UNIVERSITY OF CALIFORNIA

Santa Barbara

Probing the relationship between extension and magmatism in the lower Colorado River Extensional Corridor: Field, geochronological, and geochemical studies of Miocene volcanic rocks in the vicinity of the Whipple Mountains, CA and AZ

A dissertation submitted in partial satisfaction of the

requirements for the degree Doctor of Philosophy

in Geological Sciences

by

Mary Katherine Fidler

Committee in charge:

Professor Phillip B. Gans, Chair

Professor Bradley Hacker

Professor Matt Jackson

January 2018

The dissertation of Mary Katherine Fidler is approved.

_____

Bradley Hacker

_____

Matthew Jackson

_____

Phillip B. Gans, Committee Chair

December 2017

The relationship between extension and magmatism in the Lower Colorado River Extensional Corridor: Field, geochronological, and geochemical studies of Miocene volcanic rocks in the vicinity of the Whipple Mountains, CA and AZ

I dedicate this dissertation to the fiery women who raised me, my mom, Kathleen Fidler, and my grandmothers (by blood and in practice), Eugenia Taylor and Donna Kearney

ACKNOWLEDGEMENTS

Throughout graduate school, I have been the lucky recipient of help, mentorship, advice, and teaching from a great number of individuals. First, I would like to thank my advisor, Phil Gans, who has been a great mentor, colleague, and friend. Through his teaching and by watching his example, I have gained innumerable skills as a researcher, writer, and field geologist. But most importantly, Phil is an exemplary teacher, and his care and passion for teaching carries over into his student advising and has greatly inspired the development of my own teaching philosophy. He encouraged me to pursue every teaching opportunity available to me. Thank you for your patience and unwavering support of my academic growth and career goals.

I would also like to thank Brad Hacker, Matt Jackson, and John Cottle for serving on my committees throughout graduate school, particularly Brad and Matt for serving on my dissertation committee. Their advice, ideas, and insightful questions have greatly improved this dissertation and promoted my growth as a scientist.

I owe a debt of gratitude to several people and organizations who provided financial support for my education and for this research. I would like to especially thank Rachel Haymon and Ken MacDonald for their support through the UCSB Earth Science Department Graduate Student Opportunity Award. Their generosity gave this project a kick-start at a time when funds were tight and hope was desperately needed! Funding for tuition expenses were provided by the Earth Science Department at UCSB through the Harry Glicken Memorial Fellowship and by Shawn Byers through her generous donation to the STEM Student Support Fund. The Geological Society of America and EdMap (a component of the

USGS National Cooperative Geologic Mapping Program) also provided generous financial support for this research.

I have greatly benefited from my interactions and close friendships with a number of graduate students, particularly those in the Gans, Cottle, Hacker, Spera, and Simms research groups. I am especially thankful for the friendship and support of my housemates and colleagues, Will Junkin, Sophie Briggs, Elisabeth Steel, Josh Garber, Tyson McKinney, Alex Wrobel, and Diane Seely. Their friendship created a sense of family for me at UCSB that has carried me through every new challenge.

Finally, I would like to thank my family for their encouragement and support. My parents have always encouraged me to pursue my passions and goals with abandon. Their words of love and support have comforted and empowered me throughout my life, but especially during these five years of graduate school.

VITA OF MARY KATHERINE FIDLER
January 2018

EDUCATION:

Doctor of Philosophy in Geology
University of California Santa Barbara, January 2018

Certificate of College and University Teaching
University of California Santa Barbara, January 2018

Bachelor of Science in Environmental Geoscience
University of Notre Dame, May 2012 (Cum Laude)

PROFESSIONAL EMPLOYMENT:

2018-present	Lecturer, Department of Environmental Engineering and Earth Science, Clemson University
2016-2017	Graduate Student Researcher, Department of Earth Science, University of California, Santa Barbara
2015-2017	Associate Instructor, Department of Earth Science, University of California, Santa Barbara
2012-2016	Teaching Assistant, Department of Earth Science, University of California, Santa Barbara
2009-2012	Undergraduate Student Researcher, University of Notre Dame

TEACHING EXPERIENCE

Winter 2017 and 2016	Associate Instructor, Structural Geology, Department of Earth Science, University of California, Santa Barbara
Summer 2015	Associate Instructor, Physical Geology, Department of Earth Science, University of California, Santa Barbara

PUBLICATIONS:

***M.K. Fidler**, P.B. Gans, J.S. Lackey (2016).* Geologic map of the western Whipple Mountains and the eastern Mopah Range, southeast California: unraveling the eruptive and structural history of a synextensional Miocene volcanic province. *Abstracts with Programs - Geological Society of America*, *48*(7), Abstract no. 266-6

M.K. Fidler, *P.B. Gans (2016).* Exploring the link between crustal melting and extensional collapse; field, geochemical, and Sr-Nd isotopic evidence from pre-, syn-, and post-extensional lavas of the Whipple Mountains region, lower Colorado River extensional corridor, CA and AZ. *American Geophysical Union Fall Meeting, 2016,* Abstract V53D-3161.

M.K. Fidler*, P.B. Gans (2014).* Magmatic trigger for extensional collapse? Character and significance of pre-extensional volcanic activity in the Whipple Mountains region, lower Colorado River Extensional Corridor. *American Geophysical Union Fall Meeting, 2014,* Abstract V31E-4812

E. Steel, L. Reynolds, L. Simkins, ***M.K. Fidler*** *(2014).* Characterization of the Elephant Trees Formation, Anza Borrego with implications for determining the depositional environments of conglomeratic debris flows. *Abstracts with Programs – Geological Society of America, 46*(6), 147

M.K. Fidler *& P.B. Gans (2013).* Spatiotemporal patterns in the inception of Miocene volcanism and upper plate extensional block rotation in the vicinity of the Whipple Mountains, CA and AZ. *Abstracts with Programs - Geological Society of America,45*(7), 171.

C. Ohlin, S. Harley, J. McAlpin, R. Hocking, B. Mercado, R. Johnson, E. Villa, ***M.K. Fidler****, M. Olmstead, L. Spiccia, R.D. Britt, and W.H. Casey (2011).* Rates of water exchange for two cobalt(II) heteropolyoxotungstate compounds in aqueous solution, Chemistry - *a European Journal,*17(16), 4408-4417.

ACADEMIC HONORS:

2013 Harry Glicken Memorial Graduate Fellowship, UC Santa Barbara
2014 Preston Cloud Award, UC Santa Barbara
2014 Global Field Travel Award, UC Santa Barbara
2015 Alumni Graduate Award for Research Excellence, UC Santa Barbara
2016 Global Field Travel Award, UC Santa Barbara
2016 Lloyd and Mary Edwards Field Studies Fellowship in Earth Science, UC Santa Barbara
2016 Special Fellowship in the Stem Disciplines, UC Santa Barbara
2016 3rd place in the Best Student Geologic Mapping Competition, Geological Society of America, Fall Meeting
2017 Alumni Graduate Award for Research Excellence
2017 Muckers' Coterie Lifetime Achievement Award

GRANTS:

M.K. Fidler. Geological Society of America Graduate Student Research Grant: Using isotopes and trace element chemistry to understand source of magmatism in the vicinity of the Whipple Mountains, CA & AZ. $1777. 3/15-3/16.

P.B. Gans, ***M.K.Fidler****, and B. Gentry*. EDMAP, United States Geological Survey (USGS): Geologic Mapping of the Southwestern Whipple Mountains and Eastern Mopah Range, Southeastern California: Unraveling the Eruptive and Structural History of a Synextensional Miocene Volcanic Center. $25,677. 4/14-4/15.

M.K. Fidler. UCSB Earth Science Dept., Graduate Student Opportunity Award: Exploring the temporal and spatial relationships between extension and magmatism in the lower Colorado River extensional corridor, CA and AZ. $3,880. 6/13-6/16.

E. Steel, L. Reynolds, L. Miller, and ***M.K. Fidler***. UCSB Earth Science Dept., Graduate Student Opportunity Award: Characterization of deep and shallow marine conglomerates with implications for determining the depositional environments of the Matilija Formation, southern California. $2,066. 6/13-6/14.

ABSTRACT

Probing the relationship between extension and magmatism in the lower Colorado River Extensional Corridor: Field, geochronological, and geochemical studies of Miocene volcanic rocks in the vicinity of the Whipple Mountains, CA and AZ

by

Mary Katherine Fidler

New geologic mapping, $^{40}Ar/^{39}Ar$ geochronology, and whole rock major and trace element and Sr-Nd isotopic data of pre-, syn-, and post-extensional volcanic rocks shed light on the nature of Miocene volcanism in the lower Colorado River Extensional Corridor, CA and AZ. Detailed geologic mapping of the western Whipple Mountains and eastern Mopah Range, where the thickest accumulation of Miocene volcanic rocks is exposed in steeply tilted (~76° SW) fault blocks, reveal a four-stage volcanic history spanning the onset of normal faulting.

The earliest volcanism in this area was effusive fissure and shield eruptions of basalt and basaltic andesite totaling ~25 km^3 and producing a ~700 m thick composite surface of subdued topography. New geochronology from correlative exposures of these early lavas on the east and west sides of the corridor precisely date this early mafic volcanism from 21.1-20.0 Ma, improving existing constraints on the inception of volcanism in this part of the LCREC. The second stage consisted of primarily effusive silicic volcanism erupting ~56 km^3 from ~20-19.5 Ma, and built a 1500-2000 m thick tablelands of overlapping rhyolite

and dacite lava domes and tabular flows with subordinate pyroclastic surge and flow deposits and minor interfingering mafic lava flows. ~1.5 m.y after the onset of volcanism, three generations of normal faults formed across the field area resulting in rapid block tilting to the SSW and accumulation of syn-tectonic sediments and basaltic andesite lavas (third volcanic stage) of variable thickness in subsiding half grabens. Dips of syn-extensional strata fan upward from 67-14° SW. Total extension increased westward towards the Whipple Mountains and southwards, accommodated by rotational scissor faults. Onset of normal faulting and peak rates of associated tilting (~$2.7x10^{-4}$ degrees/yr at ~19.5 Ma) immediately followed the period of peak eruption rate ($3.9x10^{-4}$ km^3/yr from 20.1-19.9 Ma and $4.2x10^{-5}$ km^3/yr from 19.6-19.4 Ma) in the study area. The third stage of volcanism consisted of ~7.5 km^3 of basaltic andesite eruptions in the study area beginning at 19.5 Ma and persisting until ~18.8 Ma, by which time extensional tilting had ceased. In the fourth and final volcanic stage, volcanic units were channelized in fault bounded paleo-valleys, beginning with emplacement of the 18.8 Ma Peach Springs Tuff followed shortly after by scattered eruptions of ~0.04 km^3 of basalt and lastly of ~0.4 km^3 of andesite between ~18.8-16.3 Ma. Our volume estimations for the study area suggest that nearly 490 km^3 of total lava may have been erupted across the greater lower CREC in the vicinity of the Whipple Mountains.

78 Samples from the western Whipple Mountains and eastern Mopah Range (study area discussed above), Mohave Mountains, Aubrey Hills/Standard Wash, southern Whipple Mountains, and Turtle Mountains were analyzed to characterize the chemical evolution of Miocene volcanism. Pre-extensional samples are dominantly bimodal, ranging from 48.5 to 73.1 wt. % SiO_2, with a gap from 54.3 to 67.1 wt %, while syn- and post-extensional lavas are dominantly mafic and intermediate, ranging from 50.0 to 60.2 wt. % SiO_2 with minor

post-extensional rhyolites (~70 wt. % SiO_2). Many mafic and intermediate lavas are altered in the LCREC, but fresh lavas define linear trends on variation plots. $^{87}Sr/^{86}Sr$ and εNd ratios of 18 samples range from 0.706087 to 0.711366 and -1.23 to -12.37 respectively and correlate negatively with each other, indicating that assimilation of enriched crust played an important role in the evolution of Miocene lavas. The most isotopically primitive sample analyzed (a post-extensional basalt; $^{87}Sr/^{86}Sr$ = 0.706087, εNd = -1.23) is more primitive than the ancient enriched lithospheric source proposed by several authors as the likely mantle source of CREC lavas, suggesting that at least some CREC lavas represent partial melting of an OIB-like mantle source with modification by crustal assimilants affecting the most mafic lavas.

TABLE OF CONTENTS

LIST OF FIGURES

LIST OF TABLES

Introduction

Extension related magmatism is an important geodynamic process, with the majority of volcanic activity on Earth occurring at divergent margins. New divergent margins form from continental rifts, where brittle, ductile, and dilational (magmatic) extensional processes all accommodate extension at various levels within continental lithosphere. The nature of the role that magmatism plays in the initial stages of continental rifting (e.g. active versus passive role) continues to be debated after decades of study. Because fully developed rifts (divergent margins) experience considerable tectonic subsidence and sedimentation due to thinning of the continental lithosphere, the best natural laboratories to understand the nature of the relationship between extension and magmatism are in highly extended areas that did not ultimately mature into new ocean basins. As such, the Basin and Range Province of the western United States has been the focus of many pioneering studies which explore the complex relationship between continental extension and magmatism. Detailed studies of highly extended areas within the Basin and Range are key for resolving the precise temporal and spatial relationship between magmatism and extension which inform models for continental extension.

The aim of this dissertation is to understand the Cenozoic volcanic history of the lower Colorado River Extensional Corridor (LCREC) in the vicinity of the Whipple Mountains, a highly extended area within the Basin and Range Province, by combining detailed geologic mapping, geochronology, structural observations, and geochemical studies. The focus areas of the project include exposures that are dominated by Miocene volcanic rocks, including the western Whipple Mountains, eastern Mopah Range, and Turtle Mountains in CA and the Mohave Mountains, Aubrey Hills, and Standard Wash in AZ.

These regions expose variably tilted Miocene volcanic accumulations that span the duration of the region's extensional history. Each chapter of this dissertation employs a different approach to understanding the history of volcanism and its relation to extensional normal faulting in these areas. This multi-disciplinary approach results in complementary observations and a more complete picture of the igneous and tectonic processes that shaped this region.

The first chapter of this dissertation reports new detailed geologic mapping and $^{40}Ar/^{39}Ar$ geochronology of a 1.5-2 km thick accumulation of volcanic and sedimentary rocks in the western Whipple Mountains and eastern Mopah Range. We present important constraints on ages, volumes, compositions, and eruptive styles, and structural context of volcanic deposits. Results indicate that the majority of total volcanism occurred in the 1.5 million years before the onset of extensional normal faulting in this area, and that the total volume of lavas erupted in this part of the LCREC likely exceeded ~500 km^3.

The second chapter has a simple aim: to precisely date the onset of volcanism in the Whipple Mountains area and to determine whether this timing varies from east to west across this part of the corridor. New $^{40}Ar/^{39}Ar$ geochronology greatly improves existing age constraints for early volcanic units in the region, dating the onset of volcanism at ~21 Ma consistently across the corridor.

The third and final chapter of this dissertation describes the geochemical character of volcanic rocks in the vicinity of the Whipple Mountains. We present new major element, trace element, and Sr-Nd isotopic data for spanning the temporal and compositional diversity of lavas in the Whipple Mountains area. We assess the effect of various processes on the observed chemistry of CREC lavas including the effect of hydrothermal alteration on major element chemistry and of hybridization of crustal partial melts with mantle derived lavas on

isotopic data. This new data represents the most complete geochemical characterization of LCREC volcanic rocks and provides important insights into the petrogenetic evolution of these lavas.

Chapter 1 - Eruptive and structural history of a synextensional Miocene volcanic center; western Whipple Mountains and eastern Mopah Range, southeastern California

Mary Kate Fidler[1] and Phillip B. Gans[1]

[1]*Department of Earth Science, University of California, Santa Barbara, CA*

A. Abstract

New geologic mapping, major element geochemical data of 58 volcanic rocks, and 30 new $^{40}Ar/^{39}Ar$ ages shed light on the evolution of Miocene synextensional volcanism in the western Whipple Mountains and eastern Mopah Range of the lower Colorado River Extensional Corridor, southeastern California. We present important constraints on ages, volumes, compositions, and eruptive styles, and structural context of volcanic deposits.

Volcanic activity is divided into four stages, beginning with effusive fissure and shield eruptions of basalt and basaltic andesite totaling ~25 km^3 from 21-20 Ma, which spilled across an irregular landscape of pre-Tertiary basement rocks and produced a ~700 m thick composite surface with subdued topography. This was followed by a second stage of primarily effusive silicic volcanism erupting ~56 km^3 from ~20-19.5 Ma, which built a 1500-2000 m thick tablelands of overlapping rhyolitic and dacitic lava domes and tabular flows with subordinate pyroclastic surge and flow deposits. As this second stage of volcanism ended, ~1.5 m.y after the onset of volcanism, three generations of normal faults formed across the field area resulting in rapid block tilting (~$2.7x10^{-4}$ degrees /yr at 19.5 Ma) to the SSW and accumulation of syn-tectonic sediments and basaltic andesite lavas (third

volcanic stage) of variable thickness in subsiding half grabens. The third stage of volcanism consisted of ~7.5 km^3 of basaltic andesite eruptions beginning at 19.5 Ma and persisting until ~18.8 Ma, at which time extensional tilting had ceased. In the fourth and final volcanic stage, volcanic units were channelized in fault bounded paleo-valleys, beginning with emplacement of the 18.8 Ma Peach Springs Tuff followed shortly after by scattered eruptions of ~0.04 km^3 basalt and lastly of ~0.4 km^3 of andesite at ~16.5-16.3 Ma. Our volume estimations for the study area suggest that nearly 490 km^3 of total lava may have been erupted across the greater lower CREC in the vicinity of the Whipple Mountains.

The study area is divided into two structural domains based on their tilting history. The eastern domain (I) includes the western Whipple Mountains and most easterly exposures of the Mopah Range and is characterized by tilts averaging 76° for Stage 1 and 2 units, fanning dips of syn-faulting Stage 3 units from 67-14° SW, and flat-lying Stage 4 units. The western domain (II) which includes the central Mopah Range experienced considerably less total tilting during all volcanic stages. Unit and fault orientations suggest that total extension increased southwards in the study area.

B. Introduction

Scientists have been probing the relationship between continental extension and magmatism for many decades, and highly extended regions in the Basin and Range Province of the western United States have proven to be some of the best natural laboratories in which to explore the interplay between these processes. Regions which had experienced large magnitude extension were first recognized and described in the Basin and Range by Anderson (1971) and Proffett (1977), followed by such authors as Wernicke (1981), Gans

and Miller (1983), and Howard and John (1987). Then, as Cordilleran geologists recognized metamorphic core complexes (MCC) as fundamentally Cenozoic extensional features typical of highly extended regions (Crittenden et al, 1980, and references therein [particularly Coney, 1980; Davis et al, 1980; Rehrig and Reynolds, 1980]; Armstrong, 1982; Miller et al, 1983; Reynolds and Spencer; 1985; Lister and Davis; 1989), it became clear that most of these highly extended areas also exposed voluminous plutonic and/or volcanic rocks that were broadly coeval with extension (e.g., Rehrig and Reynolds, 1980). A broad temporal and spatial association of Cenozoic extension and magmatism in the Basin and Range was later expanded upon by Gans et al. (1989) and Armstrong and Ward (1991), however other authors have argued against this based on studies of specific areas (Best and Christiansen, 1991; Axen et al., 1993, Spencer et al, 1995; Putrika and Platt, 2012)

There has also been much debate about what role magmatism played in accommodating or enhancing continental extension and MCC development, particularly on whether magmatism promotes and localizes extension or is a passive consequence of extension (e.g., decompression melting). Improved geochronology and mapping in many highly extended areas throughout the US Cordillera and the world have refined models for continental extension facilitated by magmatism. The direct influence of magmatism (plutonism) in accommodating extension at depth, via magmatic accretion and dilation at depth, has been championed by many authors (Anderson, 1971; Rehrig and Reynolds, 1980; Okaya and Thompson, 1985; Gans, 1987; Gans et al., 1989; Thompson and McCarthy, 1990; Campbell-Stone and John, 2000; 2002; Laurent et al, 2015; Gans and Gentry, 2016), while others have explored the rheological influence of magmatism of promoting extension (ie. thermal triggering; Gans, 1987; Gans et al., 1989; Lister and Baldwin, 1993; Parsons and Thompson, 1993; Gans and Bohrson, 1998).

Most studies that explore this relationship focus on syntectonic plutonic rocks and relatively few explore the nature and significance of syntectonic volcanic rocks. Those that do (Gans et al. 1989; Armstrong and Ward, 1991; Gans and Bohrson, 1998; Faulds et al., 1999) note a "typical" progression of 1-3 million years of mafic to intermediate volcanism which culminates in outpourings of silicic volcanism during or immediately prior to extension, followed by a tapering of both volcanism and extension. More detailed local studies characterizing volcanism that immediately pre-dates, is coincident with, and immediately post-dates large magnitude extension such as these are needed to give insight into the broader patterns of extension-related volcanism in the US Cordillera. We present a detailed examination of a major Miocene volcanic center that lies on the western side of the Colorado River Extensional Corridor (CREC; Fig.1), a highly extended region of the Basin and Range province of the western US (Howard and John, 1987). Within the CREC, volcanism generally predated local extension by about 2 million years and persisted until the inception of extensional faulting, after which it waned in intensity but continued to erupt smaller volume syn- and post-tectonic lavas (e.g., Faulds et al., 2001).

Previous work on Miocene successions in the vicinity of the Whipple Mountains has focused mainly on the relative timing of volcanism and extension and on insights this stratigraphy gives into the structural and geomorphic evolution of the Whipple metamorphic core complex and detachment fault (Nielson and Beratan, 1990; Yin and Dunn, 1992). The Miocene volcanic and sedimentary stratigraphy in the area surrounding the Whipple Mountains has been previously described by Carr et al. (1980), Dickey et al. (1980), Hazlett (1986), Nielson and Beratan (1990), and Sherrod and Nielson (1993) and references therein. These studies mostly group volcanic rocks into broad lithostratigraphic units and present only limited information on the detailed timing and nature of individual eruptive units.

Good exposures of volcanic successions within steeply tilted fault blocks in the eastern Mopah Range and western Whipple Mountains allow us to reconstruct a complete history of volcanism in this locality and to address several important questions;

1) How did the style and composition of eruptions change leading up to and during the onset of large magnitude extension of the western Margin of the Whipple Mountains?
2) What was the total volume of magma erupted and how did eruption rates and volumes change through time?
3) How did volcanism shape the pre-extensional landscape in the vicinity of the Whipple Mountains, and how did extensional normal faulting subsequently modify the landscape and influence volcanic deposition?

We address these questions through detailed geologic mapping, structural and stratigraphic analysis, and geochemical and geochronological analysis. Our investigation charts the evolution of this major syn-extensional volcanic center, provides important new constraints on ages, volumes, compositions, and eruptive styles of volcanic deposits, and sheds light on the local tectonic and geomorphic evolution. Comparison of this volcanic terrane to others within the CREC and to both highly and moderately extended regions within the broader Basin and Range province illustrates patterns and differences among extension-related volcanic centers of the western US.

C. Regional setting and previous work

The western Whipple Mountains and Eastern Mopah Range lie in southeastern California, on the western margin of the CREC (Fig. 1) which extends from southern

Nevada to southeastern California and western Arizona. The Mopah Range is the eastern spur of the Turtle Mountains and is composed almost entirely of Tertiary volcanic and sedimentary rocks, in contrast to the main block of the Turtle Mountains which consists mainly of Precambrian gneiss and granite and Mesozoic plutons with only scattered erosional remnants of Tertiary rocks (Howard et al, 1982). The Whipple Mountains is a classic metamorphic core complex exposing a large displacement domical detachment fault that separates mid-crustal Precambrian metamorphic rocks and Mesozoic and Tertiary intrusive rocks from structurally higher, intensely faulted crystalline basement and Tertiary volcanic and sedimentary rocks (Davis et al, 1980).

The CREC lies within the larger Basin and Range province, and is interpreted to have experienced exceptionally large-magnitude crustal extension (>100%) in the Miocene (eg. Howard and John, 1987; Nielson and Beratan, 1990; Faulds et al., 1999). The lower CREC exposes several well studied metamorphic core complexes (eg. the Sacramento Mountains, Chemehuevi Mountains, Whipple Mountains, Buckskin-Rawhide Mountains, Harcuvar Mountains) and is part of a greater sinuous belt of Cordilleran MCCs stretching from Canada to Mexico (Coney, 1980). The extensional corridor sits on the fringe of the Mesozoic orogen (Burchfiel and Davis, 1981) separating ranges affected by Mesozoic deformation and plutonism to the SW from the relatively undeformed rocks of the Colorado Plateau to the northeast. Within the CREC at this latitude, Tertiary rocks lie directly on a basement of Precambrian crystalline rocks and Mesozoic and Tertiary intrusive rocks (Howard et al., 1982; Carr et al., 1980; Davis et al. 1980). The study area (Fig. 2) sits between lower plate exposures of the Whipple Mountains MCC to the east and the somewhat arbitrarily designated western boundary of the CREC in the Turtle Mountains and central Mopah Range to the west. This boundary is recognized based on the abrupt decrease

in magnitude of supracrustal normal faulting and tilting and has been interpreted as the "breakaway" or headwall region of the Whipple Detachment Fault (WDF) (Davis et al., 1980).

Previous studies showed the Mopah Range and Western Whipple Mountains expose thick sections of Tertiary volcanic and sedimentary rocks and Precambrian and Mesozoic crystalline rocks that are down-faulted along the eastern margin of the Mopah Range and are interpreted to lie in the upper plate of the WDF (eg. Carr et al, 1980; Davis et al, 1980; Hazlett, 1986). This domed fault/fault system is interpreted to have accommodated ~40 km of displacement (Davis and Lister, 1988) and displays minor NE trending antiforms and synforms (Yin and Dunn, 1992). The lower plate can be separated into two major structural domains by the gradational, SW-dipping mylonitic front, which separates rocks containing a tertiary mylonitic fabric subparallel to the WDF below the front from non-mylonitized rocks above the front (Davis et al, 1980; Davis, 1988). The lower plate rocks of the Whipple Mountains include a heterogeneous assemblage of Precambrian metamorphic and igneous rocks, Mesozoic plutons, and voluminous Miocene dikes and plutons (eg. the Chambers Well dike swarm and Wear Eagle Pluton). The Chamber's Well dikes crop out directly to the east of the field area and are proposed to be feeders of the volcanics exposed in the Eastern Mopah Range and western Whipple Mountains (Davis et al., 1982; Gans and Gentry, 2016).

The nonconformal base of the volcanic section is not exposed in the portion of the Mopah Range investigated in this study but it likely exists at depth in the field area (Hazlett, 1986, 1993) as it is observed at the northern end of the range (Nielson and Turner, 1986; Nielson and Nakata, 1993). In the NW Whipple Mountains, Yin and Dunn (1992) interpret all contacts between Precambrian gneiss and Tertiary volcanic to be exposures of the folded WDF. In the SW Whipple Mountains however, such contacts have been interpreted

differently by different authors. Carr et al. (1980), like Yin and Dunn (1992), interprets all basement-Tertiary contacts to be exposures of the WDF, whereas Gans and Gentry (2016) interpret some of these contacts as the basal nonconformity.

Previous studies of the volcanic stratigraphy of the central (Hazlett, 1986) and southern (Carr et al, 1980) Mopah Range and the western Whipple Mountains (Carr et al, 1980; Yin and Dunn, 1992; Gans and Gentry, 2016) provide a starting point for this study. These studies lay out a general sequence of volcanic events including an initial stage of basalt and basaltic andesite eruption, followed by dacite and rhyolite eruptions beginning around 20 Ma (Hazlett, 1993; Gans and Gentry, 2016). These lavas sit below a 15-30° angular unconformity above which sit conglomerates and basaltic andesite lavas (dated in disparate locations at 17 Ma and 18 Ma by Nielson and Nakata (1993) and Howard et al (1982) respectively, and at 19.5 Ma in this study) which locally display upward shallowing dips (fault growth strata). In the western Whipple Mountains, the regionally important 18.8 Ma Peach Springs Tuff (Ferguson et al, 2013; Nielson et al, 1990) also sits above this unconformity.

This study explores this volcanic stratigraphy in much more detail that has previously been described. Detailed geologic mapping and new geochronology allows us to assess eruptive rates and volumes, and to paint a clearer picture of the nature of volcanism in this region (i.e. eruptive style, types of volcanic edifices, and possible sources of volcanic deposits).

D. Methods

Geologic mapping of the western Whipple Mountains and eastern Mopah Range was

carried out during the spring and fall of 2014 and spring of 2015 using 1:4,000, 1:5,000 and 1:10,000 base maps where appropriate, depending on the geologic complexity of the area. Fidler mapped the west and southeast parts of the map area and Gans mapped the northeast part of the map area (Plate 1). Field maps were made from Google Earth imagery and mapped panels were georeferenced using ArcGIS and digitized using Adobe Illustrator. Stereographic projections of bedding and foliations were made using Allmendinger's Stereonet9 program (Allmendinger, R. W., Cardozo, N., and Fisher, D., 2012; Cardozo, N., and Allmendinger, R.W., 2013).

A total of 94 samples were collected broadly across the field area with a focus on capturing the diversity of volcanic units and the range of eruptive ages. Sample locations and rock types are given in Appendix 1. Careful attention was paid to select the least altered outcrops for $^{40}Ar/^{39}Ar$ geochronology and whole rock geochemistry. Sampling of mafic units targeted the coarse grained lava flow interiors, while for silicic units, we primarily sampled vitrophyres at the base or tops of flows. For geochemical analysis and dating of pumice rich volcaniclastic units (Tc), we sampled only juvenile pumice fragments.

A total of 30 age determinations were made from volcanic units in the field area using the $^{40}Ar/^{39}Ar$ method. Appropriate magnetic separation techniques, ultrasonic cleaning, and acid washes (HF) were used to generate purified separates of plagioclase (for andesite, dacite and rhyolite), sanidine (for Peach Springs Tuff), and holocrystalline groundmass (for basalt and basaltic andesite). All mineral separations and analyses were performed at UCSB's $^{40}Ar/^{39}Ar$ geochronology laboratory. Analyses consisted of 6 to 23 step incremental heating steps in a Staudacher-type resistance furnace with isotopes measured on a Mass Analyzer Products 216 mass spectrometer, using the procedures described by Gans (1997). Ages were reduced and spectra generated using Brad Hacker's

Eyesorecon program. Data were monitored using Taylor Creek Rhyolite sanidine and originally calibrated using an age of 27.92 Ma (Dalrymple and Duffield, 1988; Tabulated data and age spectra are in Appendix II). Ages have been recalculated (Table 1) using an adjusted assumed age of 28.35 Ma for Taylor Creek Rhyolite, in order to bring our ages into equivalence with the now widely accepted age of 28.1 Ma for Fish Canyon sanidine (Spell and McDougal et al., 2003). This brings our Peach Springs Tuff age determination of 18.77 ± 0.08 Ma into agreement with the 18.78 ± 0.02 Ma age reported by Ferguson et al. (2013). For preferred ages in which individual steps of the plateau overlap in analytical uncertainty, reported errors are ± 2 σ (95% confidence) precision. For ages where individual steps of chosen "plateau" do not overlap in analytical uncertainty, the reported error spans the age variation of all chosen steps.

The bulk-rock major oxides of 58 samples were analyzed by X-ray fluorescence (XRF) at Pomona College. Methodology and error analysis for XRF were adapted from Johnson et al. (1999) for samples analyzed at WSU, with a similar analytical method at Pomona (Lackey et al. 2012). Representative, clean, unweathered chips of all samples were powdered in a tungsten carbide head and mill and mixed with flux in a 2:1 ratio (3.5 g of sample to 7.0 g of dilithium tetraborate ($Li_2B_4O_7$)). The mixture was fused to a glass bead in a graphite crucible at 1000° C for 10 min, reground, and then fused for a second time. Beads were then polished with 1000 grit powder and analyzed. Major elements were measured at Pomona University on a single fused bead using a 3.0 kW Panalytical Axios wavelength-dispersive XRF spectrometer equipped with PE, LiF 200, GE, and PX1 industrial crystals. Concentrations are determined using reference calibration curves of 55 certified reference materials spanning a range of natural rock compositions (Lackey et el. 2012).

E. Volcanic stratigraphy of the western Whipple Mountains and eastern Mopah Range

1. Overview

The rolling hills and low jagged ridges of the westernmost Whipple Mountains and eastern Mopah Range (Fig. 3) on either side of CA Highway 95 provide nearly continuous bedrock exposure from the Whipple Mountains metamorphic core complex to the western edge of the CREC (Fig. 1, 2). This area exposes a thick section of variably tilted Miocene volcanic and subordinate sedimentary rocks. Bedrock exposures are separated by broad Quaternary pediment surfaces and alluvial washes. Tertiary strata strike WNW-ESE and dips to the SSW and lie in faulted and nonconformable contact with Proterozoic basement. Detailed mapping reveals that the volcanic stratigraphy is complex, with important lateral and vertical variations, and is repeated several times across the area by NE-dipping normal faults.

2. Classification and nomenclature of map units

Volcanic units are divided into map units based on phenocryst assemblage, rock composition (major element chemistry) and stratigraphic position (e.g., olivine- and clinopyroxene-bearing basalt flows in the lower part of the section are given the symbol $Tocb_1$ whereas stratigraphically higher flows with the same mineral assemblage are called $Tocb_2$). Mafic phenocrysts are listed in order of decreasing abundance (eg. Tocb contains olivine > clinopyroxene). Note also that rock types (eg. dacite vs. rhyolite) given to a map unit do not necessarily reflect homogeneity in composition of all lava flows within the map unit (Fig. 4). For example, silicic units of the same phenocryst assemblage and stratigraphic

position may include individual lava flows of both dacite and rhyolite. Unit names chosen therefore reflect the composition of the majority of samples analyzed for each unit.

A detailed treatment of the geochemistry and petrology of these rocks and others from across the LCREC is provided in Chapter 2. Volcanic units in the field area range from basalt to rhyolite, with an apparent compositional gap from ~60-67% SiO_2 (Fig. 4). The abundance of silicic compositions in part reflects sampling bias as these rocks are generally the freshest and easiest samples to collect for geochronology, and are also the most voluminous volcanic units in the field area.

Most mafic rocks from the base of the section (units Tttba, Tob, and Tmfu) show petrographic evidence for alteration and potassium metasomatism and thus were not analyzed. A few altered samples were analyzed, two of which (one mafic enclave (Ta) and one aphyric andesite (Taa)) contain ~12% K_2O and <<1% Na_2O – strong evidence for K-metasomatism. It is likely that some of the spread in total alkali content, particularly in our intermediate composition samples, is due to minor alteration. For example, one olivine-clinopyroxene basaltic andesite (Tocba) sample and one mafic dike sample (Tmd) have elevated total alkali contents relative to the other intermediate rocks and also show textural evidence for alteration including partial replacement of groundmass and phenocrystic plagioclase with sericite and adularia and replacement of hornblende by magnetite.

3. Proterozoic basement rocks and the basal Miocene nonconformity

Basement in the western part of the study area includes a diverse assemblage of rock types. These rocks have been described in detail by Greg Davis, Lawford Anderson, and colleagues in several petrologic studies of the Whipple Mountains (Davis et al, 1980, 1982; Davis 1988; Anderson, 1981; Anderson and Rowley 1981; Anderson et al 1988; Anderson

and Cullers, 1990) and by Howard et al (1982) in the Turtle Mountains to the East. The oldest rocks are Proterozoic banded quartzo-feldspathic gneiss, amphibolite, leucogranite, and K-feldspar megacrystic granite. Undeformed granites and innumerable hypabyssal intrusions that range from diabase to rhyolite are likely Mesozoic and Miocene respectively. Only some of the larger Miocene dacite hypabyssal intrusions are mapped (Tdi), but many more dikes of a broad range of compositions exist throughout virtually all basement exposures in the western Whipple Mountains, as reported by Gans and Gentry (2016). These authors interpreted the Miocene dikes of the western Whipple Mountains to be feeders for the thick volcanic succession exposed in the field area due to remarkable similarities in compositions, ages, magmatic evolution, and temporal relationship to local tectonism. As the complex intrusive and structural relationships displayed within basement exposures were not the focus of this study, these areas were largely mapped as a single undifferentiated unit (p€).

Regionally, it has been well documented that the Tertiary section in many areas surrounding the Whipple Mountains rests nonconformably on basement. In some areas in and near the Whipple Mountains (eg. Mohave Mountains, Aubrey Hills and Standard Wash, Eastern, Southern, and SW Whipple Mountains, Northern Turtle Mountains and Northern Mopah Range) arkosic conglomerate and sandstones (possibly of pre-Miocene age) were deposited above this nonconformity and underlie volcanic deposits (Dickey et al, 1980; Carr et al, 1980; Nielson and Turner, 1986; Nielson and Beratan, 1990; Nielson and Nakata, 1993; Howard et al 1999; Gans et al. 2016). Such sedimentary rocks, however, are not present along the basal nonconformity in the Chemehuevi Mountains (John, 1987) or within the field area. In the western Whipple Mountains, Carr et al. (1980) interpreted all of the Miocene-basement contacts to be faults, and tentatively interpreted some of these faults as

exposures of the WDF. Yin and Dunn (1992) interpreted all basement-Miocene contacts to be exposures of the WDF, and invoked E-W trending antiforms in the WDF surface to explain their map pattern. We agree that most of the basement contacts in the study area are faulted, with the exception of one WNW trending contact located a few km SE of Pyramid Butte. This contact is mostly obscured by colluvium and cut by many small mafic and silicic hypabyssal intrusions that fed overlying lava flows, but is interpreted to be nonconformable because a) it parallels the strike of overlying lava flows and b) is constrained in several places to within a meter or two with no evidence of breccia, veins, or oxidation in either the Miocene or adjacent Proterozoic rocks. This is consistent with observations by Gans and Gentry (2016), who observed similar NW-trending segments of nonconformable basement contacts in the SW Whipple Mountains, and concluded that the footwall in the SW Whipple Mountains experienced 60-70°of SW tilting. In the Mopah Range, west of the highway, the basal nonconformity is not exposed though it likely exists in the subsurface (Cross Section A) as analogous to other parts of the corridor.

4. Miocene volcanic and sedimentary stratigraphy

The Miocene succession broadly consists, in ascending order, of 1) early mafic lavas, 2) silicic lava domes that interfinger with minor flanking mafic lavas, 3) synextensional conglomerates and mafic to intermediate lavas, and 4) younger (post-tilting) capping units of Peach Springs Tuff and locally derived mafic and intermediate lavas. The following stratigraphic summary is distilled from the mapped geological relationships recorded on Plate I and summarized in Figure 5. Ages of volcanic units are summarized in Table 1.

Early mafic lavas

"Turkey-track" plagioclase-clinopyroxene-olivine basaltic andesite and olivine-clinopyroxene basalt (Tttba, Tocb$_1$, Tmu)

The oldest Tertiary unit in the field area is a porphyritic plagioclase-clinopyroxene-olivine basaltic andesite (Tttba) referred to by others colloquially as "turkey-track" or "jackstraw" porphyry due to its high proportion of large tabular flow-aligned plagioclase phenocrysts. This unit consists of many stacked ~10-20 m thick lava flows that apparently erupted in rapid succession because little to no sediments accumulated between them. This unit is best exposed in the NW portion of the map area, near the end of Cross Section B, though the same rocks can be found in the undifferentiated mafic unit (Tmu) in the SW portion of the field area. Here, alteration and poor exposure required us to map Tttba and olivine-clinopyroxene basalt flows (Tocb$_1$) together as Tmu. The porphyritic Tttba is intimately associated and interstratified with Tocb$_1$ lavas (Fig. 5). Both units are dark weathering and recessive, cropping out in low undulating hills and washes. They form steeper topography only in the SW portion of the map area where abundant ~15 m thick subhorizontal biotite dacite dikes (Tdi) cut them, creating high cliffy ledges (Fig. 3). The abundance of irregular bodies and subhorizontal intrusions of this younger dacite commonly obscures original stratigraphic relationships in these mafic units. Where mapped together, Tmu (including rocks of both Tttba and Tocb$_1$ affinities) is estimated to be up to ~700 m thick. Exposures exhibit variation in thickness due to paleotopography. Assuming an average flow thickness of 15 m, we estimate that about 50 lava flows make up this unit at its thickest point. These lava flows are highly altered within the field area, and are much better exposed in other parts of the LCREC (Aubrey Hills, Standard Wash, Mohave Mountains, and Turtle Mountains) (Figs. 1, 6).

Tttba lavas are highly porphyritic and locally contain up to 40% total phenocrysts, including 15-30% conspicuous (up to 1.5 cm) tabular flow-aligned plagioclase phenocrysts, 4-8% (1-2 mm) olivine, and 3-5% (2-3 mm) clinopyroxene, making it easily distinguishable from other mafic units (Fig. 6). $Tocb_1$ lavas contain up to 15-23% total phenocrysts of primarily olivine>clinopyroxene>>plagioclase. $Tocb_1$ lavas typically contain 8-12% (1-2 mm) olivine, 6-10% (2-3 mm) clinopyroxene, and ~1% plagioclase in a crystalline groundmass containing abundant olivine (Fig. 6). Neither Tttba nor $Tocb_1$ were dated in the field area, but correlative rocks in Standard Wash and the Aubrey Hills yielded ages of 21.0 ± 0.1 Ma and 20.61 ± 0.08 Ma respectively.

Silicic lava domes/flows and interstratified sedimentary deposits and mafic lavas

Overlying the lower mafic units are several distinct types of dacite and rhyolite lavas. These are described below in ascending order, though some of these units display complex interfingering and intrusive relationships and/or occur multiple times in the stratigraphy (Fig. 5). Some silicic lavas were too altered to be confidently assigned to any of the units described below, and were mapped as altered dacite (Tda)

Hornblende-biotite rhyolite ($Thbr_1$)

The oldest of the silicic volcanic units is a hornblende-biotite rhyolite ($Thbr_1$). This unit forms a thick steep-sided lava dome complex that is partly intrusive into the early mafic lava sequence (Fig. 5). $Thbr_1$ crops out throughout the western Whipple Mountains, where it is exposed in several imbricate fault slices, and in the steep SW slopes of the Mopah Range. Exposures in the two ranges likely occupy the same stratigraphic position. The lateral extent and dome-shaped geometry of $Thbr_1$ is best exposed in the NE portion of the field area

where it overlies tuffaceous sediments (Tts), Tttba, and $Tocb_1$, and is interstratified with and onlapped by two-pyroxene dacite (Tpd) and biotite-hornblende rhyolite (Tbhr) (Fig. 5). These lavas weather various shades of beige, pink, brick red, and lavender (Fig. 3, 7) and commonly display conspicuous streaky flow laminations parallel to platy partings. They are generally recessive, cropping out in low hills. The unit is up to 1100 m thick in the NW Whipple Mountains, where it forms the core of at least one, perhaps two stacked lava domes. It has a minimum thickness of ~150 m in the SW Whipple Mountains where it thins to one or more tabular flows.

Fresh exposures and vitrophyres of $Thbr_1$ are rare in the NW Whipple Mountains, but not uncommon in the Mopah Range. The pervasive alteration of $Thbr_1$ is indicated by chalky-looking plagioclase replaced by sericite, clays, calcite, and/or secondary k-feldspar and mafic minerals replaced by Fe-oxides. Lavas contain ~15% phenocrysts of plagioclase, hornblende and biotite with hornblende>biotite. It can be distinguished from other hornblende-biotite rhyolites which occur stratigraphically higher ($Thbr_2$) by its marked higher degree of alteration and more recessive nature. Our attempt to date the unit in the western Whipple Mountains was not successful, yielding a highly disturbed Ar spectra, but a reliable age of 19.61 ± 0.24 Ma was obtained in the Mopah Range. Based on interfingering relationships with other well dated units (Tpd, Tbhr), most exposures of $Thbr_1$ that are too altered for direct dating in the western Whipple Mountains are approximately 20.0-19.9 Ma.

Andesite inclusions (Ta)

Locally $Thbr_1$ includes abundant enclaves and rafts ranging from less than a meter to several hundred meters across of primarily andesite (Ta) that weather dark brown to black. These are observed mainly in the western Whipple Mountains, and our map underestimates

their abundance as many exposures are too small to map. The smaller exposures are clearly magmatic enclaves as they show mingling textures with the rhyolite, including delicate crenulate and quenched margins (Fig. 8). Some map out as tabular bodies within the tabular rhyolite lava flows while others are irregularly shaped and relatively equant. Some of the larger bodies mapped as Ta (such as the large exposures near the center of the cross-section B line) contain internal stratification and local rubbly and vesicular horizons, suggesting they are large xenoliths of mafic country rock that were completely enveloped by silicic lava domes, rather than magmatic enclaves. This interpretation is speculative as these exposures are highly altered and contacts are poorly exposed.

Two-pyroxene dacite (Tpd)

A distinctive silicic unit is the two-pyroxene dacite (Tpd), which consists of at least five reddish weathering lava flows separated by irregular vitrophyres. This unit is recessive (as in the NW Whipple Mountains) to resistant (as it is in the interior of the Mopah Range in the SW corner of the map – Fig. 3) and often has tan to pink weathering devitrified flow interiors and gray vitrophyres. The devitrified interiors of flows have conspicuous platy partings parallel to flow banding and vitrophyres have a well-developed perlitic texture. Generally, NW-trending exposures of Tpd are limited to a broad swath of land stretching from the SW to NE corners of the map, presumably where it has been repeated by several faults. Tpd lava flows on-lap and interfinger with $Thbr_1$, Tbhr, and hornblende-pyroxene dacites (Thpd) and are overlain by younger hornblende-biotite rhyolites ($Thbr_2$), and more Thpd flows (Fig. 5). The unit is ~550 m thick in the Mopah Range, and has a minimum thickness of ~450 m in the western Whipple Mountains (estimated in locations where there are no fault repetitions). Individual lava flows are up to 100 m thick.

Tpd lavas contain 12-18% crowded (0.2-1.5 mm) plagioclase phenocrysts and 5-8% pyroxene microphenocrysts (0.1-0.5 mm) with variable ratios of orthopyroxene to clinopyroxene. It also locally contains trace biotite and hornblende and has a glassy groundmass (Fig. 6). $^{40}Ar/^{39}Ar$ ages of 19.96 ± 0.20, 19.94 ± 0.26 and 20.03 ± 0.24 Ma were obtained for this unit in the Mopah Range as well as ages of 19.98 ± 0.32 and 19.91 ± 0.22 Ma in the western Whipple Mountains.

Biotite-hornblende rhyolite (Tbhr)

Biotite-hornblende rhyolite (Tbhr) is intimately associated with $Thbr_1$ and Tpd in the lower part of the section, displaying interfingering, on-lapping, and intrusive relationships with these units (Fig. 5). These lavas consist of tabular flows, irregular intrusions into the lower part of the section, and likely domes as well (though dome shaped geometries are not as clear as with $Thbr_1$). Tbhr is best exposed in the NE portion of the area in the Whipple Mountains, and in the SW corner in the Mopah Range. Everywhere it is exposed, the unit is recessive, forming nearly flat exposures incised by washes. Tbhr lava flows have generally fresh pumiceous breccia and vitrophyres at their bases, and devitrified and vapor phase altered interiors. The devitrified portions of the unit weather tan, pink, or red, while vitrophyres are often dark gray and have a well-developed perlitic texture. Tbhr is ~900 m thick at its thickest point in the NW Whipple Mountains where at least three flows are stacked, but is ~500 m thick in the far eastern part of the mapped area and in the Mopah Range. Individual tabular flows are estimated to be ~125-150 m thick on average.

The typical phenocryst assemblage of this unit is 10-15% plagioclase phenocrysts (up to 3 mm), and 3-5% biotite and hornblende microphenocrysts (50-400 μm). It is distinguished from $Thbr_1$ and $Thbr_2$ primarily by its greater modal abundance of biotite

compared to hornblende. Additionally, vitrophyres are better preserved compared to $Thbr_1$ and it is generally more recessive than $Thbr_2$. A single Tbhr sample in the Western Whipple Mountains yielded an age of 20.16 ± 0.26 Ma.

Hornblende-biotite rhyolite ($Thbr_2$)

The younger hornblende-biotite rhyolite unit ($Thbr_2$) consists of at least 10 tabular lava flows and 2-3 steep sided domes in the field area. The lava flows tend to form linear ridges and the domes form rounded peaks. $Thbr_2$ lavas are typically much less altered than $Thbr_1$ and Tbhr, preserving fresh phenocryst phases throughout, though flow interiors may display minor vapor phase alteration. Vitrophyres are common at the bases and tops of flows and the margins of domes. Devitrified interiors typically weather tan, yellowish gray, or light pink while vitrophyres are dark grey to black. In the SW Whipple Mountains, this unit is widespread, but parts of this section may be repeated on concealed northward dipping normal faults. In the far eastern exposures of the Mopah Range (just west of highway 95), laterally continuous vitrophyres define flow boundaries and the unit reaches its maximum thickness of ~1200 m thick. Where they can confidently be identified as tabular flows, $Thbr_2$ flows range from ~50-250 m thick.

These lavas are interleaved with many other units including Thpd, Tts, $Tocb_2$, and Taa (Fig. 5). In the SW Whipple Mountains and eastern Mopah Range (just west of highway near center of map) $Thbr_2$ forms a steeply tilted homoclinal section and clearly overlies the older silicic and mafic units (Tbhr, $Thbr_1$, Tpd, Tmu, etc.). The most ambiguous relationship observed between $Thbr_2$ and the earlier silicic units is in the SW corner of the map area in the Mopah Range. Here, a large irregularly shaped exposure of $Thbr_2$ has an ambiguous contact with $Thbr_1$ and Tpd. The peak on the western side of this exposure is entirely

devitrified, and is interpreted it to be an intrusive (at least in part) plug or a lava dome. The moderately sloping expanse of $Thbr_2$ that occupies the central and eastern parts of this exposure is entirely vitrophyric, with large portions brecciated. These rocks are interpreted to be a lava flow associated with the growth of the adjacent plug. If the eastern part of this $Thbr_2$ exposure is indeed extrusive however, it requires that the lava was erupted after the major range bounding faults developed, when $Thbr_1$ was already exposed at the surface, such that $Thbr_2$ rests in angular unconformity on $Thbr_1$.

Total phenocryst abundance in this unit ranges from 15-25%. It typically contains 8-15% plagioclase, 4-5% hornblende and ~2-3% biotite. It is distinguished from Tbhr by its much lower degree of alteration. Additionally, $Thbr_2$ is more resistant than $Thbr_1$ forming ridges and peaks whereas the latter is everywhere recessive. Excellent concordant ages were obtained for $Thbr_2$ of 19.51 ± 0.1 and 19.43 ± 0.24 Ma in the Mopah Range, and 19.49 ± 0.08 and 19.47 ± 0.2 Ma in the western Whipple Mountains, confirming its slightly younger age compared to the underlying silicic units.

Hornblende-pyroxene dacite (Thpd)

The hornblende-pyroxene dacite unit consists of two or three lava flows and is exposed only in the central part of the mapped area, in the eastern Mopah Range. This grey to pink weathering lava displays brecciated vitrophyric bases, and is interleaved with $Thbr_2$ and Tpd lavas (Fig. 5). To the east, where it is interstratified with $Thbr_2$ lava flows, Thpd lies in depositional contact above and below $Thbr_2$ lavas. However, to the west where it is interleaved with Tpd, the contacts are poorly exposed, and their nature is ambiguous. It is possible that Thpd is intrusive into Tpd rather than interstratified with it. The thpd lava flows

are ~130 m thick. Thpd is distinguished from other silicic units by its unique phenocryst assemblage.

Tuffaceous sedimentary rocks (Tts)

Tuffaceous sedimentary rocks (Tts) are common in the Tertiary section, occurring at all stratigraphic levels and in nearly all parts of the field area. Tts is closely associated with hornblende and biotite bearing silicic extrusive units and forms both laterally continuous intervals and discontinuous lenses interstratified with lava flows (Fig. 5). Exposed sections range in thickness from less than a meter (in which case it is included with the associated lava) to 430 m thick (in the SW corner of map in the Mopah Range).

Tts is pale due to an abundance of silicic pumice and ash, and is very poorly sorted, containing angular to subangular ash to lapilli and block sized fragments of hornblende and biotite bearing pumice and volcanic lithics. The composition of volcanic lithic fragments in Tts varies between different exposures, but in most instances is distinctly polymict with angular fragments of many different textural and compositional types of lava. Where it is interstratified with silicic flows or domes it contains up to up to 40% pumice and can be moderately bedded to unstratified (recording variable dips). Such deposits of Tts represent local surge, fallout, and small pyroclastic density current deposits associated with growth of silicic lava domes. Its character is different in the lower part of the section, where thin laterally continuous layers overlie the early mafic units and underlie $Thbr_1$ in the NW Whipple Mountains. Here, Tts consists of well bedded, moderately sorted, sand and pebbles of volcanic lithic fragments of variable composition.

Olivine-clinopyroxene basalt ($Tocb_2$)

At least four olivine-clinopyroxene basalt flows are interleaved with $Thbr_1$, $Thbr_2$, and Tts (Fig. 5) in the SW Whipple Mountains. The lavas are exposed in discontinuous lenses, many of which may be truncated and repeated by closely spaced faults, though exposure is poor and faults are not exposed. The unit is pale gray and recessive, and its contacts are generally poorly exposed (often covered in colluvium from neighboring silicic units). Exposures of $Tocb_2$ lavas range from 20-150 m thick, and average around 50 m thick. Due to poor exposure of this unit, it is impossible to tell if thicker exposures consist of multiple emplacement units or a single flow. No internal structure or textures could be identified. These are interpreted to be lava flows rather than intrusions because most exposures are parallel in strike to both overlying and underlying surficial Tts deposits. $Tocb_2$ is phenocryst poor, ranging from 2-3% total phenocrysts. Size of olivine to clinopyroxene is variable between flows, with some flows containing 1-2 mm clinopyroxene and 0.4-1 mm olivine, and others containing 1-3 mm olivine and 0.2-1 mm clinopyroxene. Groundmass commonly contains variolitic plagioclase and intergranular olivine and clinopyroxene. $Tocb_2$ is distinguished from $Tocb_1$ by its lower abundance and smaller size of phenocrysts as well as by stratigraphic position.

Altered Aphyric Andesite (Taa)

In the southernmost part of the SW Whipple Mountain map area are two thin lava flows of dark brown weathering nearly aphyric andesite. This localized unit is pervasively altered and contains only sparse (<1%) small phenocrysts of plagioclase and clinopyroxene (<0.3 mm). The two Taa flows are 70 and 170 m thick, and are interstratified with moderately well bedded Tts deposits and $Thbr_2$ flows (Fig. 5). Rocks of this unit have a

similar character and appearance to Ta enclaves included in $Thbr_1$, but Taa consists of lava flows and occupies a higher stratigraphic position.

Syn- to post-extensional sedimentary and volcanic units

There are several distinctly younger units that dip moderately to gently and lie in prominent angular unconformity above the steeply tilted units described above. These are interpreted to have been deposited during and after block tilting.

Younger conglomerate (Tc)

A polymict fluvial and alluvial conglomerate (Tc) rests in angular unconformity on the steeply dipping volcanic units described above. This unit is tan, yellow, or white and rarely crops out, except in gullies and steep hillslopes, as it is often covered by talus from more resistant overlying units. It is exposed in many locations throughout the Mopah Range where it directly underlies and is interbedded with olivine-clinopyroxene basaltic andesite lavas (Tocba) and only in the NW Whipple Mountains where it directly underlies the Peach Springs Tuff (Tpst) (Fig. 5). Estimated thicknesses of Tc range from as thin as a few meters to as thick as 300 m.

Tc contains a mixture of plutonic, metamorphic (basement) and volcanic clasts (lithic fragments of all underlying volcanic units, and abundant hornblende-biotite rhyolite pumice and ash), ranging in size from sand to boulders. Deposits are generally well stratified and moderately sorted. They are dominated by fluvial deposits containing channels, cross stratification, and moderately rounded clasts, but also include tabular, unsorted, clast and matrix supported debris flows, with blocks up to 50 cm. In one location in the Mopah Range

(at the base of Tc, just north of sample MP-27) Tc includes a monomict debris avalanche deposit consisting of 1-2 m angular blocks of pyroxene dacite in a sandy and pebbly matrix.

This unit is important for several reasons. It is the first in the Tertiary succession to record erosion and deposition of basement derived material, indicating crystalline basement had been exhumed at this time. Crystalline clasts may have been sourced from either the Turtle Mountain or Whipple Mountain crystalline terranes (or both), or locally within the field area. The unit is deposited in angular unconformity on the younger parts of the steeply dipping volcanic succession, and is interpreted to be faulted against the older parts. Dips are consistently intermediate between the steeply tilted section and capping units, with some areas (particularly well displayed in the Mopah Range) exhibiting decreasing dips up-section. These observations lead us to the interpretation that Tc represents half-graben basin fill deposits associated with the inception of extensional faulting.

Olivine-clinopyroxene basaltic andesite (Tocba)

Stacks of at least six olivine-clinopyroxene basaltic andesite flows (Tocba) create resistant caps on multiple ridges in the Mopah Range. This unit is widespread in the Mopah Range but not present east of Highway 95 in the Whipple Mountains, suggesting a source within the Mopah Ragne. Tocba both overlies and is interstratified with Tc, and in some places sits directly in angular unconformity on the older, steeply dipping silicic lavas (Fig. 5). Tocba is black and resistant. Slopes beneath outcrops are generally covered in meter scale boulders of talus coated in a heavy desert varnish. Flows boundaries are often subtle, but marked by slightly more resistant rubbly vesicular oxidized horizons. Locally, the unit is up to 550 m thick.

Tocba lavas contain 8-16% total phenocrysts including 2-7% plagioclase, 4-6% olivine, 2-4% clinopyroxene, and <1% Fe/Mg-oxides with sparse xenocrystic quartz rimmed by acicular clinopyroxene. In one isolated location, (sample MP-18), Tocba contains ~1% hornblende (2-3 mm) altered to magnetite. This unit looks similar to the clinopyroxene-olivine andesite of Pyramid Butte (Tcoa), but is distinguished by its abundance of olivine relative to clinopyroxene, and its association with Tc. Three lava flows within this unit, yielded consistent ages of 19.58 ± 1.02, 19.55 ± 0.25, and 19.53 ± 0.12 Ma. These ages overlap within uncertainty with ages of steeply dipping $Thbr_2$ lavas that underlie Tocba.

Peach Springs Tuff (Tpst)

The Peach Springs Tuff (Tpst), first identified and named by Young and Brennan (1974), crops out in the NW Whipple Mountains. The source of the Peach Springs Tuff is the Silver Creek Caldera near Oatman, AZ (Ferguson et al., 2013). The outflow sheet covered a large area, including the western edge of the Colorado Plateau and Transition Zone, the Colorado River Extensional Corridor, and large areas of the Mojave Desert (Young and Brennan, 1974; Glazner et al. 1986; Carr, 1991). Ferguson et al. (2013) obtained a weighted mean average age of 18.78 ± 0.02 that includes 8 of their samples (including caldera fill and outflow facies) combined with previously published ages of Nielson et al. (1990) and Miller et al. (1998). Our age for Tpst in the NW Whipple Mountains is consistent with these previously published ages (18.77 ± 0.08 Ma). This is the only volcanic unit exposed in the field area that is clearly not locally derived.

Tpst is a white, pink, and tan weathering rhyolite ignimbrite. It is unwelded to moderately welded in the field area, with ~10-15% phenocrysts of mainly sanidine (commonly chatoyant) and plagioclase with minor quartz, hornblende, biotite, and

conspicuous accessory titanite. It occurs in a NW-SE trending strip in the NW Whipple Mountains, where is sits in angular unconformity on Tc or on steeply tilted silicic units. Dips of compaction foliation are variable, but the unit's unwelded basal contact maps out as a fairly subhorizontal sheet. The distribution of Tpst and Tc coincide with and partially obscure a major NE dipping normal fault that repeats a large portion of the volcanic section. These observations suggest that Tpst flowed down or filled a NW trending ancestral fault controlled valley. In the field area, the unit reaches a maximum thickness of ~100 m.

Olivine basalt (Tob)

Overlying the Peach Springs Tuff on the northern edge of the field area as isolated hills in the western Whipple Mountains, are several lava flows of olivine basalt (Tob). These black lavas crop out similarly to Tocba and the clinopyroxene-olivine andesite (Tcoa) lavas but are distinctly younger. Tob rests unconformably on an irregular erosion surface of Tpst and in buttress unconformity against $Thbr_1$ (Fig. 5). Although its irregular lower contact makes it difficult to precisely determine the orientation of Tob, it appears to dip gently (<10°) north. The unit consists of 3-4 lava flows, each ~10 m thick. We estimate the total thickness of the unit to be ~40 m thick. Tob contains 3-8% total phenocrysts of olivine and plagioclase. We have dated 3 lava flows within this unit yielding ages of 18.76 ± 0.12, 18.74 ± 0.33 and 18.39 ± 0.12 Ma.

Clinopyroxene-olivine andesite (Tcoa)

The youngest volcanic unit in the map area consists of several clinopyroxene-olivine andesite lava flows (Tcoa). These dark red to black weathering lavas are exposed only in the western Whipple Mountains, where they form Pyramid Butte and a few lower hills to its

NW. Similar to Tocba and Tob lavas, exposures of Tcoa are typically flanked by talus slopes of heavily varnished large boulders. Tcoa lavas are surrounded by talus but inferred to sit in angular unconformity on older silicic lavas (Tpd, $Thbr_1$, $Thbr_2$, Tbhr) and Tc. Based on the elongate aspect of Tcoa exposures, these lavas were likely channelized along the same fault bound valley that controlled the distribution of Tpst. The abundance of stratified scoria deposits intercalated with lava flows in the vicinity of Pyramid Butte suggests that this was the vent area for the Tcoa lavas. This vent may have been localized by the same NE-dipping normal fault system that repeats the older volcanic succession and controlled the deposition of Tc and Tpst.

We estimate that at least 6 lava flows make up the Tcoa exposures in the field area. At its thickest point (Pyramid Butte) the unit is ~360 m thick, and thins to ~220 in the hills to the NW. Tcoa lavas typically contain ~10% plagioclase phenocrysts and <2% olivine and clinopyroxene in a microcrystalline groundmass. Though outcrop characteristics can at first appear similar, it is distinguished from the other basalt and basaltic andesite units in the field area by its sparsity of mafic phenocryst phases relative to plagioclase. Three lava flows yielded ages ranging from 16.54 ± 0.2 Ma for the lower most to 16.30 ± 0.18 Ma for the uppermost lava flows.

F. Eruptive History and evolution of volcanism in the western Whipple Mountains and eastern Mopah Range

Armed with the above unit descriptions and designations, we now describe the volcanic succession in terms of changes in the eruptive character through time. In the following section, we address several aspects of the region's volcanic history including 1)

the distribution of vents in the study area, 2) the types of vents and nature of eruptions, 3) the character of eruptive units, and 4) estimated eruptive volumes.

1. Distribution of vents in the study area

Hazlett (1986) suggested that two independent vent systems fed this volcanic terrane, one stretching the length of the Mopah Range north to the Stepladder Mountains and one in the western Whipple Mountains (Fig. 9). Evidence that vents existed in the Mopah Range is quite clear. Hazlett (1986) and Carr (1980) describe vents in the core of the Mopah Range, including large rhyolite plugs and domes, cinder cones, and dikes that feed directly into lava flows which Hazlett (1986) interpreted to represent fissure vents. Evidence used by previous workers to suggest that venting took place in the Western Whipple Mountains however is more limited, and principally includes the existence of the Chambers Well dike swarm, first described by Davis et al. (1982). Gans and Gentry (2016) convincingly argue based on chemical and geochronological similarity between the dikes of the Chambers Well swarm and the volcanic rocks of the western Whipple Mountains that these dikes are likely the hypabyssal feeders of the volcanic accumulation. Workers who have mapped portions of the volcanic rock exposure between the core of the Mopah Range and the edge of the Whipple crystalline terrane however have not recognized vent facies rocks in these highly tilted supracrustal blocks (Carr, 1980; Hazlett, 1986; Yin and Dunn, 1990; Gans and Gentry, 2016). Based on our mapping, we suggest that vents were distributed across this area and that the now tilted blocks of the eastern Mopah Range and western Whipple Mountains were part of a broad and continuous volcanic tablelands with many scattered vents rather than two separate volcanic belts (cf. Hazlett, 1986).

2. Volcanic history

For simplicity, the volcanic record is divided into 4 temporal stages (denoted as 1 to 4 from oldest to youngest; Fig. 10, 11). Stage 1 constitutes mafic volcanism that may represent either shield growth or Icelandic-type fissure eruptions. Lavas erupted in this stage dominate the total volume of erupted mafic lavas in the field area. Stage 2 spans a period of primarily silicic volcanism and immediately predates the onset of extension in the field area. These stages include dome-fed flow growth, tabular rhyolite and dacite flows and minor explosive eruptions. Silicic lavas erupted in these stages dominate the total volume of lavas erupted in the field area. Minor mafic flows are also erupted during Stage 2, likely sourced just east of the field area. Stage 3 spans the inception and majority of extensional faulting and consists of mafic volcanism and sedimentation in subsiding half-grabens. Stage 4 volcanism occurred as extensional faulting waned and volcanic units erupted during this stage were channelized in fault bounded valleys. Volcanic activity during this stage includes deposition of the Peach Springs Tuff (sourced from the Silver Creek Caldera in the Northern CREC; Ferguson, 2008) and localized mafic volcanism. Stage 4 is the longest of the five stages, but also accounts for the lowest locally erupted volume.

Before describing the character of volcanic activity and nature of volcanic deposits of each of these 4 stages, the absence of certain common volcanic features in the field area should be noted. Nowhere in the volcanic succession do we observe thick accumulations of thinly to medium bedded pyroclastic and volcaniclastic material interbedded with lava, as is characteristic, for example, of composite cones (stratovolcanoes). The vast majority of volcanic successions are dominated by lava flows, with only minor pyroclastic fall and surge deposits and reworked tuffaceous sediment that are closely related to the lavas. Also, no other diagnostic features of caldera collapse are observed such as thick intracaldera fill

sections of welded tuff, overlaps, deposits and ring faults. The only welded pyroclastic deposit in the field area is the Peach Springs Tuff which is sourced from outside the field area.

Stage 1 (21-20 Ma) – Mafic effusive volcanism

Though stage 1 volcanic rocks within the field area were too altered to date, this earliest stage of basaltic andesite eruptions began at 21 Ma continued until ~20 Ma, based on dating of virtually identical sucessions that occupy the base of the volcanic section in the Aubrey Hills (just east of the Whipple Mountains and Colorado River) and the Turtle Mountains (west of the Mopah Range). During this time, primarily basaltic andesite and minor basalt lavas (Tttba, $Tocb_1$, Tmu) erupted to form a stack of 50 ± 10 lava flows in the field area. Individual flows generally have rubbly, oxidized tops and bases and massive interiors, characteristics which suggest the majority of these lavas were emplaced as a'a flows. Individual pahoehoe flows are difficult to recognize in outcrops of ancient volcanic rocks, particularly in the heavily altered and highly faulted exposures of the western Whipple Mountains, but are likely present. Up to 20 m thick horizons of lava with no discernible internal structure are present, and these may have been emplaced as stacked and/or inflated pahoehoe flows. No pyroclastic material is observed in the Stage 1 lava sequence in the field area and there is little evidence for sedimentation between flows suggesting rapid emplacement and/or low topographic relief. Our observations are consistent with the lavas having been erupted from either a low shield vent edifice or from Icelandic-type fissure systems (eg. Pálmason, 1981; Thordarson and Höskuldsson, 2008).

Though the lateral continuity of Stage 1 lavas was impossible to assess directly in the field area due to poor exposure and colluvial cover, in the Aubrey Hills similar flows can be

traced laterally for at least 1 km confidently, and the exposure of the entire unit extends laterally for several kilometers. Based on this information, Tmu lavas may have run out distances on the scale of at least a few kilometres in the field area. The presence of mafic accumulations in the Mohave Mountains, Standard Wash, and Aubrey Hills to the east, and in the Turtle Mountains to the west that are nearly identical to the Stage 1 lavas of the western Whipple Mountains suggests that either run out distances were much greater, on the scale of several 10's of kilometers, or that Stage 1 vents were broadly distributed across the CREC at this time, or both. Dikes of similar composition and age are present in the Chamber's Well dike swarm (Gans and Gentry, 2016), and some of these may represent vents for the Stage 1 lavas in the study area.

Stage 2 (20-19.5 Ma) – Silicic dome and flow growth

An abundance of $^{40}Ar/^{39}Ar$ ages (Table 1) indicate that Stage 2 volcanism began at approximately 20 Ma and continued until about 19.5 Ma. This stage is dominated by eruption of dacite and rhyolite lavas ($Thbr_1$, Tpd, Tbhr, Thpd, $Thbr_2$) with minor input of mafic lavas ($Tocb_2$, Taa) in the later part of the period. Though analytical errors overlap for many $^{40}Ar/^{39}Ar$ ages for Stage 2 lavas, our geochronology work suggests that there may have been two distinct pulses of silicic volcanism during Stage 2, one occurring mainly between 20.1 and 19.9 Ma (erupting $Thbr_1$, Tpd, Tbhr, and Thpd and referred to below as Stage 2a) and the other occurring from about 19.6 to 19.4 Ma (erupting $Thbr_1$, $Thbr_2$, $Tocb_2$, and Taa and referred to below as Stage 2b) (Fig. 11).

All of the rhyolite and dacite lavas erupted during Stage 2 form tabular lava flows, and several also form lava domes. Each unit was emplaced as one or more lava flows that spread radially from a central vent to form tabular sheets 100-500 m thick and at least

several km^2 in area (Fig. 10). These flows likely grew endogenously, inflating and advancing in response to the magma supply from the conduit. This endogenous growth likely accounts for color banding on the scale of tens to hundreds of meters observed in some of the more highly altered units, best discernible in $Thbr_1$ exposures in the western Whipple Mountains (Fig. 7). The fact that these flows remained dispersed rather than channelized as they advanced laterally suggests that these flows were erupted onto a low relief surface (as would be expected after the fissure and/or shield eruptions of Stage 1). Run out distances for flows within the field area range from just under a kilometer to at least 7 km.

The lithologic zonations of the silicic flows of the eastern Mopah Range and western Whipple Mountains are similar to other thick rhyolite effusions elsewhere (Christiansen and Lipman, 1966; Bonnichsen and Kauffman, 1987; Duffield et al., 1995, Hildreth et al, 1999). In the best preserved flows, a devitrified felsite interior is surrounded above and below by a dense glassy vitrophyric envelope. Blocky and pumiceous primary surfaces typical of silicic lava flows (Fink et al, 1983) are not well preserved, but thin (1-5 m) glassy basal breccias are commonly observed. Evidently, these lavas advanced as blocky pumiceous flows from their source vents, with collapsed material from the flow fronts overridden by advancing flow cores much like a tractor tread.

Internal flow foliation (the product of lamellar flow within the moving liquid) is ubiquitous in all silicic units and most outcrops have platy partings along the foliation. Flow banding is defined in these rocks primarily by color, but also by differences in microlite content and alignment of platy phenocrysts. The foliation is typically subparallel to the base of flows, though on a local scale it is not uncommon for it to be inclined, contorted, or folded. While most units display an average foliation that nearly approximates paleo-horizontal (based on similarity to bedding in adjacent tuffaceous sediment), in one relatively

thick exposure of $Thbr_1$ in the western Whipple Mountains, a ~0.25 km^2 expanse of foliated lava restores to a steep dip which may represent paleo-vertical (Fig. 12). Duffield et al. (1995) concluded from his study of the Taylor Creek Rhyolite in New Mexico that the first order foliation within a dome reflects the overriding load on the viscous magma body. They observe that foliation at the base of a dome is relatively flat where the lava spreads under considerable load, and ramps steeply upwards in the upper portions of domes towards the unloaded free surface. Using this logic, the steep original foliation observed likely represents vertical movement of lava in the core of a dome, and thus this area is identified as the likely vent for most of the $Thbr_1$ exposures in the western Whipple Mountains.

The aforementioned vent is the best exposed of its kind in the steeply tilted silicic lava sequences of Stage 2a, and from its geometry, we infer the nature of the vent edifices for all the Stage 2a lavas, though vents for the other units are not readily apparent in the field area. The reconstructed thickness of this flow in the vent area (~900 m) is much greater than the distal effusive flow suggesting that this lava dome complex had an original topographic relief of >500 m. Three dimensional exposure is not adequate to determine whether the vents for the Stage 2a lavas were equant or elongate. Stage 2b rhyolites ($Thbr_2$) form several domes in the eastern Mopah Range that are more easily recognizable. These lavas, being less deeply buried, generally less altered, and in some places less tilted, often display a more evident original morphology. A large dome edifice in the Mopah Range 1.5 km east of Hwy 95 is flanked by pyroclastic deposits (mapped as Tts) which were likely overridden by and adjacent to the growing dome. The original topographic relief of the dome is impossible to assess in the tilted block, as the laterally adjacent lava flows are buried beneath alluvium, but the minimum thickness of the dome complex is 500 m. A few exposures of $Thbr_2$ on the western edge of the field area in the interior of the Mopah Range are also candidate domes.

The largest and most striking domes in the Mopah Range are the towering Mopah peaks located west of the study area in the central Mopah Range and described in detail by Hazlett (1986).

There is only minor pyroclastic material associated with the Stage 2a lava flows and domes. Pyroclastic material associated with these lava flows and domes exist primarily as thin lenses (<20 m thick) separating lava flows, many of which are smaller than map scale. Stage 2b lavas however are intimately associated with thick pyroclastic horizons (up to 400 m thick). These deposits are typically moderately to poorly stratified fall, surge, and small unwelded pyroclastic flow deposits. Tabular $Thbr_2$ lava flows override the thickest of these deposits in the interior of the Mopah Range and the western Whipple Mountains, while $Thbr_2$ domes are generally flanked by pyroclastic aprons. This difference between the abundance of pyroclastic material in Stages 2a and 2b could simply reflect a preservation problem for the older lavas, or could suggest that explosive eruptions were not tied to dome growth during Stage 2a as they were in stage 2b. Stage 2a lavas could have had lower volatile contents (likely for Tpd lavas which bear anhydrous phenocrysts) or slower magma ascent rate favoring slower degassing.

Stage 3 (19.5-18.8 Ma) – syn-faulting mafic flow fields

The character of volcanism changed abruptly from silicic to mafic eruptions (Tocba) as normal faulting and extensional block rotation began to rip the region apart. We have good age constraints on the start of this volcanic stage (19.5 Ma) and not its end, so we can only speculate on the duration of mafic volcanism. With the exception of the largely untilted portions of the Mopah range in the northwest corner of the field area, most exposures of Tocba and the underlying Tc lie in angular unconformity above the steeply tilted Stage 2

volcanic units and display moderate dips. At 18.8 Ma, the Peach Springs Tuff was deposited in the Western Whipple Mountains as a subhorizontal sheet indicating that block rotation across this part of the corridor had largely stopped by this time.

Local eruptive activity during this stage was limited to the Mopah Range and consisted primarily of basaltic andesite eruptions. Basaltic andesites were erupted into actively subsiding half-graben basins, evidenced by fanning dips and their interleaved relationship with polymict alluvial conglomerates which also display fanning dips (Cross section A, Fig. 13). In at least one location, Tocba lavas completely filled their accommodation space in one valley and spilled over the scarp of an inactive fault and into the adjacent valley (Fig. 13).

Stage 3 basaltic andesite lava flows consistently display rubbly glassy flow tops and bases and massive coarser-grained interiors, features characteristic of a'a flows. Flow foliations are often defined by flattened vesicles, and less often by platy partings. Flow foliations in the lower half of the massive interior of flows generally are subparallel to the flow base. Although slopes covered in talus make it difficult to confidently trace individual lava flows laterally along ridges in the field area, exposures of Tocba extend continuously for >4 km. These lava flows had runout distances of up to 3-5 km or more. Individual flow thicknesses range from 10 to 20 m thick.

Red oxidized scoria is locally observed at the base of flows; a good example occurs near the collection site for MP-18. Such oxidized scoria deposits are interpreted to represent near vent tephra facies. Though no direct evidence for cinder cones is preserved in the field area, the presence of scattered scoria deposits suggests that these lava flows were sourced from cinder cone vents. Cinder cones are easily eroded and thus unusually persevered in the geologic record. Hazlett (1986) however observed the eroded remains of a cinder cone in

this unit that was partially buried by an overriding lava flow in the northwest of the field area in the Mopah Range.

Stage 4 (18.8-16 Ma) – PST and small volume localized mafic eruptions

The fourth and last volcanic stage, though the longest in duration, produced the smallest volume of locally derived eruptive products. During stage 4, extensional block rotation has nearly finished and volcanic units deposited during this time remain shallowly dipping (<10°) to approximately flat lying. This stage began with the emplacement of the Peach Springs Tuff (Tpst) at 18.8 Ma which was channelized in a fault bounded paleo-valley (Fig. 10). The Peach Spring Tuff is moderately to lightly welded in the field area, and a significant percentage to the tuff has undoubtedly been lost to erosion since its deposition.

Local eruptions of basalt (Tob) followed shortly thereafter in the northernmost Whipple Mountains. These basalts exist only in the northerly extent of the western Whipple Mountains and directly overly Peach Springs Tuff.

One small eruption of andesite occurred at 18.3 Ma and then there was a gap in time until a series of andesite lavas was erupted at Pyramid Butte between ~16.5 and 16.3 Ma (Fig. 11). These lavas display the characteristic rubbly oxidized flow tops and bases and massive interiors of a'a flows. At least 5 flows can be observed on Pyramid Butte. These along with abundant tephra and scoria suggesting the vent for these lavas was here. Current exposure suggests these flows were elongate (confined to paleo-valleys) and that lavas had runout distances of at least 2.5 km.

3. Volume estimates and sources of uncertainty

Exposures of volcanic rocks in the Western Whipple Mountains and Mopah Range represent only a fraction of the original extent of the Miocene volcanic field in this area. Volcanic rocks likely covered most of the exposed crystalline bedrock and large areas of volcanic rocks are likely buried by alluvium beneath the Chemehuevi and Vidal Valleys. Hazlett (1986) used scattered inselbergs around the Mopah, Stepladder, and Western Whipple Mountains to estimate that more than 50% of the Miocene volcanic rocks erupted may be buried by Quaternary cover (Fig. 9). The exposures in the field area lie fully within the larger, partially buried area postulated by Hazlett, and the presence of inselbergs both at the northern and southern edges of the field area suggest that all Quaternary cover in the mapped area is underlain by the same volcanic rocks that crop out in the western Whipple Mountains and eastern Mopah Range.

Considering this, we present in Table 2 both minimum volumes (based only on outcrop exposures) and realistic volumes (taking into account where volcanic units likely exist beneath alluvium in the field area and where significant material has likely been lost to erosion) for lavas of each volcanic stage. The realistic volume estimates are our favored values, despite high uncertainties, are useful as a first order approximation of Miocene volcanic output. In the sections below we discuss our methods for calculating volumes for each volcanic stage, sources of uncertainty, and the effects of various interpretations on realistic volume estimates.

Methods and sources of uncertainty

All volumes are calculated by first dividing the exposure area into regions of similar average thickness of rocks for each volcanic stage (Fig. 14). The volume of the targeted

volcanic stage is calculated for each of these regions by multiplying the average thickness by the approximated original surface area of the unit within each region. Volumes of these individual regions are then summed to determine the total volume of that volcanic stage within the study area.

For volcanic units in stages 1, 2, and 4, the original surface areas are assumed to be elliptical, with radii equal to the along strike exposure length (measured directly on map) and the interpreted down dip length of the unit (measured directly on cross sections). Original surface areas of units between fault bounded blocks are assumed to be rectangular where appropriate. For Stage 3 units interpreted as fault growth strata, the wedge shaped geometry of the units is taken into account.

Owing to erosion, interpretive cross section reconstruction, and Quaternary alluvial cover, uncertainty is great for most units, resulting in a huge difference between the minimum and realistic volume estimates for many of the volcanic stages (Fig. 14). Minimum volume estimates are calculated using along strike lengths only of exposed rocks, ignoring necessary corrections for erosion and alluvial cover, and should be considered a bare minimum value that surely underrepresents the actual erupted volume. The realistic volume estimates include corrections for alluvial cover and loss due to erosion. These corrections result in large uncertainties for realistic volume estimates, but we believe the resulting calculated volumes are much closer to the actual erupted volumes than our bare minimum estimates. The methodology used to make these corrections as well as some major sources of uncertainty are illustrated in Figure 14 and discussed in greater detail in Appendix III.

Volume estimates

Stage 1: Based on the thickness and along strike length of exposures in the western Whipple mountains and extrapolation of the unit in Cross Section B, a minimum of 4 km^3 of Stage 1 lavas are estimated to have erupted within the field area. If the Stage 1 lavas also underlie the Stage 2 lavas in the Mopah Range with a similar thickness (Cross section A), the total volume erupted in the field area could be as much as 5 or 6 times greater than this figure. Our realistic estimate assuming this is true is ~25 km^3.

Stage 2: Stage 2 erupted by far the greatest volume of lava than any other stage of volcanism. Assuming these units underlie most of the alluvium in the field area, we calculate a realistic estimate of ~56 km^3 (~39 km^3 during stage 2a and ~17 km^3 during Stage 2b).

Stage 3: A bare minimum of 6 km of Tocba lavas were erupted in the field area, but due to loss of volume due to erosion, believe that 7.5 km^3 is likely a more realistic erupted volume. This volume estimate was calculated assuming a wedge shaped geometry for the Stage 3 lavas in the eastern ridges of the Mopah Rage which are interpreted to have been erupted in actively subsiding half grabens (Fig. 13; Cross-Section A).

Stage 4: We estimate a realistic volume of ~0.45 km^3 of lava was erupted locally during Stage 4 (~0.41 km^3 of andesite, most of which was erupted at pyramid butte, and only ~0.04 km^3 of basalt erupted in the northwest Whipple Mountains).

G. Structural Geology

1. Overview

This region consists of steeply SW tilted imbricate faults blocks composed of Pre-Tertiary basement overlain by Stage 1 and 2 volcanics. These steeply tilted blocks are separated by gently northeast dipping normal faults and are unconformably overlain by

younger Stage 3 and 4 sedimentary and volcanic units. Individual volcanic units generally strike WNW and dip to the SW, such that stratigraphically younger units in a conformable section appear successively toward the southwest. Normal faults of four different ages exist in the field area, each responsible for some of the total tilting experienced by Tertiary units (Fig. 15). The degree of tilting decreases from the central and eastern parts of the field area (structural domain I) towards the interior of the Mopah Range on the western edge of the field area (structural domain II).

Our interpretation of structures in the field area differs somewhat from the mapping of Carr et al. (1980), Hazlett (1986), and Yin and Dunn (1992). One major difference between our mapping and Yin and Dunn's (1992) is that we do not recognize the existence of the WDF in the field area (discussed in more detail below). We recognize many of the same major structures as those mapped by Carr et al. and Hazlett, but these authors map considerably more small scale faults than we find evidence for. Some of the discrepancies between our interpretations likely stem ultimately from disagreement on interpreting primary volcanic features.

2. Orientation of units

Orientations were collected on flow foliations of volcanic units and bedding of sedimentary units throughout the field area. Flow banding is defined in silicic lavas by color banding and flow alignment of phenocrysts, and rocks often develop partings along the foliation which could be directly measured. In mafic lavas, flow foliation was sometimes expressed as platy partings in the interior of lava flows, and sometimes as a vesicle flattening foliation. In all types of volcanic rock, flow foliations can be quite chaotic, and surfaces were chosen that were a good representation of most of the foliation in a given outcrop.

Nevertheless, flow foliations are often poor indicators of paleohorizontal, particularly in silicic lava flows and domes, and our orientations should be viewed as only giving an "average" attitude at best. Sedimentary strata within the volcanic succession provide more direct proxies for paleohorizontal. Though some sedimentary beds were likely originally deposited horizontally, many, particularly those interleaved with Stage 1 and 2 silicic lavas represent pyroclastic apron deposits and were likely emplaced with steep original dips. Such deposits can also be easily modified and deformed by later lava emplacement as well. As such, no one measurement alone is ever taken to represent the original orientation of a flow, but rather the average of many orientations across a wide area gives an estimate of paleohorizontal. Despite the complexity of possible original dips for both flow foliation and bedding, there is a remarkable overall consistency in the data and strong agreement between stratified epiclastic deposits and flow banding in lavas (Fig. 12).

Structural domains I and II are divided based on differences in average dip of Stage 2 and 3 lavas. Domain I includes all of the western Whipple Mountains and the easternmost extent of the Mopah Range, while Domain II includes the topographically higher interior of the Mopah Range on the western side of the field area (Fig. 15). Below, we describe the orientation of units in each of these two domains. Because the low relief and exceedingly rare and poor exposure of fault surfaces makes a structural analysis based on fault lineations impossible, orientations of units and strike of faults provide the only reliable constraints on how extension direction varies through time within the field area.

Domain I:

Stage 1 lavas outcrop only in Domain I, and have an average strike of 128° and dip of 76°. Stage 2a and 2b lavas are homoclinal in Domain I (Fig. 12) with average strike and

dip to be 122° and 60° respectively, based on averaging the mean vector of bedding orientations and the center of the densest cluster of foliation measurements (mean vector of foliations does not approximate paleohorizontal because some foliation data collected from the cores of lava domes likely represent something closer to paleovertical, throwing off the mean of the data set. See Fig. 12). The variation between the average orientation of Stage 1 and 2 lavas may be explained in a few different ways. First, it is important to note that Stage 1 lavas display less well developed flow foliations than Stage 2 lavas, and also contain few interbedded sedimentary horizons. Stage 1 lavas also cover a much smaller areal extent than Stage 2 lavas, and are exposed only in the far eastern side of the field area in the Whipple Mountains. Because of this, few orientation data for Stage 1 (n=11) were collected relative to Stage 2 (n-498).

It is possible that the ~16° difference of average dip between Stage 1 and Stage 2 lava represents differential tilting between the two volcanic stages, implying that extensional normal faulting and block rotation began before Stage 2 volcanism (between ~20.6-20 Ma). However, because of the small number of Stage 1 orientations and limited exposure, the variation is not statistically significant. The similar orientations of 2a and 2b units preclude growth faulting during their deposition, so the steeper dips of Stage 1 are unlikely to represent the steepest units in a longer episode of growth faulting. It is also possible that the few locations where Stage 1 orientations were discernable actually reflect variation in the degree of tilting across different fault blocks in Domain I.

The orientations of Stage 3 sedimentary rocks and lavas in Domain I are different than the older lavas they overlie (Fig. 12). The most remarkable characteristic of the Stage 3 accumulations is that they display fanning dips up section, ranging in some exposures from 67° to 14° dip from base to top (Figs. 12, 13). Our interpretation for up-section shallowing

dips of Tc and Tocba in the Mopah Range is that they were deposited in at least one actively subsiding half-graben basin. Fault A (Figs. 15, 13) is one fault that accommodated accumulation of growth strata, and was subsequently buried when accommodation space in the subsiding basin was filled and Tocba lavas overtopped the fault scarp, spilling over the footwall block. The average strike of Stage 3 units is ~152° (about 30° from the ~122° average strike of Stage 1 and 2 units)

Stage 4 lavas, which occur only in Domain I are largely untilted. The only discernably tilted Stage 4 units are exposed in the NE corner of the mapped area, where Tpst and Tob are cut by a few small offset faults, resulting in local tilting of ~8° (the 4 bedding measurements in Fig. 15 are from this location). All other exposures of Stage 4 volcanics show no evidence of tilting, and together have a horizontal average orientation.

Domain II:

All units in Domain II are considerably less tilted than their counterparts in Domain I. In addition to this another difference between Domains I and II is that in Domain II, 2a and 2b lavas are not homoclinal as they are in Domain I. Here 2b lavas lie in ~20° angular unconformity above older 2a lavas (Fig. 12). The average strike and dip of 2a lavas and sedimentary rocks is 144° and 30° respectively, while the average of 2b lavas and pyroclastic rocks is strikes 125 and dips only 9°. Though the mean vectors of these relatively small data sets overlap, field observations confirm that this difference is real (Fig. 3C). This implies that some faulting and tilting event occurred between the eruption of 2a and 2b volcanics (between 19.6-19.5 Ma) in the interior of the Mopah Range, slightly before the inception of tilting just to the east.

The average orientation of Stage 3 lavas in Domain II is horizontal. This suggests that the normal faulting which resulted in tilting of Stage 3 lavas in Domain I was limited to the eastern 2/3 of the field area and did not affect the interior of the Mopah Range. Tilting of the Mopah interior had largely ceased by 19.5 Ma.

3. Fault geometry and ages

Based on cross cutting relations and inferred or measured dips of faults (where shallow faults are interpreted to be older), the major mapped faults are grouped into 4 age groups, I-IV (Fig. 15). Few of the major faults are exposed, and due to the low topography across most of the field area, constraints on dip direction and dip amount are weak. Where fault measurements were taken, many were collected on calcified ledges that appear to be representative of the fault plane, but which do not preserve slickenlines or polish. The actual relation of these calcified ledges to the fault planes is uncertain. The oldest faults (particularly Group II) are in most places buried by either younger units or alluvium.

As such, the dip direction of most faults is inferred by the sense of offset of displaced units assuming a normal fault geometry. We assume that all faults had an original dip of ~60°, and work backwards using tilts of volcanic and sedimentary units to estimate their current dips. Because fault lineation data is so scarce (and non-existent for the many of most important faults) we do not have solid constraints on the orientation of the rotation axes for fault blocks, and assume that it occurred around an axis close to parallel to fault strike.

Group I:

The oldest faults in the field area (Faults B and C, Fig. 15) dip to the SW and displace the Tertiary section against pre-Tertiary basement rocks. Fault B dips shallowly

(~10° SW), with a sinuous trace that wraps shallow hills and gullies, while Fault C dips more steeply (~50°SW). These faults are interpreted to be the oldest in the field area for three main reasons. First, Fault B (Fig. 15) is cut by a younger structure from Group III, and secondly, the faults dip to the SW while all other younger faults dip NE. Our interpretation is that the Group I faults originally dipped to the NE, but have since been passively rotated through horizontal to their current orientations via tilting incurred during slip on younger faults. The total displacement along the Group I faults is impossible to calculate because the same units do not appear in both the exposed hanging wall and footwall of these faults. Everywhere these faults are exposed, the footwall is composed entirely of basement, and the hanging wall is composed entirely of Tertiary strata. From cross section reconstructions, a minimum bound of 500 m can be placed on normal sense displacement, but the total slip on these faults is likely much greater.

Group II:

Group II faults are enigmatic in the field area, as most are covered by younger Stage 3 and 4 strata. In these cases, the basis for recognizing them is repetition of the older Stage 1 and 2 units, the presence of Stage 3 growth strata, and the presence of linear belts of Stage 4 volcanics which were channelized in Group II fault bounded basins. Due to the common burial of these faults, and the poor exposure in places where the faults do intersect the surface, there are virtually no solid constraints on the dip of these faults. Based on the dip of repeated strata across them, and taking into account a portion of that tilting that was incurred during slip on Group 1 faults, Group II faults are interpreted to dip ~15-20° to the NE. Cross section reconstruction in the western Whipple Mountains indicated that these faults accommodate between 450 and 950 m of slip.

Group III:

Group III faults are the best exposed and most strikingly obvious faults in the field area. These faults cut the Stage 3 lavas in the Mopah range, repeating them in several NW-SE trending elongate ridges and also repeat Stage 2 units across the field area. Group III faults are estimated to dip ~40-45° to the NE, based on 15-20° SW tilts of the youngest Stage 3 (Tocba) lavas. Most of the major through-going Group III faults are unexposed and their locations where they cut Stage 2 lavas are approximated, particularly in the Mopah Range where Tpd lavas occupy both the hanging wall and footwall of faults. In the western Whipple Mountains and the SW corner of the mapped area in the Mopah Range, Group 3 faults display complex branching relationships and fault bounded lenses up to a kilometer in length. The longest faults extend for at least 10 km.

Group IV:

The youngest faults observed in the field area are located only on the northern edge of the field area in the Whipple Mountains where they cut Stage 4 units (Tob and Tpst). These are small offset normal and strike-slip faults (a few tens of meters), dipping 75-55° to the NE. Three closely spaced faults (~13 m spacing) are identified in this group, two of which branch from a single fault surface. These faults are responsible for at most 5-8° of local tilting of Stage 4 units. The lateral continuity of these faults is unconstrained, but they likely do not extend farther than a few kilometers.

H. Discussion

Tilting history:

The tilting history of Domain II is fairly straightforward. This area experienced ~20° of tilting in ~0.1 m.y. between the eruption of Stage 2a and 2b lavas (~19.6-19.5 Ma). An additional 5-10° of tilting then occurred sometime with a 0.16 Ma window between eruption of Stage 2b and Stage 3 lavas (whose ages overlap in uncertainty by about 0.16 Ma).

The tilting history of Domain I is a little more complicated. ~16° of tilting may have begun as early as 20.6 Ma between the eruption of Stage 1 and Stage 2 lavas. However, as discussed above, the evidence for this is low quality and may be an artifact of the dearth of orientation data available for Stage 1 units. Further, no structures that could have accommodated this tilting have been identified in the field area (no major faults cut only Stage 1 and not Stage 2 units). The first unquestionable evidence for block rotation is the Stage 3 growth strata which overlies tilted Stage 2 units and documents as much as 50° of tilting in some fault blocks, and an average of ~40° of tilting across the field area. This large degree of tilting was likely accommodated by two generations of normal faulting. Fault groups I and II, poorly exposed in the field area and commonly buried by Stage 3 and 4 units, are likely the structures responsible for this episode of tilting. $^{40}Ar/^{39}Ar$ ages from $Thbr_2$ and Tocba lavas which predate and postdate (respectively) this episode of extensional tilting overlap in uncertainty by 0.16 Ma (Fig. 13). This requires that 40-50° of extensional block rotation in the field area must have occurred within at most 160,000 years.

Subsequently, a final ~15-20° of tilting was accommodated by the Group III faults, which cut the Stage 3 units and are responsible for the dip of the youngest Tocba lavas in Domain I. Geochronologic constraints from Stage 3 (Tocba) and Stage 4 (Tpst) units require that this degree of tilting must have occurred within ~700,000 years (between 19.55 and 18.8 Ma).

The tilting history observed in the western Whipple Mountains and Mopah Range is not representative of the whole CREC. For example, the Peach Springs Tuff, though approximately flat lying in the study area, is steeply tilted in exposures on the eastern side of the Whipple Mountains (Howard et al., 1999), suggesting that tilting either started and finished earlier on the western side of the CREC or that it continued for a longer duration on the corridor's eastern side. Comparative discussion of the timing of extensional tilting across the CREC is beyond the scope of this study, but the tight constraints on the tilting history of the study area is an important contribution to future studies on the spatial and temporal variations in extensional block rotation across the CREC.

No place for Whipple Detachment Fault in the study area:

All workers in the Western Whipple Mountains agree that the WDF is unambiguously exposed along the base of Savahia Peak, however there has been disagreement on whether some or all of the faults separating pre-Tertiary basement from Tertiary rocks to the west of these exposures represent the same WDF surface. Yin and Dunn (1992) take interpretations of the WDF farthest. They interpret all basement-Tertiary fault contacts (Faults, B, C, and D) as exposures of a single undulating WDF surface that forms an anticlinal bulge between faults B and D and a synclinal scoop underlying all the tilted volcanic units between faults D and C. Carr et al. (1980) maps the southern continuation of Fault C as a single structure that continues toward Savahia Peak, but does not explicitly map it as the WDF. Gans and Gentry (2016), likewise do not interpret this structure to be the WDF where they map its southwestern continuation.

Our interpretation aligns closer with the mapping of Carr et al. (1980) and Gans and Gentry (2016), that none of the basement-Tertiary fault contacts are exposures of the

Whipple Detachment fault. Yin and Dunn's (1992) interpretation of a synformal WDF underlying Tertiary strata in the northwest Whipple Mountains does not adequately explain the homoclinal nature of the Stage 1 and 2 lavas in this section, which should also display deflected dips in they were also warped above an underlying WDF. Additionally, along the trace of Fault C, many small Tertiary intrusions intrude across the fault. Assuming these intrusions are related to some of the younger Tertiary volcanics in the field area, this supports Fault C being an older, passively rotated structure rather than a younger detachment surface. Our mapping is consistent with the interpretation of Gans and Gentry (2016) that the WDF, last observed at Savahia Peak, never existed this far west, and instead projects above the field area. By this interpretation, the western Whipple Mountains and Mopah Range lie in the footwall, rather than the hanging wall of the WDF.

Apparent extension direction and fault geometry in the field area:

The difference in strike between Stage 1-2 and Stage 3 units in Domain I is strikingly obvious. The average strike of Stage 1 and 2 units seems to suggest an extension direction of ~N35E, while those of Stage 3 units suggest an extension direction of ~N55E. In Domain II, the average strike of Stage 2 units also suggests an extension direction of ~N55E. This difference between the strike of older and younger volcanic units in Domain I could be explained by either a time progressive shift in the regional extension direction (that only effects Domain I), by a spatial variation in local extension direction across the field area from west to east, or by vertical axis rotations of some blocks. Because Stage 3 units are only present in the western half of the study area, it is difficult to discern whether this variation in extension direction varies spatially or temporally from strike of units alone, however the strike of faults across the field area shed additional light on the matter.

Faults across the field area of all age groups (with the exception of Fault C) appear to shift from W to E from a NNW-SSE strike to a WNW-ESE strike (Fig. 15). Additionally, some faults (particularly those in the western half of Domain I in the eastern Mopah Range) are more closely spaced to the NW and more widely spaced in the SE, resulting in a wedge shaped geometry of the intervening block. Such a geometry suggests these normal faults formed a splay of scissor faults, with greater displacement along each fault to the SE. This scenario could explain the variable strike of units from W to E, with the coincidental exposure only making it appear to be a time dependent variation. That this fanning in strike is recognized across faults of all ages, is further evidence that there was no abrupt change in the regional extension direction in the short interval between eruption of Stage 2 and Stage 3 units in the field area.

Modern analogues for volcanic stages:

Our observations suggest that the thick accumulations of Stage 1 lavas were erupted from distributed fissure vents and/or low shields. Modern analogues for this volcanism include the flood lava eruptions of Iceland (eg. Pálmason, 1981; Thordarson and Höskuldsson, 2008) or the Eastern Snake River Plain (ESRP) of the NW United States (eg. Greeley and King, 1977; Greeley, 1982). Icelandic basaltic eruptions are thought to be produced by sometimes long lived (months to decades) eruptions which produce vast flow fields with runout distances of a few 10's of kilometers and volumes approaching 20 km^3 (Thordarson and Höskuldsson, 2008). They are characterized by both relatively low-discharge (≤300 m^3/s) central vents and high-discharge (may be >1000 m^3/s) fissure eruptions. Low discharge eruptions from central vents form low shield edifices often with 3-10° sloping summit craters and 0.5-2° sloping lava aprons, while higher discharge fissure

eruptions take place on linear vent (often 10's of km long) systems demarked by rows of tightly packed cratered cones along multiple en echelon fissures. ESRP basaltic "plains-style volcanism" (Greeley and King, 1977; Greeley, 1982) is another good modern analogue for Stage 1 volcanism in the CREC. This volcanics style is typified primarily by coalesced low-profile monogenetic basaltic shields which produce a composite surface with subdued topography and shallow depositional slopes, and subordinate fissure eruptions. Unlike some of the longer lived Icelandic shield eruptions, the shields of the ESRP are formed by short-lived low-volume eruptions, affording little significant growth above the surrounding topographic surface (Hughes et al., 1999).

There are no good modern analogues for Stage 2 volcanism in the study area. No presently active volcanic fields that are not associated with a caldera exhibit the abundance of coalesced rhyolite and dacite lava domes and long-runout tabular flows observed in the western Whipple Mountains and Mopah Range. A few analogues for this volcanism are found in the ancient rock record and include the Miocene rhyolite lavas of the Bruneau-Jarbidge area of the Snake River Plain, Idaho (Bonnichsen and Kauffman, 1987), the Miocene Taylor Creek Rhyolite of Mogollon-Datil volcanic field, SW New Mexico (Duffield et al., 1995), and the Pleistocene rhyolite lava flows of the Puelche Volcanic Field, central Chilean Andes (Hildreth et al, 1999). All of these analogues are typified by overlapping domes and tabular sheets of fluid rhyolite lava, erupted from either fissures of point sources, similar to the observed geometries of the western Whipple Mountains and Mopah Range rhyolites and dacites. From their investigation of Snake River Plain rhyolites, Bonnichsen and Kauffman (1987) conclude that such eruptive styles and lava flow geometries results from a combination of high effusion rates, high temperatures, and large

volumes which impart a sufficiently low bulk viscosity to the lavas, allowing them to flow away from their vents forming sheets instead of steep sided domes.

Stage 3 and 4 volcanism in the study area display similar eruptive styles. Good modern analogues for Stage 3 and 4 volcanism are the basaltic volcanics fields of the Mojave Desert in SE California, including Cima (Wells et al., 1985) and Pisgah (Wise, 1966; Arvidson et al., 1993). These volcanics fields consist of cinder cones and associated lava flows 1-9 km in length. Lava flows are both equant and elongate and vents are occur in scattered clusters. These volcanic fields exhibit low recurrence intervals of eruptive activity, much like the Stage 3 and 4 lavas of the western Whipple Mountains and eastern Mopah Range.

Extent of Mopah-Western Whipple silicic lava dome and flow field:

Within the boundary of the study area, Stage 2 volcanism is dominated by rhyolite and dacite eruptions. It should be noted however, that this is the case only within the study area and to the west in the Mopah Range. Minor mafic and intermediate lavas ($Tocb_2$, Taa) that are intercalated with Stage 2b lavas in the mapped areas of the western Whipple Mountains thicken eastwards, and are interpreted to be sourced to the east at the same time that rhyolites were erupting in the study area. Correlative volcanic exposures in the southwest Whipple Mountains and Savahia Peak (directly east of the study area) are dominated by mafic and intermediate sections, with only minor silicic units. The preponderance of silicic and dearth of mafic eruptions in the study area and in the Mopah Range appears to be characteristic only of the far eastern side of the Miocene volcanic field.

Implications of volcanic volume estimates:

The minimum and liberal volume estimates for each volcanic stage are summarized in Figure 16. We estimate the minimum cumulative volume of Miocene volcanics erupted in the field area to be ~38 km^3, but believe our liberal cumulative volume estimate (considering alluvial cover) of ~90 km^3 is a more realistic figure. This cumulative volume estimate is only of volcanic units exposed in the confines of the study area, which is only a fraction of the total exposed Miocene volcanic rocks at this latitude of the CREC. As such, these estimates are of limited importance on their own, but they could be used to inform an estimation of the total volume of volcanic rock exposed across this part of the CREC.

By making the fairly sweeping assumption that other areas of steeply tilted volcanic rocks contain roughly the same volume per unit area as the western Whipple Mountains and eastern Mopah Range, we can speculate as to the total volume erupted in this part of the CREC. If the volcanic surface exposure in the map area (~140 km^2) corresponds to our liberal volume estimate (90 km^3), we can use a 0.64 area to volume ratio to speculate that the 760 km^2 of Miocene volcanic surface exposure in this part of the CREC may represent ~486 km^3 or more of eruptive products. The total volcanic surface exposure used in this calculation is estimated from the mapping of several authors of the Mopah Range (Hazlett, 1986), the Turtle Mountains (Stone, Paul, and Howard, 1979) the southwestern Whipple Mountains near and including Savahia Peak (Carr et al., 1980), the southern Whipple Mountains (Dickey et al., 1980), The Chemehuevi Mountains (John, 1987) the Aubrey Hills, Standard Wash, and Mohave Mountains (Howard et al., 1999), the Castaneda Hills (Lucchitta and Suneson, 1994a; 1994b), and this study. This total volume should be regarded as a rough estimate, but it does serve to give a better sense of the importance of this volcanic terrane.

Volcanic rates vs. extension rates:

The volume of volcanic products erupted in the study area varies significantly with time (Fig. 16). By dividing the minimum and liberal eruptive volume estimate for each volcanic stage by its duration, we estimate eruptive rates for each stage. These rates are should be interpreted as approximations for the purpose of comparison, and represent average rates over time periods that are much longer than the individual eruptions that produced most or all of the erupted volumes. The liberal eruptive rate calculated for Stage 1 mafic volcanism is a modest $2.5x10^{-5}$ km^3/yr. This is followed by a dramatic rate increase to $3.9x10^{-4}$ km^3/yr during Stage 2a silicic volcanism, which slows during Stage 2b volcanism to $4.2x10^{-5}$ km^3/yr. After the conclusion of local silicic volcanism and the onset of large scale extensional normal faulting and block rotation, eruptive rates drop to their lowest yet. $1.1x10^{-5}$ km^3/yr of mafic lava were erupted during Stage 3, followed by $3.9x10^{-7}$ km^3/yr in the first 0.1 million years of Stage 4, and $1.7x10^{-7}$ km^3/yr for the remainder of Stage 4 (Figure 15).

The highest eruptive rates immediately predate the onset of extensional normal faulting in the area, and the dramatic decrease coincides with the peak rates of extensional tilting (Fig. 16). Gans and Bohrson (1998) observed a similar relationship between the timing of peak volcanism and peak extension in the El Dorado Mountains of the northern CREC, where eruption rate sharply declined immediately after the onset of extensional faulting and peak rates of extension occurred during a hiatus in eruptive activity. Similar relationships are observed in several syn-extensional Miocene volcanic fields in the Basin and Range including Questa, New Mexico (Meyer and Foland, 1991), Yerrington, Nevada (Dilles and Gans, 1995), and the Vulture Mountains, Arizona (Spencer et al., 1995), to name

a few. Gans and Bohrson (1998) cite these examples to suggest that extension plays a role in suppressing volcanism.

Whether extension played a direct role in suppressing volcanic activity in the Whipple Mountains is unclear, but the relative timing of peak volcanism and peak extension in these volcanic centers suggests that volcanism plays an important role in weakening the crust and localizing extension. Although not diagnostic, the relationships observed in the western Whipple Mountains and eastern Mopah Range are consistent with a thermo-mechanical weakening model such as that proposed by Gans et al. (1989).

I. Conclusion

Geologic mapping of unprecedented detail sheds light on the volcanic and structural history and architecture of the western Whipple Mountains and eastern Mopah Range. This study is the most detailed yet on the character and age of Miocene volcanism in the region and provides important new insights into the evolution of a major volcanic field that was active immediately before and during the onset of regional large magnitude extension. Our principle conclusions from this work include the following:

1) Volcanism initiated in the western Whipple Mountains and eastern Mopah Range about 1.5 m.y. before the onset of domino-style extensional normal faulting.
2) Beginning at ~21 Ma, volcanic activity proceeded with ~1 m.y. of basalt and basaltic andesite fissure and/or shield eruptions, which flowed across an irregular though subdued crystalline terrane, forming a relatively flat volcanic field ~700 m thick. This was followed by ~0.5 m.y of eruption of rhyolite and dacite domes and tabular flows, during which time, eruptive rates reached their peak, building up a broad volcanic tableland.

3) Following this at ~19.5 Ma, extensional normal faulting began in the region, first in the central Mopah Range, and then in the eastern Mopah Range and western Whipple Mountains. In this period of peak tilting, at least two generations of NE-dipping normal faults formed half-grabens, in which syn-extensional sediments and basaltic andesite lavas accumulated.
4) Total extension increased to the SE, resulting in the development of scissor faults in the study area.
5) By 18.8 Ma, the region was broken up into NW-SE trending ranges and valleys which channelized the Peach Springs Tuff and subsequent andesite and basalt lavas which were likely localized by normal faults.
6) We estimate that ~90 km^3 of lava exists within the boundaries of the 140 km^3 study area. Using this volume to area ratio of 0.64, we speculate that across the entire CREC in the vicinity of the Whipple Mountains, nearly 490 km^3 of lava may have been erupted in the LCREC in the vicinity of the Whipple Mountains during the Miocene.

J. Acknowledgements

This mapping and associated analytical work was supported by the U.S. Geologic Survey, National Cooperative Geologic Mapping Program (EdMap), award #G14AC00080 from the period of May1, 2014 to April 30, 2015. Many thanks to Chris Older, Jason Womer, Will Junkin, and Josh Garber for assistance in the field, and to Beau Gentry for useful discussions and company as he concurrently mapped the Chambers Well dike swarm as part of the same EdMap project.

Figure 1

Figure 1. Simplified geologic map showing the regional tectonic setting of the Mopah Range and Whipple Mountains and distribution of Miocene volcanic and sedimentary rocks, Miocene plutonic rocks, pre-Miocene basement rocks and metamorphic core complexes including mylonitized footwall rocks and some of the major detachment faults and some locations discussed in text. SW = Standard Wash; AB = Aubrey Hills. Heavy dashed and barbed line marks the approximate boundaries of the highly extended Colorado River Extensional Corridor. Blue dashed line is the Colorado River (CA-AZ border), highways are dark green. Inset shows location of figure 2. This figure is modified slightly from Gans and Gentry, 2016.

Figure 1

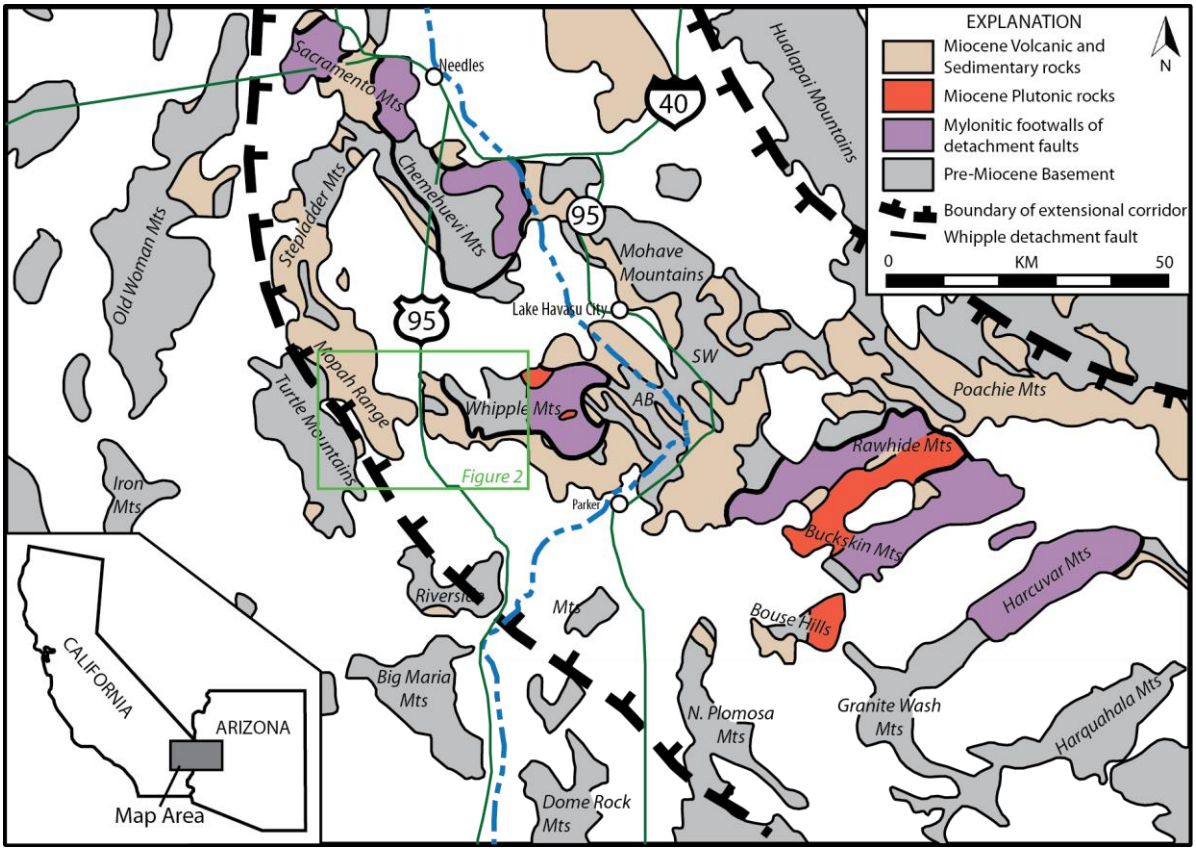
EXPLANATION
Miocene Volcanic and Sedimentary rocks
Miocene Plutonic rocks
Mylonitic footwalls of detachment faults
Pre-Miocene Basement
Boundary of extensional corridor
Whipple detachment fault
0
KM
50
N
Sacramento Mts
Needles
40
Hualapai Mountains
Old Woman Mts
Stepladder Mts
Chemehuevi Mts
95
Mohave Mountains
Lake Havasu City
95
SW
AB
Mopah Range
Turtle Mountains
Whipple Mts
Figure 2
Poachie Mts
Rawhide Mts
Iron Mts
Parker
Buckskin Mts
Harcuvar Mts
Riverside Mts
Bouse Hills
CALIFORNIA
ARIZONA
Map Area
Big Maria Mts
N. Plomosa Mts
Granite Wash Mts
Harquahala Mts
Dome Rock Mts

Figure 2

Figure 2. True color satellite image (Google Earth) showing location of map area and locations discussed in text. Inset is boundary of geologic map in plate 1. Throughout the text, the western Whipple Mountains refers to all exposures east of Highway 95 and west of the Whipple Detachment Fault, and the eastern Mopah Range refers to all exposures west of the highway and within the mapped area.

Figure 2

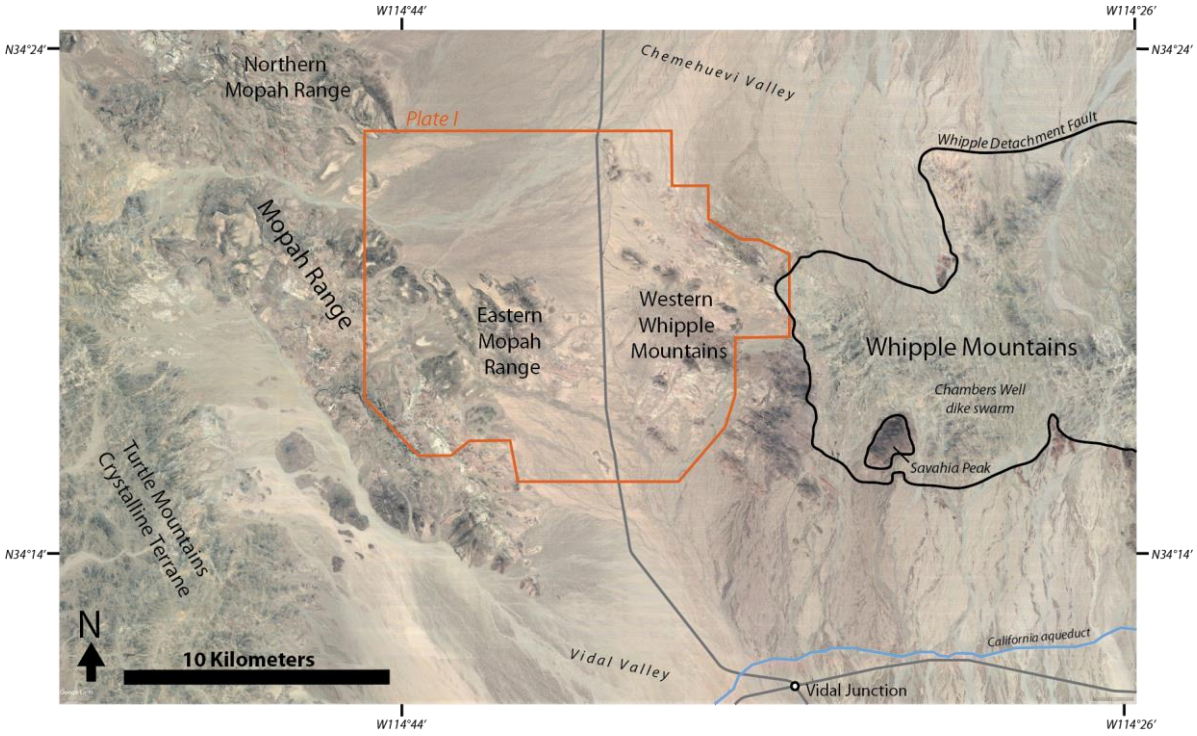
W114°44′
W114°26′
N34°24′
N34°14′
Northern
Mopah Range
Plate I
Chemehuevi Valley
Whipple Detachment Fault
Mopah Range
Eastern
Mopah
Range
Western
Whipple
Mountains
Whipple Mountains
Chambers Well
dike swarm
Savahia Peak
Turtle Mountains
Crystalline Terrane
N
10 Kilometers
Vidal Valley
California aqueduct
Vidal Junction

Figure 3

Figure 3. Field views of the western Whipple Mountains and eastern Mopah Range. (A) Typical exposure of the oldest silicic units in the W Whipple Mountains consists of gently undulating hills (foreground) covered by a veneer of red to pink colluvium; dark weathering ridges in background are mafic units cut by silicic dikes. View NW. (B) View SE from base of Tocba capping a ridge in the E Mopah Range. Pale Tc exposure in foreground. Peak on right of image in middle distance is a $Thbr_2$ lava dome discussed in text. W Whipple Mtns in distance on left. (C) Rugged interior of the Mopah Range. View south of steeply tilted Tpd lava flows (inclined fins are indurated breccias marking flow boundaries). Dips decrease farther west into the range. Monument on right in distance is a nipple of Thbr2 resting on Tts and Taa, both only gently inclined (~6°). (D) Vitrophyre with irregular fractures with smooth shiny faces (grey) and lenses of partially devitrified material (pink). Most silicic units preserved vitrophyres at their base and/or top.

Figure 3

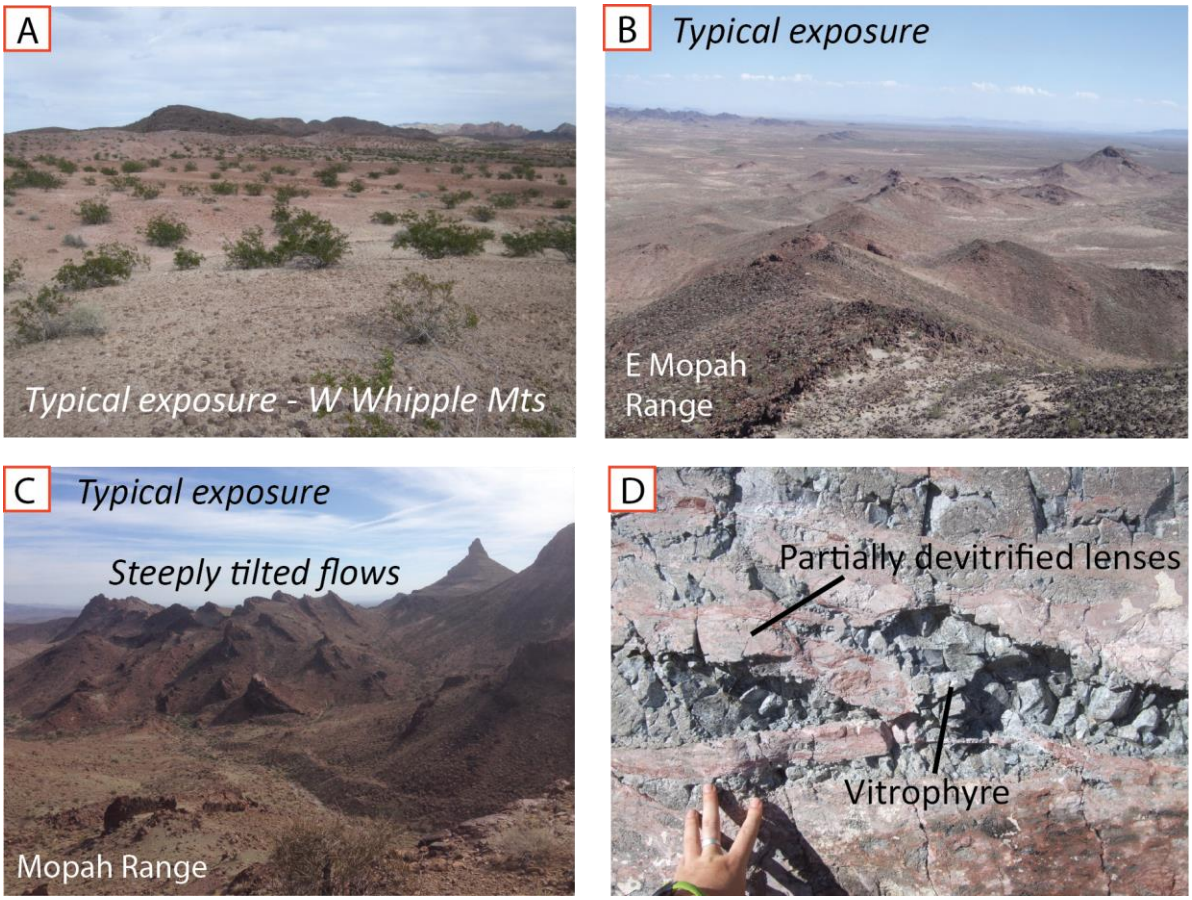
A
Typical exposure - W Whipple Mts
B
Typical exposure
E Mopah Range
C
Typical exposure
Steeply tilted flows
Mopah Range
D
Partially devitrified lenses
Vitrophyre

Figure 4

Figure 4. LeBas diagram showing total alkali vs. silica for volcanic rocks from the western Whipple Mountains and eastern Mopah Range. Samples are colored by unit. Inset shows magnified view of the cluster of points in the dacite and rhyolite fields. Samples were analyzed by XRF and normalized to 100%. Samples with the highest alkali contents (circled) have experienced K-metasomatism, indicated by low Na and high K and contain textural evidence of alteration. Samples with only slightly elevated alkali contents (circled) also contain textural evidence for alteration.

Figure 4

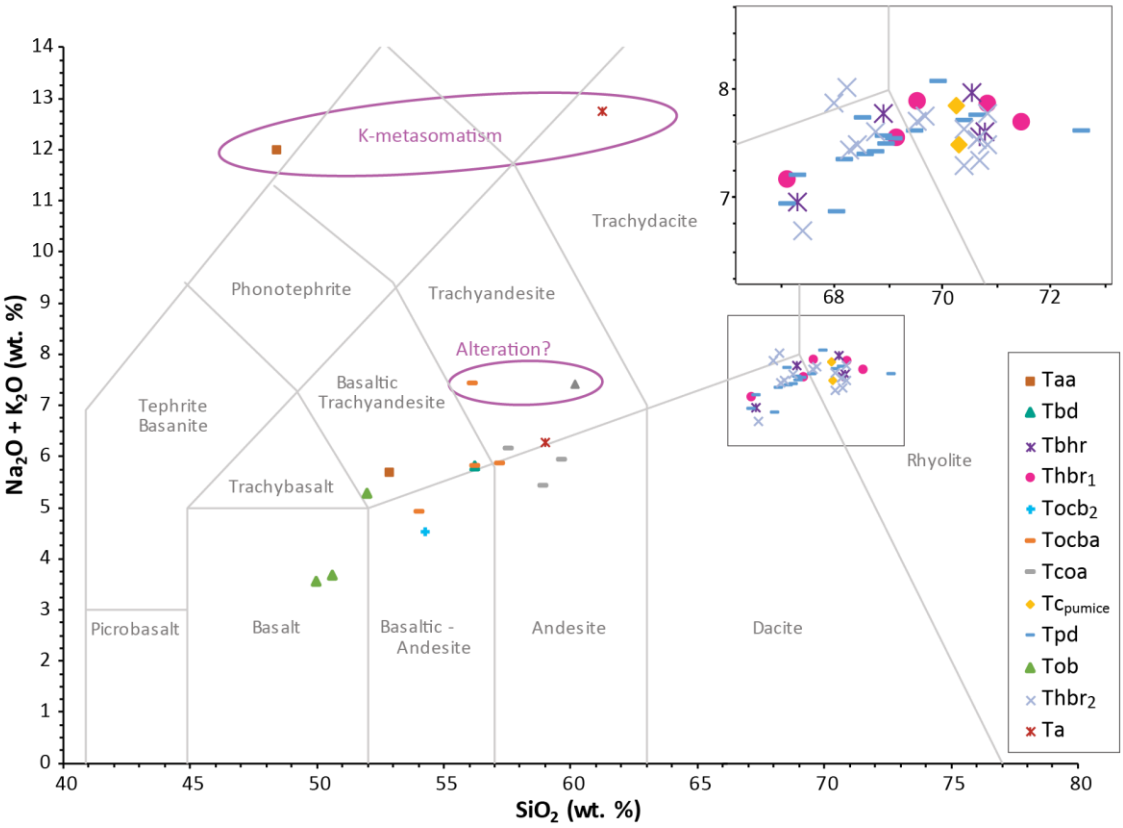
K-metasomatism
Alteration?
Trachydacite
Phonotephrite
Trachyandesite
Basaltic
Trachyandesite
Tephrite
Basanite
Trachybasalt
Rhyolite
Picrobasalt
Basalt
Basaltic -
Andesite
Andesite
Dacite
Taa
Tbd
Tbhr
Thbr1
Tocb2
Tocba
Tcoa
Tcpumice
Tpd
Tob
Thbr2
Ta
Na2O + K2O (wt. %)
SiO2 (wt. %)

Figure 5

Figure 5. Generalized stratigraphic section illustrating the mapped relationships among volcanic and sedimentary units in the field area. See map legend (Plate 1) for unit symbols. Thicknesses are not to scale, and relationships are shown systematically. The right side of the image illustrates the stratigraphic relationships in the western Whipple Mountains, whereas relationships shown on the left are more characteristic of the Mopah Range. Growth strata relationships are not shown (see cross sections, Fig. 14). Representative 40Ar/39Ar ages are placed in their approximate stratigraphic position; blue numbers are ages from the field area and red numbers are from less altered but correlative mafic units in the Aubrey Hills and Standard Wash.

Figure 5

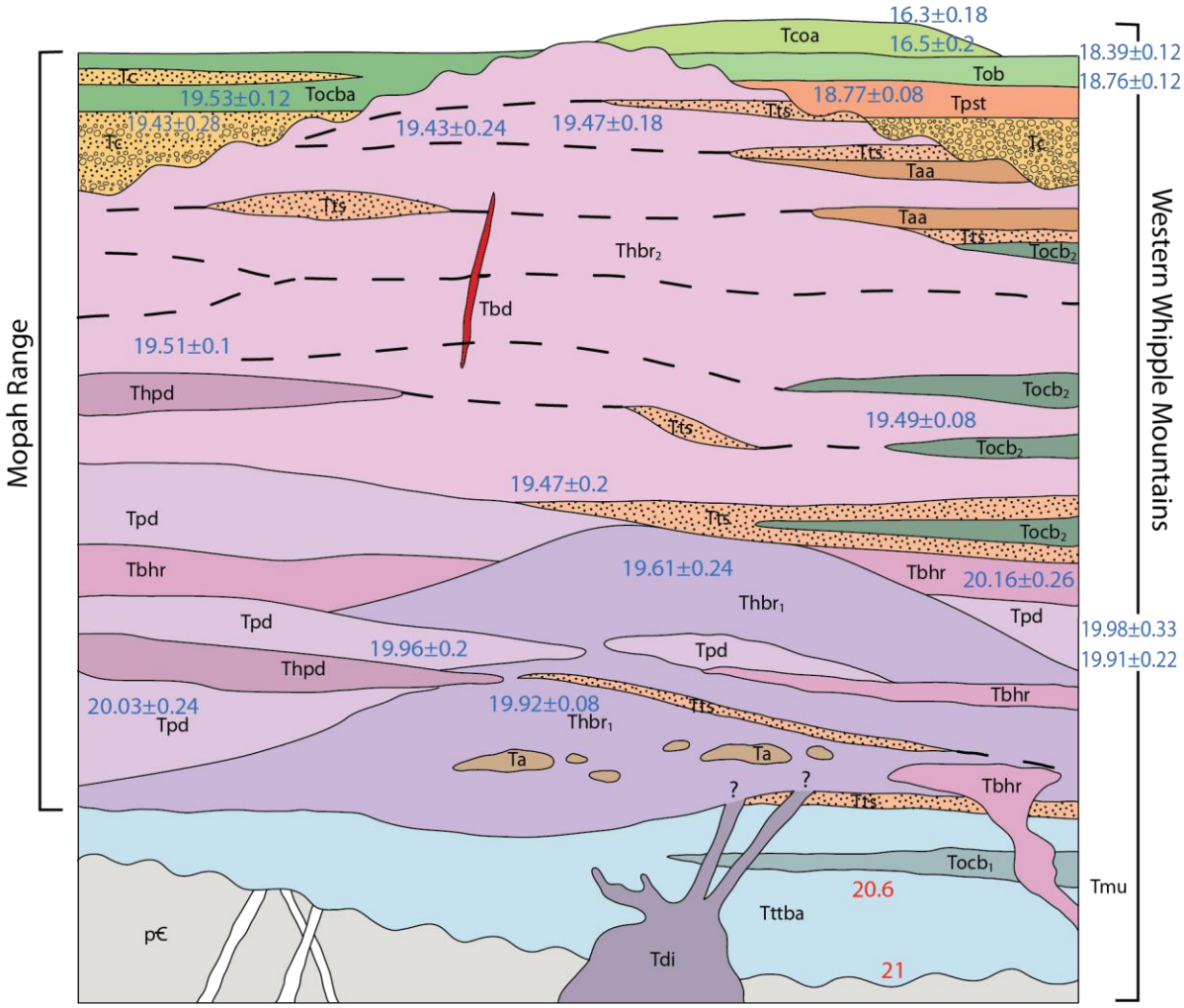
Mopah Range
Western Whipple Mountains
16.3±0.18
16.5±0.2
18.39±0.12
18.76±0.12
Tcoa
Tob
Tpst
18.77±0.08
Tc
Tocba
19.53±0.12
19.43±0.28
19.43±0.24
19.47±0.18
Tts
Taa
Thbr2
Tbd
19.51±0.1
Thpd
Tocb2
19.49±0.08
19.47±0.2
Tpd
Tbhr
19.61±0.24
Thbr1
20.16±0.26
19.96±0.2
19.98±0.33
19.91±0.22
20.03±0.24
19.92±0.08
Ta
Tocb1
Tmu
20.6
Tttba
Tdi
21
p€

Figure 6

Figure 6. Photomicrographs of typical textures of volcanic units in the western Whipple Mountains and eastern Mopah Range. A) Portion of a large (1 cm) tabular plagioclase, a characteristic feature of Tttba. B) Iddingsitized olivine and clinopyroxene phenocrysts set in a matrix of variolitic plagioclase and intergranular olivine. C) Orthopyroxene, clinopyroxene, and plagioclase phenocrysts. Variations in devitrification and microlite growth define flow bands (dashed yellow lines). D) Plagioclase phenocrysts with sieve textured rims and clear cores. E) Vitrophyre with well developed perlitic cracks and flow aligned phenocrysts and microphenocrysts of plagioclase, biotite and hornblende. Irregular chalcedony filled vugs are surrounded by devitrified glass. F) Highly sieve textured and rounded plagioclase and iddingsitized olivne phenocrysts set in a groundmass of plagioclase and intergranular clinopyroxene. “Xpl” indicates cross-polarized light. Sample name and unit are given on each photomicrograph.

Figure 6

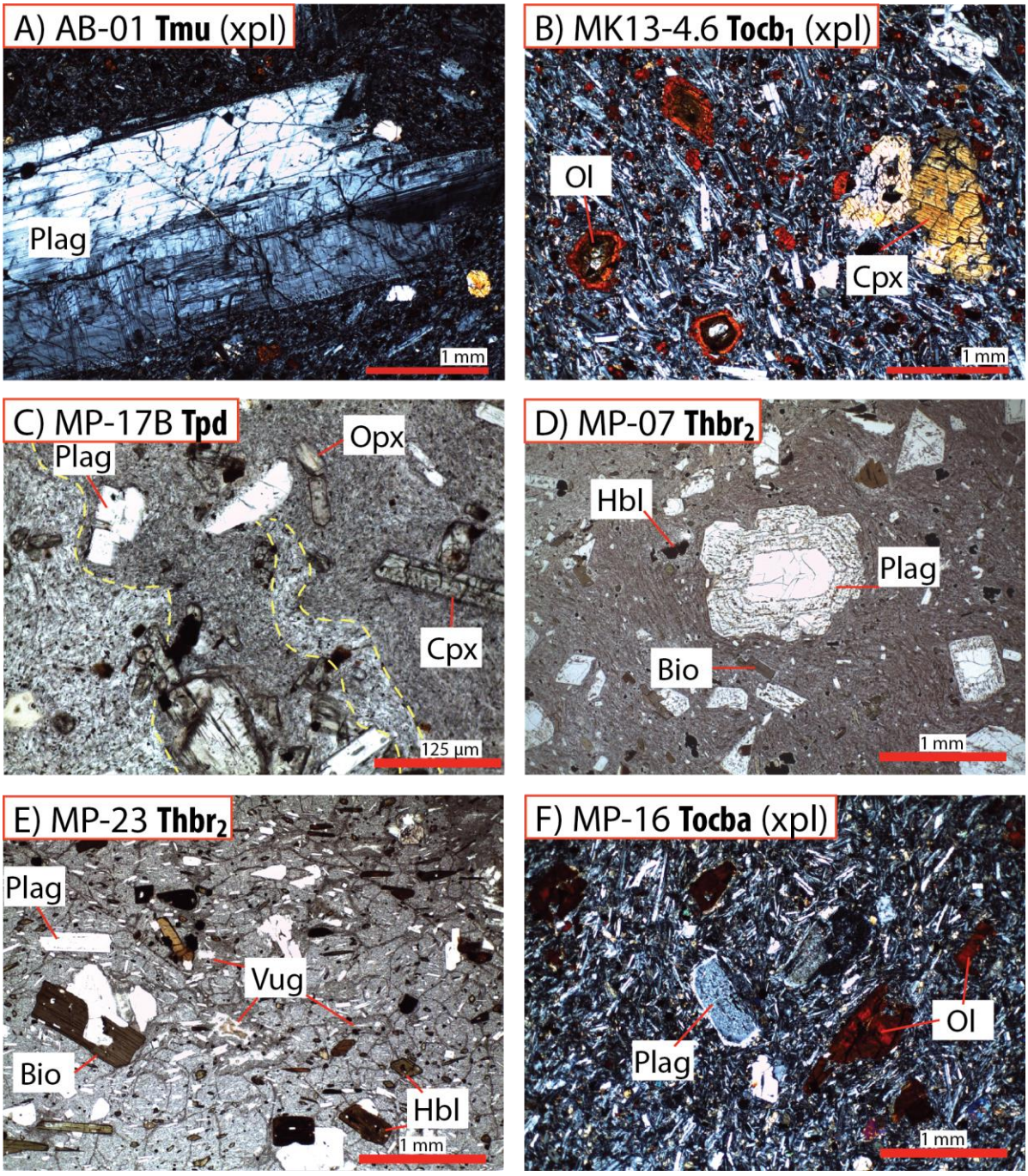
A) AB-01 Tmu (xpl)
Plag
1 mm
B) MK13-4.6 Tocb1 (xpl)
Ol
Cpx
1 mm
C) MP-17B Tpd
Plag
Opx
Cpx
125 µm
D) MP-07 Thbr2
Hbl
Plag
Bio
1 mm
E) MP-23 Thbr2
Plag
Vug
Bio
Hbl
1 mm
F) MP-16 Tocba (xpl)
Ol
Plag
1 mm

Figure 7

Figure 7. True color satellite image (Google Earth) of a well exposed area of Thbr1 in the western Whipple Mountains displaying characteristic weathering colors and internal color bands. The unit weathers shades of pink, lavender, brick red and white. Exposure of unit is outlined in white and is a single emplacement unit underlain by Tmu and overlain by Tts and Tocb2 (outlined in black) that tapers in thickness to the SW (suggesting source vent is likely located to the NW). Internal color variations do not reflect textural changes but instead may reflect endogenous growth and inflation of the lava flow.

Figure 7

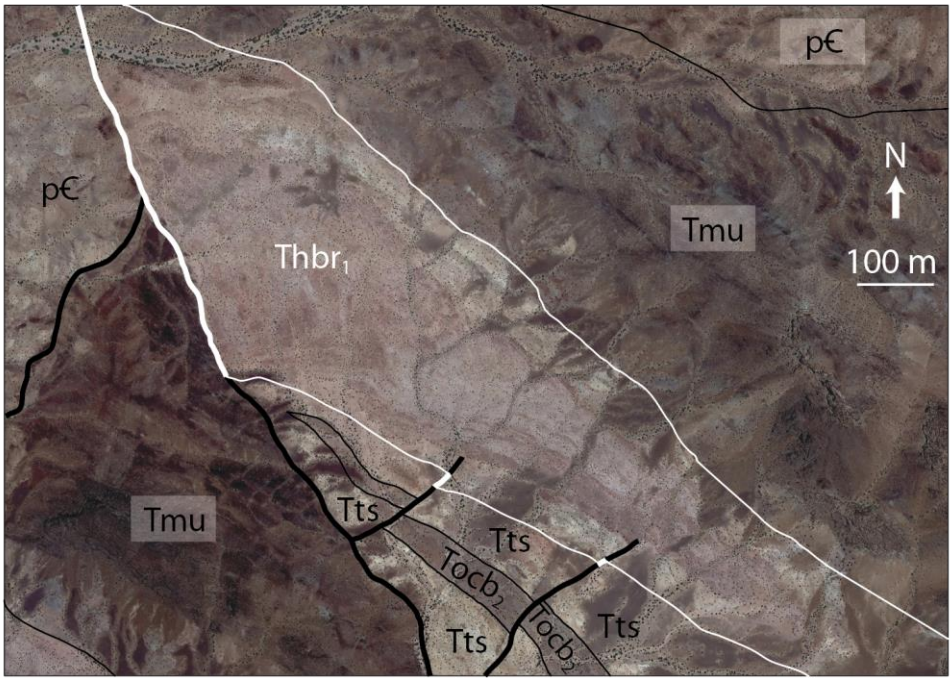

Figure 8

Figure 8. Field photos of textural relationships between andesitic enclaves (Ta) and silicic lava (Thbr1). (A) Margins between Ta enclaves and Thbr1 are delicate and crenulate, indicating the two lavas coexisted as fluids at the time of their emplacement. Margins of Ta are also quenched against Thbr1. (B) Ta exposures are completely encased in Thbr1. Ta inclusions range from only a few meters across as in the image to a few hundred meters across and are abundant in the western Whipple Mountains.

Figure 8

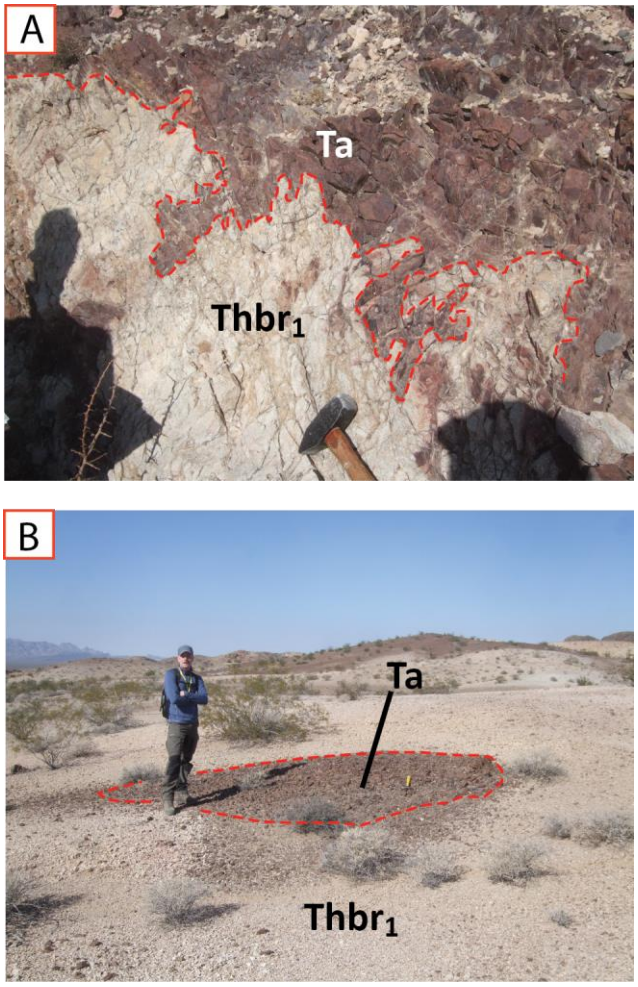

Figure 9

Figure 9. Figure from Hazlett (1986) showing the locations and geometry of his proposed volcanic belts interpreted to be vent locations for volcanic rocks west of the Whipple crystalline terrane. Figure displays current (post-extension) locations of Tertiary rocks. Reconstructing pre-extensional locations would bring the belts closer together. Dash line represents Hazlett's supposed area of original Tertiary cover, about 50% of which is buried or eroded (white). Orange inset shows location of mapped area on Plate 1, which lies entirely within Hazlett's proposed area of volcanic cover. We use this logic to calculate liberal volume estimates for lavas within the field area by extrapolating units under alluvium to the boundaries of the map area where appropriate.

Figure 9

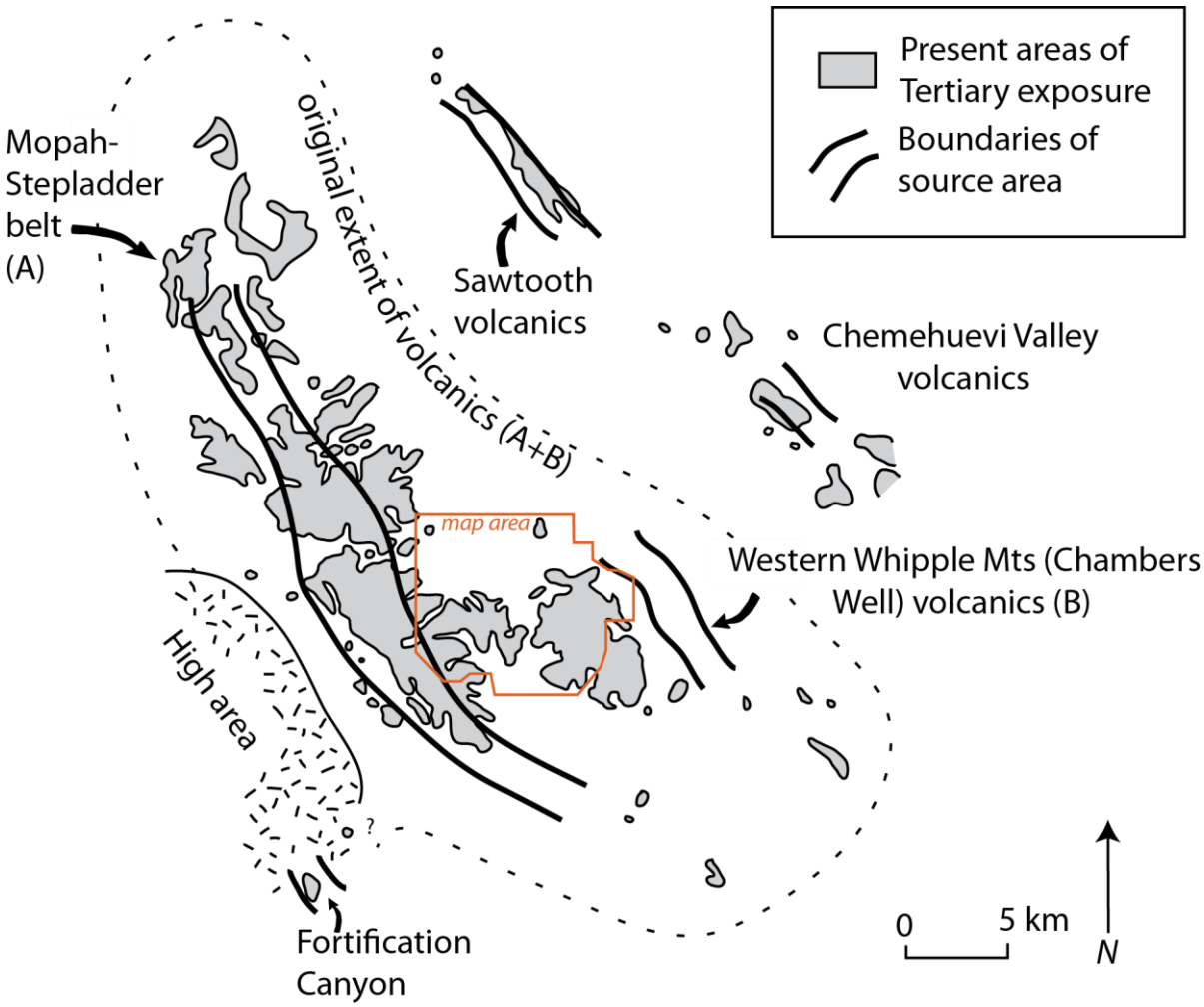
Present areas of Tertiary exposure
Boundaries of source area
Mopah-Stepladder belt (A)
original extent of volcanics (A+B)
Sawtooth volcanics
Chemehuevi Valley volcanics
map area
Western Whipple Mts (Chambers Well) volcanics (B)
High area
?
Fortification Canyon
0
5 km
N

Figure 10

Figure 10. Four-stage interpretive reconstruction of the evolution of the western Whipple Mountains and eastern Mopah Range volcanic terrane. (A) Stage 1 mafic effusive volcanism from one or more shield point sources and/or fissure systems. (B) Stage 2 silicic flow and dome growth by effusive and minor explosive eruptions. (C) Stage 3 basaltic andesite cinder cones erupt lava into actively subsiding half-grabens. (D) Stage 4 Peach Springs Tuff and relatively small local mafic lavas are channelized in valleys as extensional block rotation ends.

Figure 10

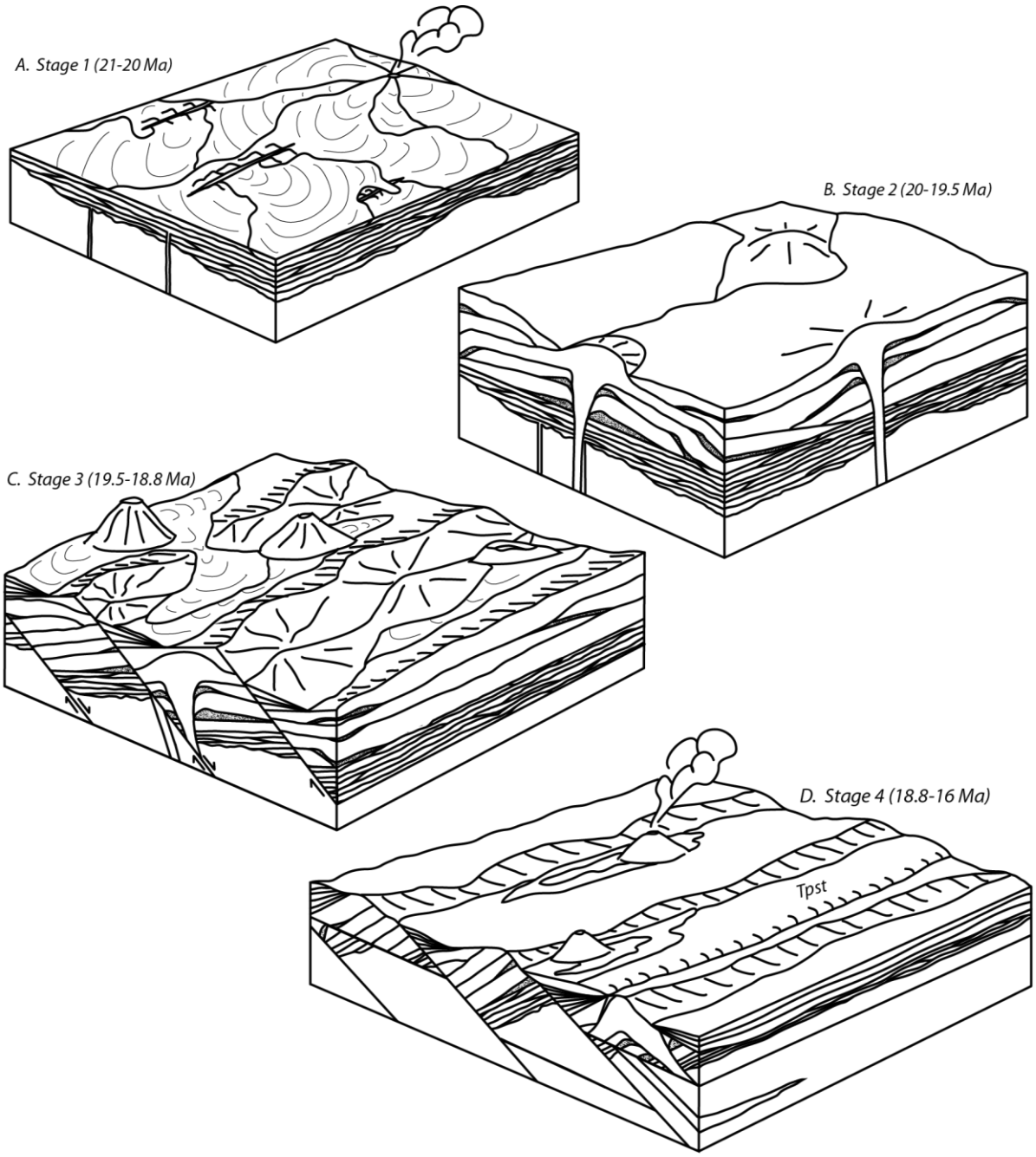
A. Stage 1 (21-20 Ma)
B. Stage 2 (20-19.5 Ma)
C. Stage 3 (19.5-18.8 Ma)
D. Stage 4 (18.8-16 Ma)
Tpst

Figure 11

Figure 11. Selected high confidence ages of volcanic units in each volcanic stage. Volcanic stages are numbered on y-axis. Although many ages from stage 2a and 2b overlap in uncertainty, the data are suggestive of two distinct pulses of volcanism during stage 2. Stage 3 ages overlap in uncertainty with all of the Stage 2b ages and some of the Stage 2a ages. Stratigraphic relations however indicate that Stage 3 lavas postdate the emplacement and ~30° of tilting of the stage 2 lavas. The three ages for Stage 3 lavas are from near the base of the unit, and may not be representative of the duration of this stage of volcanic activity.

Figure 11

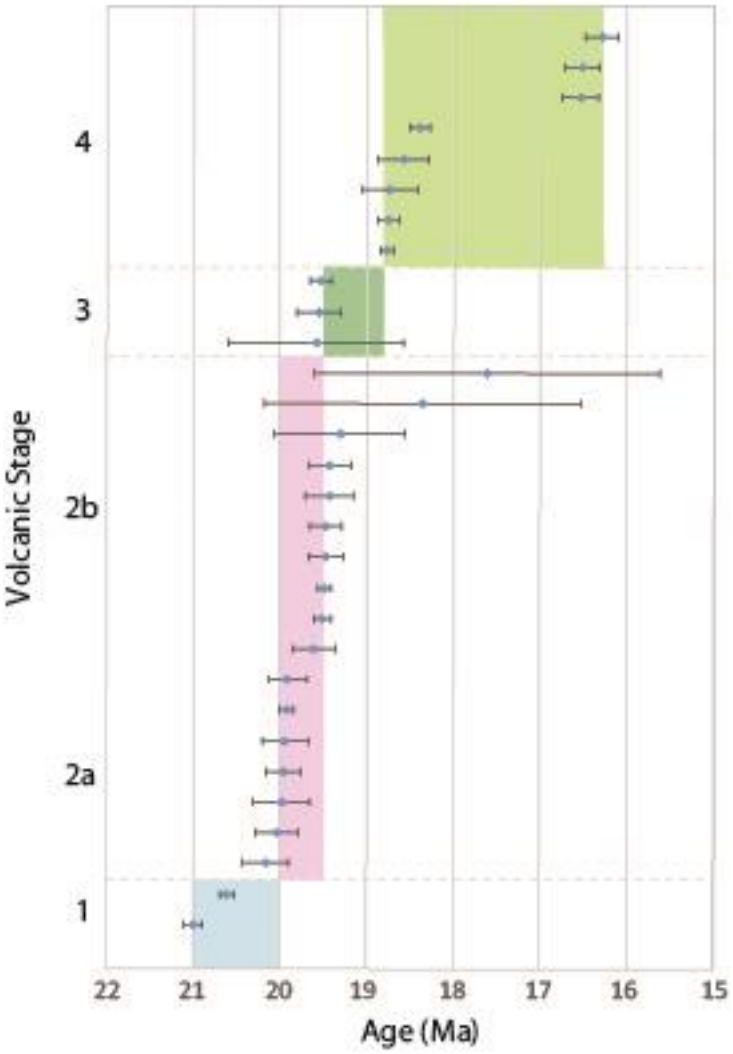

Figure 12

Figure 12. Lower hemisphere equal area stereographic projections of structural data (poles to planar elements) from the western Whipple Mountains and eastern Mopah Range. Domains I (A-D) and II (E-G) correspond to the structural domain areas in Figure 15. All bedding measurements are from stratified epiclastic or pyroclastic deposits, whereas all foliation measurements are from either laminar flow foliations (flow banding, platy partings) for lavas or flattening foliations from welded tuff (Tpst). Large dots indicate the mean vector for each data set. With the exception of Stage 3 in Domain I, bedding and the densest cluster of foliation measurements for each stage are in good agreement. A) Bedding of Stage 2a (purple) and 2b (red) deposits. B) Foliations of Stage 1 (black), Stage 2a (light blue), and Stage 2b (orange) lavas. Dashed pale blue circle encloses a cluster of orientations from the core of a Thbr1 lava dome in the western Whipple Mountains (discussed in text) which are ~90° from the densest cluster of poles to foliation (rotated around strike) and thus interpreted to represent paleovertical. There is good agreement between the bedding and foliations of Stage 2a and Stage 2b units. C) Stage 3 bedding (green) and foliation (blue). Foliation measurements are from lavas that largely overlie (some interstratification) the stratified conglomerates (bedding measurements). Shallowing upward dips from lower sedimentary beds to higher lava flows is evidence of growth faulting during Stage 3 deposition and volcanism (see Figure 14 for more detailed treatment of this data). D) Stage 4 bedding (gray) and foliation (pink) indicate nearly flat lying strata. E) Stage 2a bedding (purple) and foliation (light blue). F) Stage 2b bedding (red) and foliation (orange). G) Stage 3 foliation (no bedding measurements taken).

Figure 12


Domain I
A) Stage 2a and 2b bedding
N
n=38
n=22
B) Stage 1, 2a, and 2b foliation
N
n=11
n=290
n=148
C) Stage 3 bedding and foliation
N
n=57
n=47
D) Stage 4 bedding and foliation
N
n=4
n=48
Domain II
E) Stage 2a bedding and foliation
N
n=5
n=90
F) Stage 2b bedding and foliation
N
n=44
n=38
G) Stage 3 foliation
N
n=14

Figure 13

Figure 13. Orientations and locations of Stage 3 sedimentary and volcanic rocks that indicate growth faulting. Orientation of the location markers, data and dip indicators in A-C are rainbow colored based on their stratigraphic position, red being the lowest position and purple being the highest. A) Inset of geologic map of eastern Mopah Range showing locations of orientation data (rainbow colored dots) shown in B and C. B) Lower hemisphere stereographic projection of bedding and flow foliation measurements from Tc and Tocba. Data are poles to planes. C) Cross-section from X-Y (see A) with orientation data from B. Ball indicates approximate location of data projected onto the line of cross-section and tail indicates dip of strata. Ages of Tocba are obtained nearby (see A), and age of Stage 2 lava is our most precise stage 2 age, collected in the western Whipple Mountains. Though 3 different fault blocks containing Tocba and Tc exposures show evidence for growth faulting (decreasing dips up-section), the exposures in this location contain the most complete and continuous exposure from the base of Tc to the top of Tocba.

Figure 13

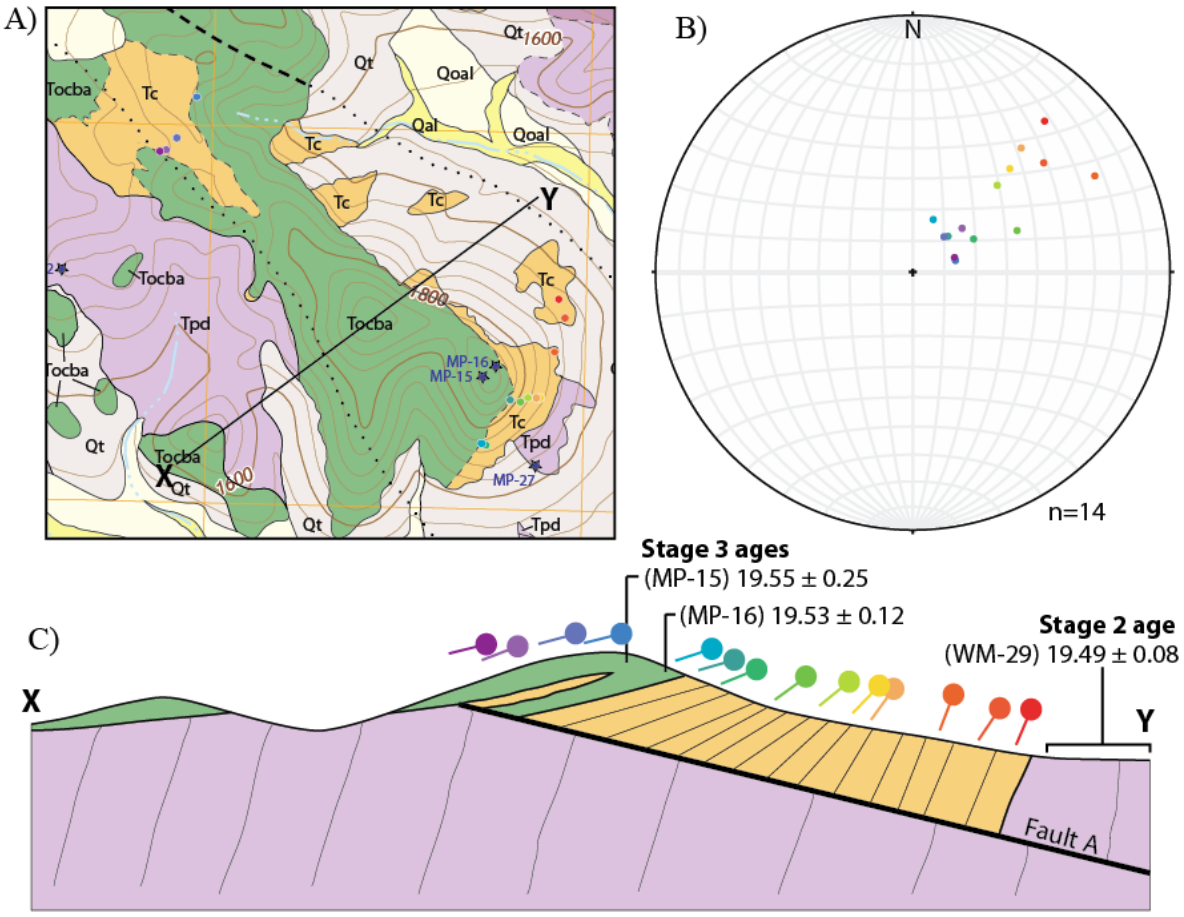
A)
Qt
1600
Tocba
Tc
Qoal
Qal
Y
Tpd
1800
MP-16
MP-15
MP-27
X
1600
B)
N
n=14
C)
Stage 3 ages
(MP-15) 19.55 ± 0.25
(MP-16) 19.53 ± 0.12
Stage 2 age
(WM-29) 19.49 ± 0.08
X
Y
Fault A

Figure 14

Figure 14. Illustration of methods for estimating volcanic rock volumes. A) Simplified geologic map of the study area showing approximate area of regions referred to in Table 2 and used in intermediate steps of total volcanic volume calculations. Region names correspond to the designated area of the same color. B) Cartoon illustration showing method for estimating along strike length of dipping units and area of flat lying units. Bold lines indicate length measured for minimum estimates and dashed lines indicate length measured for realistic estimates, for dipping (red) and flat lying (blue) units. C) Two possible cross-sections of X-Y from (B) demonstrate the effect of interpreted fault dip on estimated down-dip length of unit A.

Figure 14

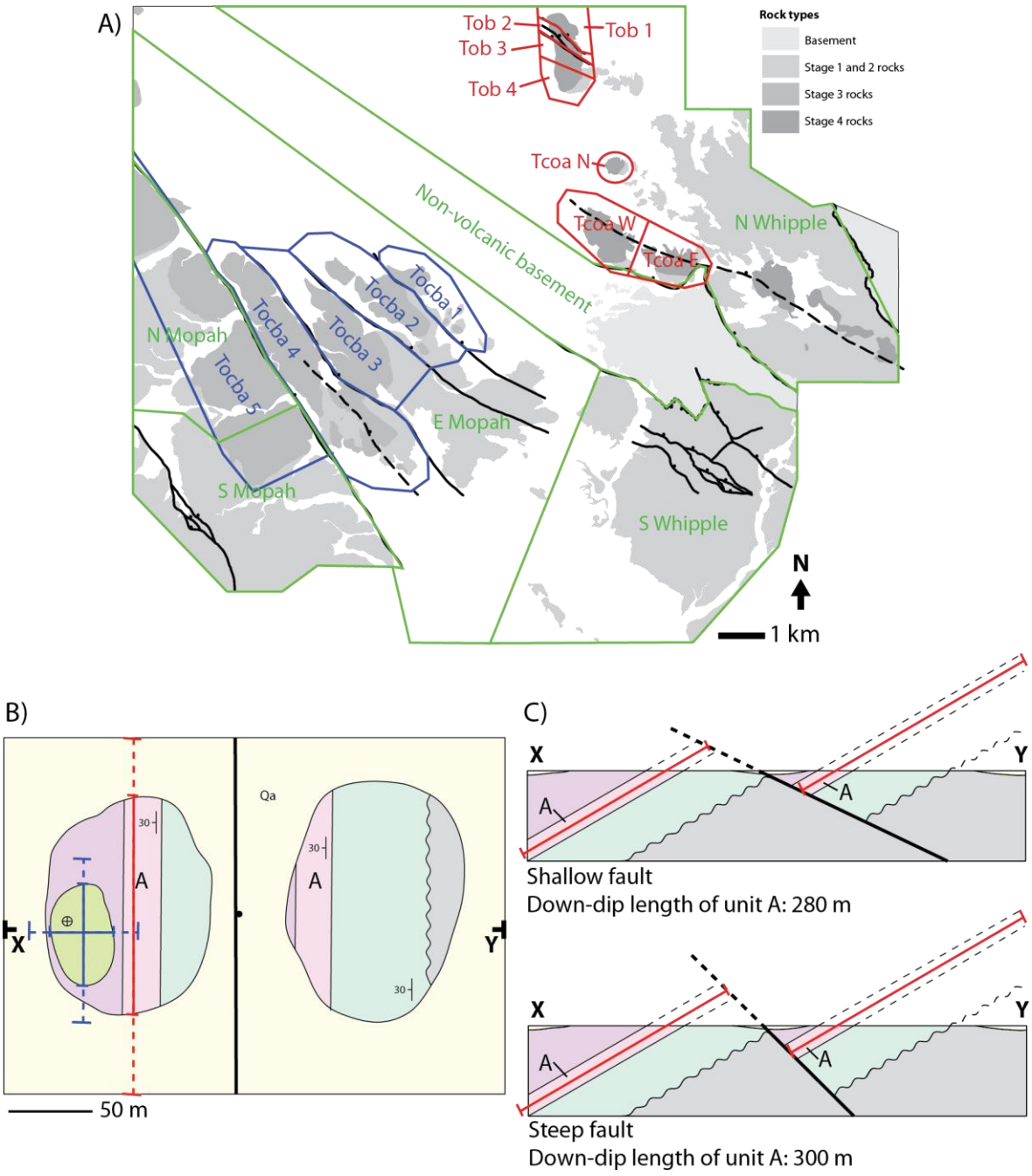
A)
Tob 2
Tob 1
Tob 3
Tob 4
Rock types
Basement
Stage 1 and 2 rocks
Stage 3 rocks
Stage 4 rocks
Tcoa N
Tcoa W
Tcoa E
Non-volcanic basement
N Whipple
Tocba 1
Tocba 2
Tocba 3
Tocba 4
Tocba 5
N Mopah
E Mopah
S Mopah
S Whipple
N
1 km
B)
Qa
A
30
X
Y
50 m
C)
X
Y
A
Shallow fault
Down-dip length of unit A: 280 m
Steep fault
Down-dip length of unit A: 300 m

Figure 15

Figure 15. Simplified structural map of the western Whipple Mountains and eastern Mopah Range. The region is approximately divided into two structural domains, I and II. These domains experienced different degrees of tilting of volcanic units in Stages 1-3. Only the major faults are shown in the figure, and these are colored according to our interpretations of relative age and given fault group names I-IV (see legend). Dashed faults are buried under younger Tertiary units or Quaternary alluvium. Relative ages of faults were determined by amount and direction of dip (steeper faults are younger) and cross-cutting relations (i.e. younger faults cut older faults, and younger faults cut younger volcanic units that older faults). Bedding and foliation data are select measurements, chosen to give an impression of the degree of tilt of various units. Inset is location of Figure 14. Named faults (A-D) discussed in the text.

Figure 15

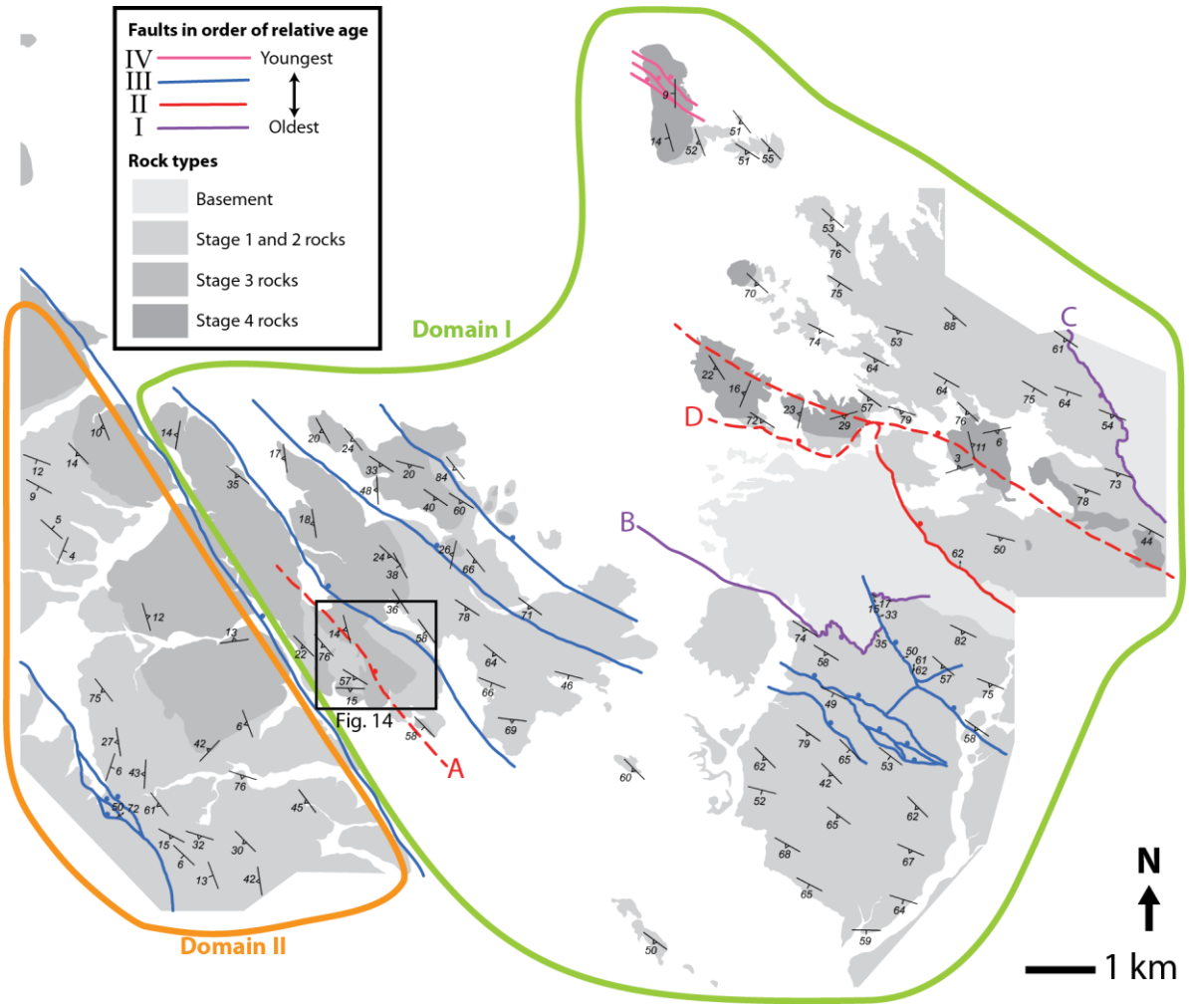
Faults in order of relative age
IV
III
II
I
Youngest
Oldest
Rock types
Basement
Stage 1 and 2 rocks
Stage 3 rocks
Stage 4 rocks
Domain I
Domain II
A
B
C
D
Fig. 14
N
1 km

Figure 16

Figure 16. Cumulative volume erupted, cumulative tilting, effective volcanic output rate, and effective extensional tilting rate vs. time for the western Whipple Mountains and eastern Mopah Range. Blue (minimum) and orange (realistic) lines are estimates for cumulative volcanic output (top) and effective eruption rate (bottom). The cumulative volume curves reflect bare minimum and realistic minimum reconstructions of original areas and thicknesses of lavas from each stage represented in figure 11 and are plotted according to radiometric ages of Table 1 (axes on left of graphs). Owing to erosion and alluvial cover, uncertainty is great for volume estimates, resulting in the large discrepancy between minimum and realistic volume and rate estimates. Black (Domain 1) and gray (Domain 2) lines are estimates for cumulative tilting for each structural domain and for effective extensional tilting rate for Domain 2 (axes on right of graphs). Color blocks represent each of the 4 volcanic stages, with stage numbers listed across top of figure.

Figure 16

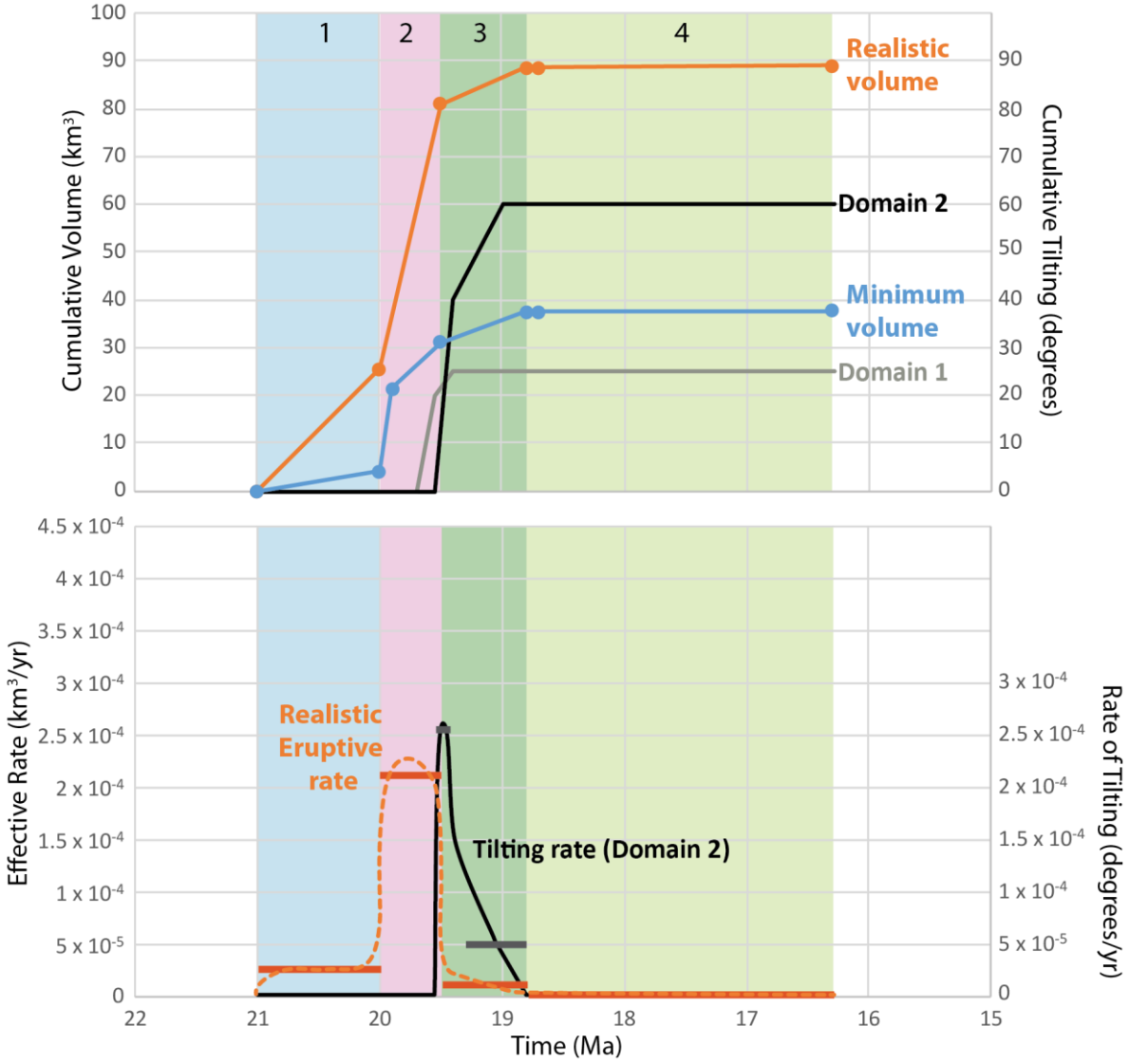
1
2
3
4
Realistic volume
Domain 2
Minimum volume
Domain 1
Cumulative Volume (km³)
Cumulative Tilting (degrees)
Realistic Eruptive rate
Tilting rate (Domain 2)
Effective Rate (km³/yr)
Rate of Tilting (degrees/yr)
Time (Ma)

Table 1. New Geochronologic Data From the Eastern Mopah Range and Western Whipple Mountains ($^{40}Ar/^{39}Ar$ Data from volcanic rocks)

Sample	Material	Map Unit	Preferred Age (Ma)	±	2σ	TFA	Comments
MP-03	Plag	$Thbr_1$	19.92	±	0.08	20.67	Excellent flat spectrum
MP-05	Plag	Tpd	<20.5			24.52	Strongly u-shaped spectrum - isochron age
MP-07	Plag	$Thbr_2$	19.51	±	0.10	19.48	Excellent flat spectrum
MP-09*	Plag	$Thbr_2$	19.43	±	0.24	19.64	Spectrum climbs to a broad flat
MP-12	Plag	Tpd	19.96	±	0.20	20.24	Excellent flat spectrum
MP-15*	GM	Tocba	19.55	±	0.25	20.00	Strong recoil with high T flat
MP-16	GM	Tocba	19.53	±	0.12	19.69	Slight recoil with high T flat
MP-18	GM	Tocba	19.58	±	1.02	19.51	Disturbed spectra
MP-19*	Plag	Tc_{pumice}	19.43	±	0.28	19.58	Spectrum climbs then flattens, low radiogenic yields
MP-21	Plag	Tpd	19.94	±	0.26	20.39	Climbs slightly to flat
MP-22	Plag	Tpd	20.03	±	0.24	20.23	Excellent flat spectrum
MP-23	Plag	$Thbr_2$	>17.66			16.36	Hump shaped spectrum, minimum age
MP-24	Plag	$Thbr_2$	19.47	±	0.18	19.79	Excellent flat spectrum
MP-26	Plag	$Thbr_1$	19.61	±	0.24	19.83	Excellent flat spectrum
WM-21	GM	Tob	18.39	±	0.12	18.28	Hump shaped spectrum, minimum age
WM-22	San	Tpst	18.77	±	0.08	18.77	Excellent flat spectrum
WM-23	GM	Tob	18.76	±	0.12	19.07	Slight Ar loss and exxess Ar, high temp. flat
WM-29	Plag	$Thbr_2$	19.49	±	0.08	19.49	Excellent flat spectra
WM-32 (14)	GM	Tob	18.74	±	0.33	18.78	Excellent flat spectrum
WM-34	Plag	Tpd	19.91	±	0.22	20.18	Excellent flat spectrum
WM-35	Plag	$Thbr_1$	17.62	±	2	15.05	Ar loss and excess Ar
WM-36*	Plag	Tpd	18.37	±	1.83	13.62	Ar loss and excess Ar
WM-38	Plag	Tpd	19.98	±	0.33	20.23	Excellent flat spectra
WM-39	Plag	Tbhr	20.16	±	0.26	20.52	Excellent flat spectra
WM-41	GM	Tcoa	18.58	±	0.3	18.73	Slight recoil and excess Ar
WM-43	Plag	Tbhr	19.31	±	0.75		Isochron Age
WM-44	Plag	$Thbr_2$	19.47	±	0.20	19.81	Excellent flat spectra
WM-48	GM	Tcoa	16.5	±	0.2	16.34	Climbs slightly to flat
WM-49*	GM	Tcoa	16.54	±	0.20	17.17	Drops with high T flat
WM-51*	GM	Tcoa	16.30	±	0.18	17.17	U-shaped spectrum with high T flat
AB-01*	GM	Tttba	20.61	±	0.08	20.95	Recoil and excess argon
MK13-4.6*	GM	$Tocb_1$	21.0	±	0.1	21.34	Recoil with high T flat, reliable age

Note: Material abbreviations: Plag - plagioclase, San - sanidine, GM - groundmass. MP, AB, and MK13 samples were collected and dated by Fidler and WM samples were collected and dated by Gans. All samples were collected within the field area with the exception of AB-01 (Aubrey Hills) and MK13-4.6 (Standard Wash).
Mineral separates were prepared and analyzed at UCSB. Preferred ages are weighted mean plateau ages from incremental heating experiments except where it is indicated in the comments that the isochron age is preferred. Ages were monitored using Taylor Creek Rhyolite sanidine, using an original calibration age of 27.92 Ma (Dalrymple and Duffield, 1988) and then recalculated using an adjusted calibration age 28.35 Ma, equivalent (R=1.00881 ± 0.00046) to the widely used Fish Canyon sanidine at 28.1 Ma (Spell and McDougal, 2003). See appendix I for tabulated data and age spectra using the original calibration age.

* denotes samples where preferred weighted mean plateau ages were calculated from temperature steps that totaled less than 50% of gas.

Table 2. Volume calculations

			*Absolute minimum**				*Realistic minimum***			
Stage	**Area**	**Thickness (m)**	**Exposure length (m)**	**Down-dip length (m)**	**Area (km^2)**	**Volume (km^3)**	**Exposure length (m)**	**Down-dip length (m)**	**Area (m^2)**	**Volume (km^3)**
1	***TOTAL 1***	725	2400	2900	5.5	**4.0**	15400	2900	35.1	**25.4**
2	2a N Whipple	1140	8520	1200	8.0	9.2	11000	1200	10.4	11.8
	2a S Whipple	300	1960	2460	3.8	1.1	3740	3060	9.0	2.7
	2a E, S Mopah	750	3940	3100	9.6	7.2	11200	3700	32.5	24.4
	TOTAL 2a					**17.5**				**38.9**
	2b N Whipple	298	1100	140	0.1	0.04	1280	140	0.1	0.04
	2b S Whipple	1300	4880	1440	5.5	7.2	5116	2422	9.7	12.7
	2b E Mopah	870	2220	780	1.4	1.2	3054	780	1.9	1.6
	2b N Mopah	360	2280	1740	3.1	1.1	3660	1940	5.6	2.0
	2b S Mopah W	360	1460	400	0.5	0.2	2300	400	0.7	0.3
	2b S Mopah E	36	1940	920	1.4	0.05	2000	1240	2.0	0.1
	TOTAL 2b					**9.7**				**16.7**
	TOTAL 2					**27.2**				**55.6**
3	Tocba 1	80	1136	520	0.6	0.05	2340	580	1.4	0.1
	Tocba 2	120	2720	700	1.9	0.2	3000	1020	3.1	0.4
	Tocba 3	240	2720	1200	3.3	0.8	3600	1200	4.3	1.0
	Tocba 4	360	4800	980	4.7	1.7	5880	980	5.8	2.1
	Tocba 5	360	6800	1480	10.1	3.6	6800	1632	11.1	4.0
	TOTAL 3					**6.4**				**7.6**
4	Tcoa W	220	1000	600	0.5	0.1	1360	680	0.7	0.2
	Tcoa E	360	960	360	0.3	0.1	1280	680	0.7	0.3
	Tcoa N	50	300	160	0.04	0.002	360	360	0.1	0.005
	TOTAL Tcoa					**0.2**				**0.4**
	Tob 1	40	460	280	0.1	0.005	640	360	0.2	0.01
	Tob 2	40	800	200	0.2	0.006	1040	200	0.2	0.01
	Tob 3	40	320	300	0.1	0.004	540	320	0.2	0.01
	Tob 4	40	380	600	0.2	0.009	400	880	0.4	0.01
	TOTAL Tob					**0.03**				**0.04**
	TOTAL 4					**0.3**				**0.5**
	Total ALL					**37.8**				**89.0**

*Absolute minimum measurements, area, and volume estimates are based strictly on exposure area.

**Realistic minimum measurements, area, and volume estimates take into account where older units are inferred under alluvial cover and where younger units likely experienced loss to erosion.

Note that all data presented in this table should be interpreted as rough estimates with large uncertainties, as described in text.

K. References

Allmendinger, R. W., Cardozo, N., and Fisher, D., 2012, Structural geology algorithms: Vectors and tensors in structural geology: Cambridge University Press

Anderson, R. Ernest. "Thin skin distension in Tertiary rocks of southeastern Nevada." *Geological Society of America Bulletin* 82.1 (1971): 43-58.

Armstrong, R. L., & Ward, P. L. (1991). Evolving geographic patterns of cenozoic magmatism in the north american cordillera; the temporal and spatial association of magmatism and metamorphic core complexes. *Journal of Geophysical Research, 96*, 13-13,224.

Arvidson, R. E., Shepard, M. K., Guinness, E. A., Petroy, S. B., Plaut, J. J., Evans, D. L., ... & Gaddis, L. R. (1993). Characterization of lava-flow degradation in the Pisgah and Cima volcanic fields, California, using Landsat Thematic Mapper and AIRSAR data. *Geological Society of America Bulletin*, *105*(2), 175-188.

Axen, G. J., Taylor, W. J., & Bartley, J. M. (1993). Space-time patterns and tectonic controls of tertiary extension and magmatism in the great basin of the western united states. *Geological Society of America Bulletin, 105*(1), 56-76.

Bonnichsen, B.; Kauffman, D.F. 1987. Physical features of rhyolite lava flows in the Snake River Plain volcanic province, southwestern Idaho. *In* The Emplacement of Silicic Domes and Lava Flows (Fink, J.H.; editor). *Geological Society of America, Special Paper*, No. 212, p. 119-145

Burchfiel, B. C., & Davis, G. A. (1981). In Ernst W. G. (Ed.), *Mojave desert and environs* Prentice-Hall, Englewood Cliffs, NJ.

Cardozo, N., and Allmendinger, R.W., 2013, Spherical projections with OSXStereonet: Computers & Geosciences, v. 51, p. 193 – 205.

Carr, W. J., Dickey, D. D., & Quinlivan, W. D. (1980). *Geologic map of the Vidal NW, Vidal Junction, and parts of the Savahia Peak SW and Savahia Peak Quadrangles, San Bernardino County, California* U. S. Geological Survey, Reston, VA.

Christiansen, R.L.; Lipman, P.W. 1966. Emplacement and thermal history of a rhyolite lava flow near Fortymile Canyon, southern Nevada. *Geological Society of America, Bulletin*, Vol. 77, p. 671-684.

Coney, P.J., 1974, Structural analysis of the Snake Range "décollement," east-central Nevada: Geological Society of America Bulletin, v. 88, p. 1237–1250.

Coney, P., 1980, Cordilleran metamorphic core complexes: An overview, in Crittenden, M. D., Coney, P. J., and Davis, G. H., eds., Cordilleran metamorphic core complexes: Geological Society of America Memoir 153, p. 7–34

Crittenden, M.D., Jr., Coney, P.J., and Davis, G.H., eds., 1980, Cordilleran Metamorphic Core Complexes: Geological Society of America Memoir 153, 490 p.

Dalrymple, G. B., and Duffield, W. A. (1988). High Precision 40Ar/39Ar dating of Oligocene rhyolites from the Mogollon-Datil volcanic field using a continuous laser system. Geophysical research letters, vol. 15, no. 5, 463-466

Davis, G.A., Anderson, J.L., Frost, E.G., and Shackelford, T.J., 1980, Mylonitization and detachment faulting in the Whipple-Bucksin-Rawhide Mountains terrane, southeastern California and western Arizona, *in* Crittenden, M.D., Coney, P.J., and Davis, G.H., eds., Cordilleran Metamorphic Core Complexes: Geological Society of America Memoir 153, p. 9-129.

Davis, G. A., & Lister, G. S. (1988). Detachment faulting in continental extension; perspectives from the southwestern U.S. cordillera. *Special Paper - Geological Society of America, 218*, 133-159. doi:http://dx.doi.org/10.1130/SPE218-p133

Davis, G. A., 1988, Rapid upward transport of mid-crustal mylonitic gneisses in the footwall of a Miocene detachment fault, Whipple Mountains, southeastern California: Geologisehes Rundschau, v. 77, p. 191-209.

Davis, G. A., J. L. Anderson, D. L. Marin, D. Krummenacher, E. G. Frost, and R. L. Armstrong (1982), Geologic and geochronologic relations in the lower plate of the Whipple detachment fault, Whipple Mountains, southeastern California: A progress report: Mesozoic-Cenozoic tectonic evolution of the Colorado River region, California, Arizona, and Nevada, April 1982, p. 409–412.

Dickey, D. D., Carr, W. J., & Bull, W. B. (1980). *Geologic map of the Parker, NW, Parker, and parts of the Whipple Mountains, SW and Whipple Wash quadrangles, California and Arizona* U. S. Geological Survey, Reston, VA.

Duffield, W.A.; Richter, D.H.; Priest, S.S. 1995. Geologic map of the Taylor Creek Rhyolite and adjacent rocks, Catron and Sierra Counties, New Mexico. *U.S. Geological Survey Map I-2399.* Scale 1:50,000. Pamphlet 16 p.

Duffield, Wendell A., Donald H. Richter, and Susan S. Priest, 1995, "Physical volcanology of silicic lava domes as exemplified by the Taylor Creek Rhyolite, Catron and Sierra Counties, New Mexico." *US Geol Surv Map I-2399*1.50,000.

Faulds, J. E., Feuerbach, D. L., Miller, C. F., & Smith, E. I. (2001). Cenozoic evolution of the northern colorado river extensional corridor, southern nevada and northwest arizona. *Guidebook - Pacific Section, American Association of Petroleum Geologists,78*, 239-271.

Faulds, J.E., Smith, E.I., and Gans, P., 1999, Spatial and temporal patterns of magmatism and extension in the northern Colorado River extensional corridor, Nevada and Arizona: A preliminary report: Nevada Petroleum Society Guidebook, p. 171-183.

Ferguson, C.A., 2008, Silver Creek caldera, probable source of the Miocene Peach Spring Tuff, Oatman Mining District, Arizona (abs.): Geological Society of America Abstracts with Programs, v. 40, no. 1, p. 33.

Ferguson, C. A., McIntosh, W. C., & Miller, C. F. (2013). Silver creek caldera; the tectonically dismembered source of the peach spring tuff. *Geology (Boulder), 41*(1), 3-6.

Fink, J. H., 1983, Structure and emplacement of a rhyolitic obsidian flow: Little Glass Mountain, Medicine Lake Highland, northern California, Geological Society of America bulletin, v. 94, p. 362-380

Foster, D. A., Schafer, C., Fanning, C. M., & Hyndman, D. W. (2001). Relationships between crustal partial melting, plutonism, orogeny, and exhumation; idaho-bitterroot batholith. *Tectonophysics, 342*(3-4), 313-350.

Foster, D. A., Miller, C. F., Harrison, T. M., & Hoisch, T. D. (1992). (Super 40) ar/ (super 39) ar thermochronology and thermobarometry of metamorphism, plutonism, and tectonic denudation in the old woman mountains area, california; with suppl. data 92-05. *Geological Society of America Bulletin, 104*(2), 176-191.

Gans, P. B. (1997). Large-magnitude Oligo-Miocene extension in southern Sonora: Implications for the tectonic evolution of northwest Mexico. *Tectonics, 16*(3), 388-408.

Gans, P.B., Mahood, G.A., and Schermer, E., 1989, Syn extensionalmagnetism in the Basin and Range Province; A case study from the eastern Great Basin: Geological Society of America Special Paper 233, 53 p.

Gans, P. B. (1987), An open-system, two-layer crustal stretching model for the Eastern Great Basin, Tectonics, 6(1), 1–12.

Gans, P. B., & Bohrson, W. A. (1998). Suppression of volcanism during rapid extension in the basin and range province, united states. *Science, 279*(5347), 66-68.

Gans, P. B., & Gentry, B. J. (2016). Dike emplacement, footwall rotation, and the transition from magmatic to tectonic extension in the whipple mountains metamorphic core complex, southeastern california. *Tectonics, 35*(11), 2564-2608.

Greeley, R., 1982, The Snake River Plain, Idaho: Representative of a new category of volcanism: Journal of Geophysical Research, v. 87, p. 2705-2712.

Greeley, R., and King, J.S., 1977, eds., Volcanism of the eastern Snake River Plain, Idaho: A Comparative planetary guidebook: Washington, D.C., National Aeronautics and Space Administration, 308 p.

Hazlett, R. W. (1986) Geology of a Tertiary volcanic center, Mopah range, San Bernardino County, California. [Ph.D. dissert.]: Los Angeles, University of Southern California, 267 p.

Hazlett; (1993). Stratigraphic section of the central Mopah Range, Calif. *In* Tertiary stratigraphy of highly extended terranes, California, Arizona, and Nevada, U.S. Geological Survey Bulletin 2053

Howard, K. A., & John, B. E. (1987). Crustal extension along a rooted system of imbricate low-angle faults; colorado river extensional corridor, california and arizona. *Geological Society Special Publications, 28*, 299-311.

Howard, K. A., Nielson, J. E., Wilshire, H. G., Nakata, J. K., Goodge, J. W., Reneau, S. L., John, B. E., Hansen, V. L. (1999), Geologic map of the Mohave Mountains area, Mohave County, western Arizona, US geological survey

Hughes, S.S., Smith, R.P., Hackett, W.R., and Anderson, S.R.,1999, Mafic Volcanism and Environmental Geology of the Eastern Snake River Plain, Idaho, *in* Hughes, S.S., and Thackray, G.D., eds., Guidebook to the Geology of Eastern Idaho: Idaho Museum of Natural History, p. 143-168.

John, B. (1987) Geologic Map of the Chemehuevi Mountains area San Bernadino County, California and Mohave county, Arizona, US Geological Survey

Johnson, D. M., Hooper, P. R., & Conrey, R. M. (1999). XRF Method XRF Analysis of Rocks and Minerals for Major and Trace Elements on a Single Low Dilution Li-tetraborate Fused Bead. *Advances in X-ray Analysis, 41*, 843-867.

Nielson and Nakata (1993). Tertiary stratigraphy and structure of the northern Turtle Mountains, Calif. *in* Tertiary stratigraphy of highly extended terranes, California, Arizona, and Nevada, U.S. Geological Survey Bulletin 2053

Lackey, J. S., Cecil, M. R., Windham, C. J., Frazer, R. E., Bindeman, I. N., & Gehrels, G. E. (2012). The Fine Gold Intrusive Suite: The roles of basement terranes and magma source development in the Early Cretaceous Sierra Nevada batholith. *Geosphere*, *8*(2), 292-313.

Laurent, V., Beaudoin, A., Jolivet, L., Arbaret, L., Augier, R., Rabillard, A., Menant, A., 2015. Interrelations between extensional shear zones and synkinematic intrusions: the example of Ikaria Island (NE Cyclades, Greece). Tectonophysics 651–652, 152–171.

Lister, G. S., and S. L. Baldwin (1993), Plutonism and the origin of metamorphic core complexes, Geology, 21(7), 607–610.

Lister, G. S., and Davis, G. S., 1989, The origin of metamorphic core complexes and detachment faults formed during Tertiary continental extension in the northern Colorado River region, U.S.A.: Journal of Structural Geology, Vol. 11, No. ½, pp. 65-94

Lucchitta, I., and Suneson, N. H. (1994a), Geologic map of the Casteaneda Hills Quadrangle, Mohave County, Arizona, US Geological Survey, Flagstaff, Arizona

Lucchitta, I., and Suneson, N. H. (1994b), Geologic map of the Casteaneda Hills SW Quadrangle, Mohave and La Paz Counties, Arizona, US Geological Survey, Flagstaff, Arizona

Nielson, J. E., & Beratan, K. K. (1990). Tertiary basin development and tectonic implications, Whipple detachment system, Colorado River extensional corridor, California and Arizona. *Journal of Geophysical Research, 95*, 599-614.

Nielson and Nakata (1993). Tertiary stratigraphy of highly extended terranes, California, Arizona, and Nevada, U.S. Geological Survey Bulletin 2053

Nielson, J. E., & Turner, R. D. (1986). *Miocene rocks of the northern turtle mountains, san bernardino county, california* Geol. Soc. Am., Boulder, CO.

Nielson, J. E., Lux, D. R., Dalrymple, G. B., & Glazner, A. F. (1990). Age of the peach springs tuff, southeastern california and western arizona. *Journal of Geophysical Research, 95*, 571-580.

Pálmason, G. (1981), Crustal rifting, and related thermo-mechanical processes in the lithosphere beneath Iceland, Geol. Rundsch., 70(1), 244–260.

Parsons, T., & Thompson, G. A. (1993). Does magmatism influence low-angle normal faulting? *Geology (Boulder), 21*(3), 247-250.

Putirka, K., & Platt, B. (2012). Basin and range volcanism as a passive response to extensional tectonics. *Geosphere, 8*(6), 1274-1285, 12.

Rehrig, W. A., and S. J. Reynolds (1980), Geologic and geochronologic reconnaissance of a northwest-trending zone of metamorphic core complexes in southern and western Arizona, in Cordilleran Metamorphic Core Complexes, Geol. Soc. Am. Mem., vol. 153, edited by M. S. Crittenden Jr., P. J. Coney, and G. H. Davis, pp. 131–157

Sherrod and Nielson, (1993), Tertiary stratigraphy of highly extended terranes, California, Arizona, and Nevada, U.S. Geological Survey Bulletin 2053

Spell, T. L., & McDougall, I. (2003). Characterization and calibration of 40 Ar/39 Ar dating standards. *Chemical Geology*, *198*(3), 189-211.

Spencer, J. E., S. M. Richard, S. J. Reynolds, R. J. Miller, M. Shafiqullah, W. G. Gilbert, and M. J. Grubensky (1995), Spatial and temporal relationships between mid-Tertiary magmatism and extension in southwestern Arizona, J. Geophys. Res., 100(B6), 10,321–10,351, doi:10.1029/94JB02817.

Stone, Paul, and Howard (1979), Compliation of geologic mapping in the Needles 1°x2° sheet, California and Arizona, US Geological Survey

Thompson, G. A., and J. McCarthy (1990), A gravity constraint on the origin of highly extended terranes, Tectonophysics, 174, 197-206

Thordarson, T., and Á. Höskuldsson (2008), Postglacial volcanism in Iceland, Jökull, 58, 197–228.

Wells, S. G., Dohrenwend, J. C., McFadden, L. D., Turrin, B. D., and Mahrer, K. D., 1985, Late Cenozoic landscape evolution on lava flow surfaces of the Cima volcanic field, Mojave Desert, California: Geological Society of America Bulletin, v. 96, p. 1518-1529.

Wernicke, B., Walker, J. D., and Beaufait, M. S., 1985, Structural discordance between Neogene detachments and frontal Sevier thrusts, central Mormon Mountains, southern Nevada: Tectonics, v. 4, p. 213–246

Whitney, D.L., Teyssier, C., Rey, P., Buck, W.R., 2013. Continental and oceanic core complexes. Geological Society of America Bulletin 125 (3/4), 273–298.

Wise, W. S., 1966, Geologic map of the Pisgah and Sunshine Cone lava fields: National Aeronautics and Space Administration Technical Letter, v. 11, 8 p.

Yin, A., & Dunn, J. F. (1992). Structural and stratigraphic development of the whipple-chemehuevi detachment fault system, southeastern california; implications for the geometrical evolution of domal and basinal low-angle normal faults. *Geological Society of America Bulletin*, *104*(6), 659-674.

Chapter 2 - New constraints on timing of initiation of volcanism in the vicinity of the Whipple Mountains, Lower Colorado River Extensional Corridor, CA and AZ

Mary Kate Fidler[1] and Phillip B. Gans[1]

[1]*Department of Earth Science, University of California, Santa Barbara, CA*

A. Abstract

Early mafic volcanic units in the Whipple Mountains area have proven difficult to precisely date, particularly on the eastern side of the corridor (e.g. Mohave Mountains area) where many exposures have been subject to K-metasomatism. These rocks have previously yielded K-Ar and zircon fission track ages from 23-20 Ma with large analytical and geologic uncertainties. We present new $^{40}Ar/^{39}Ar$ ages of the freshest available early volcanic units from the ranges surrounding the Whipple Mountains that are more precise than previously published ages for these volcanic successions. Within the early mafic succession, the oldest ages are ~21.1 Ma, and ages get as young as 18.0 Ma. The basal flows from the Turtle Mountains on the western side of the corridor (21.17 ± 0.10 Ma) and the Standard Wash on the eastern side of the corridor (21.00 ± 0.10 Ma) overlap in analytical uncertainty. Presented ages indicate that no lavas older than ~21.1 Ma are present in the volcanic exposures surrounding the Whipple Mountains, and that there is no significant E-W variation in the timing of initiation of volcanism in this part of the corridor.

B. Introduction

Volcanism is commonly closely associated with crustal extension around the world, and though it is observed in both continental and oceanic rift systems, the exact nature of the relationship between extension and volcanism remains controversial in the Basin and Range. As discussed in Chapter 1, there has been a long standing debate over the role of magmatism in extensional environments. Most notably, debate has focused on whether magmatism is a passive consequence of tectonism (e.g. decompression melting) or if mantle derived melts play an active role triggering and/or localizing extension.

Some authors who favor an active influence of magmatism on continental extension have explored the impact of magmatic influx on crustal rheology (i.e. thermal triggering; Gans, 1987; Gans et al., 1989; Lister and Baldwin, 1993; Parsons and Thompson, 1993; Gans and Bohrson, 1998). Parsons and Thompson (1993) proposed that the processes of intrusion (thermal erosion), release of volatiles associated with magmatism, and partial melting of the crust are likely important promoters of rheological weakening. They also propose that intrusions may explain the paradox of low angle normal faulting because transient stress pulses associated with dike emplacement can re-orient principles stresses.

Despite plausibility of many of these mechanism, debate has persisted because the precise timing of the onset of volcanism relative to the onset of tectonic extension has been variably documented by different authors. Authors such as Gans et al. (1989), Armstrong and Ward (1991), Gans and Bohrson (1998), and Faulds et al. (1999) document in several highly extended areas that volcanism predates extension, compatible with a thermal weakening model. Controversy continues however because other authors (eg. Putrika and Platt, 2012) argue that volcanism postdates extension, and that volcanism is therefore a passive response to extensional tectonics.

The Colorado River Extensional Corridor (CREC; Figure 17) is one of the places where volcanic successions have been studied in order to explore whether a causal relationship with extension exists. Early authors noted the northward migration of both extension (Glazner and Bartley, 1984) and volcanism (Glazner and Supplee, 1982) in the corridor, attributing this pattern to the northward migration of the Mendocino Triple Junction. The best constraints on the relative timing of extension and volcanism come from the northern CREC (NCREC) where Gans (1989) and Faulds and colleagues (1994, 1999, 2001) concluded that volcanism immediately predated the inception of extension through most of the corridor.

The age of the onset of volcanism in the lower CREC (LCREC; defined here as the part of the CREC south of the Dead Mountains) in the vicinity of the Whipple Mountains has been less precisely constrained than in other parts of the corridor, particularly on the eastern side of the corridor where >1 km thick accumulations of early mafic volcanics have proven difficult to date. Since the pioneering work in the Whipple Mountains by Davis et al. (1980) on the Whipple Detachment Fault, this area has been a key example in competing models of continental extension. Thus, it is a valuable place to explore the role that magmatism may have played in its extensional history.

In this study, we present new $^{40}Ar/^{39}Ar$ ages for the oldest volcanic rocks spanning the width of the CREC in the vicinity of the Whipple Mountains (Figure 18). This data substantially improves existing constraints for the onset of volcanism in this part of the corridor. Precisely dating initiation of volcanism in this area is key for future studies of both local and regional scale magmatic patterns and for evaluating the applicability of passive vs. active rifting models for the LCREC.

C. Geologic setting

1. Extensional history

The general geologic history and importance of the CREC is described in Chapter 1. In short, the LCREC has accommodated more than 100% of northeast-directed Miocene crustal extension (Davis et al., 1980; Howard and John 1987; Reynolds and Spencer, 1985; Nielson and Beratan, 1990) over a relatively narrow area (~150 km) coupled with voluminous volcanic outpourings and synextensional sedimentation. Direct evidence of extension within the corridor includes both exhumation of middle crustal rocks along the WDF and faulting at shallow crustal levels.

Researchers in the area have successfully dated the onset of extension normal faulting in numerous locations up and down the corridor. Commonly, the maximum age of onset of faulting is determined by dating the youngest, most steeply tilted unit that predates significant tilt fanning or angular unconformities, and the the upper age is constrained by dating flat lying, unfaulted strata (e.g. Faulds et al, 1995, 1999; Nielson and Beratan, 1995; Campbell and John, 1996; Harlan et al, 1998; Chapter 1). Faulds et al. (2001) found that volcanism propagated northward up the CREC from ~22 Ma in the south to ~12 in the north and predated the inception of extension by 1 to 4 million years, which also propagated northward at rates of about 2 to 3 cm/yr (Gans et al, 1989; Faulds et al, 1999). Eruptive rates generally peaked just prior to extension throughout the corridor and declined significantly during peak extension (e.g. Faulds et al, 1995; Gans and Bohrson, 1998).

In the vicinity of the Whipple mountains however, directly dating the earliest volcanic units and the onset of extension has been hampered by pervasive alteration, poor sample selection, and geochronologic methods with relatively large uncertainties (primarily

K-Ar) that have resulted in conflicting data. Detailed studies of the stratigraphy and sedimentary evolution of upper plate basins have provided insights into the geometry and kinematics of extension in this area (e.g. Miller and John, 1988; Nielson and Beratan, 1995). Foster et al (1990) and John and Foster (1993) performed thermochronology in the lower plate in order to date the inception of rapid cooling associated with Miocene slip on the Chemehuevi detachment faults. Using these indirect methods to date extension, they hypothesized that extension may have begun as early as 24-22 Ma, though other authors working on the Cenozoic sedimentary and volcanic stratigraphy have found no evidence that extensional faulting began earlier than ~20 Ma (e.g. Nielson and Beratan, 1995).

2. Previous work on age of early LCREC volcanics

Many volcanic rocks in the Whipple Mountains area have proven difficult to reliably date by traditional K-Ar methods, resulting in conflicting ages and large uncertainties. The oldest volcanic units, having experienced deepest burial, are more likely to be effected by hydrothermal alteration (eg. K-metasomatism; Beratan, 1999) making the base of the volcanic section difficult to precisely date in some areas. Existing published ages for early volcanic units of the ranges surrounding the Whipple Mountains are outlined below and summarized in Figures 19 and 20. Unless otherwise specified, all previously published age data discussed below are K-Ar ages that have been recalculated from original dates (using monitor ages of Dalrymple and Duffield, 1988) to reflect recent advances in calibrating monitor ages (Spell and McDougal, 2003). Ages discussed below represent the most widely accepted ages for early volcanism in the Whipple Mountains area, most of which are included in the stratigraphic summaries by Sherrod and Neilson (1993) and references therein. The majority of these ages are cited from personal communications and their

original data were never published, making it impossible to evaluate the analytical and geologic uncertainties of these ages.

On the eastern side of the corridor, In the Crossman Peak Block of the Mohave Mountains, Standard Wash, and Aubrey Hills, few ages exist for lavas in the lower ~600 m of the volcanic section. Beratan (1990) dated the lowest volcanic unit in the Aubrey Hills, a tuff interbedded with mafic lava flows ~350 m from the base of the section, and obtained a highly imprecise zircon fission track age of 23 ± 2.4 Ma. Ages from much higher in the section (~950-1400 m above the base) from Nakata et al. (1990) yield rhyolite biotite ages from 20.8 ± 1.6 to 19.4 ± 0.6 Ma, and a mafic whole rock age of 20.1 ± 0.6 Ma. To the North in the Mohave Mountains, the oldest rocks dated were also well above the base of the section and yield ages of 21.8 ± 0.5 for a mafic whole rock sample (Nielson, 1993) and 20.8 ± 0.5 and 20.2 ± 0.5 Ma for biotite and plagioclase respectively from a tuff (Nielson et al., 1993).

The ranges on the western side of the corridor have yielded more consistent ages of early volcanism. Erosional remnants of basalt and basaltic andesite that cap the high crystalline terrane of the southern Turtle Mountains were approximately dated to be ~20.3 Ma by Woodward-McNiell and associates (1974). Just east in the southern Turtle Mountains where K-metasomatism is less widespread, more units have been dated close to the base of the section. The lowest unit dated was an andesite lava flow, which gave the same whole rock age of 20.3 ± 0.5 Ma as biotite from the Mopah Peak rhyolite plug in the central Mopah Range (also 20.3 ± 0.5 Ma; Nielson and Nakata, 1993). Tuffs interbedded with the oldest mafic lavas of the northern Turtle Mountains yielded biotite ages of 20.5 ± 1.0 and 20.3 ± 0.7 Ma (Howard et al, 1982) and biotite from two rhyolite feeder dikes that cut this part of the section were dated to be 19.8 ± 0.2 and 20.0 ± 0.2 Ma (Nielson and Nakata, 1993). Just

to the south, in the central Mopah Range, a flow near the top of the older mafic succession gave a whole rock age of 20.7 ± 0.4 Ma (Hazlett, 1993). In the Northern Stepladder Mountains, the earliest volcanic units are dated to a similar precision. The whole rock separate of the basal flow of the volcanic section, a basanite lava, was dated at 22.0 ± 0.5 Ma, and the overlying tuff gave a biotite age of 21.2 ± 0.5 Ma and a plagioclase age of 20.2 ± 0.5 Ma (Howard et al., 1993). All of these ages were obtained from lavas near the base of the section.

D. Methods

1. Sampling

The focus of sampling was to collect fresh samples as close as possible to the base of the section in regions where thick accumulations of volcanic rock are exposed (Figure 18). Sampling of mafic units targeted the coarse-grained lava flow interiors for dating of holocrystalline groundmass separates. In these rocks, potassium is concentrated in the rims of late crystalizing groundmass plagioclase. Analyzing coarse holocrystalline groundmass also minimizes the effects of reactor induced recoil which disproportionately affects glasses and fine grained groundmass, though recoil is not eliminated completely. Sampling of silicic units targeted vitrophyric horizons for analysis of plagioclase phenocrysts.

2. $^{40}Ar/^{39}Ar$ Geochronology

A total of 13 age determinations were made from volcanic units in the field area using the $^{40}Ar/^{39}Ar$ method (Table 3; Figure 21; Appendix V). Mineral separation and analytical techniques are described in Chapter 1. All data were monitored using Taylor

Creek Rhyolite sanidine. Samples were originally calibrated using an age of 27.92 Ma (Dalrymple and Duffield, 1988) and were recalculated using an adjusted assumed age of 28.35 Ma for Taylor Creek Rhyolite, in order to bring our ages into equivalence with the now widely accepted age of 28.1 Ma for Fish Canyon sanidine (Spell and McDougal, 2003). For preferred ages in which individual steps of the plateau overlap in analytical uncertainty, reported errors are ± 2 σ (95% confidence) precision. For ages where individual steps of chosen "plateau" do not overlap in analytical uncertainty, the reported error spans the age variation of all chosen steps.

E. Results

A summary of both the pre-existing dating and representative new ages of early volcanic rocks of the Turtle Mountains, Stepladder Mountains and Sawtooth Range, Mopah Range, western Whipple Mountains, eastern Chemehuevi Mountains, Aubrey Hills and Standard Wash, and Mohave Mountains (Crossman Peak Block) is presented in Figures 19 and 20, and new ages are presented in Table 3 representative age spectra are shown in Figure 21 (tabulated data and all age spectra in Appendix V). New ages for the base of the volcanic section in the Turtle Mountains, Aubrey Hills/Standard Wash, and Mohave Mountains greatly improves constraints on onset of volcanism in these ranges where precise geochronology was lacking (Figure 20).

The most reliable age for LCREC early volcanism comes from the basal lava flow in the southern Turtle Mountains, an olivine-clinopyroxene basalt (TTM-01). A groundmass separate yielded a slightly "u" shaped age spectrum with a weighted mean age of 21.17 ± 0.10 Ma, precisely dating the inception of volcanism on the eastern edge of the corridor. The

overlying plagioclase-clinopyroxene-olivine basaltic andesite flow (TTM-02) is much less reliable, showing strong reactor induced recoil and no plateau. The assigned age of 21.07 ± 0.2 for this unit is interpretive.

The Aubrey Hills and Standard Wash are interpreted to contain correlative sections repeated across a buried normal fault. A groundmass separate from the basal olivine-clinopyroxene basalt directly overlying Proterozoic basement in Standard Wash (MK13-4.6) produced an age spectrum with some reactor induced recoil and a high temperature flat yielding a weighted mean age of 21.00 ± 0.10 Ma. This is the highest quality age obtained on the eastern side of the corridor, and we interpret it to precisely date the inception of volcanism in this region. The next best age comes from a "turkey-track" plagioclase-clinopyroxene-olivine basaltic andesite in the Aubrey Hills (AB-01). A groundmass separate produced a u-shaped age spectrum displaying both recoil and excess argon. A high temperature flat at the base of the "u" yielded a weighted mean age of 20.61 ± 0.08 Ma and is interpreted as a reliable age. Unreliable ages were obtained from groundmass separates of an olivine-clinopyroxene basalt ~15 m above the base of the section in Standard Wash (MK13-4.4) and another turkey-track basaltic andesite in the Aubrey Hills (MK13-2.4). We interpret the 18.9 ± 1.0 Ma age of the former to be a hydrothermal alteration age due to unrealistically high K/Ca ratios, and assign an uncertain, interpretive age of 19.8 ± 0.5 Ma to the latter which displays a disturbed spectrum.

One lower mafic sample was dated from the Mohave Mountains, just east of Lake Havasu City, ~300 m above the base of the section (MHV-10). A groundmass separate of this "turkey-track" basaltic andesite displayed recoil with a high temperature flat, yielding a weighted mean age of 20.90 ± 0.15 Ma. This age is consistent with that obtained for the lowest flow in the nearby Standard Wash (MK13-4.6). Two moderately dipping

clinopyroxene-olivine basaltic andesite lavas sit in ~40° angular unconformity above the older succession containing MHV-10. Both of these samples (MHV-01 and MHV-04) yielded lightly disturbed spectra with reactor induced recoil. Our preferred ages for these samples are 19.50 ± 0.15 and 19.4 ± 0.3 Ma respectively.

Two other lavas were dated from the northern end of the Mohave Mountains. A steeply tilted basalt (MHV-14) that directly overlies basement and arkosic conglomerate displayed a disturbed, hump-shaped spectrum, exhibiting both Ar loss and recoil. Our best approximation of the age of this sample is 18.5 ± 0.3 Ma, but high K/Ca rations suggests that this is likely a hydrothermal age. A steeply tilted basaltic andesite (MHV-12) which overlies this lava by ~300 m gave an older, more reliable age. A groundmass separate produced an excellent simple flat spectrum, yielding a weighted mean age of 19.89 ± 0.08 Ma.

Lastly two ages are presented from rhyolites low in the section in the northern Mopah Range near the Craik perlite mine (MK13-7.1) and Mopah Springs (MK13-7.4), both yielding excellent simple flat spectra for plagioclase separates and weighted mean ages of 20.32 ± 0.08 and 20.25 ± 0.08 Ma respectively.

F. Discussion

1. No evidence for E-W variation in age on onset of volcanism

The two most reliable $^{40}Ar/^{39}Ar$ ages for early mafic volcanism come from the basal lava flows on opposite sides of the corridor. Armed with this we are confident that we have precisely dated the inception of volcanism on the western and eastern sides of the corridor at 21.17 ± 0.10 and 21.00 ± 0.10 Ma, respectively. These data, and other previously published ages from the northern Mopah Range are consistent, showing that volcanism began at

approximately the same time across this portion of the corridor. Based on Howard and John's (1987) estimate that these locations have been extended by ~50 km since the Miocene, at the time of early volcanism, these sample sites were likely 15-20 km apart. These data are consistent with previously published ages for the LCREC, but significantly reduce uncertainties allowing for comparison with published ages of extensional onset.

One implication to consider, is what this consistency of ages of initial volcanism across the corridor may imply about the eruptive centers. It is possible that these lavas erupted from separate fissure vents spaced across the corridor, spreading and overlapping with each other to form a composite surface. Alternatively, consistent ages and remarkable petrologic similarity may suggest that some of these lava flows (particularly the oldest ones) are in fact single flows from monogenetic eruptions with runout distances upwards of ~15-20 km. If this is the case, the thicker sections of early mafic lavas to the east and thinner sections to the west could indicate that the source for these early mafic lavas existed on the eastern side of the corridor prior to the inception of extension.

2. Volcanism began at ~21 Ma in the Whipple Mountains area

This study provides evidence that the inception of volcanism, consisting of outpourings of mainly mafic volcanism, began at ~21.1 Ma. This finding agrees with the some of the previously published geochronology discussed above (e.g. Sherrod et al., 1993 and references therein), though analytical uncertainties of this new data are smaller, allowing us to dismiss some previously published older ages such as ages up to 25 Ma (Spencer et al., 1995) and the 23 Ma age presented by Beratan (1990) which is commonly cited as the age of inception of volcanism for this region (e.g. Putrika and Platt, 2012). Some of the older ages for inception of extension (e.g. Foster, 1990; 1993) are also suspect as they are not supported

by any of the stratigraphic or structural relations in the Miocene section. However, based on the 19-20 Ma age for the onset of extension presented by Nielson and Beratan (1990; 1995) and Chapter 1, it appears that volcanism predated the inception of extension by 1-2 Ma.

G. Conclusion

New $^{40}Ar/^{39}Ar$ geochronology for early volcanic rocks in the Whipple Mountains area provide new precise constraints for the timing of the earliest volcanic activity in this part of the CREC. Volcanism began at ~21.1 Ma on both the western and eastern sides of the LCREC in the vicinity of the Whipple Mountains. Consistent ages of the basal basalt flows on both the most easterly and westerly exposures of Miocene volcanic rocks in this part of the LCREC suggest that there was no E-W variation in the timing of the onset of volcanism across the corridor. Ages presented are consistent with previously published ages of these volcanic succession but provide improved precision in age resolution.

Figure 17

Figure 17. Generalized map of the western US showing major physiographic provinces, and important tectonic features, and approximate boundaries of the Colorado River Extensional Corridor. Gray shading is the approximate extent of the Basin and Range physiographic province. Black areas are Cordilleran metamorphic core complexes. W, Whipple Mountains; LV, Las Vegas; MTJ, Mendocino triple junction. Red inset is location of Figure 18. Figure edited slightly from Gans and Bohrson, 1998.

Figure 17

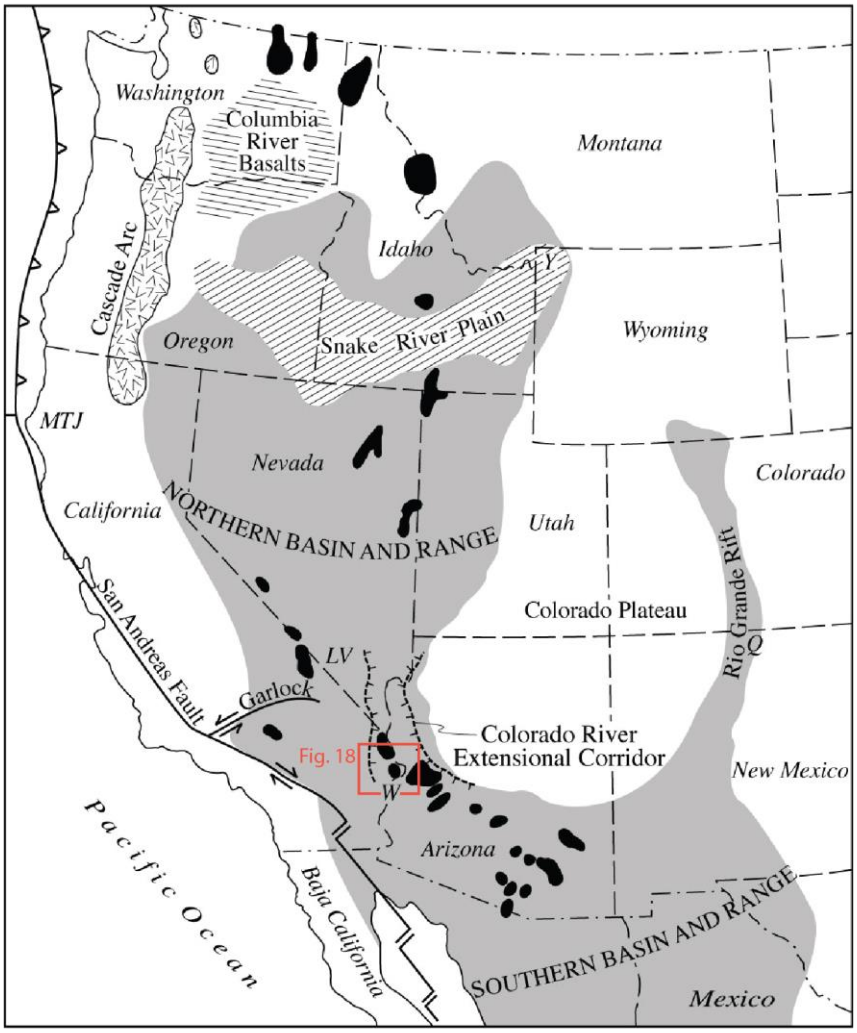
Washington
Columbia River Basalts
Montana
Idaho
Cascade Arc
Oregon
Snake River Plain
Wyoming
MTJ
Nevada
Colorado
California
NORTHERN BASIN AND RANGE
Utah
Rio Grande Rift
Colorado Plateau
San Andreas Fault
LV
Garlock
Colorado River Extensional Corridor
Fig. 18
New Mexico
Arizona
Pacific Ocean
Baja California
SOUTHERN BASIN AND RANGE
Mexico

Figure 18

Figure 18. Simplified geologic map of the Whipple Mountains region of the LCREC with locations discussed in text. Mapping simplified from Yin and Dunn, 1992. Clockwise from the NW corner - SL, Stepladder Mountains; SR, Sawtooth Range; CH, Chemehuevi Mountains; MHV, Mohave Mountains (Crossman Peak Block); SW, Standard Wash; AB, Aubrey Hills; WWM, Western Whipple Mountains; MP, Mopah Range; TTM, Turtle Mountains; NT, Northern Turtle Mountains. Numbers are locations of samples presented in this study. (1) AB-01, MK13-2.4, (2) MK13-4.4, MK13-4.6, (3) MHV-01, MHV-04, MHV-10, (4) MHV-12, MHV-14, (5) TTM-01, TTM-02, (6) MK13-7.4, (7) MK13-7.1.

Figure 18

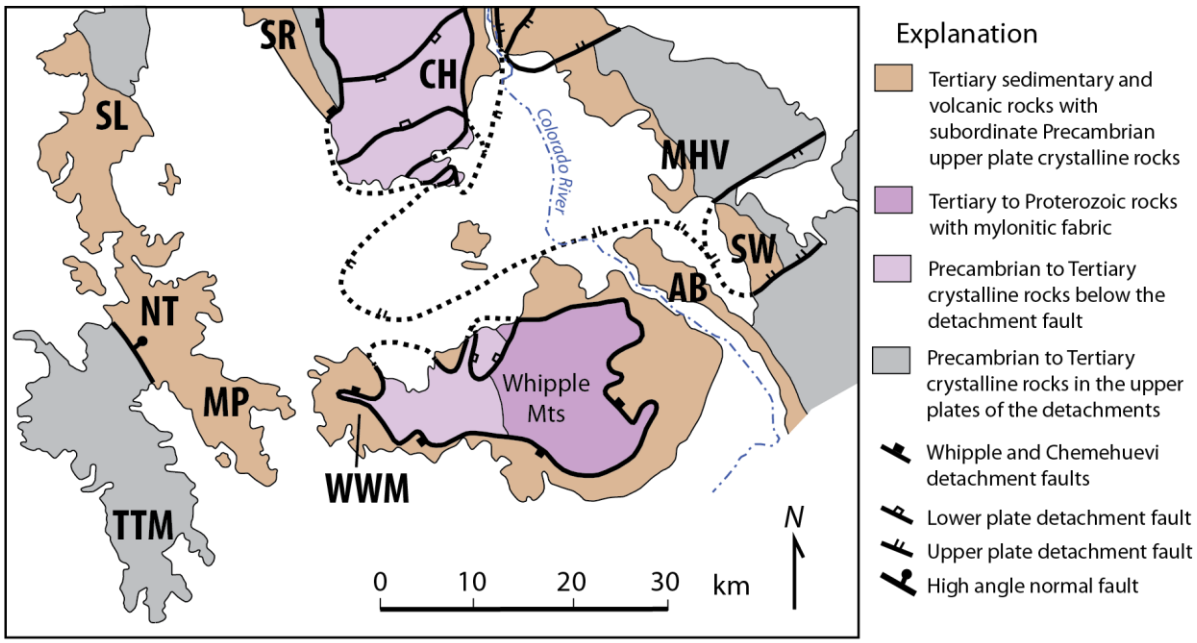
SR
CH
SL
Colorado River
MHV
SW
AB
NT
MP
Whipple
Mts
WWM
TTM
0
10
20
30
km
N
Explanation
Tertiary sedimentary and volcanic rocks with subordinate Precambrian upper plate crystalline rocks
Tertiary to Proterozoic rocks with mylonitic fabric
Precambrian to Tertiary crystalline rocks below the detachment fault
Precambrian to Tertiary crystalline rocks in the upper plates of the detachments
Whipple and Chemehuevi detachment faults
Lower plate detachment fault
Upper plate detachment fault
High angle normal fault

Figure 19

Figure 19. Generalized Tertiary stratigraphic sections and geochronological summary of early volcanic rocks (up to 18.8 Ma in age, pre-Peach Springs Tuff) in the LCREC, arranged approximately from west to east (left to right). Acronyms at base of column correspond to locations in Figure 2. Stratigraphic sections are after columns and/or descriptions in Howard et al. (1980, 1993), Nielson and Nakata (1993), Hazlett (1993), Miller and John (1993), Nielson (1993a, 1993b), and Chapter 1 of this dissertation. They are highly simplified and meant to illustrate variations in relative importance of mafic vs. silicic volcanism across the LCREC, rather than the details of stratigraphic relationships. Stratigraphic positions of all ages are approximate. Red ages are from various previous workers (discussed in text, K-Ar age recalculated to Fish Canyon Tuff age of 28.1 Ma). Green ages are from Chapter 1 of this dissertation. Blue ages are presented in this study. Black ages are the 18.8 Ma Peach Springs Tuff (Ferguson et al., 2013).

Figure 19

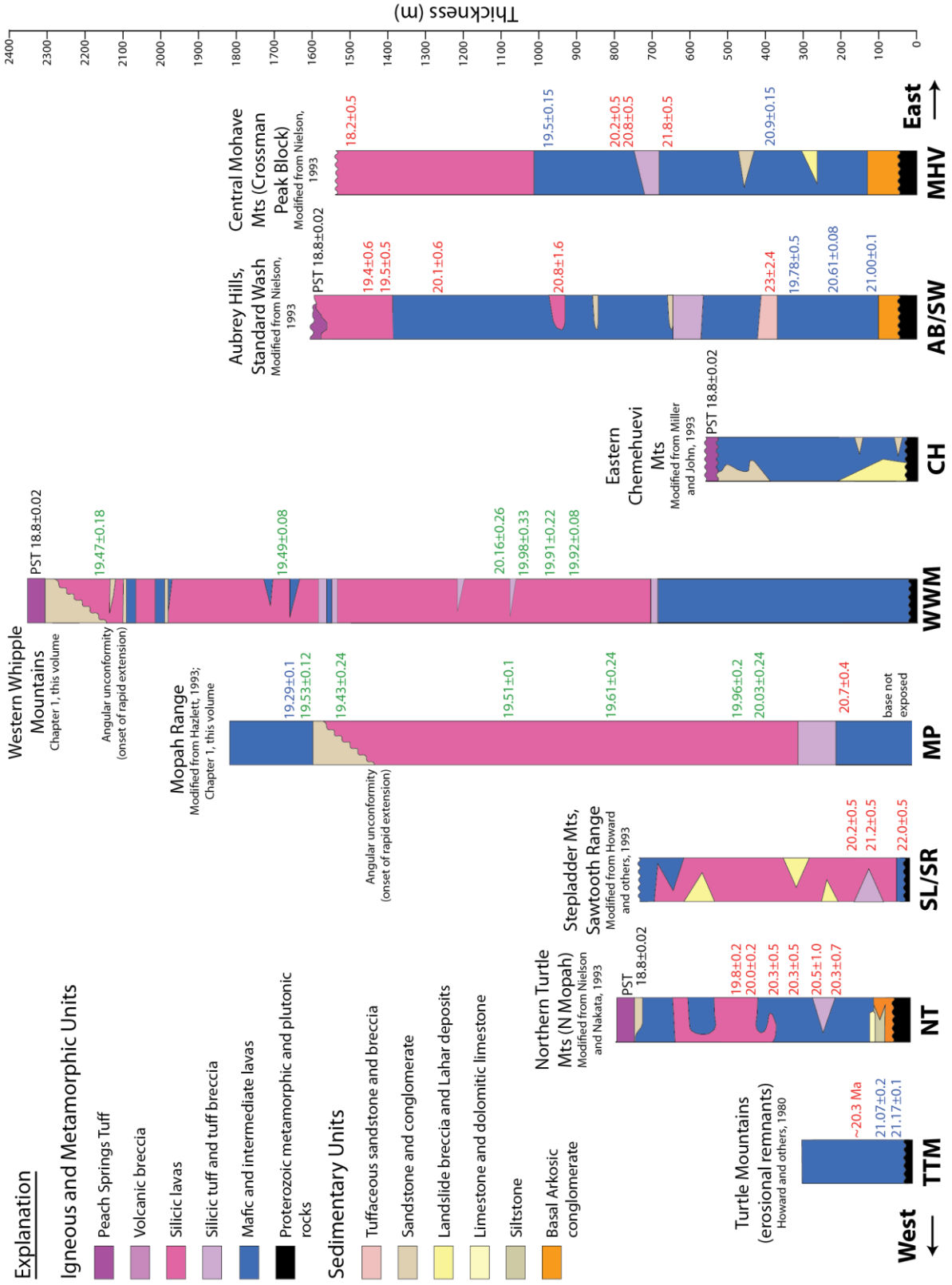
Thickness (m)
2400
2300
2200
2100
2000
1900
1800
1700
1600
1500
1400
1300
1200
1100
1000
900
800
700
600
500
400
300
200
100
0
Explanation
Igneous and Metamorphic Units
Peach Springs Tuff
Volcanic breccia
Silicic lavas
Silicic tuff and tuff breccia
Mafic and intermediate lavas
Proterozoic metamorphic and plutonic rocks
Sedimentary Units
Tuffaceous sandstone and breccia
Sandstone and conglomerate
Landslide breccia and Lahar deposits
Limestone and dolomitic limestone
Siltstone
Basal Arkosic conglomerate
West
East
Turtle Mountains (erosional remnants)
Howard and others, 1980
~20.3 Ma
21.07±0.2
21.17±0.1
TTM
Northern Turtle Mts (N Mopah)
Modified from Nielson and Nakata, 1993
PST 18.8±0.02
19.8±0.2
20.0±0.2
20.3±0.5
20.3±0.5
20.5±1.0
20.3±0.7
NT
Stepladder Mts, Sawtooth Range
Modified from Howard and others, 1993
20.2±0.5
21.2±0.5
22.0±0.5
SL/SR
Mopah Range
Modified from Hazlett, 1993; Chapter 1, this volume
19.29±0.1
19.53±0.12
Angular unconformity (onset of rapid extension)
19.43±0.24
19.51±0.1
19.61±0.24
19.96±0.2
20.03±0.24
20.7±0.4
base not exposed
MP
Western Whipple Mountains
Chapter 1, this volume
PST 18.8±0.02
Angular unconformity (onset of rapid extension)
19.47±0.18
19.49±0.08
20.16±0.26
19.98±0.33
19.91±0.22
19.92±0.08
WWM
Eastern Chemehuevi Mts
Modified from Miller and John, 1993
PST 18.8±0.02
CH
Aubrey Hills, Standard Wash
Modified from Nielson, 1993
PST 18.8±0.02
19.4±0.6
19.5±0.5
20.1±0.6
20.8±1.6
23±2.4
19.78±0.5
20.61±0.08
21.00±0.1
AB/SW
Central Mohave Mts (Crossman Peak Block)
Modified from Nielson, 1993
18.2±0.5
19.5±0.15
20.2±0.5
20.8±0.5
21.8±0.5
20.9±0.15
MHV

Figure 20

Figure 20. Previously published and new age constraints for pre-Peach Spring Tuff volcanism (<18.8 Ma) in Whipple Mountains area, LCREC. All ages presented in this study are shown in blue except MK13-4.4 which is interpreted to represent an alteration age. Previously published ages are shown in yellow and orange, grouped by study (alternating colors are for ease of distinguishing ages from each study). Oldest ages presented in this study are consistent with most previously published ages for early volcanism in the region, but constrain the onset of volcanism much more tightly.

Figure 20

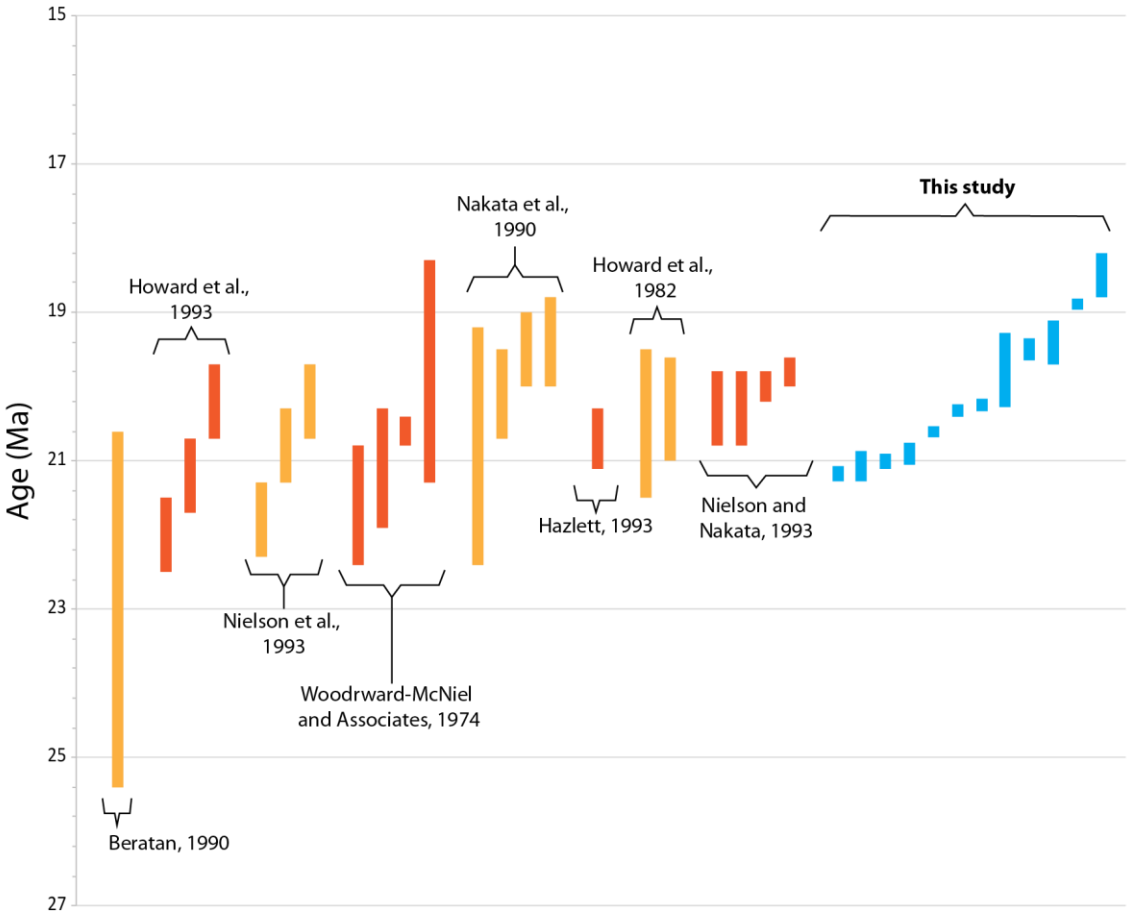
15
17
19
21
23
25
27
Age (Ma)
Howard et al., 1993
Nakata et al., 1990
Howard et al., 1982
This study
Nielson et al., 1993
Woodrward-McNiel and Associates, 1974
Hazlett, 1993
Nielson and Nakata, 1993
Beratan, 1990

Figure 21

Figure 21. Representative $^{40}Ar/^{39}Ar$ age spectra for early volcanic units from the Whipple Mountains region, LCREC. Interpreted weighted mean plateau age (WMPA) and 2σ uncertainty calculated from shaded steps. Integrated total fusion age (TFA). Sample name at top of each spectra, gm = groundmass and plag = plagioclase.

Figure 21

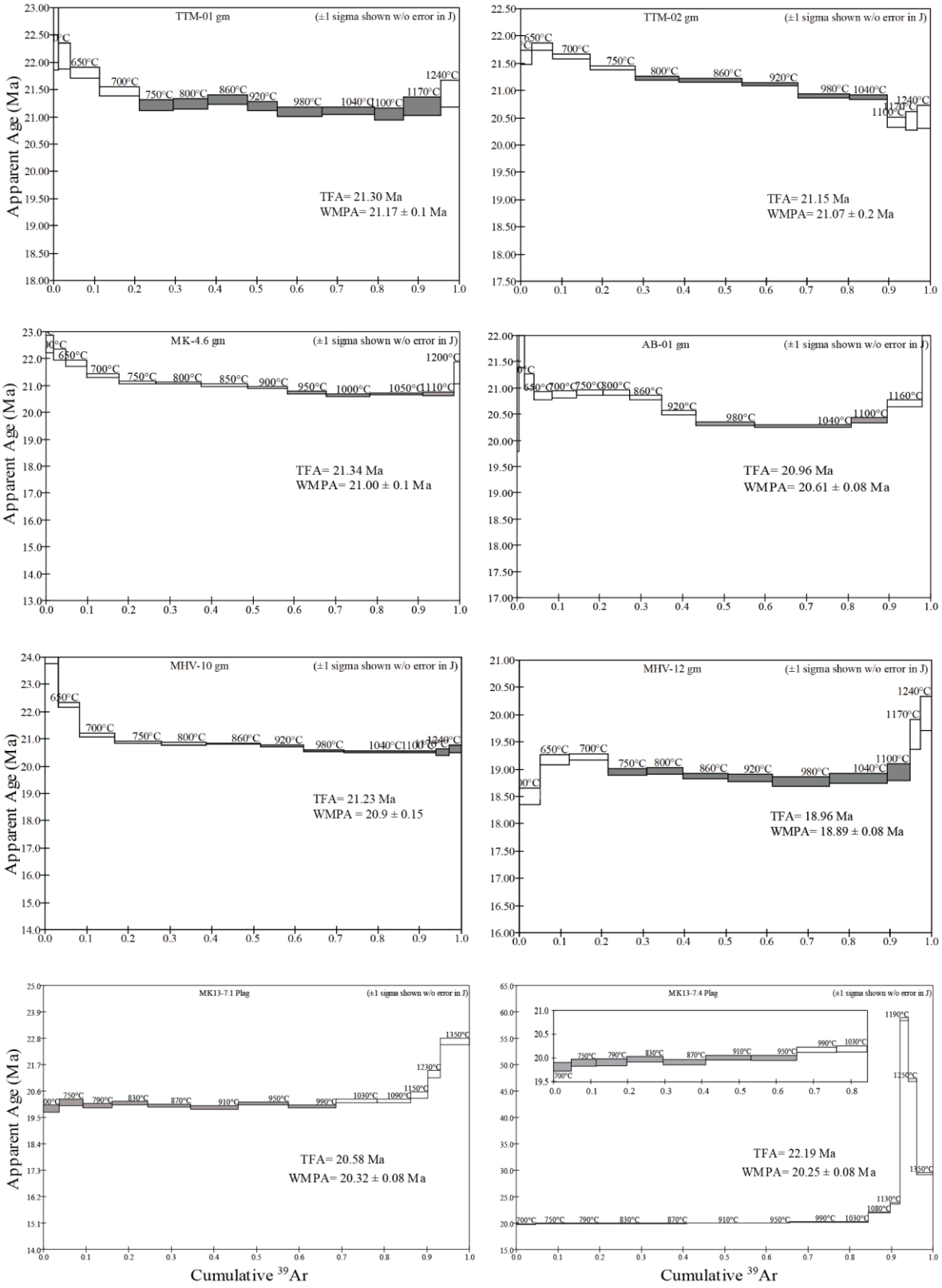
TTM-01 gm
(±1 sigma shown w/o error in J)
TFA= 21.30 Ma
WMPA= 21.17 ± 0.1 Ma
TTM-02 gm
(±1 sigma shown w/o error in J)
TFA= 21.15 Ma
WMPA= 21.07 ± 0.2 Ma
MK-4.6 gm
(±1 sigma shown w/o error in J)
TFA= 21.34 Ma
WMPA= 21.00 ± 0.1 Ma
AB-01 gm
(±1 sigma shown w/o error in J)
TFA= 20.96 Ma
WMPA= 20.61 ± 0.08 Ma
MHV-10 gm
(±1 sigma shown w/o error in J)
TFA= 21.23 Ma
WMPA = 20.9 ± 0.15
MHV-12 gm
(±1 sigma shown w/o error in J)
TFA= 18.96 Ma
WMPA= 18.89 ± 0.08 Ma
MK13-7.1 Plag
(±1 sigma shown w/o error in J)
TFA= 20.58 Ma
WMPA= 20.32 ± 0.08 Ma
MK13-7.4 Plag
(±1 sigma shown w/o error in J)
TFA= 22.19 Ma
WMPA= 20.25 ± 0.08 Ma
Apparent Age (Ma)
Cumulative ^{39}Ar

Table 3. New Geochronologic Data From the Lower Colorado River Extensional Corridor in the vicinity of the Whipple Mountains ($^{40}Ar/^{39}Ar$ Data from volcanic rocks)

Sample	Material	Preferred Age (Ma)	±	2σ	TFA	Comments
MK13-7.1†	Plag	20.32	±	0.08	20.58	Excellent flat spectrum
MK13-7.4†	Plag	20.25	±	0.08	22.19	Excellent flat spectrum
AB-01*†	GM	20.61	±	0.08	20.96	Recoil and excess argon
MK13-2.4*†	GM	19.8	±	0.5	19.94	Disturbed spectrum
MK13-4.4*†	GM	18.9	±	1.0	18.79	K/Ca ratios indicate alteration - hydrothermal age
MK13-4.6*†	GM	21.00	±	0.10	21.34	Recoil with high T flat, reliable age
TTM-01	GM	21.17	±	0.10	21.3	Excellent flat spectrum
TTM-02	GM	21.07	±	0.20	21.15	Strong recoil, no plateau, interpreted age
MHV-01	GM	19.50	±	0.15	19.71	Disturbed spectrum with recoil
MHV-04*	GM	19.4	±	0.3	19.92	Bouncy spectrum plus recoil
MHV-10*	GM	20.90	±	0.15	21.23	Recoil with high T flat
MHV-12	GM	18.89	±	0.08	18.96	Excellent flat spectrum
MHV-14*	GM	18.5	±	0.3	18.37	Highly disturbed hump-shaped spectrum, Ar loss and recoil

Note: Material abbreviations: Plag - plagioclase, Bio - Biotite, GM - groundmass. MP, AB, TTM, MHV and MK13 samples were collected and dated by Fidler and WM samples were collected and dated by Gans. Mineral separates were prepared and analyzed at UCSB. Preferred ages are weighted mean plateau ages from incremental heating experiments except where it is indicated in the comments that the isochron age is preferred.

* denotes samples where preferred weighted mean plateau ages were calculated from temperature steps that totaled less than 50% of gas.

† Ages were monitored using Taylor Creek Rhyolite sanidine, using an original calibration age of 27.92 Ma (Dalrymple and Duffield, 1988) and then recalculated using an adjusted calibration age 28.35 Ma, equivalent (R=1.00881 ± 0.00046) to the widely used Fish Canyon sanidine at 28.1 Ma (Spell and McDougal, 2003). See Appendix V for tabulated data and age spectra using the original calibration age.

All other ages were calculated using a calibration age for TCR of 28.35 Ma, equivalent to FCT at 28.1 Ma (Spell and McDougal, 2003). See Appendix V for tabulated data and spectra.

H. References

Armstrong, R. L., & Ward, P. L. (1991). Evolving geographic patterns of cenozoic magmatism in the north american cordillera; the temporal and spatial association of magmatism and metamorphic core complexes. *Journal of Geophysical Research, 96*, 13-13,224.

Beratan, K.K., 1990, Basin development during Miocene detachment faulting, Whipple Mountains, southeastern California: Los Angeles, University of Southern California, Ph.D. Dissertation, 267 p.

Beratan, K. K. (1999). Miocene potassium metasomatism, Whipple Mountains, southeastern California: A datable tracer of extension-related fluid transport. *Geology*, *27*(3), 259-262.

Caliza, J.P. and Morton, J. L., 1980, Compilation of isotopic ages within the Needles 1 by 2° quadrangle, California and Arizona: U.S. Geological Survey Open-file Report 80-1303

Campbell, E. A., John, B. E. (1996) Constraints on extension related plutonism from modeling of the Colorado River gravity high: GSA Bulletin, v. 108; no. 10; P. 1242-1255

Dalrymple, G. B., and Duffield, W. A. (1988). High Precision 40Ar/39Ar dating of Oligocene rhyolites from the Mogollon-Datil volcanic field using a continuous laser system. Geophysical research letters, vol. 15, no. 5, 463-466

Davis, G.A., Anderson, J.L., Frost, E.G., and Shackelford, T.J., 1980, Mylonitization and detachment faulting in the Whipple-Bucksin-Rawhide Mountains terrane, southeastern California and western Arizona, *in* Crittenden, M.D., Coney, P.J., and Davis, G.H., eds., Cordilleran Metamorphic Core Complexes: Geological Society of America Memoir 153, p. 9-129.

Faulds, J.E., Smith, E.I., and Gans, P., 1999, Spatial and temporal patterns of magmatism and extension in the northern Colorado River extensional corridor, Nevada and Arizona: A preliminary report: Nevada Petroleum Society Guidebook, p. 171-183.

Faulds, J. E., Gans, P. B., and Smith, E. I., 1994, Spatial and temporal patterns of extension in the northern Colorado River extensional corridor, northwestern Arizona and southern Nevada: Geological Society of America Abstracts with Programs, v. 26, no. 2, p. 51.

Faulds, J.E., Feuerbach, D.L., Reagan, M., Metcalf, R.V., Gans, P., and Walker, J.D., 1995, The Mount Perkins block, northwestern Arizona: An exposed cross section of an evolving, preextensional to synextensional magmatic system: Journal of Geophysical Research, v. 100, no. B8, p. 15,249-15,266.

Faulds, J. E., Feuerbach, D. L., Miller, C. F., & Smith, E. I. (2001). Cenozoic evolution of the northern colorado river extensional corridor, southern nevada and northwest arizona. *Guidebook - Pacific Section, American Association of Petroleum Geologists,78*, 239-271.

Foster, D. A., Harrison, T. M., Miller, C. F., Howard, K. A., Haxel, G. B., & Simpson, R. W. (1990). The (super 40) ar/ (super 39) ar thermochronology of the eastern mojave desert, california, and adjacent western arizona with implications for the evolution of metamorphic core complexes. *Journal of Geophysical Research, 95*, 5-20,024.

Gans, P. B. (1987). An open‐system, two‐layer crustal stretching model for the Eastern Great Basin. *Tectonics*, *6*(1), 1-12.

Gans, P. B., & Bohrson, W. A. (1998). Suppression of volcanism during rapid extension in the basin and range province, united states. *Science, 279*(5347), 66-68.

Gans, P. B., Mahood, G. A., & Schermer, E. R. (1989). Synextensional magmatism in the basin and range province; a case study from the eastern great basin. *Special Paper - Geological Society of America, 233*, 53-53.

Glazner, A. F., & Bartley, J. M. (1984). Timing and tectonic setting of tertiary low-angle normal faulting and associated magmatism in the southwestern united states. *Tectonics, 3*(3), 385-396.

Glazner, A. F., & Supplee, J. A. (1982). Migration of Tertiary volcanism in the southwestern United States and subduction of the Mendocino fracture zone. *Earth and Planetary Science Letters*, *60*(3), 429-436.

Harlan, S. S., Duebendorfer, E. M., & Deibert, J. E. (1998). New (super 40) ar/ (super 39) ar isotopic dates from miocene volcanic rocks in the lake mead area and southern las vegas range, nevada. *Canadian Journal of Earth Sciences = Revue Canadienne Des Sciences De La Terre, 35*(5), 495-503.

Hazlatt, R. W. (1993). Stratigraphic Section of the Central Mopah Range, Calif., *US Geological Survey Bulletin*, *2053*, 127-129.

Howard, K. A., Christiansen, P. P., & John, B. E. (1993). Cenozoic stratigraphy of northern Chemehuevi Valley and flanking Stepladder Mountains and Sawtooth Range, southeastern California. *US Geological Survey Bulletin*, *2053*, 123-126.

Howard, K. A., & John, B. E. (1987). Crustal extension along a rooted system of imbricate low-angle faults; Colorado River extensional corridor, California and Arizona. *Geological Society Special Publications, 28*, 299-311.

Howard, K.A., Stone Paul, Pernokas, M.A., and Marvin, R.F., 1982, Geologic and geochronologic reconnaissance of the Turtle Mountains area California: west border of

the Whipple Mountains detachment terrane, in Frost, E.G., and Martin, D.L., eds., Mesozoic-Cenozoic tectonic evolution of the Colorado River region, California, Arizona, and Nevada (Anderson-Hamilton Volume): San Diego, Calif., Cordilleran Publishers, p. 341-354.

John, B. E., & Foster, D. A. (1993). Structural and thermal constraints on the initiation angle of detachment faulting in the southern basin and range; the chemehuevi mountains case study. *Geological Society of America Bulletin, 105*(8), 1091-1108.

Lister, G. S., and S. L. Baldwin (1993), Plutonism and the origin of metamorphic core complexes, Geology, 21(7), 607–610.

Miller, J. M. G., & John, B. E. (1988). Detached strata in a tertiary low-angle normal fault terrane, southeastern california; a sedimentary record of unroofing, breaching, and continued slip. *Geology (Boulder), 16*(7), 645-648.

Nakata, J.K, Pernokas, M.A., Howard, K.A., Nielson, J.E., and Shannon, J.R., 1990, K-Ar and fission-track ages (dates) of volcanic, intrusive, altered, and metamorphic rocks in the Mohave Mountains area, west-central Arizona: Isochron West, no. 56, p. 8-20.

Nielson, J. E. (1993). Stratigraphic and Structural Correlation of Tertiary Strata of the Mohave Mountains and Aubrey Hills, Ariz., *US Geological Survey Bulletin, 2053*, 127-129.

Nielson, J. E., & Beratan, K. K. (1990). Tertiary basin development and tectonic implications, Whipple detachment system, Colorado River extensional corridor, California and Arizona. *Journal of Geophysical Research, 95*, 599-614.

Nielson, J. E., & Beratan, K. K. (1995). Stratigraphic and structural synthesis of a Miocene extensional terrane, southeast California and west-central Arizona. *Geological Society of America Bulletin*, *107*(2), 241-252.

Nielson, J. E., & Nakata, J. K. (1993). Tertiary stratigraphy and structure of the northern Turtle Mountains. *California: US Geological Survey Bulletin*, *2053*, 127-129.

Parsons, T., & Thompson, G. A. (1993). Does magmatism influence low-angle normal faulting? *Geology (Boulder), 21*(3), 247-250.

Putirka, K., & Platt, B. (2012). Basin and range volcanism as a passive response to extensional tectonics. *Geosphere, 8*(6), 1274-1285, 12.

Reynolds, S. J., & Spencer, J. E. (1985). Evidence for large-scale transport on the Bullard detachment fault, west-central Arizona. *Geology*, *13*(5), 353-356.

Simpson, C., Schweitzer, J., and Howard, K. A., 1991, A reinterpretation of the timing, position, and significance of part of the Sacramento Mountains detachment fault, southeastern California: Geological Society of America Bulletin, v. 103, p. 751-761.

Spell, T. L., & McDougall, I. (2003). Characterization and calibration of $^{40}Ar/^{39}$ Ar dating standards. *Chemical Geology*, *198*(3), 189-211.

Woodward-McNiel and Associates, 1974, *in* Southern California Edison Company, Information concerning site characteristics, Vidal Nuclear Generating Station: Appendices 2.5-E and 2.5-I

Chapter 3 - Geochemical characteristics of pre-, syn- and post extensional volcanic rocks in the Whipple Mountains region, CA and AZ

Mary Kate Fidler[1] and Phillip B. Gans[1]

[1]*Department of Earth Science, University of California, Santa Barbara, CA*

A. Abstract

The Colorado River extensional corridor (CREC) is a superb natural laboratory for exploring the relationship between continental magmatism and extension. We present new major, trace, and Sr-Nd isotopic data for Whipple Mountains area lavas spanning the temporal, spatial, and compositional diversity of volcanism in this region. Major element XRF analyses of fresh rocks indicate that the Whipple Mountains are lavas are calc-alkaline and metaluminous, and major element oxides vary linearly with SiO_2. Alteration textures are present in some of these lavas and have the greatest effect on K, Na, and Ca. Sr, Zr, and REE are depleted in more evolved magmas and Nb/Th correlates negatively suggesting that both crystal fractionation and assimilation processes were operating during magma evolution. Sr and Nd isotopes provide clear evidence of crustal assimilation. $^{87}Sr/^{86}Sr$ varies positively and εNd varies negatively with increasing SiO_2, and project away from the OIB array and towards regional proterozoic crust in εNd versus $^{87}Sr/^{86}Sr$ space. The most primitive sample analyzed is more primitive than published assessments of regional enriched mantle lithosphere, but more evolved than OIB. All together, these data suggest that Whipple Mountains area lavas represent asthenospheric mantle melts which have both fractionated and extensively hybridized with crustal partial melts.

B. Introduction

The Basin and Range province of the western US is an archetypical example of a continental rift. Studies of its ranges, particularly in highly extended areas, have driven the development of many influential models for continental extension and extension-related magmatism. Despite significant advances in our understanding of this region over 50 years of active research, the relationship between magmatism and tectonics in the Basin and Range remains controversial. Continental-scale Cenozoic magmatic patterns in the Basin and Range have been variously attributed to the roll-back of a once-flat subducting Farallon plate (Coney and Reynolds, 1977; Best and Christiansen, 1991; Spencer et al., 1995; Dickinson, 2002), active upwelling of hot asthenosphere (Gans et al.,1989; Hawkesworth et al., 1995; Hooper et al., 1995; Wang et al., 2002), decompression melting due to stretching of the continental lithosphere (Glazner and Bartley, 1985; Wernicke et al., 1987; Putrika and Platt, 2012, Farmer and DePaolo), and the expansion of a slab window related to the northward migration of the Mendocino Triple Junction (Glazner and Bartley, 1984; Severinghaus and Atwater, 1990). Knowledge of the character and evolution of both pre- and syn-extensional volcanic centers, the spatial distribution of volcanism in extensional provinces, and the contributions of different mantle and crustal sources to melts can be used to evaluate tectonic models for Miocene volcanism in the southwest U.S.

The nature of volcanic rocks in the lower Colorado River Extensional Corridor (LCREC) in the vicinity of the Whipple Mountains has been less thoroughly characterized than those to the north. Thick accumulations of variably tilted volcanic rocks in the Whipple Mountains and ranges to the NE and SW provide an excellent opportunity to sample the full

suite of synextensional volcanic rocks in this part of the corridor and to address several important questions:

1) What is the compositional variation of Miocene volcanic rocks in the LCREC? Are there systematic compositional differences between pre-, syn- and post-extensional volcanic rocks?
2) What is the areal distribution of volcanic rock types in the CREC?
3) What differentiation processes are responsible for the evolution of lavas in the LCREC (i.e. fractional crystallization vs. assimilation)?
4) What is the likely mantle source for the mafic endmembers of LCREC lavas?

In this study, we present new whole rock major and trace element data and Sr and Nd isotopic data from volcanic rocks that span the width of the CREC in the vicinity of the Whipple Mountains. This data substantially improves existing knowledge of the geochemical and isotopic character of Miocene lavas associated with large magnitude extensional normal faulting and block rotation in the region.

C. Geologic Setting

1. Tectonic setting of the CREC and Whipple Mountains

The tectonic setting of the CREC and importance of the Whipple Mountains in studies of crustal extension are described more thoroughly in Chapters 1 and 2. The CREC extends from southern Nevada to southeastern California and western Arizona (Figure 17; Davis et al, 1980; Reynolds and Spencer, 1985; Howard and John, 1987; Davis and Lister, 1988, Spencer and Reynolds, 1998a) and is part of a sinuous belt of Cordilleran metamorphic core complexes (MCC) that stretches from Canada to Mexico (Figure 17;

Coney, 1980). The 70-150 km wide CREC is an extensional belt south of Las Vegas, Nevada that includes parts of Nevada, California, and Arizona and the Colorado River (eg. Howard and John, 1987, Faulds et al., 1990).

2. Distribution of volcanic rocks and summary of volcanic stratigraphy

Chapter 1 of this dissertation provides a thorough description of the eruptive history and volcanic rock units of the western Whipple Mountains and Mopah Range, which include most of the samples that are used in this study. The volcanic rock types present in the western Whipple Mountains and eastern Mopah Range are representative of the volcanics throughout the greater LCREC at this latitude. As such, we refer the reader to Chapter 1 for detailed unit descriptions and for the petrographic character of these rocks. Though the range of rock types are generally similar across the corridor, there are important variations in the abundance of different volcanic units from east to west, particularly of pre-18.8 Ma units (pre-Peach Spring Tuff; Figure 19). Several authors have mapped and described the early Tertiary rocks of the LCREC (Stone et el.,1979, Turtle Mountains; Hazlett, 1986, Central Mopah Range; Carr et al., 1980, SW Whipple Mountains and S Mopah Range; Dickey et al., 1980, S Whipple Mountains; John, 1987, Chemehuevi Mountains; Pike and Hansen, 1982, Nielson and Beratan, 1990, and Howard et al., 1999, Aubrey Hills, Standard Wash, and Mohave Mountains; Nielson and Beratan, 1990, E Whipple Mountains; Chapter 1 of this Dissertation, W Whipple Mountains and E Mopah Range), and Sherrod and Nielson (1993) compiled work by many authors in a USGS Bulletin providing a detailed summary of its Tertiary stratigraphy.

All combined, this work shows that early volcanism (pre-18.8 Ma Peach Springs Tuff; Ferguson et al., 2013) was dominated by mafic and intermediate effusions, including

basalts, basaltic andesite, andesite and trachyte, and punctuated by rhyolite tuffs on the eastern side of the corridor. These early mafic accumulations reached nearly 1.5 km thick in some areas (eg. Aubrey Hills; Nielson and Beratan, 1990), and were followed by eruptions of dacite and rhyolite lavas totaling just a few hundred meters thick (Figure 19). On the western side of the corridor, we observe the same pattern of volcanic activity – early mafic and intermediate effusions followed by eruption of silicic lavas. However, the earliest mafic lavas here account for a much smaller percentage of the total pre-Peach Springs Tuff volcanic stratigraphy compared to the eastern side of the corridor and the volume of silicic lavas was much greater (Figure 19).

Following the early mafic and silicic volcanic phases, the corridor abruptly underwent widespread extensional failure, as evidenced by large degrees of tilting of the older Tertiary units (Nielson and Beratan,1990; Gans and Gentry, 2016; Chapter 1 of this dissertation) overlain in sharp angular unconformity by only slightly younger syn-extensional volcanic and sedimentary strata. The onset of rapid faulting and block rotation occurred at ~19.5 Ma on the western and eastern sides of the corridor, but extended for a longer period in the east (Chapter 1; Nielson and Beratan, 1990, 1995). This is most clearly demonstrated by variable orientations of the 18.8 Ma Peach Springs Tuff (Ferguson et al., 2013) from flat lying in the west (post-faulting) to moderately dipping in the east (syn-faulting). Syn- and post-extensional eruptions occurred at much slower rates and was less widespread that pre-extensional volcanism. In all parts of the corridor, volcanism shifted back to primarily mafic and intermediate compositions following the inception of extensional faulting, with only minor rhyolite eruptions.

3. Previous work on geochemistry and petrogenesis of LCREC (Whipple Regions) volcanics

Previous work characterizing the Tertiary volcanic stratigraphy of the Whipple Mountains region shows that volcanism was calc-alkalic to alkai-calcic, and metaluminous to peraluminous, spanning a range of compositions from basalt to rhyolite. Major element and select trace element compositions of volcanic and subvolcanic units have been documented by several authors, including Suneson and Luchitta (1978, 1979, 1980, 1981), Suneson (1980), Nakata (1982), Hazlett (1986, 1990), Bradshaw et al. (1993), LaForge (2015), and Gans and Gentry (2016).

Many studies have concluded that Cenozoic basalts in the CREC older than ~12 Ma were sourced from ancient enriched lithospheric mantle ($\varepsilon Nd < \sim 4$ and $^{87}Sr/^{86}Sr > \sim 0.705$; e.g., Daley and DePaolo, 1992; Feuerbach et al. 1993; Bradshaw et al., 1993; Metcalf et al., 1995; DePaolo and Daley, 2000) with minor assimilation of regional Proterozoic crust and that more silicic igneous rocks appear to represent hybrids of these enriched mantle melts and Proterozoic crust (Miller and Wooden, 1994; Allen et al. 1995; Bachl et al. 2001). The Proterozoic crust of the Mojave region is characterized by high to very high measured $^{87}Sr/^{86}Sr$ (~0.710 to 0.80) and low to very low εNd (~-15 to -22; Bennett and DePaolo, 1987; Miller and Wooden, 1994). Others argue that basalts throughout the SW United States are isotopically heterogenous suggesting they have an asthenospheric primary source and variable additions of lithospheric mantle and/or crustal mafic partial melts (Glazner and Farmer, 1992; Reiners, 2002; Ramos and Reid, 2005).

Few studies have presented isotopic data for the lavas of the LCREC. Bradshaw et al., (1993) and DePaulo and Daley (2000) present Sr, Nd and Pb ratios for several samples

from the Mohave Mountains area, but both studies focused only on basalt lavas, excluding the abundant intermediate and silicic units in the area. Bradshaw et al. (1993) concluded that basalts in the CREC could be divided into two groups with distinct petrogenesis – an earlier group derived from partial melting on an enriched mantle lithosphere, variation in which they attribute to variable degrees of mantle partial melting, and a younger more primitive group derived from the asthenospheric upper mantle. More work has been done on the petrogenesis of Cenozoic magmas in the NCREC, particularly in the plutons and volcanic rocks of the El Dorado Mountains and Lake Mead area (Faulkner et al., 1995; Bachl et al., 2001; Miller and Miller, 2002; McDowell et al., 2016). These studies all conclude that Tertiary magmas were produced from a combination of enriched mantle and crustal derived material, but generally discount significant crustal contamination on the most mafic units. These studies do not fully resolve or quantify the magnitude of crustal assimilation in CREC lavas, particularly for the most primitive and most evolved end members.

D. Methods

1. Sampling

A total of 78 samples were collected from various locations across the CREC from volcanic exposures surrounding the Whipple Mountains (Figure 18) for geochemical analysis and geochronology. The focus of sampling for geochemical analysis was to capture the diversity of volcanic units and to sample both sides of the extensional corridor. Samples from the western Whipple Mountains and eastern Mopah Range are described in Chapter 1, with locations given in Appendix I, while rock types and locations of samples from other parts of the corridor (Turtle Mountains, norther Mopah Range, southwest Whipple

Mountains, Mohave Mountains, Aubrey Hills, and Standard Wash) are given in Appendix IV. Careful attention was paid to select the least altered outcrops for whole rock geochemistry, with the exception of four strongly altered samples. These four samples (WM-6, WM-7, WM-32(12), and WW-6) display clear chemical evidence of K-metasomatism including elevated K_2O (11-12%) and low Na_2O (0-1.9%; Table 4). These samples are not included in most of the geochemical plots discussed below. Despite our efforts to select the least altered samples, many mafic and intermediate samples show minor to moderate textural and chemical evidence for alteration (Figure 22). Sampling of mafic units targeted the coarse-grained lava flow interiors, while for silicic units, we sampled vitrophyres at the base or tops of flows when possible and devitrified portions of flows when vitrophyres were not present. In many studies, major and trace element abundances have been shown to be effected by both low temperature ion exchange with groundwater in hydrated glasses (low, Si, Na, Li, high K, Al, Sr and Ba relative to fresh obsidian), and by both high temperature fractionation and volatile transport and low temperature ion exchange, differential solution, and absorption by secondary phases in the devitrified interiors (low Li, Cs, U, Mo, and F, and high Sr, Ba, and Eu relative to fresh obsidian) of silicic flows (Lipman, 1965; Zielinski, 1977; Noh and Boles, 1989). This is an obstacle to obtaining original magmatic compositions in the field area, as nearly all preserved glasses are perlitic. Surface weathering, and in some areas, minor to intense hydrothermal alteration (potassic, propylitic, sericitic) due to circulating hydrothermal fluids compound the difficulty of obtaining reliable magmatic compositions. Considerable effort was devoted to obtaining the freshest possible samples as indicated by degree of freshness of volcanic crystalline phases.

2. Whole rock geochemistry

The bulk-rock major oxides of 78 samples were analyzed by x-ray fluorescence (XRF) at Pomona College (Table 4). Methodology and error analysis for XRF were adapted from Johnson et al. (1999) for samples analyzed at WSU, with a similar analytical method at Pomona (Lackey et al. 2012). Representative, clean, unweathered chips of all samples were powdered in a tungsten carbide head and mill and mixed with flux in a 2:1 ratio (3.5 ± 0.0001 g of sample to 7.0 ± 0.0001 g of dilithium tetraborate ($Li_2B_4O_7$)). The mixture was fused to a glass bead in a graphite crucible at 1000° C for 10 min, reground, and then fused for a second time. 2-3 mm shards of glass were chipped off each bead using a dremel tool, mounted in epoxy and polished to 1 μm finish for laser ablation quadrupole inductively coupled mass spectrometry (LA-ICP-MS) trace element analysis. Beads were then polished to ~15 μm finish and analyzed. Major, minor, and a suite of trace elements (we report Cu, Zn, Rb, Sr, Y, Zr, and Ga in this study) were measured at Pomona University on a single fused bead using a 3.0 kW Panalytical Axios wavelength-dispersive XRF spectrometer equipped with PE, LiF 200, GE, and PX1 industrial crystals. Concentrations are determined using reference calibration curves of 55 certified reference materials spanning a range of natural rock compositions (Lackey et el. 2012).

Whole rock trace elements (Sc, Ti, Cr, Co, Ni, Cs, Ba, La, Ce, Pr, Nd, Sm, Eu, Gd, Tb, Dy, Ho, Er, Tm, Yb, Lu, Hf, Th, and U) were measured at UCSB by LA-Q-ICP-MS. Samples were ablated using 50 μm wide by 250 μm long line scans at a rate of 4 μm/second for ~2 minutes of data each. A set of whole-rock reference materials were measured at the beginning and end of each analytical session and a primary and secondary reference material were measured between every 9-10 unknowns. Data were analyzed in three analytical sessions, and the specific standards used varied between sessions, but include USGS

reference glasses (BHVO-1G, BHVO-2G, BCR-2G, AGV-2), MPI-DING reference glasses (ATHO-G, ML3B-G, GOR-132-G, StHs 6/80-G, T1-G), and NIST SRM 612. Reference material pairs used as primary and secondary standards in various analytical sessions include ATHO-G, AGV-2, BHVO-1, StHs6/80-G, and T1-G. Data were reduced using the "Trace elements IS" data reductions scheme in Iolite v2.5 (Paton et al., 2011) using Ca as the internal standard (measured by XRF) with a UCSB in-house routine (J. Garber, personal communication). ^{160}Gd and ^{157}Gd measurements were complicated by interferences by $^{144}Nd^{16}O$ and $^{141}Pr^{16}O$ respectively, resulting in an apparent negative anomaly in chondrite normalized values. We present ^{157}Gd where possible as the interference is smaller for this isotope (Table 4).

3. Sr and Nd isotope geochemistry

Sr and Nd isotopic compositions of 18 samples spanning the compositional and age range of the volcanic suite were analyzed by Thermal ionization mass spectrometry (TIMS) at the University of North Carolina. Powdered samples were dissolved in steel jacketed Parr vessels with Hf and HNO_3. The samples were split and Sr separated from one portion using Eichrom Sr-spec, while Nd was separated from the other portion following a three step protocol involving AGW50x-4 resin and HCl, Eichrom TRU resin, and AGW50x-4 resin with 2-methyllactic acid (MLA). Six Sr isotopic compositions were measured on the VG Sector 54 and 12 were measured on the IsotopX Phoenix and an internal standard correction was applied to equate the values from the two machines. All Nd isotopic concentrations were measured on the Phoenix. The Sr analytical methods used at UNC are reported in Hedman et al. (2009), and external precision is estimated to be 20 ppm (2σ). Nd was run as

an oxide on the IsotopX Phoenix, using oxide corrections from Harvey and Baxter (2009), and external precision is estimated to be better than 20 ppm (2σ).

E. Results

Samples are divided into two main groups based on their age relative to the onset of extension (Figures 22, 23, and 24). The first group consists of steeply tilted units (~110-50° of total tilting) interpreted to pre-date the onset of extensional normal faulting and block rotation. We refer to these rocks as "pre-extensional," as they pre-date the onset of tectonic extension, though the region did experience dilational-extension (diking) during this time (Gans and Gentry, 2016). The second group consists of moderately to gently dipping units (35-0° of total tilting) which are interpreted to post-date most or all normal faulting and block rotation. We refer to these rocks as syn- to post- extensional units.

1. Alteration textures

Many CREC samples show textural evidence of alteration (Figures 25). Based on the petrographic observations described below, samples were grouped by degree of alteration (strong, moderate, minor and unaltered). All altered samples are elevated in total alkalis relative to unaltered samples, which define a linear trend on a TAS diagram (Figure 22).

In the most strongly altered rocks, phenocrystic and groundmass plagioclase are completely replaced by K-bearing phases like adularia and sericite as well as quartz. Intense calcite veining and/or replacement of groundmass is common (Figure 25). In more silicic samples, hornblende phenocrysts are replaced by magnetite and clay minerals. Wt. % K_2O is high, ranging from 10-12 wt. % in the 4 strongly altered samples (Figure 23). In moderately altered samples, replacement of plagioclase by adularia, sericite and quartz is complete in the

groundmass and patchy within phenocrysts. Plagioclase phenocrysts may be pseudomorphed by mats of fine-grained adularia, resulting in twinning which appears to have fuzzy, or diffuse boundaries. In several moderately altered mafic to intermediate samples, hydrothermal biotite has grown in the groundmass in altered patches of plagioclase phenocrysts (Figure 25). Evidence of strong to moderate alteration is generally easily recognizable in hand sample, as both groundmass and phenocrystic plagioclase crystals are milky-colored and opaque and do not exhibit cleavage flashes.

Minor alteration is evidenced by subtler textures which may be easily overlooked in hand samples, as plagioclase phenocrysts generally appear translucent and give bright cleavage flashes and clinopyroxene phenocrysts appear fresh and stable. Petrographic evidence of alteration in these rocks include replacement by adularia within small areas of plagioclase phenocrysts, such as along fractures or within distinct oscillatory zones. Glass inclusions within plagioclase phenocrysts are replaced by clay minerals and patchy replacement of groundmass by chalcedony is commonly observed. Twinning in groundmass plagioclase is generally not very sharp as a result of pseudomorphing by adularia. Olivine is typically partially to fully replaced by clay and Fe-oxide minerals (Figure 25). These textures are distinct from unaltered rocks, which generally display sharp twinning in both phenocrystic and groundmass plagioclase and fresh mafic phases, with the exception of olivine which is commonly iddingsitized.

2. Major element geochemistry

Major element compositions of volcanic rocks from the Whipple Mountains and surrounding ranges are presented in Table 4 and Figures 22, 23, 24, and 26. Analyzed rocks

are dominantly calc-alkalic (Figure 24) and display a wide range of mafic and intermediate compositions (basalt, trachybasalt, basaltic-andesite, basaltic-trachyandesite, andesite and trachyandesite), and a tight grouping of silicic compositions (dacite and rhyolite; Figure 22). The mafic and intermediate rocks are metaluminous, whereas silicic rocks span the boundary between metaluminous and peraluminous (Figure 24). SiO_2 content ranges from 48.5 to 73.1 wt. %, with a gap from 61 to 67 wt. % (Table 4).

Pre-extensional samples display a bimodal distribution of SiO_2, with a compositional gap from 54.3 to 67.1 wt. % SiO_2, except for a single intermediate sample (WM-9; Figure 22). This sample displays evidence of alteration including and may not reflect an original magmatic composition. Nearly all syn- to post-extensional samples are mafic and intermediate, ranging from 50.0 to 60.2 wt. % SiO_2, except for a single rhyolite pumice clast from a syn-extensional conglomerate in the Mopah Range and a late stage rhyolite dike in Standard Wash. The pumice may have been either sourced from outside the study area or eroded from an existing pre-extensional unit. Major element data define trends that are broadly linear on Harker diagrams for all oxides except Al_2O_3 and P_2O_5 (Figure 23) and show typical trends for compatible and incompatible elements (Harker, 1909).

3. Trace element geochemistry

In contrast to the relatively smooth trends exhibited by major elements, many trace elements are weakly correlated with increasing SiO_2 (e.g. Rb, Ba), while others are depleted at high silica concentrations (e.g. Sr, Nd, Zr; Figure 26). Depletion in Sr in more evolved rocks likely represents fractionation of plagioclase, while depletion of Zr may represent fractionation of a Zr or Ti-rich phase such as zircon or rutile. Rare earth elements (REE) are enriched relative to chondrite (McDonough and Sun, 1995) with mafic lavas more enriched

in REE than silicic lavas (Figure 26). This may be due to either fractionation of a REE-rich phase from more evolved lavas or to mixing with some REE depleted material. No such crustal reservoir has been identified, making the former the more likely explanation. These observations together suggest that crystal fractionation processes were operating as LCREC lavas evolved. Despite variable degrees of enrichment, chondrite normalized profiles are similar in shape with very few samples displaying a slight Eu anomaly. All REE profiles have a negative slope with La/Yb ranging from 4-34 (Figure 26).

Though depletions of certain elements in more evolved lavas suggests crystal fractionation, trace element data also provides strong evidence for crustal assimilation. Nb/Th is high in the mantle and low in the crust. LCREC lavas Nb/Th correlate negatively with $^{87}Sr/^{86}Sr_{(i)}$ (Figure 27), which is consistent with isotopic enrichment due to mixing of mantle and crustal material.

4. Sr and Nd isotopes

LCREC lavas do not plot on the mantle array for OIB, rather they form an array towards regional Proterozoic crust. $^{87}Sr/^{86}Sr_{(i)}$ values range from 0.706087 to 0.711366 while $\varepsilon Nd_{(i)}$ values range from -1.23 to -12.37 (Table 5, Figures 27 and 28). $^{87}Sr/^{86}Sr_{(i)}$ increases and $\varepsilon Nd_{(i)}$ decreases with increasing SiO_2 (Figure 28), providing compelling evidence for crustal assimilation. $\varepsilon Nd_{(i)}$ correlates negatively with $^{87}Sr/^{86}Sr_{(i)}$, but this correlation is much stronger among pre-extensional samples than among syn- to post-extensional samples. This may suggest assimilation of more isotopically heterogeneous crustal material in the more silicic samples relative to the mafic samples.

The mafic pre-extensional samples plot within the field of enriched mantle basalts from the Mojave region (Feurbach et al., 1993) on $^{87}Sr/^{86}Sr_{(i)}$ versus $\varepsilon Nd_{(i)}$ plots. Silicic pre-

extensional samples plot in the same field as the Mojave and western Arizona region Mesozoic plutonic rocks (Miller and Wooden, 1994; Allen et al., 1995; Kapp et al., 2002), somewhat more primitive values than most of the Proterozoic crust (Miller and Wooden, 1994). Most syn- to post-extensional units (both mafic and intermediate in composition) plot between the mafic and silicic pre-extensional units in this space, except for the most mafic sample analyzed, a post-extensional olivine basalt (WM-32(14)) which is more primitive, plotting between the fields of enriched basalts and typical ocean island basalts (Figure 28). All samples, except for WM-32(14) which is slightly more primitive, are consistent with measured Sr and Nd isotope ratios from the NCREC (Faulkner et al., 1995; Bachl et al., 2001; Miller and Miller, 2002; McDowell et al., 2016).

F. Discussion

1. Mantle source and crustal assimilants

The mafic pre-extensional samples plot within the field of enriched mantle basalts from the Mojave region (Feurbach et al., 1993) on $^{87}Sr/^{86}Sr_{(i)}$ versus $\varepsilon Nd_{(i)}$ plots. Similar isotopic values in NCREC basalts have led previous workers to conclude that such basalts are sourced strictly from an enriched subcontinental mantle lithosphere. However, multiple lines of evidence suggest that LCREC lavas analyzed were likely sourced from an OIB-like mantle source rather than the enriched mantle lithosphere, and that all lavas analyzed were subsequently contaminated by crustal partial melts:

1) The most primitive sample analyzed is less evolved than regional enriched basalts, but plots outside of OIB and MORB arrays in $\square Nd_{(i)}$ versus $^{87}Sr/^{86}Sr_{(i)}$ space. Thus, it can neither have been sourced from the same enriched mantle

proposed as the source of regional enriched basalts, nor can it represent a pure asthenospheric melt.

2) On $\varepsilon Nd_{(i)}$ versus $^{87}Sr/^{86}Sr_{(i)}$ plots, all of our most mafic samples form a tight linear array that projects toward Proterozoic basement values (Figure 28).
3) These mafic samples display increasing $^{87}Sr/^{86}Sr_{(i)}$ and decreasing $\varepsilon Nd_{(i)}$ with increasing SiO_2, trends which can be most easily explained by low degrees of crustal assimilation.
4) Proterozoic zircons were separated from at least one of the mafic samples analyzed (AB-01) and Gans and Gentry (2016) report that all mafic dikes of the Chambers Well Swarm, including early mafic dikes considered to be feeders of the early mafic volcanics in the western Whipple Mountains, contain abundant Mesozoic and Proterozoic zircon.

These lines of evidence suggest that even the most mafic LCREC lavas experienced some degree of crustal assimilation, and we attribute this as the cause of isotopic variation in these samples.

The pre-extensional silicic volcanism which followed shortly on the heels of early pre-extensional mafic volcanism lie along the same array as the early mafic lavas, defining a mixing line between OIB and regional crustal rocks. There is some variation in this array, perhaps due to assimilation of crustal materials of variable isotopic signatures and Sr and Nd contents. Ability to model this mixing is limited by uncertainty in the mantle source (as all lavas likely experienced some degree of crustal assimilation) as well as uncertainty in the proportions of various Proterozoic and Mesozoic crustal assimilants involved in this hybridization. As both Mesozoic and Proterozoic xenocrystic zircons are routinely found in

Miocene dikes of Chambers Well (Gans and Gentry, 2016), it is clear that crustal assimilants are heterogeneous.

Syn- to post-extensional intermediate and mafic lavas display the widest variability in isotopic ratios, and though they are also consistent with hybridization of mantle partial melts with the crust, together, they do not define a clear mixing line with a well-defined crustal source. It is likely that multiple distinct crustal reservoirs were responsible for hybridizing with mantle partial melts to form the wide range of signatures observed in these lavas.

2. Potential Implications

Chapter 1 demonstrates that the volume of erupted LCREC lavas in the vicinity of the Whipple mountains alone are on the order of 500 km^3. This study shows that these lavas consist of material both from the mantle and from the crust. Taking this work further, to quantifying the relative amount of crustal material vs. mantle material comprising LCREC lavas would be an important contribution to our understanding of the volcanic and tectonic evolution of the CREC. Generating some bounds on both the amount of hot mantle-derived basalt fluxing the crust and the degree of partial melting experienced by the crust could shed light on the thermal and rheological state of the CREC crust. Such information would be useful for modeling the effects of thermo-mechanical weakening on the extensional collapse of the corridor.

G. Conclusion

XRF and ICP-MS major and trace element data, and the first reported Sr-Nd isotopic data for volcanic rocks spanning the width of the LCREC in the vicinity of the Whipple

Mountains allow for a thorough characterization of syn-extensional volcanism and provide important new constraints on petrogenesis. This is the most detailed geochemical study on lavas in this part of the corridor, and represents a substantial contribution to our understanding of CREC volcanism and its relation to large magnitude extension. Our principle conclusions from this work include the following:

1) Pre-extensional volcanic activity consisted of a period of basalt and basaltic andesite volcanism followed by primarily dacite and rhyolite volcanism. Following the onset of rapid extension, most lavas erupted in the LCREC were of intermediate composition with minor eruption of more primitive basalt. Linear major element trends are consistent with mixing of mantle and crustal derived material playing a major role in magma petrogenesis.
2) Trace element variations suggest that both crystal fractionation and assimilation processes were operating during LCREC evolution.
3) Sr and Nd Isotopic signatures of LCREC lavas indicate that CREC basalts were not derived exclusively from the enriched mantle lithosphere, but were likely derived from an OIB-like mantle source and subsequently assimilated Mojave Pro terozoic and/or Mesozoic crust. Pre-extensional silicic lavas represent hybridization of primitive mantle and with greater amounts of crustal material.
4) The demonstrated importance of crustal partial melts in the evolution of the voluminous pre-extensional volcanics of the LCREC is consistent with a model of extensional failure localized and driven by thermal weakening of the crust.

H. Acknowledgements

I am grateful for assistance in the field over three field seasons from Beau Gentry, Chris Older, Jason Womer, Will Junkin, and Josh Garber. Thank you also to Josh Garber for

help reducing ICP-MS trace element data, Jade Star Lackey for XRF analyses, and to Drew Coleman and Ryan Mills and their students for assistance with Sr and Nd isotope analyses. An extra special thank you to Frank Spera and Jenna Adams for helpful discussions about AFC processes and modeling. This work was funded by grants from the U.S. Geologic Survey, National Cooperative Geologic Mapping Program (EdMap), award #G14AC00080, from the period of May1, 2014 to April 30, 2015, the Geological Society of America, and the generous donation of Rachel Haymon and Ken Macdonald to UCSB department of Earth Science Graduate Student Research Grants.

Figure 22

Figure 22. Total alkalis vs. SiO_2 for volcanic rocks of the Whipple Mountains region, LCREC. Samples are colored by age relative to the onset of rapid large magnitude extensional faulting and block tilting, and symbol shapes designate sample location. Sample location acronyms in key are the samples as in Figure 2. Samples were analyzed by XRF and normalized to 100%. Several samples with the highest alkali contents, particularly those of lowest SiO_2 content, contain textural evidence for alteration and may not represent original erupted compositions.

Figure 22

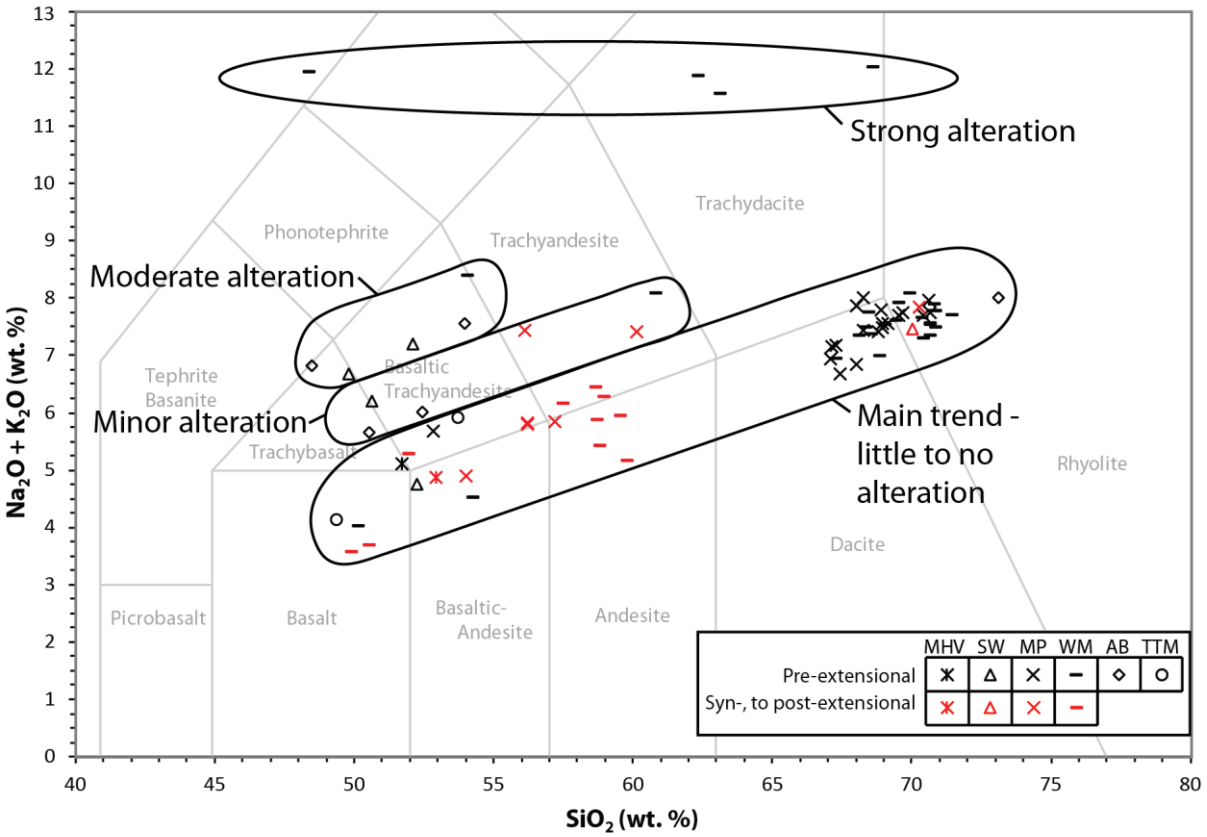
Strong alteration
Moderate alteration
Minor alteration
Main trend - little to no alteration
Phonotephrite
Trachyandesite
Trachydacite
Tephrite Basanite
Basaltic Trachyandesite
Trachybasalt
Rhyolite
Dacite
Picrobasalt
Basalt
Basaltic-Andesite
Andesite
MHV SW MP WM AB TTM
Pre-extensional
Syn-, to post-extensional
$Na_2O + K_2O$ (wt. %)
SiO_2 (wt. %)

Figure 23

Figure 23. Major element oxides vs. SiO_2 for volcanic rocks of the Whipple Mountains region, LCREC. Samples shapes are the same as Figure 4, and sample location acronyms in key are same as in Figure 2. Black = pre-extensional, red = syn- and post-extensional, dark grey = minor alteration, light grey = moderate alteration. Minor and moderate alteration samples show textural evidence of alteration and are circled in Figure 2. Strongly altered samples are not shown. Samples were analyzed by XRF and normalized to 100%.

Figure 23

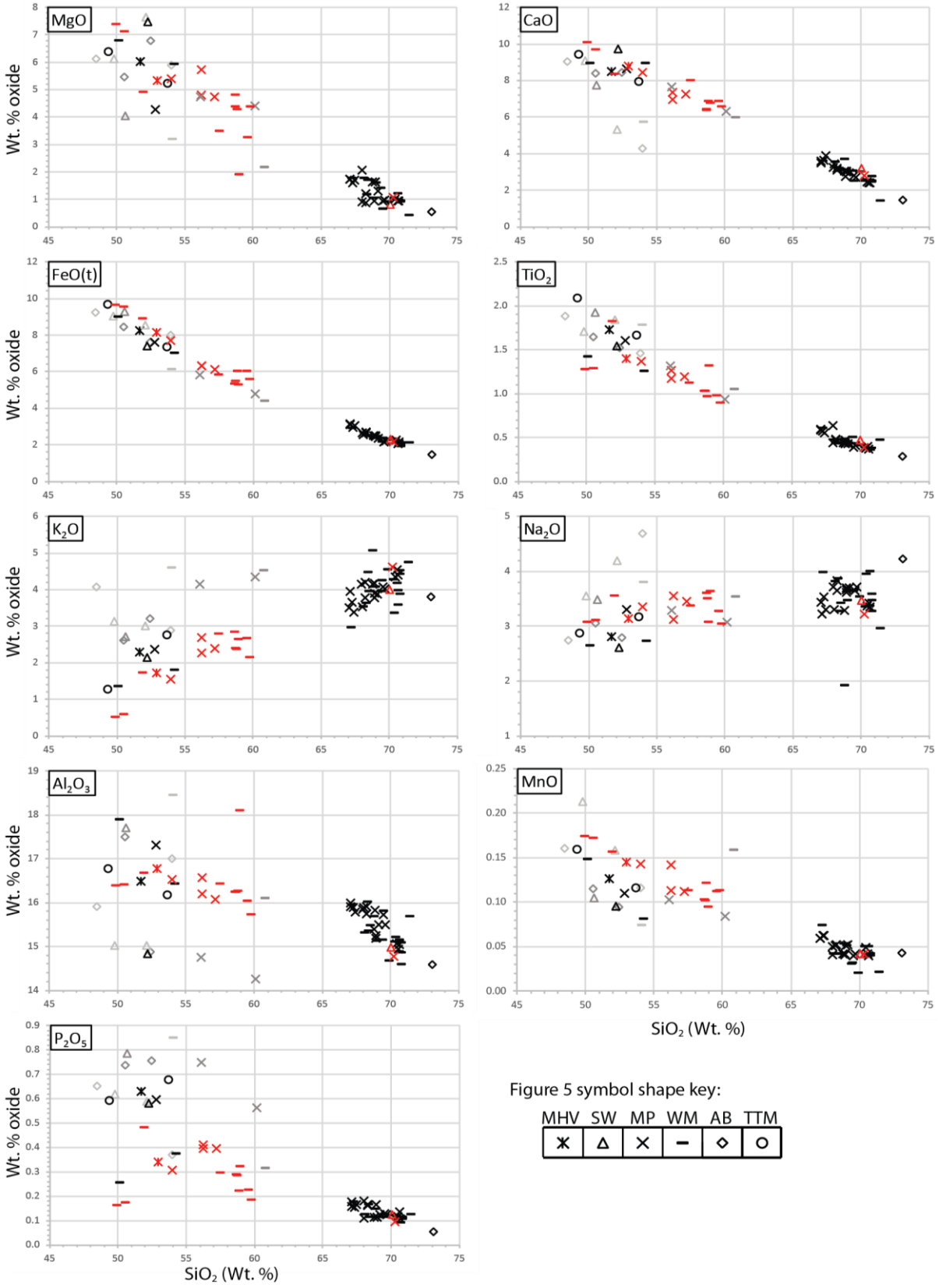
MgO
CaO
FeO(t)
TiO2
K2O
Na2O
Al2O3
MnO
P2O5
Wt. % oxide
SiO2 (Wt. %)
Figure 5 symbol shape key:
MHV SW MP WM AB TTM

Figure 24

Figure 24. Select igneous classifications of LCREC lavas. Symbol colors are the same as in Figure 5. A) Modified alkali lime index (MALI) indicates that all unaltered samples are calc-alkalic to calcic. B) Aluminum saturation index indicates that CREC lavas are overwhelmingly metaluminous, with silicic samples grouping at the metaluminous-peraluminous boundary.

Figure 24

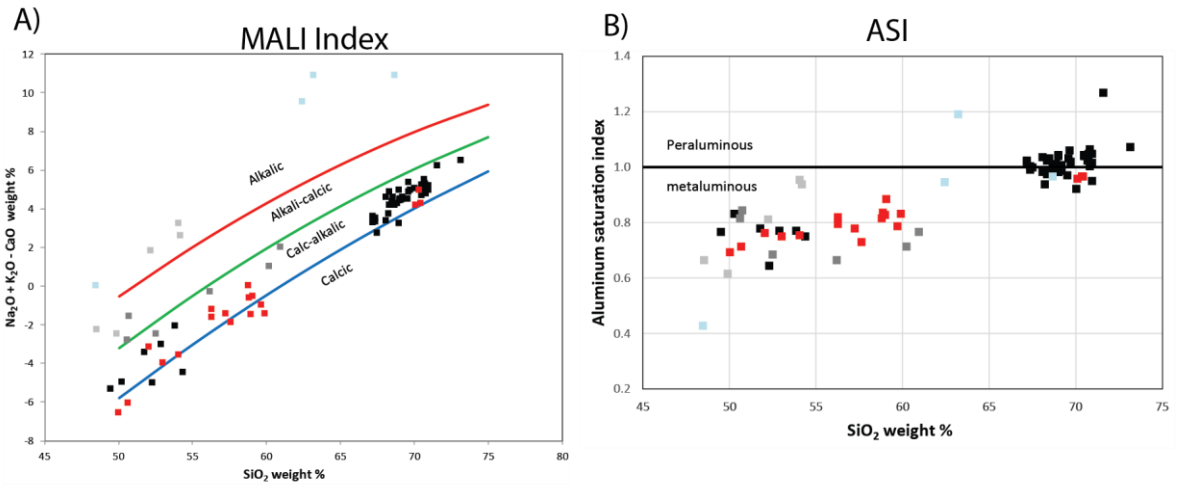
A)
MALI Index
Alkalic
Alkali-calcic
Calc-alkalic
Calcic
$Na_2O + K_2O - CaO$ weight %
SiO_2 weight %
B)
ASI
Peraluminous
metaluminous
Aluminum saturation index
SiO_2 weight %

Figure 25

Figure 25. Representative photomicrographs contrasting samples displaying strong (A, B), moderate (C), minor (D), and no (E) textural evidence of secondary alteration. Each image shows cross-polarized light on the left and plane light on the right, with the exception of D, which shows cross-polarized light on the top and plane light on the bottom in the left photomicrograph and only cross-polarized light in the right photomicrograph. Mineral abbreviations are Plag = Plagioclase, Cpx = clinopyroxene, Ol = oliving, Fe-ox = iron oxides, Qtz = quartz, Cc = calcite.

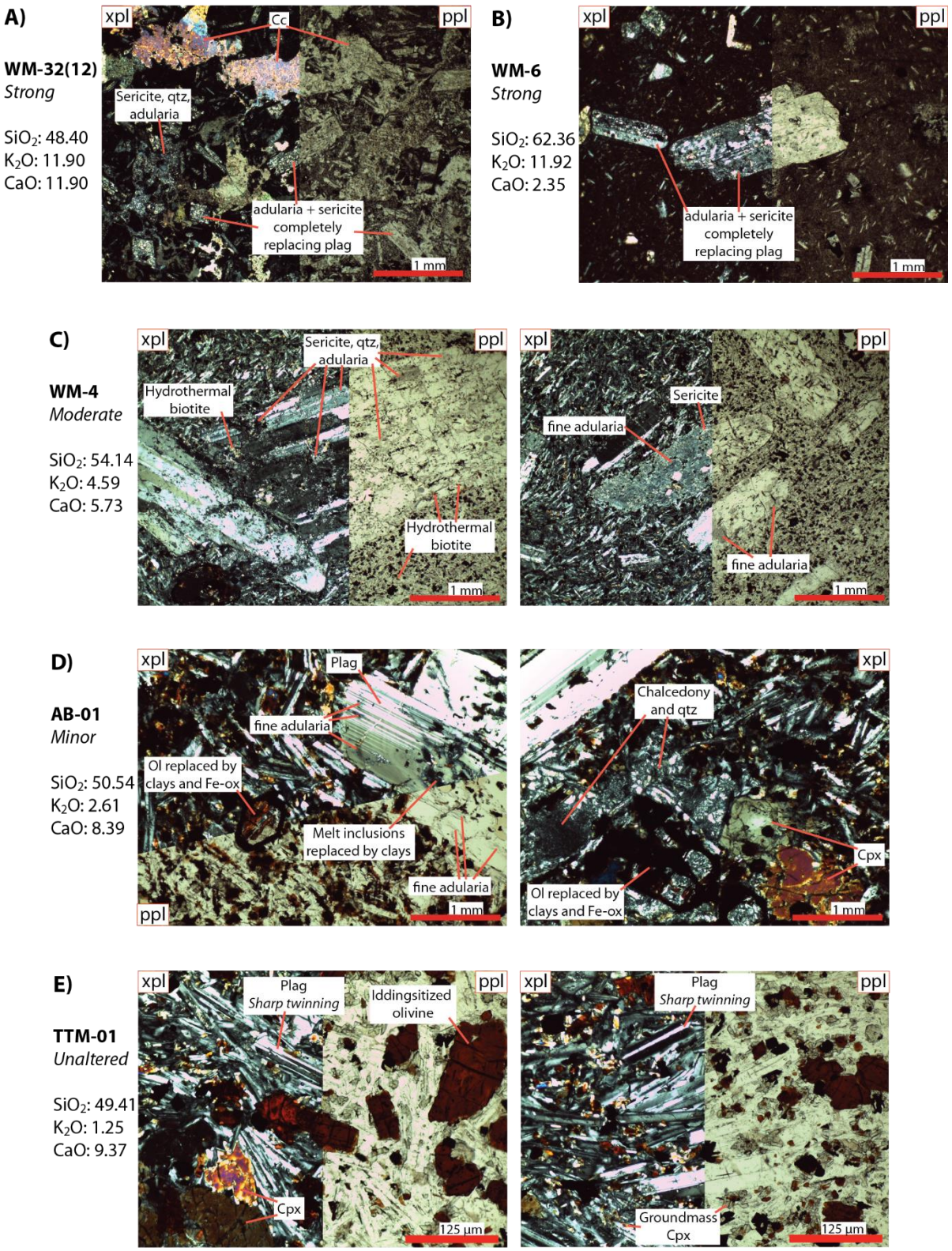
A)
WM-32(12)
Strong
SiO2: 48.40
K2O: 11.90
CaO: 11.90
xpl
ppl
Cc
Sericite, qtz, adularia
adularia + sericite completely replacing plag
1 mm
B)
WM-6
Strong
SiO2: 62.36
K2O: 11.92
CaO: 2.35
xpl
ppl
adularia + sericite completely replacing plag
1 mm
C)
WM-4
Moderate
SiO2: 54.14
K2O: 4.59
CaO: 5.73
xpl
ppl
Sericite, qtz, adularia
Hydrothermal biotite
Hydrothermal biotite
1 mm
xpl
ppl
Sericite
fine adularia
fine adularia
1 mm
D)
AB-01
Minor
SiO2: 50.54
K2O: 2.61
CaO: 8.39
xpl
ppl
Plag
fine adularia
Ol replaced by clays and Fe-ox
Melt inclusions replaced by clays
fine adularia
1 mm
xpl
Chalcedony and qtz
Cpx
Ol replaced by clays and Fe-ox
1 mm
E)
TTM-01
Unaltered
SiO2: 49.41
K2O: 1.25
CaO: 9.37
xpl
ppl
Plag
Sharp twinning
Iddingsitized olivine
Cpx
125 µm
xpl
ppl
Plag
Sharp twinning
Groundmass Cpx
125 µm

Figure 26

Figure 26. Trace element characteristics of Whipple Mountains area volcanic rocks. Symbology in variation plots is the same as Figure 5. Whole rock, chondrite normalized, rare earth element (REE) plot in bottom graph (normalized to McDonough and Sun, 1995). Only representative samples with relatively smooth REE profiles are shown (samples with spikey REE profiles are primarily silicic samples with low REE concentrations. Data are in Table 4). Profiles are colored by SiO_2 content (red, <52%; orange, 52-57%; light green, 57-63%; dark green, 63-70%; blue, >70%).

Figure 26

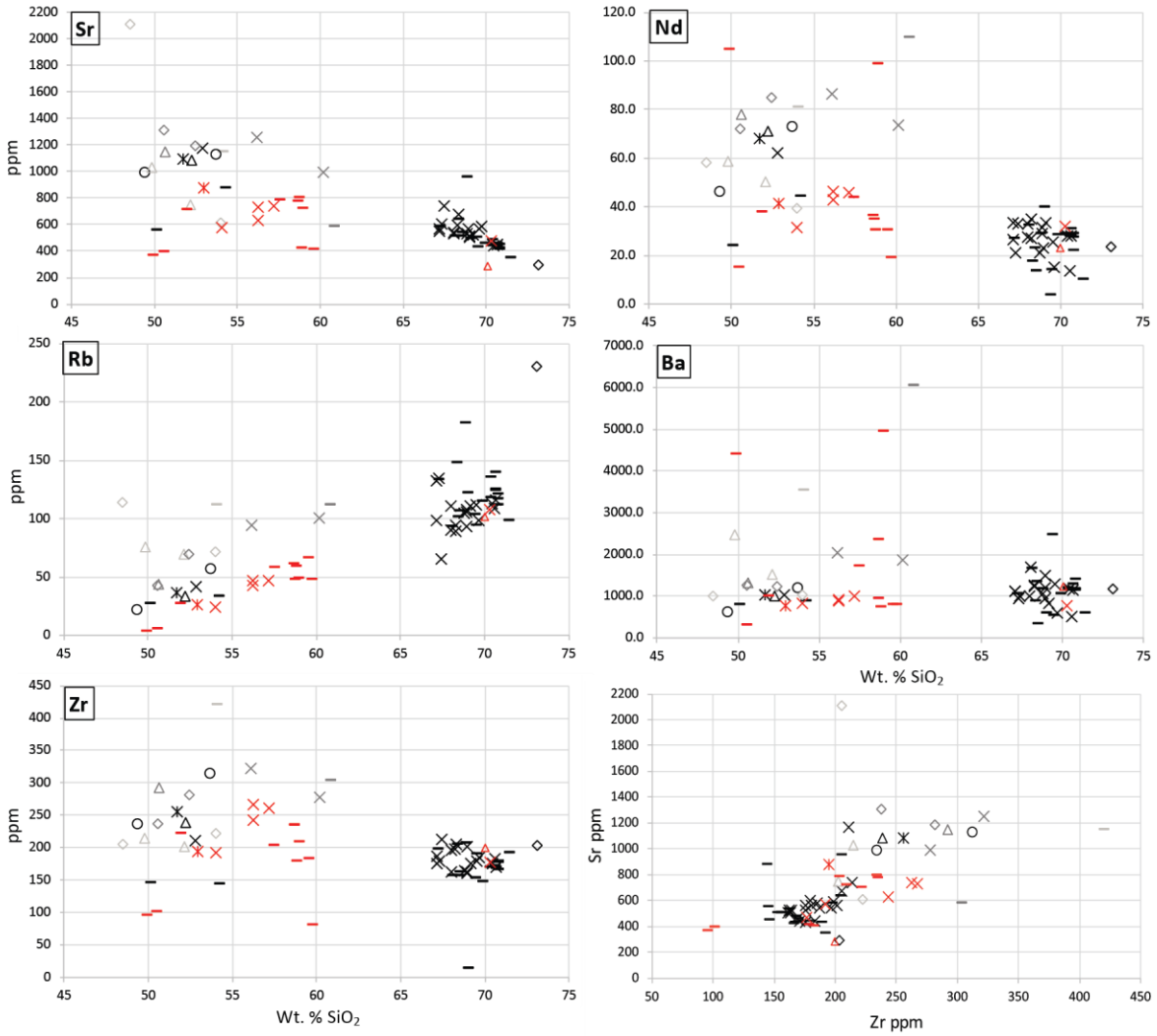
Sr
ppm
Nd
Rb
ppm
Ba
Wt. % SiO2
Zr
ppm
Wt. % SiO2
Sr ppm
Zr ppm

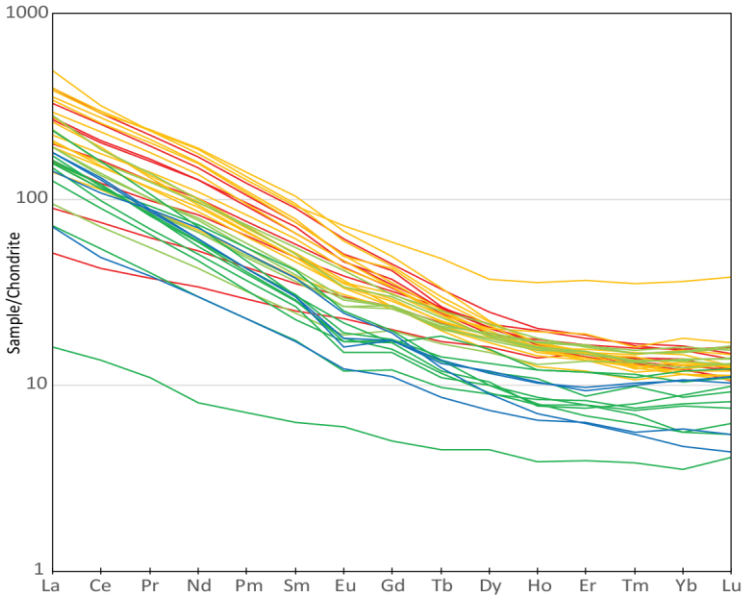
Sample/Chondrite
1000
100
10
1
La
Ce
Pr
Nd
Pm
Sm
Eu
Gd
Tb
Dy
Ho
Er
Tm
Yb
Lu

Figure 27

Figure 27. Initial Sr and Nd isotope variation diagrams for Whipple Mountains area volcanic rocks. For A-C, symbology is the same as Figures 22 and 23. For D, black are pre-extensional and red are post-extensional lavas.

Figure 27

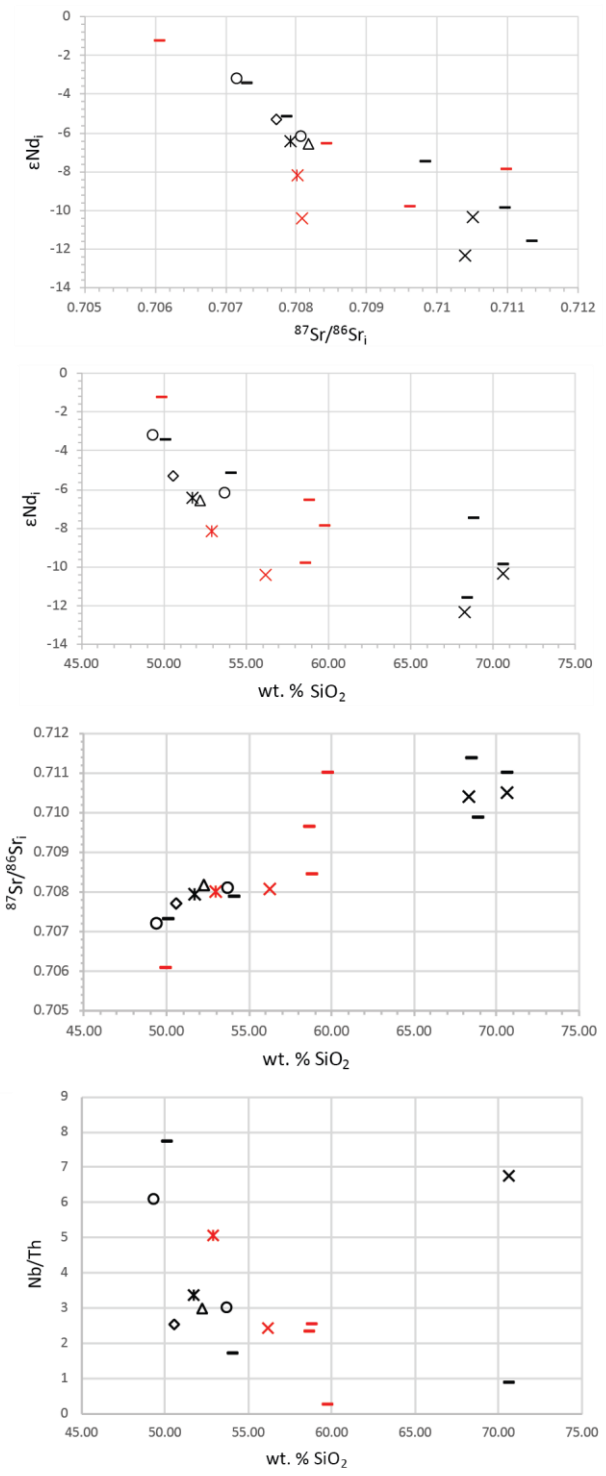

Figure 28

Figure 28. Initial Sr-Nd isotopic compositions of LCREC samples compared with compositions of regionally significant lithologies of the eastern Mojave and western Arizona terranes. Proterozoic crust (Miller and Wooden, 1994); Lower crustal xenoliths (Hanchar et al. 1994); Mesozoic intrusives (Miller and Wooden, 1994; Allen et al. 1995; Kapp et al., 2002); Other CREC units (Faulkner et al., 1995; Bachl et al., 2001; Miller and Miller, 2002; McDowell et al., 2016); Enriched basalts (Feurbach et al., 1993); enriched mantle xenoliths in Cenozoic basalts (Beard and Glazner, 1995; Mukasa and Wilshire, 1997); OIB and MORB array (Jackson, 2007).

Figure 28

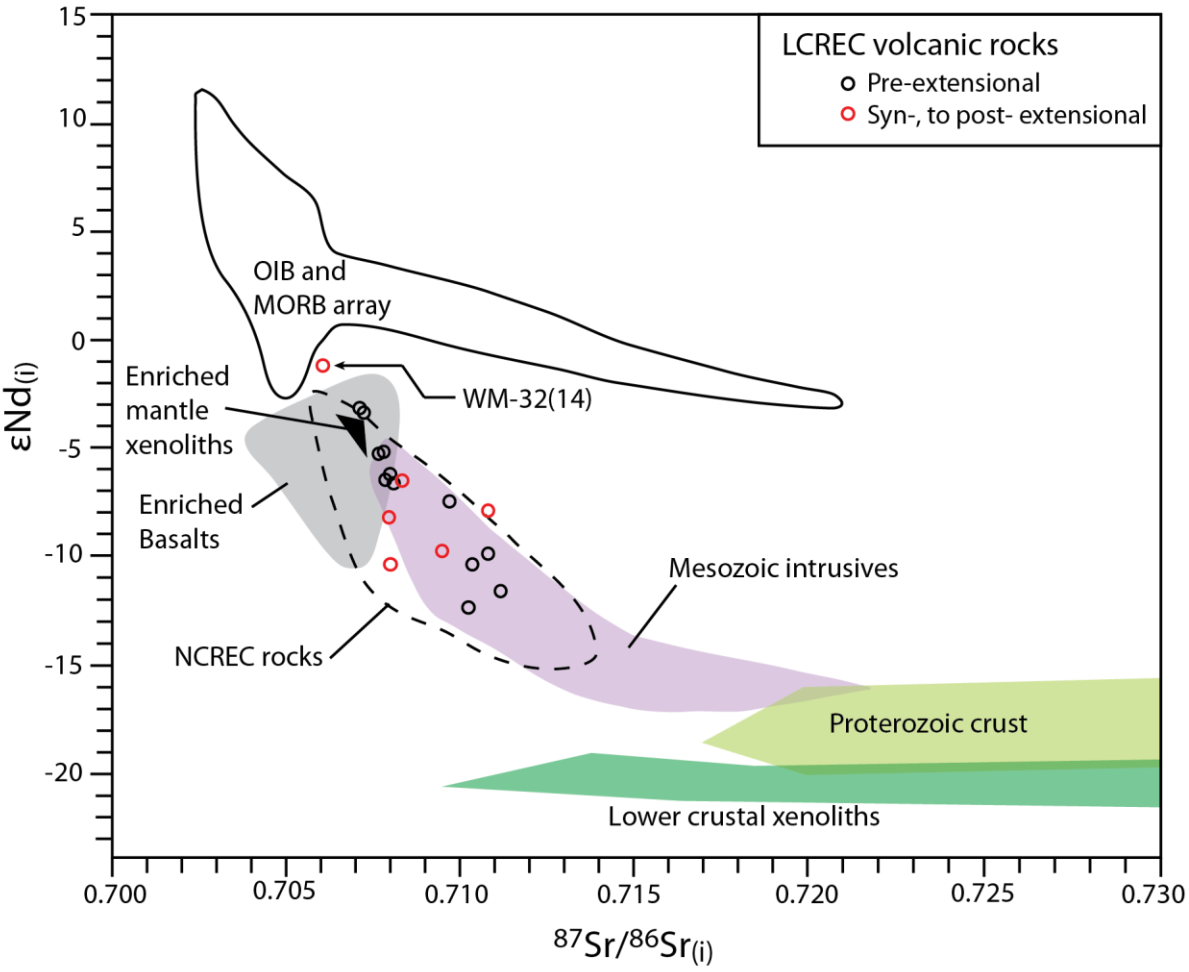
LCREC volcanic rocks
Pre-extensional
Syn-, to post- extensional
OIB and
MORB array
WM-32(14)
Enriched
mantle
xenoliths
Enriched
Basalts
NCREC rocks
Mesozoic intrusives
Proterozoic crust
Lower crustal xenoliths
εNd(i)
87Sr/86Sr(i)
15
10
5
0
-5
-10
-15
-20
0.700
0.705
0.710
0.715
0.720
0.725
0.730

Table 4. Major, minor and trace element compositions

NAME	AB-01	AB-02*	MK13-2.1	MK13-2.3	MK13-2.4	MK13-4.1*	MK13-4.2	MK13-4.3
SiO_2	50.54	73.11	53.98	48.48	52.45	70.03	49.80	50.63
TiO_2	1.64	0.29	1.46	1.89	1.52	0.47	1.70	1.93
Al_2O_3	17.50	14.60	17.00	15.91	14.89	14.98	15.03	17.70
Fe_2O_3	9.47	1.64	9.01	10.38	8.55	2.59	10.13	10.43
FeO(t)	8.43	1.46	8.02	9.24	7.61	2.30	9.01	9.28
MnO	0.11	0.04	0.12	0.16	0.09	0.04	0.21	0.10
MgO	5.45	0.54	5.90	6.13	6.78	0.82	6.12	4.04
CaO	8.39	1.45	4.26	9.04	8.43	3.21	9.10	7.73
Na_2O	3.05	4.22	4.68	2.74	2.79	3.46	3.56	3.49
K_2O	2.61	3.80	2.88	4.08	3.21	4.00	3.12	2.70
P_2O_5	0.74	0.05	0.37	0.65	0.76	0.13	0.62	0.79
Total	**99.52**	**99.73**	**99.68**	**99.45**	**99.47**	**99.74**	**99.39**	**99.54**
Sc	16.8	4.6	23.6	22.9	21.3	5.9	24.8	17.4
Ti	10390	2866	9737	11100	9504	3956	10645	12046
V	198.5	54.4	203.5	214.6	185.8	82.1	173.4	214.6
Cr	162.0	16.9	77.4	130.7	450.5	22.8	388.4	48.8
Co	179.6	179.0	200.8	183.0	164.4	242.8	231.6	242.5
Ni	97.7	9.0	38.3	76.7	183.6	16.4	125.4	43.7
Cu	24	15	34	28	58	21	60	98
Zn	130	37	91	107	85	46	101	115
Rb	43	231	72	114	69	101	76	43
Sr	1316	293	613	2114	1190	288	1029	1153
Y	32	18	28	29	28	18	27	35
Zr	238	204	223	206	282	200	215	293
Ga	22	18	20	20	20	18	17	22
Cs	0.8	3.0	0.7	23.2	0.5	3.6	0.9	0.5
Ba	1265	1165	1025	1016	1244	1227	2478	1333
La	78.2	43.3	49.3	63.6	94.8	41.0	66.0	95.2
Ce	156.1	79.2	93.8	125.3	184.3	71.8	128.6	178.4
Pr	18.7	7.7	10.7	15.0	22.0	7.7	15.4	20.6
Nd	72.2	23.5	39.7	58.6	85.3	23.2	58.9	78.3
Sm	11.6	4.1	6.8	9.8	14.1	4.1	10.6	13.3
Eu	3.3	0.9	1.9	2.7	3.4	0.9	2.6	3.5
Gd	8.4	2.5	5.6	7.0	8.7	2.9	7.4	9.0
Tb	1.1	0.5	0.8	0.9	1.1	0.5	0.9	1.2
Dy	5.5	3.0	4.6	5.1	5.4	2.3	5.1	6.1
Ho	1.0	0.6	0.9	0.9	0.9	0.5	0.9	1.1
Er	2.7	1.1	2.4	2.3	2.5	1.4	2.3	3.0
Tm	0.4	0.4	0.4	0.3	0.3	0.3	0.3	0.4
Yb	2.4	1.8	2.5	2.0	2.2	1.2	2.2	2.5
Lu	0.3	0.4	0.4	0.3	0.3	0.3	0.3	0.3
Hf	5.9	5.8	5.2	4.6	6.6	4.7	4.9	6.5
Th	10.2	12.9	6.1	5.9	13.4	10.3	6.4	10.9
U	1.3	2.6	1.1	1.0	2.5	1.8	1.0	2.1

Table 4. Major, minor and trace element compositions (continued)

NAME	MK13-4.4	MK13-4.6	MP-02*	MP-05	MP-06*	MP-07*	MP-09*	MP-12
SiO_2	52.13	52.23	68.01	67.29	68.92	68.27	68.25	68.79
TiO_2	1.85	1.54	0.63	0.58	0.47	0.48	0.47	0.44
Al_2O_3	15.03	14.83	15.85	15.89	15.83	15.92	15.75	15.40
Fe_2O_3	9.63	8.30	2.97	3.32	2.77	3.00	3.03	2.82
FeO(t)	8.57	7.39	2.65	2.96	2.47	2.67	2.69	2.51
MnO	0.16	0.10	0.04	0.06	0.04	0.05	0.05	0.04
MgO	7.65	7.47	0.92	1.59	0.94	1.20	0.87	1.64
CaO	5.31	9.73	3.22	3.62	2.76	3.18	3.09	3.06
Na_2O	4.20	2.61	3.72	3.54	3.62	3.65	3.83	3.28
K_2O	3.01	2.14	4.15	3.64	4.17	3.78	4.19	4.14
P_2O_5	0.59	0.58	0.18	0.15	0.16	0.17	0.16	0.11
Total	**99.55**	**99.53**	**99.70**	**99.70**	**99.69**	**99.68**	**99.68**	**99.72**
Sc	22.1	23.4	8.5	7.1	5.6	6.1	5.8	7.1
Ti	11912	9790	4915	4267	3592	3995	4063	3455
V	172.1	192.1	108.7	87.7	71.2	72.6	87.0	83.8
Cr	316.5	426.3	51.4	35.5	27.1	36.2	30.1	41.5
Co	134.3	183.5	194.7	193.1	174.1	272.2	190.8	183.7
Ni	181.4	204.1	17.7	20.5	12.9	13.6	12.2	29.8
Cu	71	44	34	26	30	29	31	33
Zn	94	94	56	60	56	59	58	53
Rb	70	33	90	134	93	89	94	104
Sr	750	1085	543	602	569	679	597	529
Y	26	24	18	17	15	17	15	14
Zr	202	239	197	180	202	206	199	165
Ga	18	19	20	20	19	21	21	20
Cs	0.3	0.2	0.9	1.3	0.6	1.4	1.1	1.1
Ba	1524	1007	1019	958	1214	1228	1275	1049
La	52.9	81.7	38.8	30.0	46.8	50.2	42.0	31.5
Ce	108.3	159.4	69.3	55.1	79.1	91.5	74.4	60.7
Pr	13.0	18.8	7.5	6.1	8.8	9.6	9.2	6.3
Nd	50.7	71.5	27.6	21.5	31.6	35.3	27.4	21.4
Sm	9.1	11.1	3.7	3.3	5.2	5.2	4.1	4.2
Eu	2.4	2.8	1.3	1.0	1.1	1.5	1.1	0.9
Gd	6.8	7.1	3.6	3.4	4.6	4.0	3.8	2.4
Tb	0.9	0.9	0.5	0.4	0.6	0.7	0.6	0.4
Dy	4.9	4.7	3.0	2.6	3.5	3.5	3.2	2.3
Ho	0.9	0.8	0.6	0.4	0.5	0.8	0.5	0.4
Er	2.3	2.3	1.7	1.2	1.3	1.4	1.2	1.1
Tm	0.3	0.3	0.4	0.2	0.3	0.3	0.2	0.2
Yb	1.9	1.8	1.4	1.4	0.6	1.9	1.4	1.1
Lu	0.3	0.3	0.2	0.2	0.3	0.3	0.2	0.2
Hf	4.7	5.8	4.5	4.4	5.1	5.5	4.7	3.1
Th	5.9	10.2	9.7	8.4	10.2	10.9	9.8	8.5
U	1.0	1.5	1.7	1.4	1.3	1.5	1.4	1.3

Table 4. Major, minor and trace element compositions (continued)

NAME	MP-13	MP-14	MP-15	MP-16	MP-18	MP-19	MP-21*	MP-22
SiO_2	70.35	54.00	57.19	56.21	56.12	70.28	68.93	68.95
TiO_2	0.37	1.36	1.19	1.27	1.32	0.38	0.43	0.44
Al_2O_3	14.62	16.53	16.07	16.57	14.75	14.77	15.24	15.20
Fe_2O_3	2.34	8.64	6.88	7.10	6.56	2.42	2.76	2.82
FeO(t)	2.08	7.69	6.12	6.32	5.84	2.15	2.46	2.51
MnO	0.04	0.14	0.11	0.11	0.10	0.04	0.04	0.05
MgO	1.21	5.41	4.72	4.80	4.73	1.06	1.64	1.63
CaO	3.16	8.42	7.24	7.38	7.67	2.81	3.00	3.03
Na_2O	2.73	3.36	3.45	3.55	3.28	3.23	3.66	3.70
K_2O	4.76	1.55	2.40	2.26	4.14	4.61	3.90	3.78
P_2O_5	0.13	0.31	0.40	0.41	0.75	0.09	0.11	0.11
Total	**99.71**	**99.71**	**99.65**	**99.66**	**99.43**	**99.70**	**99.72**	**99.71**
Sc	4.6	23.5	18.3	19.6	16.2	3.8	6.2	6.9
Ti	3167	9194	7863	8474	8437	2993	3514	3556
V	74.3	194.7	151.5	165.0	154.3	59.1	77.8	77.6
Cr	22.5	148.7	146.7	141.6	169.4	67.0	34.7	48.4
Co	436.5	230.2	166.2	146.1	163.8	62.0	146.8	162.2
Ni	14.6	62.1	74.6	65.3	87.6	36.0	14.8	28.6
Cu	36	51	53	48	72	20	22	25
Zn	47	89	85	84	91	47	49	50
Rb	90	23	47	42	94	107	107	105
Sr	430	574	741	735	1259	476	510	506
Y	19	27	23	25	27	20	14	14
Zr	170	192	263	268	322	178	162	164
Ga	16	19	20	21	20	19	20	18
Cs	1.3	0.3	0.4	0.3	1.0	0.4	1.4	1.0
Ba	1237	827	1015	894	2037	760	1484	956
La	38.2	33.6	67.4	66.3	92.5	33.7	47.4	35.0
Ce	71.0	69.2	115.1	115.0	180.7	66.7	87.5	60.3
Pr	7.5	8.1	12.8	12.5	22.3	8.2	9.1	6.4
Nd	23.1	31.5	45.8	46.4	86.8	32.3	29.0	23.4
Sm	4.3	5.7	7.5	7.6	15.5	5.6	5.2	3.9
Eu	0.8	1.7	1.9	2.0	3.8	1.4	1.1	0.8
Gd	3.1	5.1	6.0	5.8	9.9	3.8	3.5	3.0
Tb	0.5	0.8	0.8	0.8	1.2	0.5	0.6	0.4
Dy	2.5	4.4	4.5	4.6	5.5	2.2	3.1	2.5
Ho	0.4	0.9	0.9	0.9	0.9	0.4	0.6	0.5
Er	1.3	2.5	2.4	2.3	2.4	1.0	1.8	1.3
Tm	0.3	0.4	0.3	0.4	0.3	0.1	0.4	0.2
Yb	1.4	2.4	2.0	2.1	1.9	0.8	1.2	0.9
Lu	0.3	0.3	0.3	0.3	0.3	0.1	0.4	0.2
Hf	4.1	4.1	6.1	5.8	7.8	3.0	5.2	4.4
Th	10.5	4.1	10.9	10.5	16.7	6.0	13.6	11.3
U	1.7	0.7	1.2	1.1	3.0	1.1	2.3	1.3

Table 4. Major, minor and trace element compositions (continued)

NAME	MP-23	MP-24	MP-25	MP-26	MP-27*	MP-28	MP-31	MP-32
SiO_2	67.42	70.60	60.15	69.15	68.03	69.67	70.66	70.44
TiO_2	0.55	0.39	0.93	0.43	0.44	0.41	0.37	0.38
Al_2O_3	15.78	14.94	14.27	15.50	15.88	15.49	15.05	15.07
Fe_2O_3	3.44	2.33	5.36	2.65	2.85	2.48	2.42	2.52
FeO(t)	3.06	2.07	4.77	2.36	2.54	2.21	2.15	2.24
MnO	0.06	0.04	0.08	0.05	0.05	0.04	0.04	0.05
MgO	1.71	0.94	4.40	1.31	2.08	0.99	0.94	1.02
CaO	3.87	2.39	6.33	2.93	3.43	2.72	2.41	2.43
Na_2O	3.30	3.41	3.07	3.69	3.31	3.71	3.35	3.36
K_2O	3.38	4.55	4.34	3.87	3.54	4.03	4.39	4.34
P_2O_5	0.17	0.13	0.56	0.12	0.11	0.12	0.11	0.12
Total	**99.68**	**99.72**	**99.51**	**99.71**	**99.71**	**99.68**	**99.73**	**99.73**
Sc	8.2	4.2	11.9	3.7	6.2	5.2	6.3	6.1
Ti	3980	3229	6355	2855	4060	3716	2711	2754
V	77.7	64.6	113.9	54.4	86.1	74.1	55.9	60.9
Cr	24.8	13.3	158.7	76.1	30.3	13.7	12.2	14.6
Co	147.9	34.3	157.8	73.4	210.4	39.2	155.4	171.8
Ni	15.5	14.7	91.6	45.1	12.5	15.7	9.3	10.0
Cu	23	21	45	21	25	24	15	18
Zn	61	42	74	48	54	55	30	34
Rb	65	109	100	110	111	98	116	112
Sr	740	450	997	525	533	589	449	439
Y	21	19	25	17	14	15	17	18
Zr	214	184	278	176	162	186	171	176
Ga	20	19	19	19	20	21	18	20
Cs	0.7	0.5	0.7	0.4	1.6	0.6	1.3	1.5
Ba	1006	514	1859	845	1686	589	1148	1190
La	50.3	17.0	80.0	37.1	50.7	19.6	42.6	42.3
Ce	90.6	29.9	153.6	70.6	93.1	34.3	78.0	78.7
Pr	9.6	3.6	18.7	8.6	9.9	4.2	8.1	8.1
Nd	33.3	13.8	73.6	33.6	33.2	15.5	28.0	28.1
Sm	5.3	2.5	12.4	6.1	4.7	3.0	4.5	4.6
Eu	1.2	0.7	3.0	1.4	1.5	0.8	1.0	1.0
Gd	4.7	2.2	8.3	3.9	4.5	2.5	3.5	3.3
Tb	0.8	0.3	1.0	0.5	0.6	0.4	0.5	0.5
Dy	3.1	1.8	5.0	2.5	4.4	2.0	3.0	3.0
Ho	0.6	0.4	0.8	0.4	0.6	0.4	0.6	0.6
Er	2.0	1.0	2.2	1.1	2.2	1.1	1.5	1.6
Tm	0.3	0.1	0.3	0.2	0.3	0.2	0.2	0.2
Yb	1.6	0.9	1.9	0.9	1.5	1.0	1.7	1.7
Lu	0.3	0.1	0.3	0.1	0.3	0.1	0.3	0.3
Hf	5.7	2.5	7.0	3.3	6.8	2.8	4.8	4.7
Th	14.4	2.7	15.3	6.8	12.8	3.1	12.7	12.8
U	1.5	0.8	2.4	1.1	1.9	0.9	2.2	2.3

Table 4. Major, minor and trace element compositions (continued)

NAME	MP-33	MP-34*	MP-35	MP-36	MP-37	WM-4	WM-6	WM-7
SiO_2	56.21	67.11	67.12	52.83	69.54	54.14	62.36	68.61
TiO_2	1.17	0.58	0.60	1.60	0.39	1.78	0.87	0.44
Al_2O_3	16.20	15.99	15.92	17.31	15.73	18.45	16.87	14.70
Fe_2O_3	7.08	3.54	3.47	8.56	2.43	6.89	3.73	2.20
FeO(t)	6.30	3.15	3.09	7.62	2.16	6.13	3.32	1.96
MnO	0.14	0.06	0.06	0.11	0.04	0.07	0.10	0.05
MgO	5.74	1.73	1.72	4.29	0.95	3.20	1.23	0.43
CaO	6.93	3.61	3.51	8.64	2.80	5.73	2.35	1.10
Na_2O	3.12	3.44	3.21	3.31	3.64	3.79	1.93	0.63
K_2O	2.68	3.50	3.95	2.38	4.06	4.59	9.99	11.43
P_2O_5	0.39	0.16	0.18	0.60	0.13	0.85	0.22	0.11
Total	**99.67**	**99.71**	**99.72**	**99.62**	**99.70**	**99.49**	**99.65**	**99.70**
Sc	18.8	14.1	8.1	18.9	6.0	26.1	4.7	-0.1
Ti	6887	3280	3913	8960	2802	15473	2798	1043
V	161.4	57.7	80.2	185.5	61.5	196.6	64.3	23.8
Cr	178.6	1023.7	20.3	37.5	13.9	49.9	24.3	18.4
Co	215.6	106.7	210.2	193.9	166.3	413.7	104.5	55.5
Ni	100.9	14.5	21.3	39.9	9.0	23.6	12.0	12.0
Cu	45	17	24	50	16	45	21	22
Zn	66	44	35	73	39	89	123	82
Rb	47	132	98	42	111	111	271	275
Sr	633	570	550	1172	565	1149	306	87
Y	23	15	16	24	13	33	25	15
Zr	244	176	188	212	181	421	401	208
Ga	21	20	20	21	20	23	22	16
Cs	0.5	1.1	1.8	0.4	1.4	2.3	1.2	0.4
Ba	911	1132	1117	1039	1307	3553	815	319
La	62.3	46.6	38.8	70.7	37.7	118.2	32.4	12.6
Ce	117.5	64.4	74.8	142.4	74.1	198.6	58.6	22.8
Pr	12.3	8.0	7.6	16.6	7.7	22.0	6.0	2.3
Nd	43.0	33.6	26.9	62.4	25.7	81.3	22.4	9.1
Sm	7.2	4.6	4.3	9.7	4.2	13.7	3.0	1.5
Eu	1.9	1.2	1.0	2.7	1.0	4.1	1.0	0.3
Gd	5.3	4.1	3.5	6.7	3.1	11.8	2.9	1.4
Tb	0.7	0.8	0.5	0.9	0.4	1.8	0.5	0.2
Dy	4.2	3.4	2.9	4.5	2.3	9.2	2.2	1.2
Ho	0.8	0.9	0.6	0.8	0.4	2.0	0.5	0.2
Er	2.2	1.8	1.4	2.2	1.3	5.9	1.1	0.6
Tm	0.3	0.2	0.2	0.3	0.2	0.9	0.2	0.1
Yb	2.2	1.8	1.4	2.0	1.2	5.9	1.0	0.5
Lu	0.3	0.4	0.2	0.3	0.2	0.9	0.2	0.1
Hf	5.5	5.8	4.9	5.3	4.7	21.9	4.0	1.7
Th	10.5	13.1	10.0	9.7	10.3	26.3	8.8	4.0
U	1.5	1.5	2.4	1.8	1.8	4.9	1.3	0.5

Table 4. Major, minor and trace element compositions (continued)

NAME	WM-8*†	WM-9*	WM-13†	WM-14	WM-15	WM-20	WM-21	WM-24
SiO_2	68.91	60.88	50.20	58.78	58.72	51.99	50.59	59.61
TiO_2	0.48	1.05	1.41	1.03	1.03	1.83	1.29	0.97
Al_2O_3	15.67	16.09	17.89	16.24	16.23	16.67	16.41	16.03
Fe_2O_3	2.66	4.95	10.08	6.14	6.00	10.00	10.70	6.74
FeO(t)	2.37	4.40	8.97	5.47	5.34	8.90	9.52	6.00
MnO	0.05	0.16	0.15	0.10	0.10	0.16	0.17	0.11
MgO	1.06	2.16	6.79	4.79	4.36	4.89	7.10	3.25
CaO	3.69	5.99	8.92	6.42	6.34	8.36	9.67	6.87
Na_2O	1.92	3.54	2.65	3.49	3.60	3.56	3.11	3.27
K_2O	5.07	4.53	1.36	2.38	2.83	1.71	0.57	2.67
P_2O_5	0.15	0.32	0.25	0.28	0.29	0.48	0.17	0.22
Total	**102.03**	**99.66**	**108.67**	**99.66**	**99.50**	**99.63**	**99.78**	**99.75**
Sc	7.0	32.0	32.5	17.1	17.6	22.1	27.7	22.0
Ti	3049	18670	8615	7026	7040	11821	8663	6853
V	61.7	314.3	172.0	146.4	140.1	204.0	201.8	157.0
Cr	16.0	72.2	157.3	122.9	134.3	247.1	250.7	90.7
Co	128.9	804.0	149.2	184.9	185.2	142.7	208.1	237.7
Ni	12.5	27.2	72.4	79.6	78.6	129.3	102.1	40.2
Cu	14	30	12	45	51	62	73	40
Zn	49	74	235	74	72	96	93	62
Rb	182	111	27	47	61	27	5	66
Sr	955	584	558	802	777	710	398	411
Y	15	28	26	26	26	30	22	26
Zr	207	305	147	235	236	223	103	184
Ga	19	20	19	19	19	20	19	17
Cs	38.7	4.1	0.4	0.5	0.5	0.2	0.1	0.8
Ba	1169	6056	800	947	2376	991	322	793
La	45.5	151.5	21.3	45.8	45.6	38.1	12.3	37.5
Ce	79.6	294.2	46.4	83.1	85.2	75.9	26.4	70.1
Pr	8.5	31.5	5.8	9.4	9.4	9.2	3.5	8.0
Nd	29.4	110.1	24.2	35.3	36.5	37.9	15.5	30.6
Sm	4.1	11.1	5.2	5.8	6.3	7.3	3.7	5.6
Eu	1.3	4.7	1.7	1.6	1.7	2.2	1.3	1.5
Gd	4.2	14.7	5.3	5.3	5.3	6.4	4.0	5.1
Tb	0.4	1.6	0.8	0.7	0.7	0.9	0.6	0.8
Dy	2.6	10.8	4.6	4.4	4.3	5.3	4.0	4.8
Ho	0.6	2.3	1.0	0.9	0.8	1.1	0.8	0.9
Er	1.5	4.9	2.7	2.3	2.4	2.9	2.4	2.7
Tm	0.2	0.6	0.4	0.3	0.3	0.4	0.3	0.4
Yb	1.7	10.5	2.5	2.2	2.2	2.6	2.1	2.4
Lu	0.2	1.1	0.4	0.3	0.3	0.4	0.3	0.4
Hf	5.7	26.8	3.6	5.5	5.5	5.3	2.6	4.5
Th	11.7	54.9	2.5	8.7	8.7	4.3	1.2	7.9
U	2.1	9.1	0.5	1.0	1.9	0.9	0.4	1.0

Table 4. Major, minor and trace element compositions (continued)

NAME	WM-25A	WM-25B*	WM-26*	WM-27*	WM-28	WM-29*	WM-32(12)	WM-32(14)*
SiO_2	68.59	69.96	71.50	59.01	69.56	70.89	48.40	49.96
TiO_2	0.44	0.41	0.47	1.31	0.50	0.38	1.11	1.27
Al_2O_3	15.48	14.68	15.68	18.09	15.80	14.85	14.84	16.38
Fe_2O_3	2.82	2.54	2.39	5.91	2.66	2.23	9.70	10.83
FeO(t)	2.51	2.26	2.13	5.26	2.37	1.99	8.63	9.64
MnO	0.04	0.02	0.02	0.09	0.03	0.04	0.26	0.17
MgO	1.71	0.90	0.41	1.91	0.66	0.92	0.34	7.38
CaO	3.14	2.99	1.43	6.77	2.48	2.53	11.90	10.08
Na_2O	3.42	3.53	2.96	3.63	3.65	3.27	0.09	3.07
K_2O	3.96	4.55	4.74	2.65	4.25	4.51	11.90	0.50
P_2O_5	0.11	0.12	0.12	0.32	0.12	0.11	0.17	0.16
Total	**99.71**	**99.71**	**99.72**	**99.68**	**99.73**	**99.73**	**98.70**	**99.80**
Sc	8.3	5.7	1.8	32.2	4.5	6.2	34.2	28.8
Ti	3080	3320	1628	17736	3339	4276	10140	13489
V	76.0	81.5	33.4	301.2	68.5	88.1	236.2	281.0
Cr	44.9	51.6	26.2	72.4	12.1	38.4	311.7	81.4
Co	111.9	207.2	118.3	965.2	35.5	274.7	293.5	532.5
Ni	21.6	27.3	13.2	25.3	14.3	14.1	126.2	34.9
Cu	27	26	24	42	22	22	60	77
Zn	55	40	41	77	47	43	69	91
Rb	106	115	98	49	94	117	264	3
Sr	536	459	351	721	436	448	1063	372
Y	16	14	15	25	17	19	21	22
Zr	164	148	194	211	190	181	102	97
Ga	20	19	19	22	19	19	8	18
Cs	0.4	1.4	0.5	2.6	0.5	1.3	0.2	5.3
Ba	355	1062	604	4973	530	1407	285	4405
La	17.3	35.2	18.0	165.2	18.0	44.2	13.2	159.3
Ce	33.3	65.5	29.7	289.0	31.5	70.7	28.9	299.3
Pr	3.8	7.0	3.3	29.4	3.8	7.4	3.8	31.0
Nd	13.8	28.9	10.2	99.1	14.2	27.5	16.9	104.7
Sm	2.6	4.4	2.5	14.4	2.7	3.4	4.4	18.5
Eu	0.7	1.1	0.4	4.2	0.8	1.0	1.5	3.7
Gd	2.4	3.0	1.5	12.6	2.2	5.1	4.6	11.2
Tb	0.4	0.2	0.2	1.9	0.3	0.5	0.7	2.2
Dy	2.2	2.1	1.4	10.4	1.8	2.0	4.7	9.7
Ho	0.5	0.5	0.3	2.1	0.3	0.6	1.0	2.0
Er	1.3	1.3	1.0	5.8	1.0	1.8	2.6	6.5
Tm	0.2	0.2	0.1	1.4	0.1	0.3	0.4	1.1
Yb	1.3	1.0	0.6	4.0	0.8	2.4	2.6	5.1
Lu	0.2	0.2	0.1	1.1	0.1	0.4	0.4	0.9
Hf	2.0	4.4	2.3	19.4	2.6	5.4	2.7	15.1
Th	3.5	10.4	5.7	48.3	2.8	12.0	1.3	45.9
U	0.5	1.7	0.8	8.6	0.8	1.9	0.3	7.4

Table 4. Major, minor and trace element compositions (continued)

NAME	WM-33(14)	WM-34*	WM-35*	WM-36	WM-38	WM-39†	WM-41	WM-43
SiO_2	69.48	68.50	70.87	68.17	69.10	70.72	57.56	67.32
TiO_2	0.43	0.43	0.35	0.47	0.45	0.37	1.12	0.61
Al_2O_3	15.15	15.35	14.58	15.31	15.12	14.88	16.43	15.96
Fe_2O_3	2.43	2.76	2.16	2.95	2.78	2.37	6.54	3.28
FeO(t)	2.16	2.46	1.92	2.63	2.47	2.11	5.82	2.92
MnO	0.03	0.04	0.04	0.04	0.05	0.04	0.11	0.07
MgO	1.42	1.70	0.95	1.75	1.59	1.20	3.48	1.76
CaO	3.04	3.09	2.76	3.55	2.99	2.50	7.99	3.59
Na_2O	3.64	3.26	3.46	3.81	3.46	4.00	3.36	3.97
K_2O	3.96	4.47	4.42	3.53	4.06	3.57	2.79	2.97
P_2O_5	0.11	0.11	0.10	0.12	0.11	0.09	0.30	0.18
Total	**99.69**	**99.72**	**99.71**	**99.72**	**99.72**	**101.84**	**99.68**	**99.70**
Sc	4.2	6.3	5.8	6.9	21.9	8.7	21.6	7.1
Ti	1731	3431	3247	4049	2182	2768	11215	4504
V	26.7	83.7	70.7	92.3	67.0	67.2	209.9	83.0
Cr	34.5	55.5	52.5	26.2	182.4	38.2	34.0	23.1
Co	42.6	211.4	203.2	167.3	245.4	212.8	113.9	148.9
Ni	11.9	29.8	27.9	14.5	0.0	29.5	35.0	20.6
Cu	25	21	17	30	20	12	54	26
Zn	50	48	43	55	50	44	73	55
Rb	103	101	112	93	122	139	58	133
Sr	507	513	417	511	498	434	790	589
Y	14	15	17	14	170	14	28	18
Zr	154	157	178	157	14	169	205	199
Ga	19	20	19	20	19	20	19	19
Cs	0.1	1.2	1.2	1.9	0.0	1.8	1.5	1.4
Ba	2463	1351	1161	1662	594	1295	1731	1050
La	3.8	33.4	36.5	56.2	37.2	52.2	56.9	40.7
Ce	8.4	57.9	66.6	98.5	35.7	100.3	97.2	72.5
Pr	1.0	6.3	7.1	9.9	9.2	9.0	11.6	7.8
Nd	3.7	23.0	22.2	32.7	40.2	31.3	44.3	27.3
Sm	0.9	3.7	4.2	4.5	10.7	4.3	8.2	4.6
Eu	0.3	1.0	0.9	1.2	1.7	1.1	2.3	1.1
Gd	1.0	2.9	2.5	3.4	0.0	3.6	6.1	3.5
Tb	0.2	0.4	0.5	0.7	0.2	0.4	0.9	0.5
Dy	1.1	2.3	2.5	3.9	0.0	2.5	5.2	3.3
Ho	0.2	0.4	0.7	0.7	3.2	0.4	1.0	0.7
Er	0.6	1.1	0.8	1.9	3.0	1.4	2.6	1.9
Tm	0.1	0.2	0.2	0.3	1.4	0.2	0.4	0.3
Yb	0.6	0.8	1.6	1.9	0.0	1.2	2.4	1.7
Lu	0.1	0.2	0.3	0.3	3.4	0.2	0.4	0.3
Hf	0.8	4.0	4.1	6.0	3.3	5.4	7.5	5.4
Th	0.5	10.0	10.3	15.3	14.2	17.0	9.4	10.2
U	0.3	1.5	1.3	2.7	6.1	2.3	2.6	1.9

Table 4. Major, minor and trace element compositions (continued)

NAME	WM-44*	WM-48†	WW-2	WW-6	WW-10	WW-13	WW-18	WW-19
SiO_2	68.41	58.89	70.41	63.12	54.29	70.44	70.73	70.69
TiO_2	0.47	0.97	0.39	0.85	1.25	0.40	0.38	0.38
Al_2O_3	16.00	16.26	15.10	15.93	16.43	15.21	15.14	15.10
Fe_2O_3	2.83	6.76	2.51	5.36	7.86	2.58	2.48	2.40
FeO(t)	2.51	6.02	2.24	4.77	7.00	2.29	2.21	2.14
MnO	0.04	0.12	0.05	0.19	0.08	0.05	0.05	0.04
MgO	1.19	4.27	0.99	1.38	5.93	1.05	0.99	0.99
CaO	3.06	6.84	2.52	0.64	8.93	2.58	2.52	2.49
Na_2O	3.87	3.07	3.36	0.28	2.72	3.94	3.37	3.37
K_2O	3.62	2.36	4.28	11.32	1.80	3.36	3.96	4.18
P_2O_5	0.16	0.22	0.12	0.23	0.37	0.12	0.11	0.11
Total	**99.65**	**105.77**	**99.73**	**99.31**	**99.67**	**99.73**	**99.73**	**99.73**
Sc	6.5	23.0	6.5	9.2	25.7	6.4	6.2	6.1
Ti	3193	5280	2789	5035	7216	2939	2823	2747
V	64.8	122.0	55.1	103.7	169.4	64.7	57.9	59.0
Cr	46.7	95.7	13.1	6.9	169.8	13.9	13.4	12.1
Co	170.7	198.8	152.2	120.7	148.4	174.7	173.2	172.6
Ni	23.2	41.4	9.3	56.1	71.5	10.4	10.1	10.4
Cu	32	35	15	13	50	16	14	20
Zn	56	63	30	1126	79	30	36	28
Rb	147	59	117	266	33	135	124	125
Sr	644	422	440	333	880	482	461	441
Y	15	27	18	20	19	17	18	19
Zr	206	180	171	197	145	170	171	172
Ga	21	18	18	22	20	20	18	18
Cs	0.9	0.7	1.4	0.7	0.3	1.6	1.5	1.5
Ba	893	740	1205	3023	898	1187	1169	1147
La	29.4	37.0	44.6	30.5	48.2	42.5	42.9	42.5
Ce	53.3	70.9	81.3	61.4	98.1	80.6	82.1	81.0
Pr	5.5	8.2	8.4	6.6	11.8	8.1	8.2	8.2
Nd	18.0	30.5	29.3	24.0	44.4	28.9	28.1	28.2
Sm	3.0	5.4	5.0	4.5	7.6	4.5	4.7	4.4
Eu	0.8	1.5	1.0	1.2	2.1	0.9	1.0	0.9
Gd	2.7	5.4	3.9	3.7	5.3	3.7	3.6	3.5
Tb	0.4	0.8	0.5	0.5	0.7	0.5	0.5	0.5
Dy	2.6	4.6	3.2	3.1	3.8	3.0	2.8	2.9
Ho	0.5	0.9	0.6	0.6	0.7	0.5	0.6	0.6
Er	0.9	2.6	1.7	1.7	1.9	1.7	1.7	1.6
Tm	0.2	0.4	0.3	0.2	0.3	0.3	0.2	0.3
Yb	0.9	2.6	2.0	1.6	1.8	1.7	1.7	1.7
Lu	0.1	0.4	0.3	0.2	0.3	0.2	0.3	0.3
Hf	4.1	4.4	4.9	4.5	3.7	4.7	4.7	4.7
Th	9.6	7.9	13.9	7.4	7.6	12.9	13.5	12.8
U	1.7	1.0	2.2	1.6	1.7	2.2	2.1	2.2

Table 4. Major, minor and trace element compositions (continued)

NAME	WW-21	TTM-01†	TTM-02†	MHV-04†	MHV-10†	SWM-03†
SiO_2	70.89	49.41	53.76	52.93	51.70	59.83
TiO_2	0.37	2.08	1.65	1.40	1.73	0.89
Al_2O_3	15.07	16.76	16.16	16.77	16.49	15.73
Fe_2O_3	2.37	10.82	8.21	9.13	9.26	6.28
FeO(t)	2.11	9.63	7.31	8.13	8.24	5.59
MnO	0.04	0.16	0.11	0.14	0.13	0.11
MgO	0.94	6.36	5.19	5.33	6.02	4.38
CaO	2.46	9.37	7.89	8.77	8.49	6.57
Na_2O	3.59	2.86	3.16	3.14	2.81	3.03
K_2O	3.89	1.25	2.73	1.72	2.30	2.13
P_2O_5	0.11	0.59	0.68	0.34	0.63	0.18
Total	**99.74**	**109.28**	**106.85**	**107.80**	**107.79**	**104.73**
Sc	5.9	22.7	16.6	27.1	19.9	16.5
Ti	2757	12306	9705	8282	10197	3711
V	58.5	185.5	143.0	162.6	168.1	95.2
Cr	12.9	164.0	166.8	96.4	201.9	73.8
Co	373.7	140.1	158.9	157.4	117.3	125.2
Ni	9.8	102.2	122.3	44.3	141.8	45.1
Cu	22	48	70	52	69	39
Zn	22	95	94	90	100	60
Rb	121	21	56	26	37	48
Sr	422	986	1125	880	1091	5577
Y	19	23	24	28	26	14
Zr	167	235	314	195	256	82
Ga	18	20	21	22	22	17
Cs	1.5	0.3	0.7	0.3	0.7	0.5
Ba	1185	611	1166	770	1036	796
La	43.4	47.7	85.3	45.8	78.3	22.5
Ce	80.9	99.7	169.7	92.3	157.4	43.9
Pr	8.2	11.7	19.7	10.9	18.2	5.1
Nd	29.1	46.3	72.6	41.6	68.3	19.5
Sm	4.7	8.6	11.6	7.3	11.2	3.6
Eu	1.0	2.4	2.8	2.0	2.9	1.0
Gd	3.7	6.7	8.5	6.3	8.3	3.9
Tb	0.5	0.9	1.0	0.9	1.0	0.6
Dy	3.1	4.7	5.2	5.0	5.0	3.7
Ho	0.6	0.9	0.9	1.1	0.9	0.7
Er	1.6	2.3	2.4	3.0	2.4	2.2
Tm	0.2	0.3	0.3	0.4	0.3	0.3
Yb	1.6	2.0	2.1	2.9	2.2	2.2
Lu	0.3	0.3	0.3	0.4	0.3	0.3
Hf	4.9	5.3	7.8	5.1	6.2	3.3
Th	13.1	5.4	12.2	4.5	9.3	3.9
U	2.2	1.0	2.3	0.7	1.5	2.6

Table 4. Oxides are in weight percent and trace elements are in parts per million.
All oxides and Cu, Zn, Rb, Sr, Y, Zr, and Ga were measured by XRF at Pomona, while Sc, Ti, Cr, Co, Ni, Cs, Ba, La, Ce, Pr, Nd, Sm, Eu, Gd, Tb, Dy, Ho, Er, Tm, Yb, Lu, Hf, Th, and U were measured by LA-Q-ICP-MS at UCSB.
Oxides are normalized to 100% excluding LOI.
*Samples with low HREE contents that display spiky chondrite normalized REE profiles. These samples are not displayed in Figure #.
†Samples for which ^{157}Gd was measured. For all other samples, ^{160}Gd was measured.

Table 5. Sr and Nd isotopic data for Whipple Mountains area volcanic rocks

Sample	$^{87}Sr/^{86}Sr_o$	$^{143}Nd/^{144}Nd_o$	$^{87}Sr/^{86}Sr_i$	$^{143}Nd/^{144}Nd_i$	εNd_i
AB-01	0.707741	0.512346	0.707714	0.512333	-5.29
MK13-4.6	0.708197	0.512279	0.708171	0.512279	-6.58
MHV-04	0.708025	0.512199	0.708001	0.512186	-8.17
MHV-10	0.707951	0.512286	0.707923	0.512274	-6.45
MP-07	0.710505	0.511983	0.710402	0.511971	-12.37
MP-16	0.708120	0.512190	0.708075	0.512086	-10.39
MP-24	0.710690	0.512086	0.710499	0.512075	-13.35
TTM-01	0.707189	0.512453	0.707171	0.512439	-3.23
TTM-02	0.708121	0.512295	0.708080	0.512283	-6.27
WM-4	0.707964	0.512351	0.707885	0.512338	-5.19
WM-8	0.710018	0.512232	0.709861	0.512220	-7.49
WM-13	0.707356	0.512445	0.707317	0.512429	-3.43
WM-15	0.709686	0.512115	0.709625	0.512103	-9.82
WM-32	0.706093	0.512564	0.706086	0.512541	-1.23
WM-34	0.711527	0.512021	0.711365	0.512008	-11.64
WM-39	0.711244	0.512109	0.710983	0.512097	-9.89
WM-48	0.708534	0.512285	0.708419	0.512271	-6.51
SWM-03	0.711005	0.512221	0.711003	0.512217	-7.92

A. References

Allen, C. M., Wooden, J. L., Howard, K. A., Foster, D. A., & Tosdal, R. M. (1995). Sources of the Early Cretaceous plutons in the Turtle and West Riverside Mountains, California: anomalous Cordilleran interior intrusions. *Journal of Petrology, 36*(6), 1675-1700.

Armstrong, R. L., & Ward, P. L. (1991). Evolving geographic patterns of cenozoic magmatism in the north american cordillera; the temporal and spatial association of magmatism and metamorphic core complexes. *Journal of Geophysical Research, 96*, 13-13,224.

Axen, G. J., Taylor, W. J., & Bartley, J. M. (1993). Space-time patterns and tectonic controls of tertiary extension and magmatism in the great basin of the western united states. *Geological Society of America Bulletin, 105*(1), 56-76.

Bachl, C. A., Miller, C. F., Miller, J. S., & Faulds, J. E. (2001). Construction of a pluton: Evidence from an exposed cross section of the Searchlight pluton, Eldorado Mountains, Nevada. *Geological Society of America Bulletin, 113*(9), 1213-1228.

Beard, B. L., & Glazner, A. F. (1995). Trace element and Sr and Nd isotopic composition of mantle xenoliths from the Big Pine volcanic field, California. *Journal of Geophysical Research: Solid Earth, 100*(B3), 4169-4179.

Bennett, V. C., & DePaolo, D. J. (1987). Proterozoic crustal history of the western United States as determined by neodymium isotopic mapping. *GSA Bulletin, 99*(5), 674-685.

Beratan, K.K., 1990, Basin development during Miocene detachment faulting, Whipple Mountains, southeastern California: Los Angeles, University of Southern California, Ph.D. Dissertation, 267 p.

Best, M. G., & Christiansen, E. H. (1991). Limited extension during peak tertiary volcanism, great basin of nevada and utah.*Journal of Geophysical Research, 96*, 13-13,528.

Bradshaw, T. K., Hawkesworth, C. J., & Gallagher, K. (1993). Basaltic volcanism in the southern basin and range; no role for a mantle plume. *Earth and Planetary Science Letters, 116*(1-4), 45-62.

Carr, W. J., Dickey, D. D., & Quinlivan, W. D. (1980). *Geologic map of the Vidal NW, Vidal Junction, and parts of the Savahia Peak SW and Savahia Peak Quadrangles, San Bernardino County, California* U. S. Geological Survey, Reston, VA.

Campbell, E. A., John, B. E. (1996) Constraints on extension related plutonism from modeling of the Colorado River gravity high: GSA Bulletin, v. 108; no. 10; P. 1242-1255

Coney, P., 1980, Cordilleran metamorphic core complexes: An overview, in Crittenden, M. D., Coney, P. J., and Davis, G. H., eds., Cordilleran metamorphic core complexes: Geological Society of America Memoir 153, p. 7–34

Coney, P. J., & Harms, T. A. (1984). Cordilleran metamorphic core complexes; cenozoic extensional relics of mesozoic compression. *Geology (Boulder), 12*(9), 550-554.

Coney, P. J., & Reynolds, S. J. (1977). Cordilleran benioff zones. *Nature (London), 270*(5636), 403-406.

Daley, E. E., & DePaolo, D. J. (1992). Isotopic evidence for lithospheric thinning during extension: Southeastern Great Basin. *Geology*, *20*(2), 104-108.

Dalrymple, G. B., and Duffield, W. A. (1988). High Precision 40Ar/39Ar dating of Oligocene rhyolites from the Mogollon-Datil volcanic field using a continuous laser system. Geophysical research letters, vol. 15, no. 5, 463-466

Davis, G.A., Anderson, J.L., Frost, E.G., and Shackelford, T.J., 1980, Mylonitization and detachment faulting in the Whipple-Bucksin-Rawhide Mountains terrane, southeastern California and western Arizona, *in* Crittenden, M.D., Coney, P.J., and Davis, G.H., eds., Cordilleran Metamorphic Core Complexes: Geological Society of America Memoir 153, p. 9-129.

Davis, G.A, and Lister, G.S., 1988, Detachment faulting in continental extension; perspectives from the southwestern U.S. Cordillera: in Clark, S.P., Jr., et al., eds., Processes in continental lithosphere deformation: Geological Society of America Special Paper 218, p. 133-159.

DePaolo, D. J., & Daley, E. E. (2000). Neodymium isotopes in basalts of the southwest basin and range and lithospheric thinning during continental extension. *Chemical Geology*, *169*(1), 157-185.

Dickinson, W. R. (2002). The basin and range province as a composite extensional domain. *International Geology Review*, *44*(1), 1-38.

Dickey, D. D., Carr, W. J., & Bull, W. B. (1980). *Geologic map of the Parker, NW, Parker, and parts of the Whipple Mountains, SW and Whipple Wash quadrangles, California and Arizona* U. S. Geological Survey, Reston, VA.

Faulds, J. E., Feuerbach, D. L., Miller, C. F., & Smith, E. I. (2001). Cenozoic evolution of the northern colorado river extensional corridor, southern nevada and northwest arizona. *Guidebook - Pacific Section, American Association of Petroleum Geologists,78*, 239-271.

Faulds, J.E., Smith, E.I., and Gans, P., 1999, Spatial and temporal patterns of magmatism and extension in the northern Colorado River extensional corridor, Nevada and Arizona: A preliminary report: Nevada Petroleum Society Guidebook, p. 171-183.

Faulds, J.E., Geissman, J.W., and Mawer, C.K., 1990, Structural development of a major extensional accommodation zone in the Basin and Range province, northwestern Arizona and southern Nevada: Geological Society of America Memoir 176, p. 37-76.

Faulds, J.E., Feuerbach, D.L., Reagan M. ., Metcalf, R.V., Gans, P., and Walker, J.D., 1995, The Mount Perkins block, northwestern Arizona: An exposed cross section of an evolving, preextensional to synextensional magmatic system: Journal of Geophysical Research, v. 100, no. B8, p. 15,249-15,266.

Falkner, C. M., Miller, C. F., Wooden, J. L., & Heizler, M. T. (1995). Petrogenesis and tectonic significance of the calc-alkaline, bimodal Aztec Wash pluton, Eldorado Mountains, Colorado River extensional corridor. *Journal of Geophysical Research: Solid Earth*, *100*(B6), 10453-10476.

Ferguson, C. A., McIntosh, W. C., & Miller, C. F. (2013). Silver creek caldera; the tectonically dismembered source of the peach spring tuff. *Geology (Boulder), 41*(1), 3-6.

Feuerbach, D. L., Smith, E. I., Walker, J. D., & Tangeman, J. A. (1993). The role of the mantle during crustal extension: Constraints from geochemistry of volcanic rocks in the Lake Mead area, Nevada and Arizona. *Geological Society of America Bulletin*, *105*(12), 1561-1575.

Foster, D. A., Harrison, T. M., Miller, C. F., Howard, K. A., Haxel, G. B., & Simpson, R. W. (1990). The (super 40) ar/ (super 39) ar thermochronology of the eastern mojave desert, california, and adjacent western arizona with implications for the evolution of metamorphic core complexes. *Journal of Geophysical Research, 95,* 5-20,024.

Gans, P. B. (1997). Large-magnitude Oligo-Miocene extension in southern Sonora: Implications for the tectonic evolution of northwest Mexico. *Tectonics*, *16*(3), 388-408.

Gans, P. B., & Bohrson, W. A. (1998). Suppression of volcanism during rapid extension in the basin and range province, united states. *Science*, *279*(5347), 66-68.

Gans, P. B., & Gentry, B. J. (2016). Dike emplacement, footwall rotation, and the transition from magmatic to tectonic extension in the whipple mountains metamorphic core complex, southeastern california. *Tectonics*, *35*(11), 2564-2608.

Gans, P. B., Mahood, G. A., & Schermer, E. R. (1989). Synextensional magmatism in the basin and range province; a case study from the eastern great basin. *Special Paper - Geological Society of America, 233,* 53-53.

Glazner, A. F., & Bartley, J. M. (1984). Timing and tectonic setting of tertiary low-angle normal faulting and associated magmatism in the southwestern united states. *Tectonics, 3*(3), 385-396.

Glazner, A. F., & Farmer, G. L. (1992). Production of isotopic variability in continental basalts by cryptic crustal contamination. *MH*, *2*, 0-70330.

Hanchar, J. M., Miller, C. F., Wooden, J. L., Bennett, V. C., & Staude, J. M. G. (1994). Evidence from xenoliths for a dynamic lower crust, eastern Mojave Desert, California. *Journal of Petrology*, *35*(5), 1377-1415.

Harker, A. (1909). *The natural history of igneous rocks*. Macmillam.

Harlan, S. S., Duebendorfer, E. M., & Deibert, J. E. (1998). New (super 40) ar/ (super 39) ar isotopic dates from miocene volcanic rocks in the lake mead area and southern las vegas range, nevada. *Canadian Journal of Earth Sciences = Revue Canadienne Des Sciences De La Terre*, *35*(5), 495-503.

Harvey, J., and E. F. Baxter (2009), An improved method for TIMS high precision neodymium isotope analysis of very small aliquots (1–10 ng), Chem. Geol., 258(3), 251–257.

Hawkesworth, C., Turner, S., Gallagher, K., Hunter, A., Bradshaw, T., & Rogers, N. (1995). Calc-alkaline magnetism, lithospheric thinning and extension in the basin and range. *Journal of Geophysical Research*, *100*, 10-10,286.

Hazlett, R. W. (1986) Geology of a Tertiary volcanic center, Mopah range, San Bernardino County, California. [Ph.D. dissert.]: Los Angeles, University of Southern California, 267 p.

Hazlett, R. W. (1990). Extension-related Miocene volcanism in the Mopah Range volcanic field, southeastern California. *Geological Society of America Memoirs*, *174*, 133-146.

Hazlatt, R. W. (1993). Stratigraphic Section of the Central Mopah Range, Calif., *US Geological Survey Bulletin*, *2053*, 127-129.

Hedman, K. M., B. B. Curry, T. M. Johnson, P. D. Fullagar, and T. E. Emerson (2009), Variation in strontium isotope ratios of archaeological fauna in the Midwestern United States: A preliminary study, J. Archaeol. Sci., 36(1), 64–73.

Hooper, P. R., Bailey, D. G., & McCarley Holder, ,G.A. (1995). Tertiary calc-alkaline magmatism associated with lithospheric extension in the pacific northwest. *Journal of Geophysical Research*, *100*, 10-10,319.

Howard, K. A., Goodge, J. W., & John, B. E. (1982). In Frost E. G., Martin D. L. (Eds.), *Detached crystalline rocks of the mohave, buck, and bill williams mountains, western arizona* Cordilleran Publ., San Diego, CA.

Howard, K. A., & John, B. E. (1987). Crustal extension along a rooted system of imbricate low-angle faults; Colorado River extensional corridor, California and Arizona. *Geological Society Special Publications, 28*, 299-311.

Howard, K. A., Nielson, J. E., Wilshire, H. G., Nakata, J. K., Goodge, J. W., Reneau, S. L., John, B. E., Hansen, V. L. (1999), Geologic map of the Mohave Mountains area, Mohave County, western Arizona, US geological survey

Howard, K.A., Stone Paul, Pernokas, M.A., and Marvin, R.F., 1982, Geologic and geochronologic reconnaissance of the Turtle Mountains area California: west border of the Whipple Mountains detachment terrane, in Frost, E.G., and Martin, D.L., eds., Mesozoic-Cenozoic tectonic evolution of the Colorado River region, California, Arizona, and Nevada (Anderson-Hamilton Volume): San Diego, Calif., Cordilleran Publishers, p. 341-354.

Jackson, M. G., Hart, S. R., Koppers, A. A., Staudigel, H., Konter, J., Blusztajn, J., ... & Russell, J. A. (2007). The return of subducted continental crust in Samoan lavas. *Nature*, *448*(7154), 684-687.

John, B. E., 1987a, Geologic map of the Chemehuevi Mountains area, San Bernardino County, California, and Mohave County, Arizona: U.S. Geological Survey Open-File Report 87–666, scale 1:24 000.

John, B. E., 1987b, Geometry and evolution of a mid-crustal extensional fault system: Chemehuevi Mountains, southeastern California, *in* Coward, M. P., Dewey, J. F., and Hancock, P. L., eds., Continental extensional tectonics: Geological Society of London Special Paper 28, p. 313–335.

John, B. E., & Foster, D. A. (1993). Structural and thermal constraints on the initiation angle of detachment faulting in the southern basin and range; the chemehuevi mountains case study. *Geological Society of America Bulletin, 105*(8), 1091-1108.

Johnson, D. M., Hooper, P. R., & Conrey, R. M. (1999). XRF Method XRF Analysis of Rocks and Minerals for Major and Trace Elements on a Single Low Dilution Li-tetraborate Fused Bead. *Advances in X-ray Analysis*, *41*, 843-867.

Kapp, J. D. A., Miller, C. F., & Miller, J. S. (2002). Ireteba pluton, Eldorado Mountains, Nevada: Late, deep-source, peraluminous magmatism in the Cordilleran Interior. *The Journal of geology*, *110*(6), 649-669.

Lackey, J. S., Cecil, M. R., Windham, C. J., Frazer, R. E., Bindeman, I. N., & Gehrels, G. E. (2012). The Fine Gold Intrusive Suite: The roles of basement terranes and magma source development in the Early Cretaceous Sierra Nevada batholith. *Geosphere*, *8*(2), 292-313.

LaForge, Justin S., Insights into Low-Angle Normal Fault Initiation near the Brittle-Plastic Transition; a Micro- to Macroscale Documentation of the Mohave Wash Fault System,

Chemehuevi Mountains, Southeastern CA, MS, Department of Geology and Geophysics, December, 2015.

Lipman, P. W. (1965). *Chemical comparison of glassy and crystalline volcanic rocks* (No. 1201-D). US Govt. Print. Off.

Lister, G. S., and S. L. Baldwin (1993), Plutonism and the origin of metamorphic core complexes, Geology, 21(7), 607–610.

Metcalf, R. V., Smith, E. I., Walker, J. D., Reed, R. C., & Gonzales, D. A. (1995). Isotopic disequilibrium among commingled hybrid magmas: evidence for a two-stage magma mixing-commingling process in the Mt. Perkins Pluton, Arizona. *The Journal of Geology*, *103*(5), 509-527.

McDowell, S. M., Overton, S., Fisher, C. M., Frazier, W. O., Miller, C. F., Miller, J. S., & Economos, R. C. (2016). Hafnium, oxygen, neodymium, strontium, and lead isotopic constraints on magmatic evolution of the supereruptive southern Black Mountains volcanic center, Arizona, USA: A combined LASS zircon–whole-rock study. *American Mineralogist*, *101*(2), 311-327.

McDonough, W. F., & Sun, S. S. (1995). The composition of the Earth. *Chemical geology*, *120*(3-4), 223-253.

Miller, J. M. G., & John, B. E. (1988). Detached strata in a tertiary low-angle normal fault terrane, southeastern california; a sedimentary record of unroofing, breaching, and continued slip. *Geology (Boulder), 16*(7), 645-648.

Miller, C. F., & Miller, J. S. (2002). Contrasting stratified plutons exposed in tilt blocks, Eldorado Mountains, Colorado River Rift, NV, USA. *Lithos*, *61*(3), 209-224.

Miller, C. F., & Wooden, J. L. (1994). Anatexis, hybridization and the modification of ancient crust: Mesozoic plutonism in the Old Woman Mountains area, California. *Lithos*, *32*(1-2), 111-133.

Mukasa, S. B., & Wilshire, H. G. (1997). Isotopic and trace element compositions of upper mantle and lower crustal xenoliths, Cima volcanic field, California: implications for evolution of the subcontinental lithospheric mantle. *Journal of Geophysical Research: Solid Earth*, *102*(B9), 20133-20148.

Nakata, J.K, Pernokas, M.A., Howard, K.A., Nielson, J.E., and Shannon, J.R., 1990, K-Ar and fission-track ages (dates) of volcanic, intrusive, altered, and metamorphic rocks in the Mohave Mountains area, west-central Arizona: Isochron West, no. 56, p. 8-20.

Nielson, J. E., & Beratan, K. K. (1990). Tertiary basin development and tectonic implications, Whipple detachment system, Colorado River extensional corridor, California and Arizona. *Journal of Geophysical Research, 95*, 599-614.

Nielson, J. E., & Beratan, K. K. (1995). Stratigraphic and structural synthesis of a Miocene extensional terrane, southeast California and west-central Arizona. *Geological Society of America Bulletin*, *107*(2), 241-252.

Nielson, J. E., & Nakata, J. K. (1993). Tertiary stratigraphy and structure of the northern Turtle Mountains. *California: US Geological Survey Bulletin*, *2053*, 127-129.

Nielson, J. E. (1993). Stratigraphic and Structural Correlation of Tertiary Strata of the Mohave
Mountains and Aubrey Hills, Ariz., *US Geological Survey Bulletin*, *2053*, 127-129.

Noh, J. H., & Boles, J. R. (1989). Diagenetic alteration of perlite in the Guryongpo area, Republic of Korea. *Clays and Clay Minerals*, *37*(1), 47-58.

Paton, C., Hellstrom, J., Paul, B., Woodhead, J., and Hergt, J. (2011). Iolite: Freeware for the visualization and processing of mass spectrometric data. Journal of Analytical Atomic Spectrometry, 26(12), 2508-2518.

Parsons, T., & Thompson, G. A. (1993). Does magmatism influence low-angle normal faulting? *Geology (Boulder)*, *21*(3), 247-250.

Pike, J. E. N., & Hansen, V. L. (1982). Complex Tertiary stratigraphy and structure, Mohave Mountains, Arizona: A preliminary report. *Mesozoic-Cenozoic tectonic evolution of the Colorado River region, California, Arizona, and Nevada: San Diego, Cordilleran Publishers*, 91-96.

Putirka, K., & Platt, B. (2012). Basin and range volcanism as a passive response to extensional tectonics. *Geosphere*, *8*(6), 1274-1285, 12.

Ramos, F. C., & Reid, M. R. (2005). Distinguishing melting of heterogeneous mantle sources from crustal contamination: Insights from Sr isotopes at the phenocryst scale, Pisgah Crater, California. *Journal of Petrology*, *46*(5), 999-1012.

Rehrig, W. A., and S. J. Reynolds (1980), Geologic and geochronologic reconnaissance of a northwest-trending zone of metamorphic core complexes in southern and western Arizona, in Cordilleran Metamorphic Core Complexes, Geol. Soc. Am. Mem., vol. 153, edited by M. S. Crittenden Jr., P. J. Coney, and G. H. Davis, pp. 131–157

Reiners, P. W. (2002). Temporal-compositional trends in intraplate basalt eruptions: Implications for mantle heterogeneity and melting processes. *Geochemistry, Geophysics, Geosystems*, *3*(2), 1-30.

Reynolds, S. J., & Spencer, J. E. (1985). Evidence for large-scale transport on the Bullard detachment fault, west-central Arizona. *Geology*, *13*(5), 353-356.

Severinghaus, J., & Atwater, T. (1990). Cenozoic geometry and thermal state of the subducting slabs beneath western north america. *Memoir - Geological Society of America, 176*, 1-22.

Sherrod and Nielson, (1993), Tertiary stratigraphy of highly extended terranes, California, Arizona, and Nevada, U.S. Geological Survey Bulletin 2053

Spell, T. L., & McDougall, I. (2003). Characterization and calibration of $^{40}Ar/^{39}$ Ar dating standards. *Chemical Geology, 198*(3), 189-211.

Simpson, C., Schweitzer, J., and Howard, K. A., 1991, A reinterpretation of the timing, position, and significance of part of the Sacramento Mountains detachment fault, southeastern California: Geological Society of America Bulletin, v. 103, p. 751-761.

Spencer, J. E., Richard, S. M., Reynolds, S. J., Miller, R. J., Shafiqullah, M., Gilbert, W. G., & Grubensky, M. J. (1995). Spatial and temporal relationships between mid-tertiary magnetism and extension in southwestern arizona. *Journal of Geophysical Research, 100*, 10-10,351.

Spencer, J. E., and Reynolds, S. J., 1989, Tertiary structure, stratigraphy, and tectonics of the Buckskin Mountains, *in* Spencer, J. E., and Reynolds, S. J., eds., Geology and mineral resources of the Buckskin and Rawhide Mountains, west-central Arizona: Arizona Geological Survey Bulletin 198, p. 103–167.

Stone, Paul, and Howard (1979), Compliation of geologic mapping in the Needles 1°x2° sheet, California and Arizona, US Geological Survey

Wang, K., Plank, T., Walker, J. D., & Smith, E. I. (2002). A mantle melting profile across the Basin and Range, SW USA. *Journal of Geophysical Research: Solid Earth, 107*(B1).

Ward, P. L. (1991). On plate tectonics and the geologic evolution of southwestern north america. *Journal of Geophysical Research,96*, 12-12,496.

Wernicke, B. P., Christiansen, R. L., England, P. C., & Sonder, L. J. (1987). Tectonomagmatic evolution of Cenozoic extension in the North American cordillera. *Geological Society Special Publications, 28*, 203-221

Yin, A., & Dunn, J. F. (1992). Structural and stratigraphic development of the whipple-chemehuevi detachment fault system, southeastern california; implications for the geometrical evolution of domal and basinal low-angle normal faults. *Geological Society of America Bulletin, 104*(6), 659-674.

Zielinski, R. A., Lipman, P. W., & Millard, H. T. (1977). Minor-element abundances in obsidian, perlite, and felsite of calc-alkalic rhyolites. *American Mineralogist, 62*(5-6), 426-437.

Appendix I

Sample locations and rock types for samples within Plate 1

Sample name	Unit	Latitude	Longitude
MP-1	$Thbr_2$	34°17'55.63"N	114°40'7.34"W
MP-2	$Thbr_2$	34°17'52.47"N	114°40'10.48"W
MP-3	$Thbr_1$	34°17'52.11"N	114°40'11.90"W
MP-4	Thpd	34°17'48.86"N	114°40'13.36"W
MP-5	Tpd	34°17'46.43"N	114°40'18.66"W
MP-6	Tbh	34°17'38.47"N	114°40'28.47"W
MP-7	$Thbr_2$	34°17'29.61"N	114°40'21.98"W
MP-08	$Thbr_2$	34°17'33.11"N	114°40'19.70"W
MP-09	$Thbr_2$	34°18'19.39"N	114°40'20.19"W
MP-10	$Thbr_2$	34°17'49.92"N	114°40'48.55"W
MP-11	$Thbr_2$	34°17'53.50"N	114°40'47.97"W
MP-12	Tpd	34°18'9.37"N	114°41'1.28"W
MP-13	Tc	34°18'22.29"N	114°41'15.72"W
MP-14	Tocba	34°18'23.95"N	114°41'18.15"W
MP-15	Tocba	34°17'44.18"N	114°41'17.34"W
MP-16	Tocba	34°17'44.93"N	114°41'16.67"W
MP-17A	Tpd	34°19'19.01"N	114°40'52.81"W
MP-17B	Tpd	34°19'18.70"N	114°40'53.41"W
MP-18	Tocba	34°18'53.46"N	114°41'59.87"W
MP-19	Tc	34°18'35.61"N	114°41'21.04"W
MP-20	Tc	34°18'38.21"N	114°43'27.90"W
MP-21	Tpd	34°17'45.45"N	114°42'13.81"W
MP-22	Tpd	34°17'53.12"N	114°42'2.36"W
MP-23	$Thbr_2$	34°17'14.01"N	114°40'14.08"W
MP-24	$Thbr_2$	34°19'22.80"N	114°44'31.37"W
MP-25	Tbd	34°19'15.59"N	114°44'35.07"W
MP-26	$Thbr_1$	34°16'17.34"N	114°42'45.42"W
MP-27	Tpd	34°17'37.58"N	114°41'14.72"W
MP-28	$Thbr_2$	34°16'45.19"N	114°41'56.81"W
MP-29	Tbhr	34°17'56.40"N	114°40'27.51"W
MP-30	Tpd	34°18'23.43"N	114°39'35.35"W
MP-31	Tpd	34°17'47.15"N	114°43'54.54"W
MP-32	Tpd	34°17'38.56"N	114°44'0.69"W

Sample name	Unit	Latitude	Longitude
MP-33	Tpd	34°16'54.75"N	114°43'46.38"W
MP-34	Tpd	34°17'2.23"N	114°43'38.06"W
MP-35	$Thbr_2$	34°16'39.57"N	114°43'54.92"W
MP-36	Taa	34°16'29.74"N	114°43'21.25"W
MP-37	$Thbr_2$	34°16'30.33"N	114°42'26.16"W
WW-1	$Thbr_2$	34°17'33.77"N	114°37'5.88"W
WW-2	$Thbr_2$	34°17'29.92"N	114°36'27.09"W
WW-3	$Thbr_2$	34°18'2.79"N	114°36'43.50"W
WW-4	$Thbr_2$	34°17'48.92"N	114°37'19.88"W
WW-5	Tmu	34°18'2.39"N	114°36'6.90"W
WW-6	Tmu	34°17'52.19"N	114°37'4.10"W
WW-7	Tmu	34°17'48.35"N	114°36'51.92"W
WW-8	$Thbr_2$	34°16'17.11"N	114°37'50.21"W
WW-9	Taa	34°16'24.63"N	114°37'50.26"W
WW-10	$Tocb_2$	34°16'33.42"N	114°37'54.12"W
WW-11	$Thbr_2$	34°16'51.65"N	114°37'43.35"W
WW-12	$Thbr_2$	34°17'0.43"N	114°37'37.75"W
WW-13	$Thbr_2$	34°17'2.84"N	114°37'33.68"W
WW-14	$Thbr_2$	34°17'5.85"N	114°37'28.05"W
WW-15	$Thbr_2$	34°17'7.95"N	114°37'25.02"W
WW-16	$Tocb_2$	34°17'15.19"N	114°37'41.31"W
WW-17	$Thbr_1$	34°17'18.14"N	114°37'40.66"W
WW-18	$Thbr_2$	34°17'4.84"N	114°36'59.80"W
WW-19	$Thbr_2$	34°17'18.09"N	114°36'56.11"W
WW-20	$Tocb_2$	34°17'30.37"N	114°36'35.63"W
WW-21	$Thbr_2$	34°17'41.92"N	114°36'41.37"W
WW-22	$Thbr_1$	34°17'54.03"N	114°36'36.76"W
WW-23	Tmu	34°18'9.00"N	114°36'37.92"W
WW-24	Tdi	34°20'16.35"N	114°35'57.96"W
WM-20	Tob	34°21'38.27"N	114°38'56.04"W
WM-21	Tob	34°21'38.84"N	114°38'58.85"W
WM-22	Tpst	34°21'42.16"N	114°38'47.26"W
WM-23	Tob	34°21'39.85"N	114°38'44.77"W
WM-24	Tcoa	34°19'41.59"N	114°38'15.94"W
WM-25A	Tpd	34°19'57.94"N	114°37'10.63"W
WM-25B	Tpd	34°19'57.94"N	114°37'10.63"W
WM-26	$Thbr_1$	34°19'57.76"N	114°36'37.69"W
WM-27	Tpd	34°20'13.67"N	114°36'27.11"W
WM-28	$Thbr_1$	34°20'17.81"N	114°36'26.21"W
WM-29	$Thbr_2$	34°17'11.83"N	114°38'30.62"W
WM-31(12)	Ta	34°22'5.23"N	114°38'53.12"W
WM-32 (12)	Taa	34°16'23.38"N	114°37'50.41"W

Sample name	Unit	Latitude	Longitude
WM-32 (14)	Taa	34°22'16.75"N	114°39'8.57"W
WM-33(12)	$Thbr_2$	34°16'17.36"N	114°37'46.78"W
WM-33(14)	Tpd	34°21'42.44"N	114°38'32.14"W
WM-34	Tpd	34°21'41.80"N	114°38'27.56"W
WM-35	$Thbr_1$	34°21'37.01"N	114°38'43.22"W
WM-36	Tpd	34°21'50.08"N	114°38'15.86"W
WM-37	Tpd	34°21'33.95"N	114°38'2.94"W
WM-38	Tpd	34°20'18.60"N	114°37'37.78"W
WM-39	Tbhr	34°20'24.25"N	114°37'39.83"W
WM-40	Tcoa	34°20'38.47"N	114°38'17.16"W
WM-41	Tcoa	34°20'40.56"N	114°38'20.40"W
WM-42	$Thbr_1$	34°20'39.48"N	114°37'59.52"W
WM-43	Tbhr	34°20'47.47"N	114°37'22.19"W
WM-44	$Thbr_2$	34°19'42.78"N	114°37'11.24"W
WM-48	Tcoa	34°19'42.38"N	114°37'29.60"W
WM-49	Tcoa	34°19'36.95"N	114°37'26.58"W
WM-50	Tcoa	34°19'40.40"N	114°37'44.36"W
WM-51	Tcoa	34°19'44.90"N	114°37'46.56"W
WM-53	Tcoa	34°19'41.63"N	114°38'16.40"W

Appendix II

Tabulated $^{40}Ar/^{39}Ar$ data and age spectra discussed in Chapter 1. All mineral separations and analyses were performed at UCSB's $^{40}Ar/^{39}Ar$ geochronology laboratory.

Sample: SB65-119; 12MK-MP-03 Plag; J=0.0029196

T	t	40(mol)	40/39	38/39	37/39	36/39	K/Ca	∑ 39Ar	40Ar*	Age (Ma)
700	14	1.5e-14	4.2957	0.0e+0	9.3760	0.0018	0.052	0.05645	0.875	19.7 ± 0.1
750	14	1.6e-14	4.0277	0.0e+0	9.7370	0.0010	0.050	0.12398	0.928	19.6 ± 0.1
790	14	1.9e-14	3.9486	0.0e+0	9.8217	0.0008	0.050	0.20490	0.941	19.5 ± 0.1
830	14	2.3e-14	3.9145	0.0e+0	9.8893	0.0006	0.050	0.30148	0.957	19.6 ± 0.1
870	14	2.6e-14	3.9107	0.0e+0	9.8706	0.0006	0.050	0.41279	0.956	19.6 ± 0.1
910	14	2.8e-14	3.9241	0.0e+0	9.7512	0.0006	0.050	0.52997	0.953	19.6 ± 0.1
950	14	2.8e-14	3.9488	0.0e+0	9.5957	0.0006	0.051	0.64674	0.952	19.7 ± 0.1
990	14	2.5e-14	4.0667	0.0e+0	9.3439	0.0010	0.052	0.74963	0.926	19.7 ± 0.1
1030	14	2.0e-14	4.3194	0.0e+0	9.0181	0.0017	0.054	0.82761	0.882	20.0 ± 0.1
1080	14	1.7e-14	5.1197	0.0e+0	8.6124	0.0033	0.057	0.88225	0.810	21.7 ± 0.1
1130	14	9.7e-15	5.3430	0.0e+0	8.6165	0.0045	0.057	0.91228	0.751	21.0 ± 0.2
1190	14	9.5e-15	6.0642	0.0e+0	8.8836	0.0055	0.055	0.93842	0.733	23.3 ± 0.2
1250	14	9.3e-15	7.1681	0.0e+0	9.0616	0.0074	0.054	0.95994	0.696	26.1 ± 0.3
1350	14	1.9e-14	7.8036	0.0e+0	8.5423	0.0086	0.057	1.00000	0.674	27.5 ± 0.2

Total fusion age, TFA= 20.36 ± 0.04 Ma (including J)
Weighted mean plateau age, WMPA= 19.62 ± 0.04 Ma (including J)
Inverse isochron age =19.47 ± 0.09 Ma. (MSWD =1.08; 40Ar/36Ar=336.4 ± 16.2)
Steps used: 750, 790, 830, 870, 910, 950, 990, (2–8/14 or 69% ∑ 39Ar
t = dwell time in minutes.
40(mol) = moles corrected for blank and reactor-produced 40.
Ratios are corrected for blanks, decay, and interference.
∑39Ar is cumulative, 40Ar* = rad fraction.

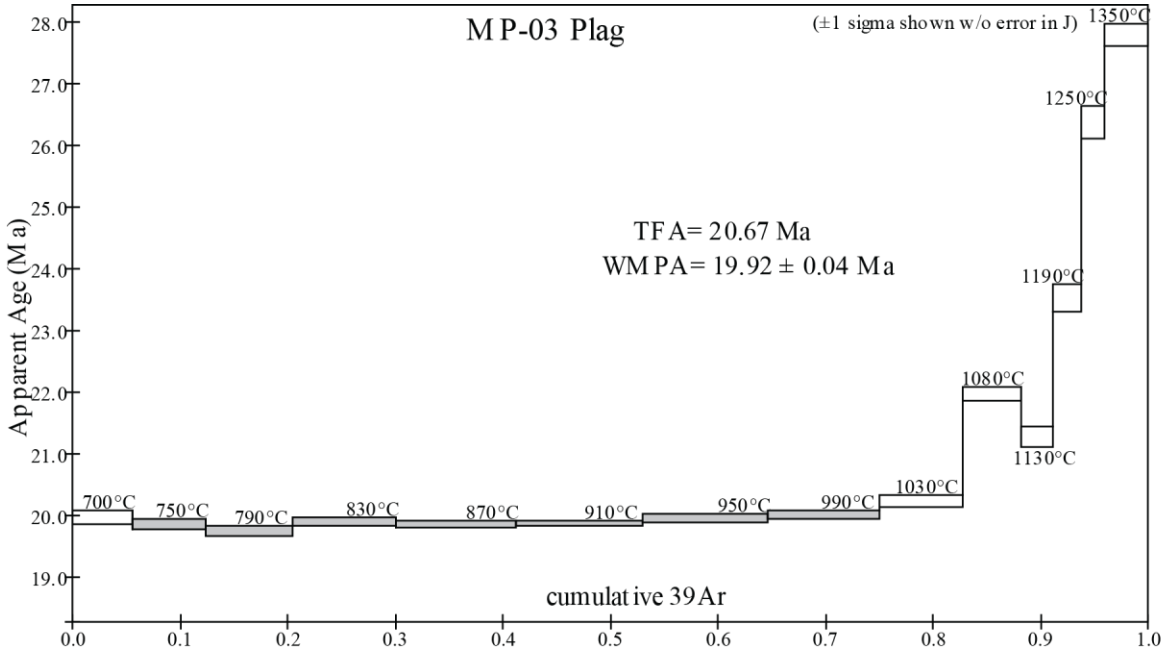

Sample: SB65-110; 12MK-MP-05 Plag; J=0.0030121

T	t	40(mol)	40/39	38/39	37/39	36/39	K/Ca	∑ 39Ar	40Ar*	Age (Ma)
720	14	8.8e-13	262.4930	0.0e+0	8.8050	0.8687	0.056	0.05661	0.022	31.2 ± 1.0
720	14	4.1e-13	232.5033	1.3e-3	8.7407	0.7678	0.056	0.08646	0.024	30.2 ± 1.2
680	14	1.7e-13	288.9294	0.0e+0	8.8220	0.9601	0.056	0.09667	0.018	28.1 ± 5.9
700	12	1.3e-13	178.8025	0.0e+0	8.8817	0.5889	0.055	0.10912	0.027	25.9 ± 3.3
720	12	1.3e-13	146.9425	0.0e+0	8.9937	0.4812	0.054	0.12467	0.032	25.6 ± 2.6
740	12	1.5e-13	121.8886	8.0e-4	9.0513	0.3988	0.054	0.14625	0.033	21.8 ± 1.8
760	12	1.7e-13	105.7205	0.0e+0	9.0076	0.3433	0.054	0.17417	0.040	23.1 ± 1.6
780	12	1.8e-13	88.3774	8.7e-4	9.0377	0.2854	0.054	0.20864	0.046	21.9 ± 1.1
800	12	1.9e-13	79.2999	0.0e+0	9.0230	0.2553	0.054	0.24942	0.049	20.9 ± 1.1
820	12	1.9e-13	70.0489	0.0e+0	8.9835	0.2239	0.055	0.29543	0.056	21.0 ± 0.8
840	12	2.0e-13	63.5631	0.0e+0	8.9879	0.2018	0.055	0.34751	0.062	21.2 ± 0.7
860	12	2.0e-13	58.4978	0.0e+0	8.9886	0.1848	0.055	0.40486	0.066	21.0 ± 0.6
890	12	2.2e-13	51.7751	0.0e+0	8.9548	0.1618	0.055	0.47671	0.077	21.4 ± 0.5
920	12	2.3e-13	48.2666	0.0e+0	8.9520	0.1499	0.055	0.55916	0.082	21.5 ± 0.5
950	12	2.6e-13	48.9601	0.0e+0	8.8865	0.1524	0.055	0.64884	0.080	21.2 ± 0.5
980	12	2.7e-13	52.1299	0.0e+0	8.8352	0.1625	0.055	0.73816	0.079	22.2 ± 0.5
1010	12	2.8e-13	65.6225	0.0e+0	8.7076	0.2063	0.056	0.81062	0.071	25.2 ± 0.2
1010	12	2.1e-13	76.8431	0.0e+0	8.6381	0.2456	0.057	0.85803	0.056	23.1 ± 0.9
1040	12	2.6e-13	97.3461	0.0e+0	8.5692	0.3138	0.057	0.90395	0.047	24.9 ± 1.1
1070	12	3.2e-13	147.6787	0.0e+0	8.3348	0.4796	0.059	0.94080	0.040	32.1 ± 0.7
1070	12	2.6e-13	188.7142	0.0e+0	8.2464	0.6184	0.059	0.96374	0.032	32.1 ± 2.4
1100	12	2.1e-13	189.4829	7.2e-4	8.1420	0.6193	0.060	0.98253	0.034	34.8 ± 2.9
1130	12	1.9e-13	184.5665	1.3e-3	8.0600	0.6012	0.061	1.00000	0.037	37.2 ± 3.0

Total fusion age, TFA= 24.15 ± 0.21 Ma (including J)
Weighted mean plateau age, WMPA= 21.46 ± 0.20 Ma (including J)
Inverse isochron age =20.18 ± 0.45 Ma. (MSWD =1.30; 40Ar/36Ar=296.8 ± 0.4)
Steps used: 740, 760, 780, 800, 820, 840, 860, 890, 920, 950, 980, (6–16/23 or 61% ∑ 39Ar
t = dwell time in minutes.
40(mol) = moles corrected for blank and reactor-produced 40.
Ratios are corrected for blanks, decay, and interference.
∑39Ar is cumulative, 40Ar* = rad fraction.

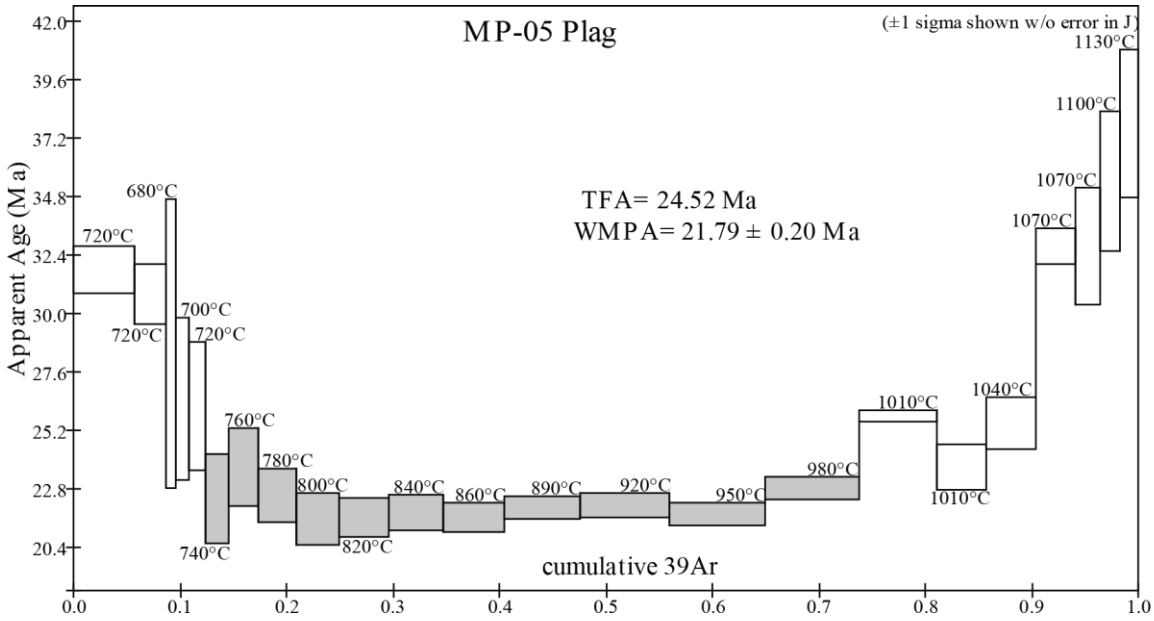

Sample: SB65-107; 12MK-MP-07 Plag; J=0.0030356

T	t	40(mol)	40/39	38/39	37/39	36/39	K/Ca	∑ 39Ar	40Ar*	Age (Ma)
700	14	1.0e-13	23.9544	1.0e+0	18.2648	0.0749	0.027	0.05770	0.076	8.6 ± 0.6
750	14	4.5e-14	9.3272	9.2e-3	7.4431	0.0203	0.066	0.12246	0.358	18.2 ± 0.2
800	14	4.1e-14	6.1784	0.0e+0	7.0559	0.0090	0.069	0.21140	0.569	19.1 ± 0.1
850	14	4.2e-14	4.9286	0.0e+0	6.9894	0.0047	0.070	0.32415	0.720	19.3 ± 0.1
900	14	4.3e-14	4.4115	0.0e+0	6.9399	0.0030	0.071	0.45402	0.796	19.1 ± 0.1
950	14	4.0e-14	4.3332	0.0e+0	6.8418	0.0028	0.072	0.57701	0.812	19.2 ± 0.1
1000	14	3.2e-14	4.5846	0.0e+0	6.7300	0.0035	0.073	0.66994	0.774	19.3 ± 0.1
1050	14	2.3e-14	5.7433	0.0e+0	6.5995	0.0073	0.074	0.72393	0.623	19.5 ± 0.2
1100	14	1.9e-14	6.9655	0.0e+0	6.2734	0.0110	0.078	0.76013	0.532	20.2 ± 0.3
1140	14	2.4e-14	4.8712	0.0e+0	6.1933	0.0044	0.079	0.82449	0.732	19.4 ± 0.2
1180	14	1.8e-14	4.9920	0.0e+0	6.4686	0.0045	0.076	0.87256	0.735	20.0 ± 0.2
1220	14	1.6e-14	5.6713	0.0e+0	6.6694	0.0064	0.073	0.91106	0.666	20.6 ± 0.3
1260	14	1.7e-14	7.1094	0.0e+0	6.7016	0.0102	0.073	0.94335	0.574	22.2 ± 0.3
1350	14	4.1e-14	9.6774	0.0e+0	6.9487	0.0164	0.071	1.00000	0.499	26.3 ± 0.2

Total fusion age, TFA= 19.19 ± 0.06 Ma (including J)
Weighted mean plateau age, WMPA= 19.22 ± 0.05 Ma (including J)
Inverse isochron age =19.17 ± 0.12 Ma. (MSWD =1.07; 40Ar/36Ar=297.7 ± 4.7)
Steps used: 800, 850, 900, 950, 1000, 1050, (3–8/14 or 60% ∑ 39Ar
t = dwell time in minutes.
40(mol) = moles corrected for blank and reactor-produced 40.
Ratios are corrected for blanks, decay, and interference.
∑39Ar is cumulative, 40Ar* = rad fraction.

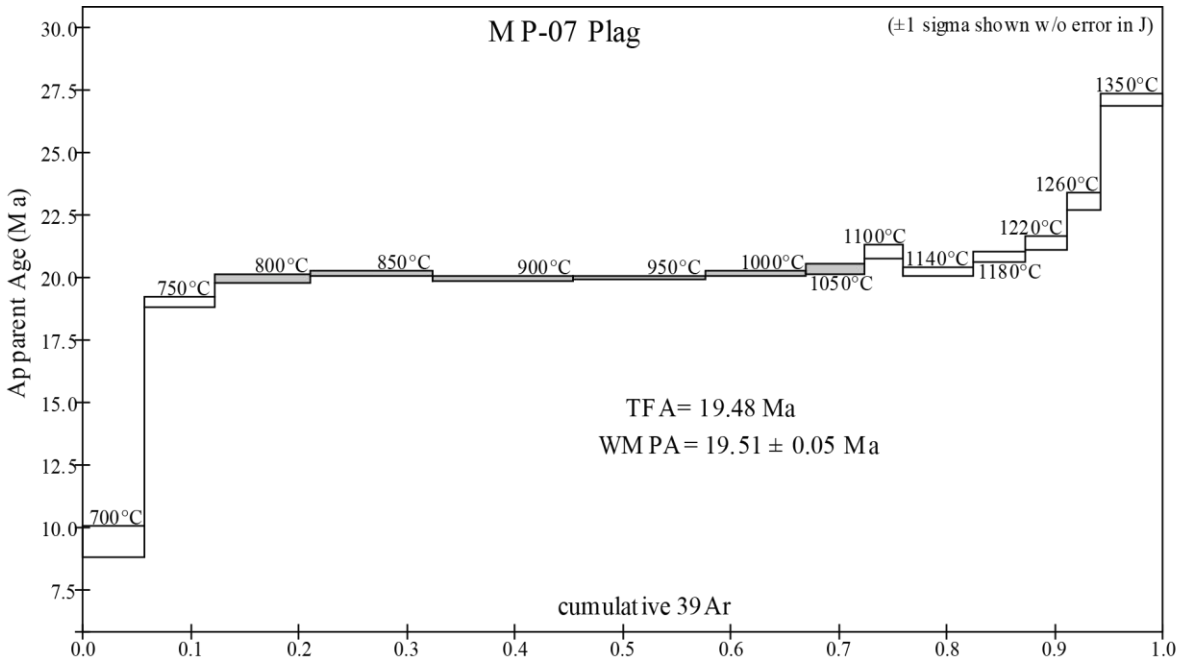

Sample: SB67-132; MK-MP-09 Plag; J=0.0032010

T	t	40(mol)	40/39	38/39	37/39	36/39	K/Ca	∑ 39Ar	40Ar*	Age (Ma)
800	14	2.4e-14	3.7977	0.0e+0	4.4560	0.0018	0.11	0.19136	0.859	18.7 ± 0.1
880	15	2.7e-14	3.6777	0.0e+0	5.3062	0.0013	0.092	0.41214	0.896	18.9 ± 0.2
950	15	2.5e-14	3.7411	0.0e+0	5.7473	0.0014	0.085	0.61160	0.889	19.1 ± 0.2
1030	15	2.1e-14	4.1670	0.0e+0	5.5130	0.0028	0.089	0.76329	0.800	19.2 ± 0.2
1160	14	2.4e-14	7.3912	0.0e+0	4.5228	0.0137	0.11	0.86219	0.451	19.2 ± 0.2
1350	14	3.4e-14	7.4965	0.0e+0	6.0796	0.0127	0.081	1.00000	0.500	21.5 ± 0.2

Total fusion age, TFA= 19.34 ± 0.09 Ma (including J)
Weighted mean plateau age, WMPA= 19.14 ± 0.12 Ma (including J)
Inverse isochron age =18.90 ± 0.13 Ma. (MSWD =1.43; 40Ar/36Ar=299.1 ± 3.7)
Steps used: 950, 1030, 1160, (3–5/6 or 45% ∑ 39Ar
t = dwell time in minutes.
40(mol) = moles corrected for blank and reactor-produced 40.
Ratios are corrected for blanks, decay, and interference.
∑39Ar is cumulative, 40Ar* = rad fraction.

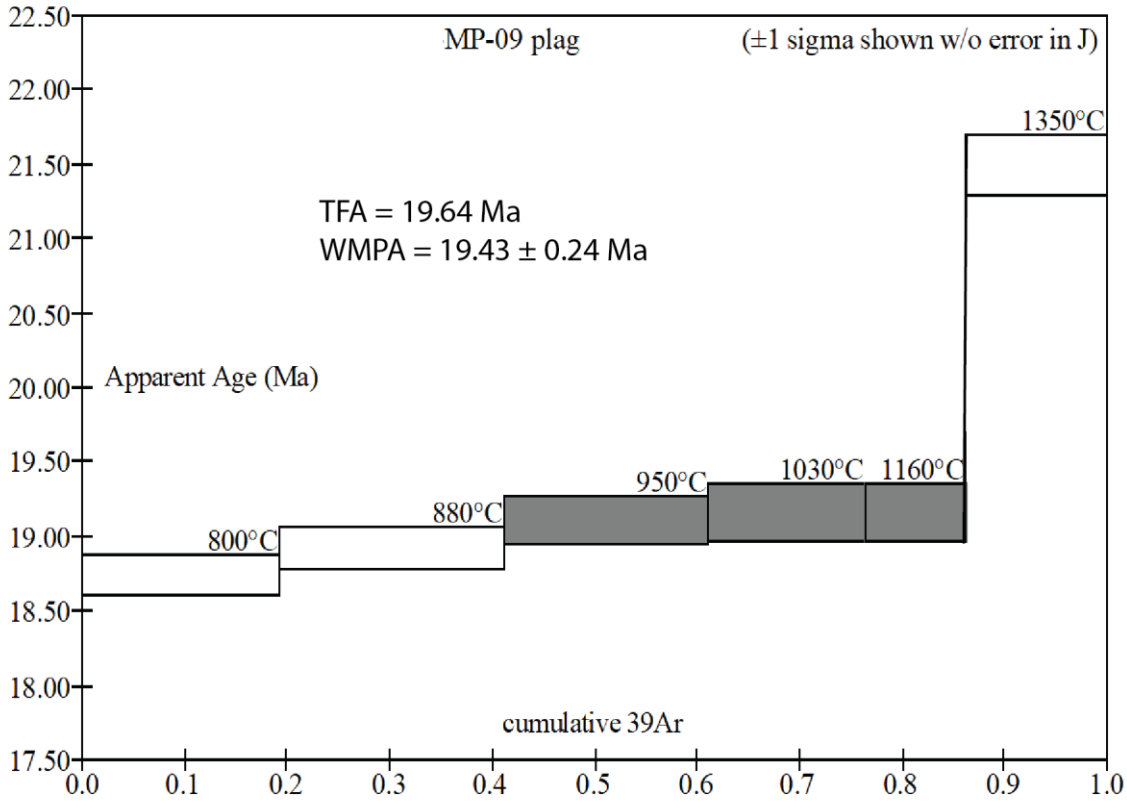

Sample: SB67-134; MK-MP-12 Plag; J=0.0031920

T	t	40(mol)	40/39	38/39	37/39	36/39	K/Ca	∑ 39Ar	40Ar*	Age (Ma)
800	14	1.5e-14	4.1229	0.0e+0	7.0062	0.0026	0.070	0.12482	0.816	19.3 ± 0.3
880	15	2.0e-14	3.7614	0.0e+0	7.1150	0.0011	0.069	0.31210	0.916	19.7 ± 0.2
950	15	2.4e-14	3.6151	0.0e+0	7.0544	0.0007	0.069	0.53751	0.945	19.6 ± 0.2
1030	15	2.6e-14	3.7108	0.0e+0	6.9162	0.0009	0.071	0.77626	0.925	19.7 ± 0.2
1160	14	1.5e-14	3.9162	0.0e+0	6.6298	0.0016	0.074	0.90963	0.883	19.8 ± 0.3
1350	14	1.6e-14	5.9903	0.0e+0	6.2144	0.0065	0.079	1.00000	0.677	23.2 ± 0.3

Total fusion age, TFA= 19.94 ± 0.10 Ma (including J)
Weighted mean plateau age, WMPA= 19.66 ± 0.10 Ma (including J)
Inverse isochron age =19.38 ± 0.38 Ma. (MSWD =0.04; 40Ar/36Ar=347.2 ± 13.4)
Steps used: 880, 950, 1030, 1160, (2–5/6 or 78% ∑ 39Ar
t = dwell time in minutes.
40(mol) = moles corrected for blank and reactor-produced 40.
Ratios are corrected for blanks, decay, and interference.
∑39Ar is cumulative, 40Ar* = rad fraction.

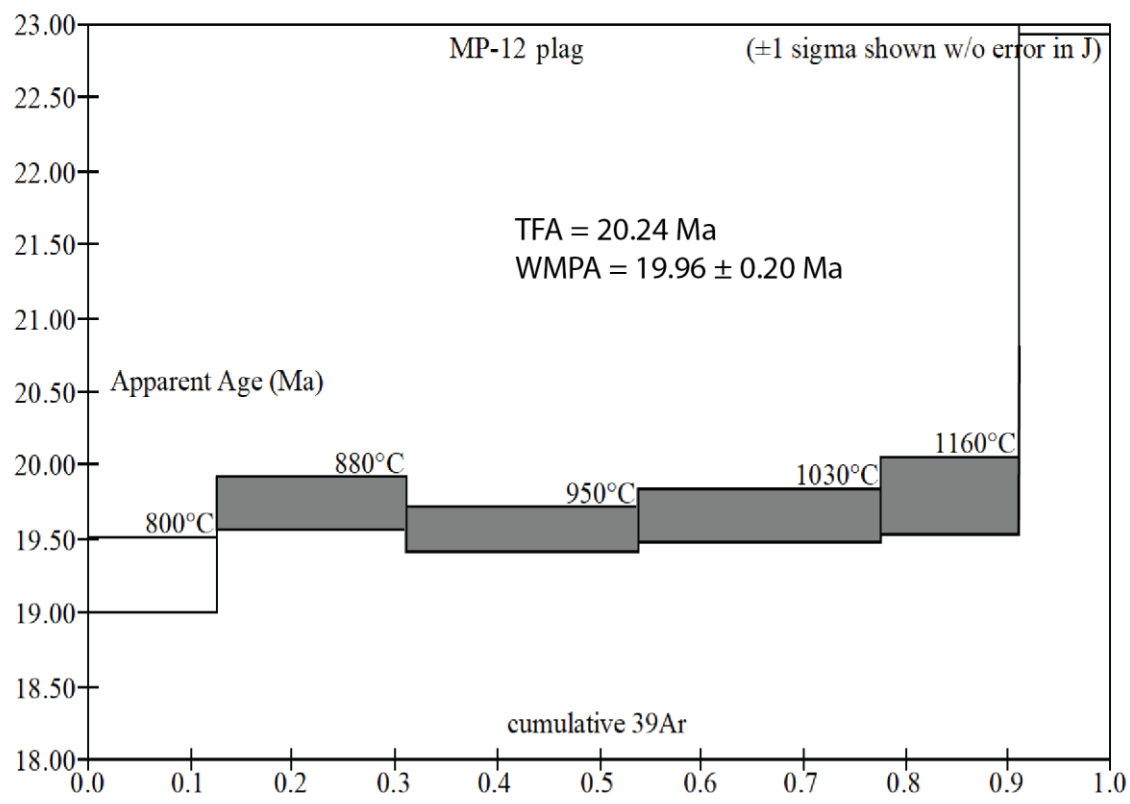

Sample: SB67-135; MK-MP-15 GM; J=0.0031851

T	t	40(mol)	40/39	38/39	37/39	36/39	K/Ca	∑ 39Ar	40Ar*	Age (Ma)
680	12	6.0e-14	4.5314	0.0e+0	0.6758	0.0030	0.73	0.19403	0.807	20.9 ± 0.1
750	12	5.6e-14	3.9371	0.0e+0	0.6036	0.0015	0.81	0.40226	0.890	20.0 ± 0.1
820	12	4.6e-14	3.8191	0.0e+0	0.5713	0.0014	0.86	0.57871	0.893	19.5 ± 0.1
890	12	4.4e-14	3.7803	0.0e+0	0.5473	0.0013	0.90	0.75021	0.896	19.4 ± 0.1
960	12	3.0e-14	4.1493	0.0e+0	0.6173	0.0026	0.79	0.85582	0.812	19.3 ± 0.1
1030	12	2.6e-14	4.6043	0.0e+0	0.7692	0.0044	0.64	0.93977	0.719	18.9 ± 0.1
1100	12	1.9e-14	5.6396	0.0e+0	1.6706	0.0082	0.29	0.99005	0.573	18.5 ± 0.1
1170	12	5.7e-15	8.5051	1.1e-3	14.0675	0.0186	0.035	1.00000	0.352	17.1 ± 0.7

Total fusion age, TFA= 19.70 ± 0.06 Ma (including J)
Weighted mean plateau age, WMPA= 19.26 ± 0.06 Ma (including J)
Inverse isochron age =19.77 ± 0.46 Ma. (MSWD =119.39; 40Ar/36Ar=290.5 ± 30.3)
Steps used: 890, 960, 1030, (4–6/8 or 36% ∑ 39Ar
t = dwell time in minutes.
40(mol) = moles corrected for blank and reactor-produced 40.
Ratios are corrected for blanks, decay, and interference.
∑39Ar is cumulative, 40Ar* = rad fraction.

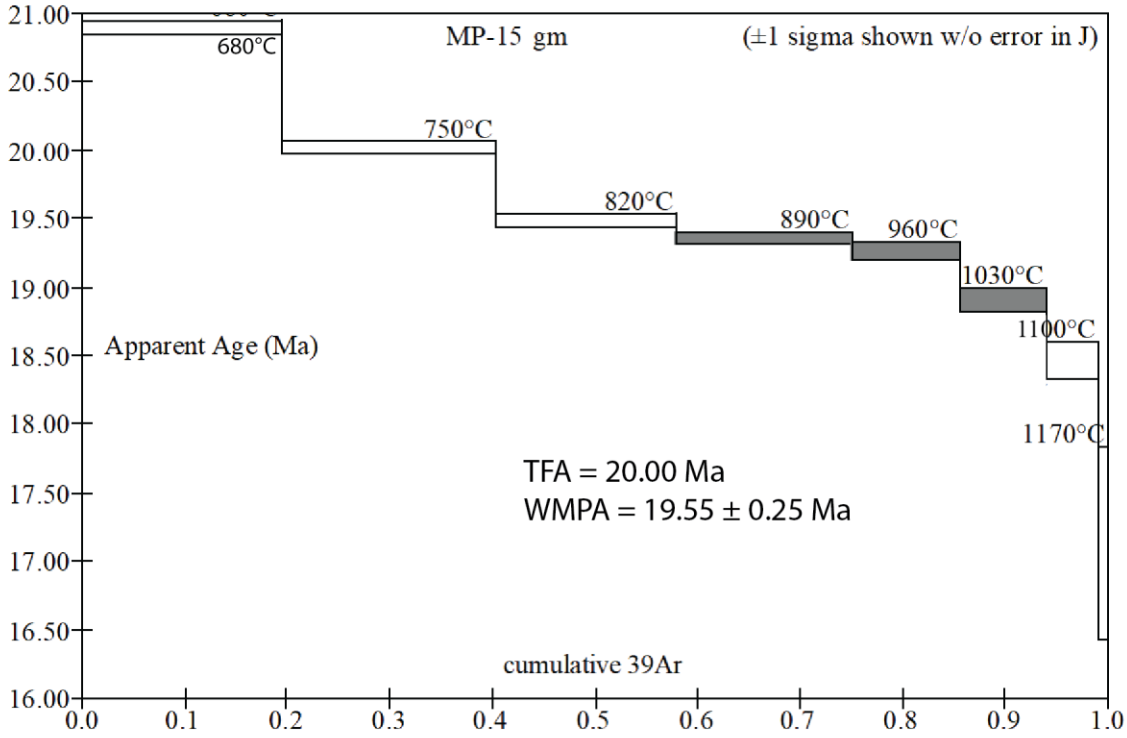

Sample: SB67-137; MK-MP-16 GM; J=0.0031750

T	t	40(mol)	40/39	38/39	37/39	36/39	K/Ca	∑ 39Ar	40Ar*	Age (Ma)
670	14	2.3e-14	4.4199	0.0e+0	1.1429	0.0031	0.43	0.10580	0.792	19.9 ± 0.1
740	14	3.6e-14	3.9601	0.0e+0	0.9409	0.0017	0.52	0.28519	0.872	19.7 ± 0.1
810	14	3.1e-14	3.7730	0.0e+0	0.8020	0.0013	0.61	0.44944	0.901	19.4 ± 0.1
880	14	3.6e-14	3.6304	0.0e+0	0.6864	0.0008	0.71	0.64671	0.932	19.3 ± 0.1
960	14	3.3e-14	3.8272	0.0e+0	0.6353	0.0015	0.77	0.81690	0.883	19.3 ± 0.1
1040	14	2.7e-14	4.2076	0.0e+0	0.7405	0.0029	0.66	0.94436	0.797	19.1 ± 0.1
1160	14	1.3e-14	4.7334	3.7e-4	4.4346	0.0048	0.11	1.00000	0.699	18.8 ± 0.2

Total fusion age, TFA= 19.39 ± 0.06 Ma (including J)
Weighted mean plateau age, WMPA= 19.24 ± 0.06 Ma (including J)
Inverse isochron age =19.36 ± 0.09 Ma. (MSWD =0.38; 40Ar/36Ar=280.9 ± 4.7)
Steps used: 880, 960, 1040, (4–6/7 or 49% ∑ 39Ar
t = dwell time in minutes.
40(mol) = moles corrected for blank and reactor-produced 40.
Ratios are corrected for blanks, decay, and interference.
∑39Ar is cumulative, 40Ar* = rad fraction.

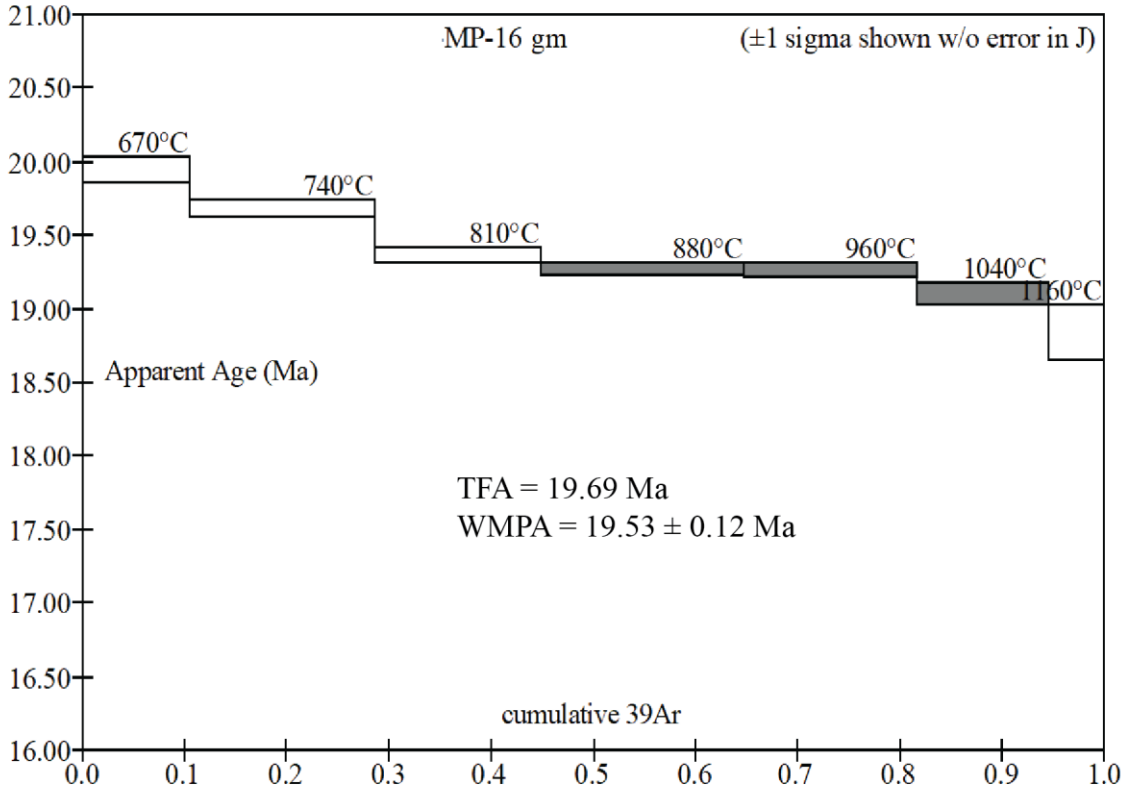

Sample: SB67-138; MK-MP-18 GM; J=0.0031700

T	t	40(mol)	40/39	38/39	37/39	36/39	K/Ca	∑ 39Ar	40Ar*	Age (Ma)
670	14	4.8e-14	3.7222	0.0e+0	0.4375	0.0009	1.1	0.12337	0.931	19.7 ± 0.1
740	14	8.1e-14	3.5884	0.0e+0	0.3186	0.0004	1.5	0.33984	0.967	19.7 ± 0.1
810	14	8.9e-14	3.5244	0.0e+0	0.2555	0.0003	1.9	0.58404	0.972	19.5 ± 0.1
880	14	6.8e-14	3.4849	0.0e+0	0.2662	0.0003	1.8	0.77290	0.971	19.3 ± 0.1
960	14	4.6e-14	3.4721	0.0e+0	0.3483	0.0007	1.4	0.90049	0.944	18.6 ± 0.1
1040	14	2.6e-14	3.7204	0.0e+0	0.4994	0.0018	0.98	0.96725	0.853	18.1 ± 0.1
1160	14	1.3e-14	3.9262	1.4e-3	3.5128	0.0035	0.14	1.00000	0.738	16.5 ± 0.2

Total fusion age, TFA= 19.22 ± 0.06 Ma (including J)
Weighted mean plateau age, WMPA= 19.29 ± 0.06 Ma (including J)
Inverse isochron age =19.75 ± 0.27 Ma. (MSWD =157.42; 40Ar/36Ar=151.9 ± 41.5)
Steps used: 670, 740, 810, 880, 960, 1040, 1160, (1–7/7 or 100% ∑ 39Ar
t = dwell time in minutes.
40(mol) = moles corrected for blank and reactor-produced 40.
Ratios are corrected for blanks, decay, and interference.
∑39Ar is cumulative, 40Ar* = rad fraction.

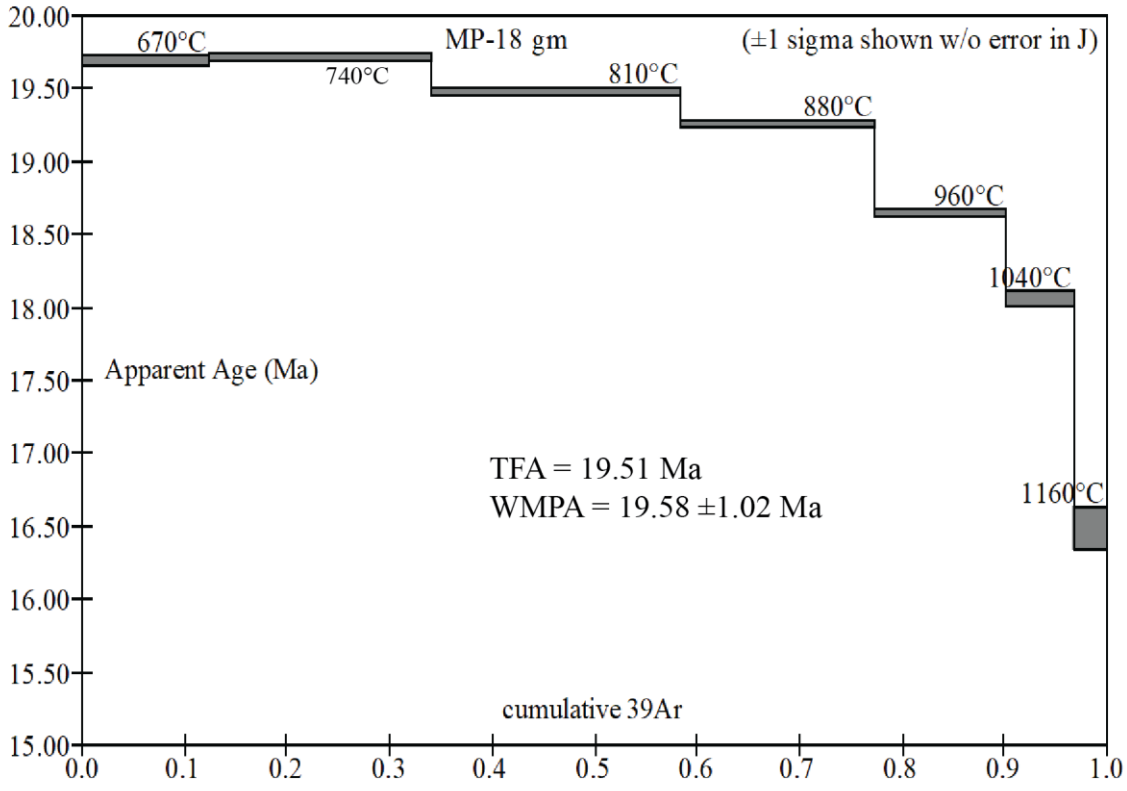

Sample: SB67-140; MK-MP-19 Plag; J=0.0031595

T	t	40(mol)	40/39	38/39	37/39	36/39	K/Ca	∑ 39Ar	40Ar*	Age (Ma)
800	14	1.0e-13	16.9440	0.0e+0	4.3995	0.0465	0.11	0.19129	0.190	18.2 ± 0.2
880	15	8.7e-14	12.0587	0.0e+0	5.4404	0.0295	0.090	0.41476	0.276	18.9 ± 0.2
950	15	8.0e-14	10.5008	0.0e+0	5.3697	0.0241	0.091	0.65198	0.321	19.1 ± 0.2
1030	15	7.4e-14	11.6595	0.0e+0	5.1575	0.0280	0.095	0.84922	0.290	19.2 ± 0.2
1160	14	7.1e-14	25.1194	0.0e+0	4.9378	0.0729	0.099	0.93620	0.143	20.3 ± 0.3
1350	14	2.3e-14	11.2609	0.0e+0	5.0705	0.0240	0.097	1.00000	0.370	23.6 ± 0.3

Total fusion age, TFA= 19.29 ± 0.10 Ma (including J)
Weighted mean plateau age, WMPA= 19.14 ± 0.14 Ma (including J)
Inverse isochron age =19.96 ± 1.21 Ma. (MSWD =1.13; 40Ar/36Ar=289.5 ± 7.9)
Steps used: 950, 1030, (3–4/6 or 43% ∑ 39Ar
t = dwell time in minutes.
40(mol) = moles corrected for blank and reactor-produced 40.
Ratios are corrected for blanks, decay, and interference.
∑39Ar is cumulative, 40Ar* = rad fraction.

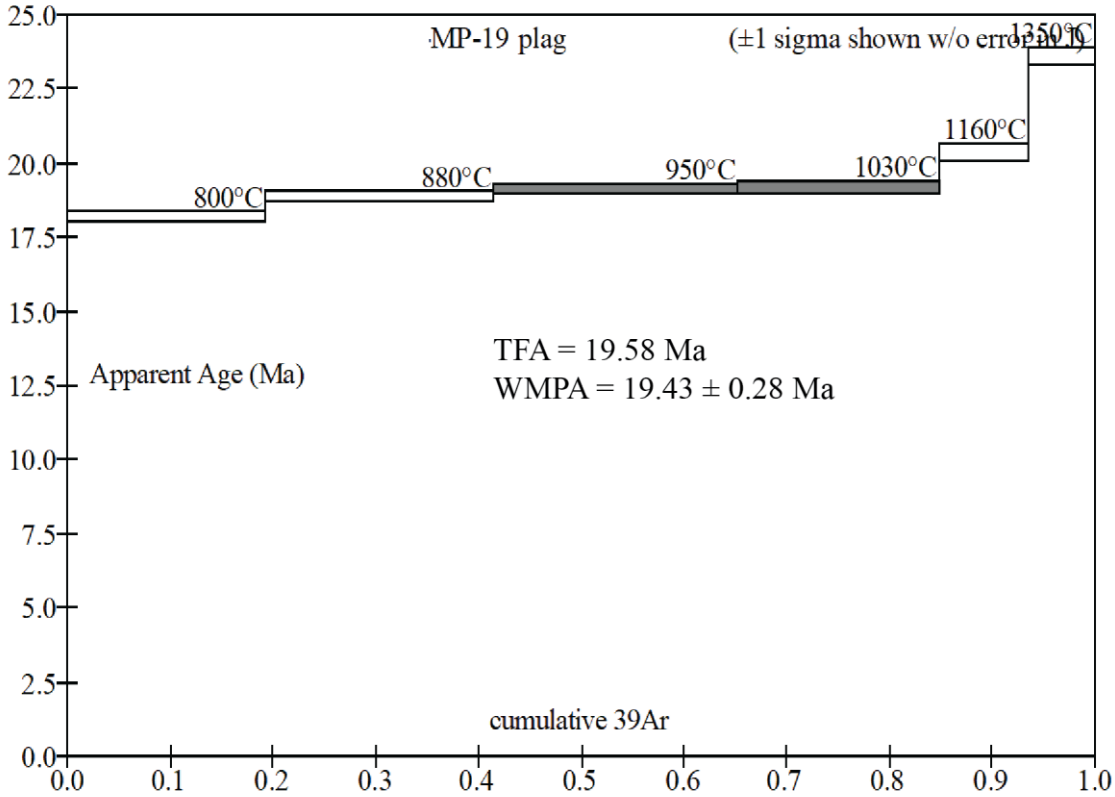

Sample: SB67-142; MK-MP-21 Plag; J=0.0031510

T	t	40(mol)	40/39	38/39	37/39	36/39	K/Ca	∑ 39Ar	40Ar*	Age (Ma)
800	14	2.2e-14	5.6922	0.0e+0	8.5394	0.0077	0.057	0.15429	0.602	19.4 ± 0.3
880	15	2.6e-14	4.6935	0.0e+0	8.6939	0.0042	0.056	0.36833	0.738	19.6 ± 0.2
950	15	2.6e-14	4.3697	0.0e+0	8.5901	0.0030	0.057	0.59822	0.795	19.6 ± 0.2
1030	15	2.6e-14	5.1373	0.0e+0	8.2062	0.0056	0.060	0.80023	0.679	19.7 ± 0.2
1160	14	1.6e-14	6.2417	0.0e+0	7.7527	0.0086	0.063	0.90359	0.595	21.0 ± 0.3
1350	14	1.5e-14	6.2528	0.0e+0	7.0504	0.0073	0.069	1.00000	0.657	23.2 ± 0.3

Total fusion age, TFA= 20.08 ± 0.11 Ma (including J)
Weighted mean plateau age, WMPA= 19.64 ± 0.13 Ma (including J)
Inverse isochron age =19.51 ± 0.53 Ma. (MSWD =0.09; 40Ar/36Ar=300.8 ± 6.7)
Steps used: 880, 950, 1030, (2–4/6 or 65% ∑ 39Ar
t = dwell time in minutes.
40(mol) = moles corrected for blank and reactor-produced 40.
Ratios are corrected for blanks, decay, and interference.
∑39Ar is cumulative, 40Ar* = rad fraction.

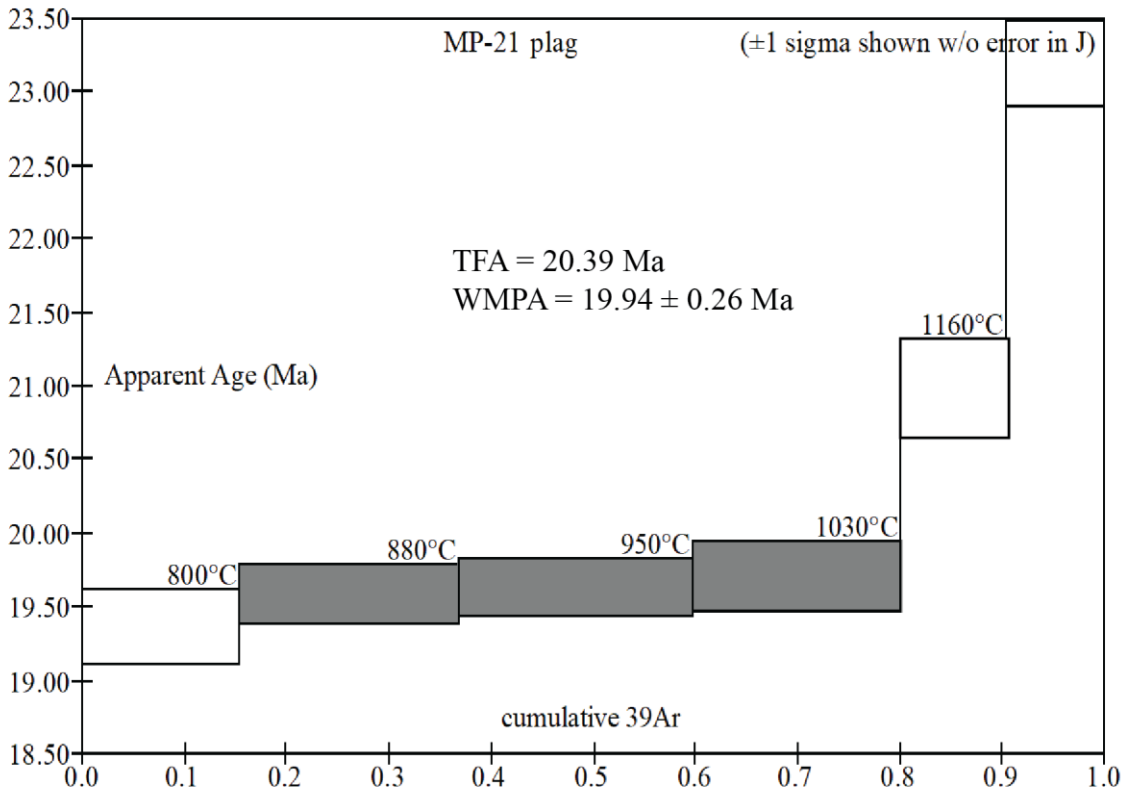

Sample: SB67-145; MK-MP-22 Plag; J=0.0031370

T	t	40(mol)	40/39	38/39	37/39	36/39	K/Ca	∑ 39Ar	40Ar*	Age (Ma)
800	14	1.6e-14	4.2492	0.0e+0	8.4522	0.0027	0.058	0.14206	0.812	19.4 ± 0.2
880	15	2.2e-14	3.8933	0.0e+0	8.5104	0.0014	0.058	0.35070	0.894	19.6 ± 0.2
950	15	2.4e-14	3.7736	0.0e+0	8.3995	0.0009	0.058	0.58814	0.927	19.7 ± 0.2
1030	15	2.2e-14	3.8368	0.0e+0	8.1377	0.0011	0.060	0.80107	0.919	19.8 ± 0.2
1160	14	1.2e-14	4.2467	0.0e+0	7.7592	0.0021	0.063	0.90425	0.851	20.3 ± 0.3
1350	14	1.7e-14	6.7941	0.0e+0	6.9208	0.0099	0.071	1.00000	0.570	21.8 ± 0.3

Total fusion age, TFA= 19.93 ± 0.11 Ma (including J)
Weighted mean plateau age, WMPA= 19.73 ± 0.12 Ma (including J)
Inverse isochron age =19.92 ± 0.21 Ma. (MSWD =0.41; 40Ar/36Ar=262.7 ± 15.8)
Steps used: 880, 950, 1030, (2–4/6 or 66% ∑ 39Ar
t = dwell time in minutes.
40(mol) = moles corrected for blank and reactor-produced 40.
Ratios are corrected for blanks, decay, and interference.
∑39Ar is cumulative, 40Ar* = rad fraction.

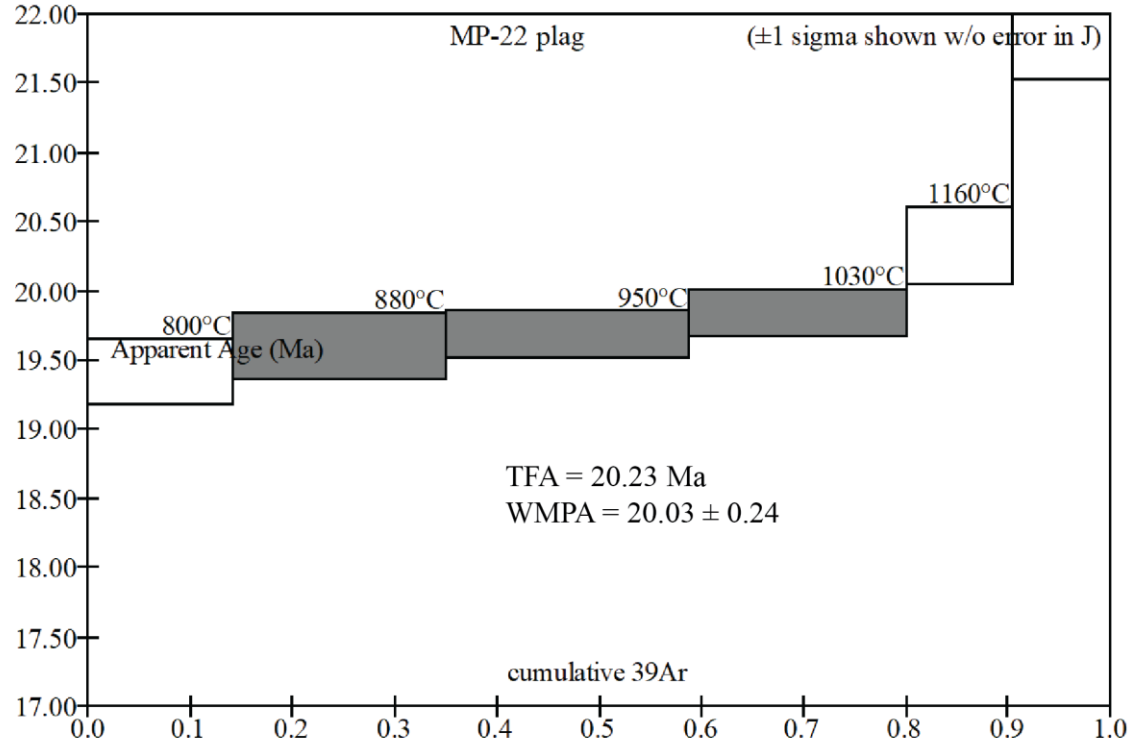

Sample: SB67-147; MK-MP-23 Plag; J=0.0031100

T	t	40(mol)	40/39	38/39	37/39	36/39	K/Ca	∑ 39Ar	40Ar*	Age (Ma)
800	14	1.4e-13	34.7651	0.0e+0	6.5156	0.1081	0.075	0.16901	0.081	15.8 ± 0.4
880	15	1.1e-13	21.6297	0.0e+0	6.8197	0.0627	0.072	0.38722	0.144	17.4 ± 0.2
950	15	9.6e-14	18.2349	0.0e+0	6.7524	0.0510	0.073	0.60501	0.173	17.6 ± 0.3
1030	15	9.8e-14	22.4423	0.0e+0	6.4522	0.0656	0.076	0.78621	0.137	17.1 ± 0.3
1160	14	1.5e-13	59.5226	0.0e+0	6.1681	0.1929	0.079	0.89050	0.043	14.2 ± 0.6
1350	14	2.7e-13	111.7406	0.0e+0	6.2679	0.3711	0.078	0.99237	0.019	11.7 ± 0.4
1350	14	5.2e-14	280.7476	1.4e-3	7.7337	0.9474	0.063	1.00000	0.003	4.4 ± 6.0

Total fusion age, TFA= 16.11 ± 0.15 Ma (including J)
Weighted mean plateau age, WMPA= 17.39 ± 0.15 Ma (including J)
Inverse isochron age =19.04 ± 1.33 Ma. (MSWD =0.26; 40Ar/36Ar=290.5 ± 2.0)
Steps used: 880, 950, 1030, (2–4/7 or 62% ∑ 39Ar
t = dwell time in minutes.
40(mol) = moles corrected for blank and reactor-produced 40.
Ratios are corrected for blanks, decay, and interference.
∑39Ar is cumulative, 40Ar* = rad fraction.

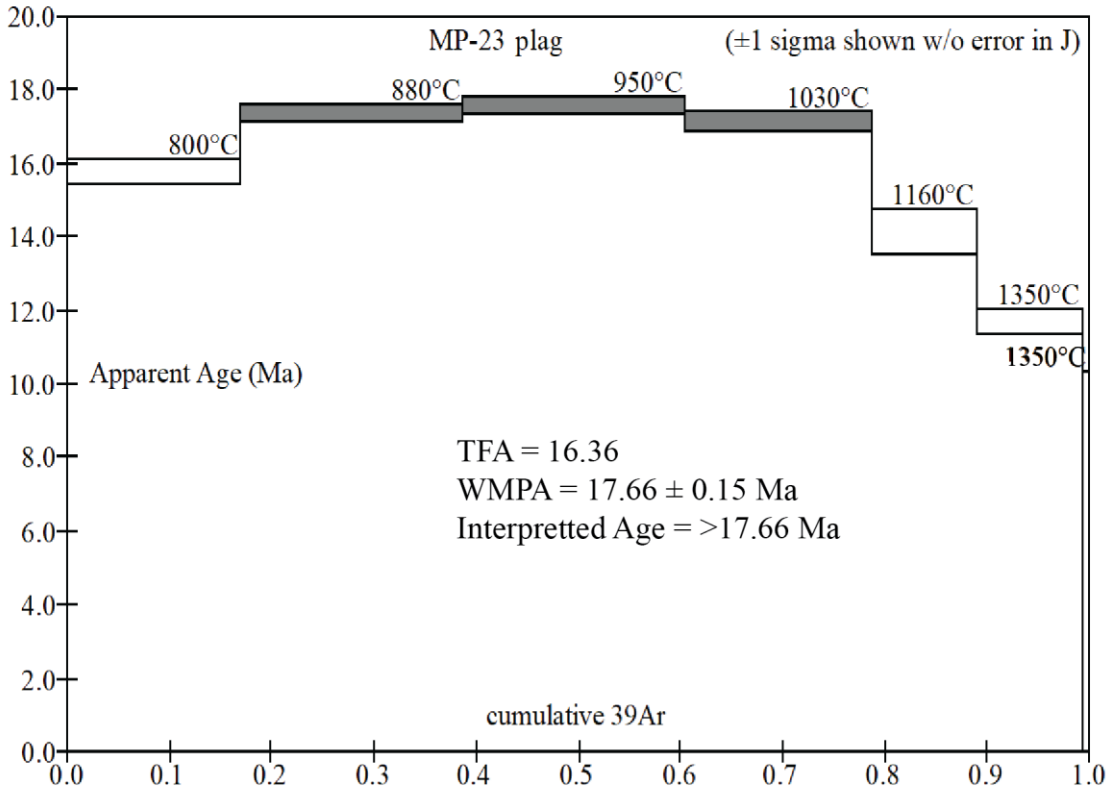

Sample: SB67-149; MK-MP-24 Plag; J=0.0030880

T	t	40(mol)	40/39	38/39	37/39	36/39	K/Ca	∑ 39Ar	40Ar*	Age (Ma)
800	14	2.5e-14	5.2247	0.0e+0	5.4419	0.0061	0.090	0.14866	0.656	19.0 ± 0.2
880	15	2.8e-14	4.4438	0.0e+0	5.6991	0.0034	0.086	0.34762	0.776	19.1 ± 0.2
950	15	3.0e-14	4.2587	0.0e+0	5.5972	0.0027	0.088	0.56819	0.815	19.2 ± 0.1
1030	15	3.2e-14	4.4377	0.0e+0	5.3557	0.0033	0.091	0.79384	0.781	19.2 ± 0.1
1160	14	2.3e-14	6.4483	0.0e+0	5.1046	0.0100	0.096	0.90465	0.543	19.4 ± 0.2
1350	14	3.7e-14	12.2085	0.0e+0	5.0932	0.0276	0.096	1.00000	0.332	22.4 ± 0.3

Total fusion age, TFA= 19.49 ± 0.09 Ma (including J)
Weighted mean plateau age, WMPA= 19.18 ± 0.09 Ma (including J)
Inverse isochron age =19.13 ± 0.16 Ma. (MSWD =0.76; 40Ar/36Ar=298.0 ± 5.0)
Steps used: 800, 880, 950, 1030, 1160, (1–5/6 or 90% ∑ 39Ar
t = dwell time in minutes.
40(mol) = moles corrected for blank and reactor-produced 40.
Ratios are corrected for blanks, decay, and interference.
∑39Ar is cumulative, 40Ar* = rad fraction.

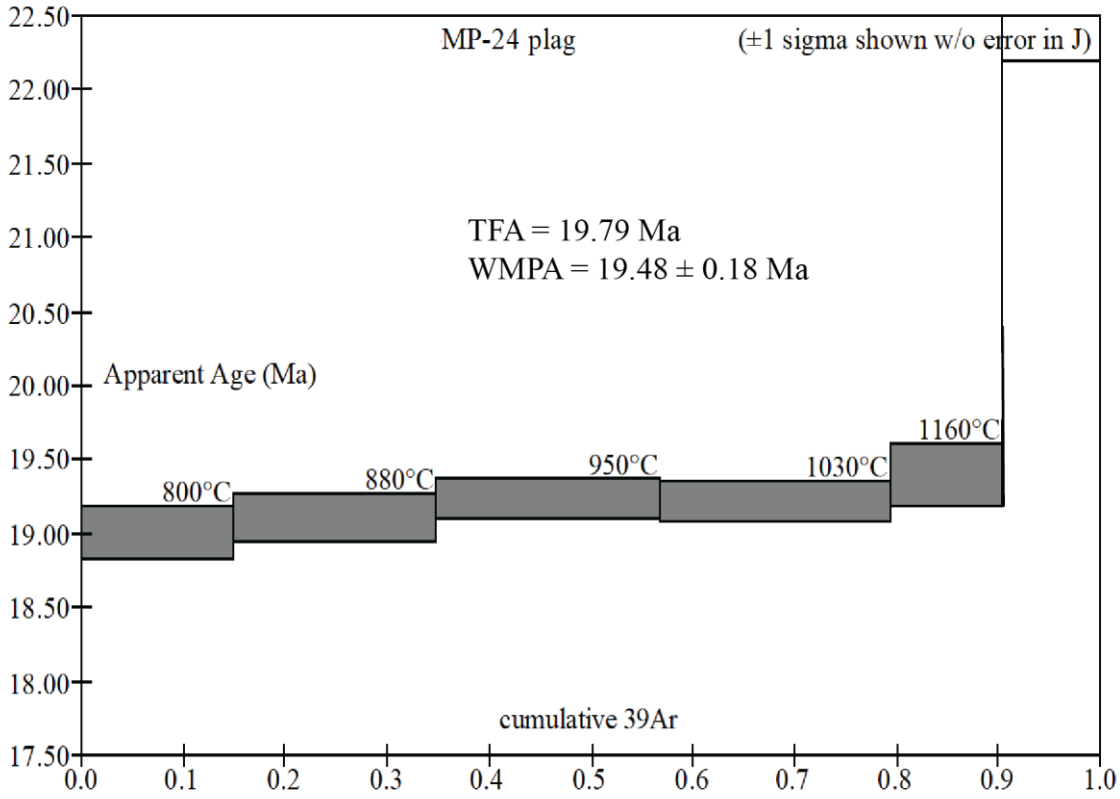

Sample: SB67-151; MK-MP-26 Plag; J=0.0030680

T	t	40(mol)	40/39	38/39	37/39	36/39	K/Ca	∑ 39Ar	40Ar*	Age (Ma)
800	14	1.8e-14	4.4817	0.0e+0	8.7800	0.0034	0.056	0.18258	0.777	19.2 ± 0.3
880	15	1.9e-14	4.0861	0.0e+0	9.3302	0.0019	0.053	0.39779	0.860	19.4 ± 0.2
950	15	1.8e-14	4.0122	0.0e+0	9.2369	0.0017	0.053	0.60027	0.875	19.3 ± 0.2
1030	15	1.7e-14	4.4396	0.0e+0	8.8698	0.0031	0.055	0.78093	0.792	19.4 ± 0.2
1160	14	1.6e-14	7.2166	0.0e+0	8.4480	0.0125	0.058	0.88042	0.487	19.3 ± 0.4
1350	14	2.1e-14	8.2139	0.0e+0	8.2328	0.0148	0.060	1.00000	0.467	21.1 ± 0.3

Total fusion age, TFA= 19.53 ± 0.12 Ma (including J)
Weighted mean plateau age, WMPA= 19.31 ± 0.12 Ma (including J)
Inverse isochron age =19.31 ± 0.17 Ma. (MSWD =0.12; 40Ar/36Ar=295.5 ± 2.3)
Steps used: 800, 880, 950, 1030, 1160, (1–5/6 or 88% ∑ 39Ar
t = dwell time in minutes.
40(mol) = moles corrected for blank and reactor-produced 40.
Ratios are corrected for blanks, decay, and interference.
∑39Ar is cumulative, 40Ar* = rad fraction.

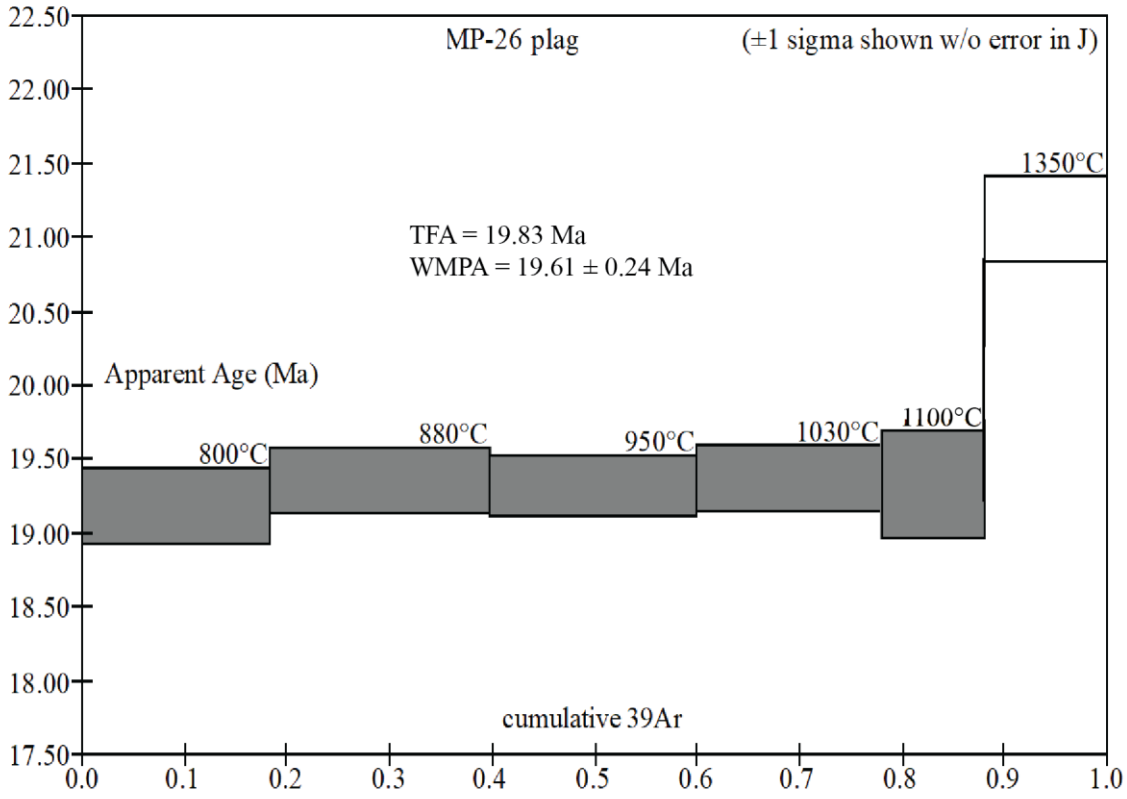

Sample: SB66-116; AB-01 GM; J=0.0041919

T	t	40(mol)	40/39	38/39	37/39	36/39	K/Ca	∑ 39Ar	40Ar*	Age (Ma)
500	14	6.2e-15	8.9490	0.0e+0	0.9545	0.0210	0.51	0.00554	0.306	20.6 ± 0.8
550	14	7.1e-15	4.8058	0.0e+0	0.7240	0.0065	0.68	0.01746	0.601	21.7 ± 0.3
600	14	1.1e-14	3.5476	0.0e+0	0.6913	0.0025	0.71	0.04137	0.792	21.1 ± 0.2
650	14	1.7e-14	3.1331	0.0e+0	0.6986	0.0012	0.70	0.08450	0.885	20.9 ± 0.1
700	14	2.2e-14	2.9481	0.0e+0	0.6806	0.0006	0.72	0.14398	0.942	20.9 ± 0.1
750	14	2.3e-14	2.9088	0.0e+0	0.5361	0.0004	0.91	0.20817	0.956	20.9 ± 0.1
800	14	2.4e-14	2.9447	0.0e+0	0.3984	0.0006	1.2	0.27285	0.944	20.9 ± 0.1
860	14	2.9e-14	2.9454	0.0e+0	0.3576	0.0006	1.4	0.35123	0.940	20.8 ± 0.1
920	14	3.0e-14	2.9043	0.0e+0	0.3769	0.0006	1.3	0.43310	0.940	20.5 ± 0.1
980	14	5.1e-14	2.8697	0.0e+0	0.4099	0.0006	1.2	0.57540	0.941	20.3 ± 0.1
1040	14	8.4e-14	2.8870	0.0e+0	0.4592	0.0006	1.1	0.80803	0.934	20.3 ± 0.0
1100	14	3.3e-14	3.0908	0.0e+0	1.2530	0.0013	0.39	0.89446	0.877	20.4 ± 0.1
1160	14	3.5e-14	3.3331	0.0e+0	5.1137	0.0020	0.096	0.98002	0.826	20.7 ± 0.1
1250	14	1.1e-14	4.2817	0.0e+0	4.7921	0.0038	0.10	1.00000	0.739	23.8 ± 0.2

Total fusion age, TFA= 20.64 ± 0.04 Ma (including J)
Weighted mean plateau age, WMPA= 20.30 ± 0.04 Ma (including J)
Inverse isochron age =20.21 ± 0.10 Ma. (MSWD =0.43; 40Ar/36Ar=312.7 ± 10.5)
Steps used: 980, 1040, 1100, (10–12/14 or 46% ∑ 39Ar
t = dwell time in minutes.
40(mol) = moles corrected for blank and reactor-produced 40.
Ratios are corrected for blanks, decay, and interference.
∑39Ar is cumulative, 40Ar* = rad fraction.

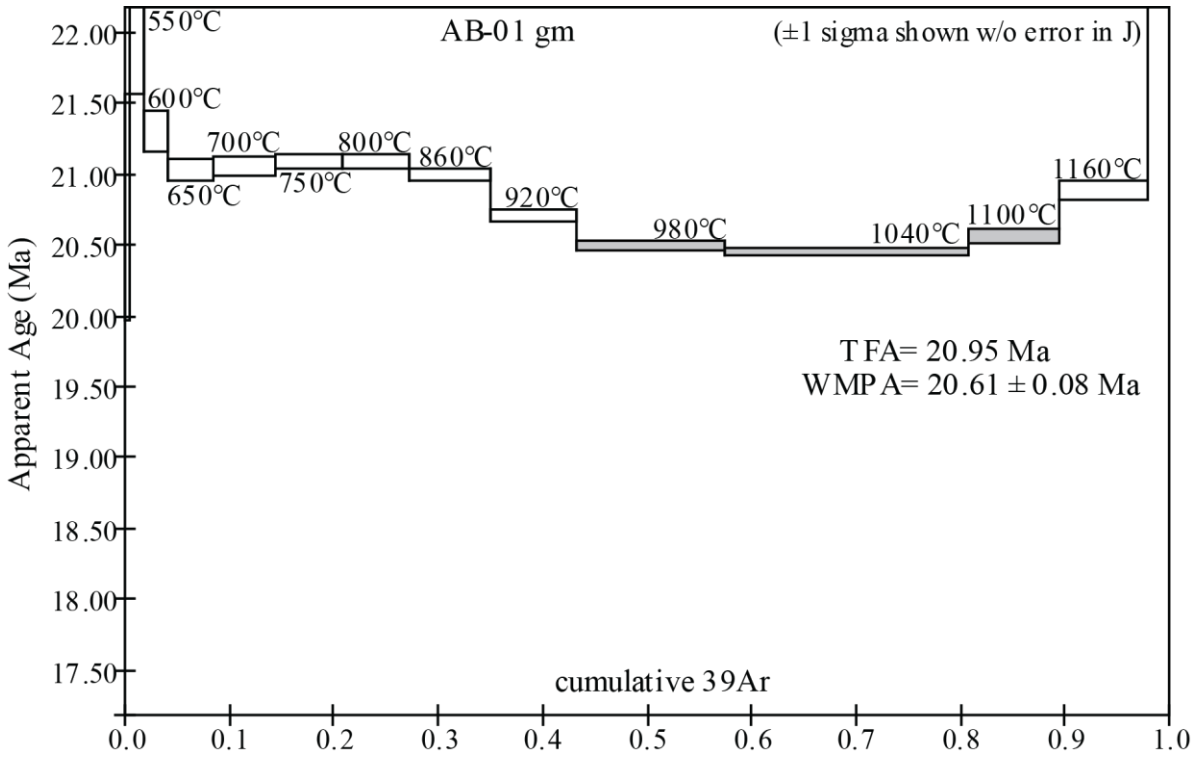

Sample: SB66-129; MK-4.6 GM; J=0.0041286

T	t	40(mol)	40/39	38/39	37/39	36/39	K/Ca	∑ 39Ar	40Ar*	Age (Ma)
550	14	1.4e-14	7.1482	0.0e+0	1.3106	0.0139	0.37	0.01923	0.426	22.5 ± 0.3
600	14	1.4e-14	4.7632	0.0e+0	1.4259	0.0060	0.34	0.04810	0.628	22.1 ± 0.2
650	14	2.0e-14	3.7383	0.0e+0	1.2261	0.0027	0.40	0.09851	0.789	21.8 ± 0.1
700	14	2.6e-14	3.1902	0.0e+0	1.2491	0.0010	0.39	0.17614	0.905	21.4 ± 0.1
750	14	2.9e-14	3.0509	0.0e+0	0.9444	0.0007	0.52	0.26608	0.935	21.1 ± 0.1
800	14	3.6e-14	3.1429	0.0e+0	0.6691	0.0010	0.73	0.37609	0.906	21.1 ± 0.1
850	14	3.5e-14	3.0233	0.0e+0	0.5463	0.0006	0.90	0.48693	0.938	21.0 ± 0.1
900	14	3.0e-14	2.9912	0.0e+0	0.4271	0.0006	1.1	0.58379	0.945	20.9 ± 0.1
950	14	2.9e-14	3.0493	0.0e+0	0.4818	0.0008	1.0	0.67654	0.918	20.7 ± 0.1
1000	14	3.3e-14	3.0430	0.0e+0	0.6620	0.0009	0.74	0.78217	0.915	20.6 ± 0.1
1050	14	4.1e-14	3.0308	0.0e+0	0.6241	0.0008	0.79	0.91161	0.921	20.7 ± 0.1
1110	14	2.4e-14	3.1155	8.6e-5	1.8314	0.0011	0.27	0.98661	0.896	20.7 ± 0.1
1200	14	6.4e-15	4.6859	0.0e+0	16.5279	0.0060	0.030	1.00000	0.619	21.5 ± 0.4

Total fusion age, TFA= 21.02 ± 0.05 Ma (including J)
Weighted mean plateau age, WMPA= 20.68 ± 0.05 Ma (including J)
Inverse isochron age =20.68 ± 0.29 Ma. (MSWD =0.80; 40Ar/36Ar=295.5 ± 40.3)
Steps used: 950, 1000, 1050, 1110, (9–12/13 or 40% ∑ 39Ar
t = dwell time in minutes.
40(mol) = moles corrected for blank and reactor-produced 40.
Ratios are corrected for blanks, decay, and interference.
∑39Ar is cumulative, 40Ar* = rad fraction.

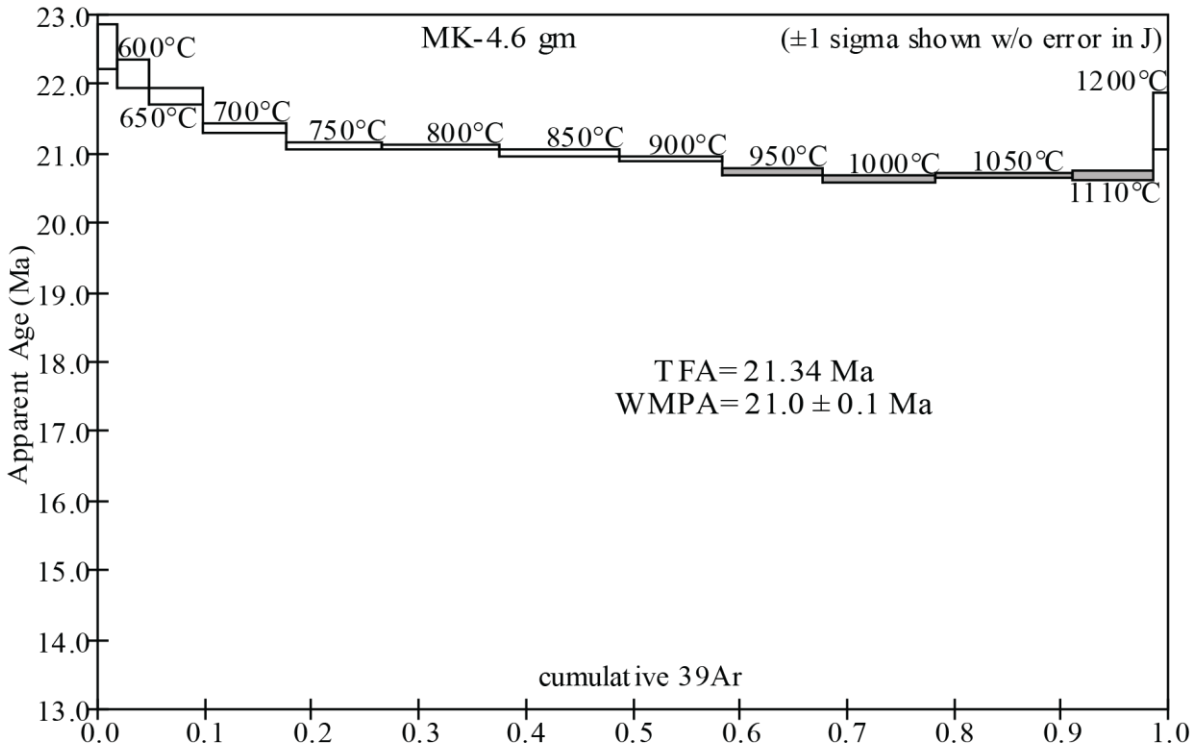

Sample: SB63-77; WM-21 GM; J=0.0034593

T	t	40(mol)	40/39	38/39	37/39	36/39	K/Ca	∑ 39Ar	40Ar*	Age (Ma)
550	18	1.3e-14	8.8195	0.0e+0	3.0360	0.0210	0.16	0.03280	0.295	16.2 ± 0.3
600	18	1.0e-14	5.0936	0.0e+0	4.3687	0.0079	0.11	0.07702	0.540	17.1 ± 0.2
650	18	1.4e-14	4.1829	0.0e+0	4.8384	0.0043	0.10	0.14915	0.698	18.1 ± 0.1
700	18	1.7e-14	3.7386	0.0e+0	4.5905	0.0028	0.11	0.25216	0.781	18.1 ± 0.1
750	18	1.8e-14	3.6088	0.0e+0	3.7482	0.0021	0.13	0.36174	0.827	18.5 ± 0.1
800	18	1.8e-14	3.8549	0.0e+0	3.6764	0.0030	0.13	0.46763	0.772	18.5 ± 0.1
850	18	1.5e-14	3.6638	0.0e+0	3.6481	0.0024	0.13	0.55757	0.804	18.3 ± 0.1
910	18	1.6e-14	3.8788	0.0e+0	5.1931	0.0032	0.094	0.64688	0.758	18.3 ± 0.1
960	18	1.6e-14	4.3487	0.0e+0	6.1263	0.0049	0.080	0.72605	0.670	18.1 ± 0.1
1010	18	1.8e-14	6.3240	0.0e+0	5.3680	0.0117	0.091	0.79063	0.452	17.7 ± 0.1
1060	18	2.1e-14	7.4448	0.0e+0	4.9882	0.0155	0.098	0.85185	0.385	17.8 ± 0.2
1130	18	3.2e-14	8.7268	1.9e-4	7.6100	0.0198	0.064	0.93284	0.331	17.9 ± 0.2
1200	18	1.7e-14	8.1776	0.0e+0	42.4602	0.0184	0.012	0.97921	0.336	17.1 ± 0.3
1280	18	7.4e-15	8.2815	0.0e+0	63.0798	0.0184	0.008	1.00000	0.345	17.7 ± 0.5

Total fusion age, TFA= 18.00 ± 0.05 Ma (including J)
Weighted mean plateau age, WMPA= 17.93 ± 0.07 Ma (including J)
Inverse isochron age =18.10 ± 0.18 Ma. (MSWD =1.54; 40Ar/36Ar=292.9 ± 2.3)
Steps used: 960, 1010, 1060, 1130, (9–12/14 or 29% ∑ 39Ar)
t = dwell time in minutes.
40(mol) = moles corrected for blank and reactor-produced 40.
Ratios are corrected for blanks, decay, and interference.
∑39Ar is cumulative, 40Ar* = rad fraction.

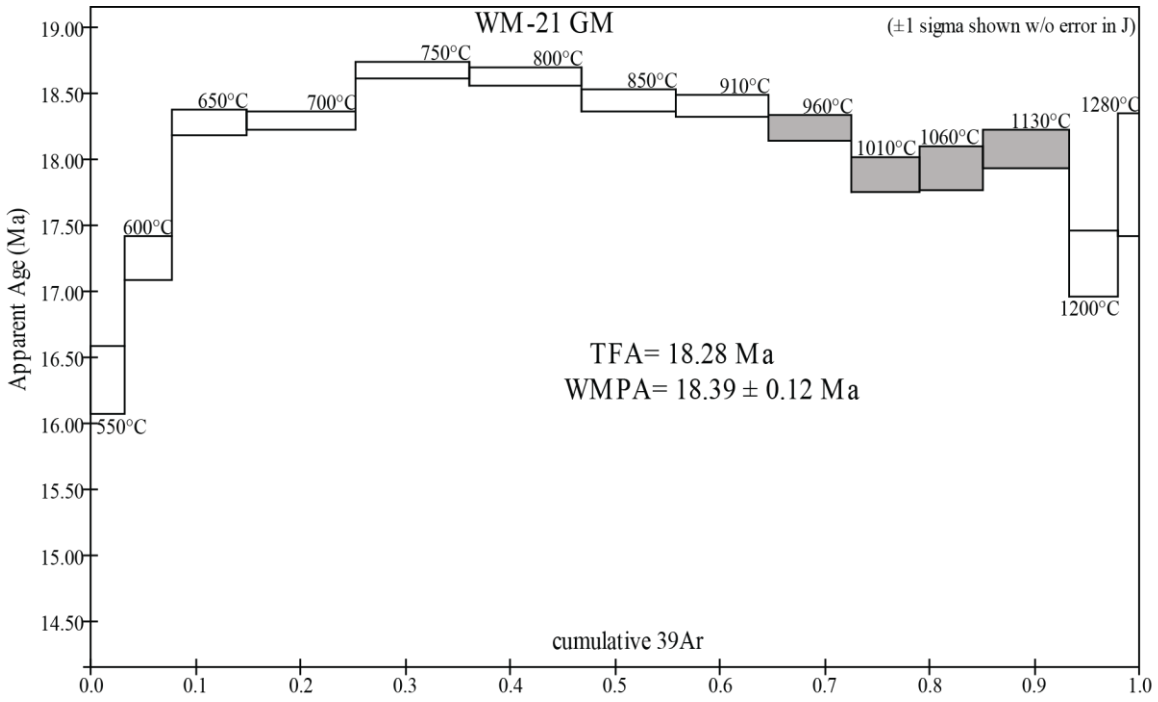

Sample: SB63-76; WM-22 San; J=0.0034668

T	t	40(mol)	40/39	38/39	37/39	36/39	K/Ca	∑ 39Ar	40Ar*	Age (Ma)
650	18	2.5e-15	3.8685	2.2e-2	0.0952	0.0031	5.1	0.00406	0.761	18.3 ± 0.6
730	18	6.2e-15	3.4596	1.0e-3	0.4392	0.0017	1.1	0.01536	0.857	18.4 ± 0.2
800	18	1.1e-14	3.2013	0.0e+0	0.0524	0.0007	9.3	0.03746	0.935	18.6 ± 0.1
860	18	1.7e-14	3.0885	0.0e+0	0.0337	0.0005	15	0.07216	0.950	18.3 ± 0.1
920	18	2.7e-14	3.0454	0.0e+0	0.0276	0.0003	18	0.12712	0.972	18.4 ± 0.1
980	18	4.0e-14	3.0259	0.0e+0	0.0242	0.0002	20	0.20943	0.979	18.4 ± 0.0
1040	18	5.3e-14	3.0140	0.0e+0	0.0249	0.0001	20	0.32001	0.986	18.5 ± 0.0
1100	18	6.2e-14	3.0112	0.0e+0	0.0271	0.0001	18	0.44881	0.988	18.5 ± 0.0
1150	18	4.6e-14	3.0270	0.0e+0	0.0414	0.0002	12	0.54367	0.981	18.5 ± 0.0
1200	18	6.9e-14	3.0090	0.0e+0	0.0828	0.0001	5.9	0.68730	0.986	18.5 ± 0.0
1260	18	1.1e-13	3.0053	0.0e+0	0.0474	0.0001	10	0.91804	0.990	18.5 ± 0.0
1350	18	4.0e-14	3.0480	0.0e+0	0.2299	0.0002	2.1	1.00000	0.984	18.7 ± 0.0

Total fusion age, TFA= 18.49 ± 0.04 Ma (including J)
Weighted mean plateau age, WMPA= 18.49 ± 0.04 Ma (including J)
Inverse isochron age =18.49 ± 0.05 Ma. (MSWD =1.50; 40Ar/36Ar=282.5 ± 16.4)
Steps used: 650, 730, 800, 860, 920, 980, 1040, 1100, 1150, 1200, 1260, (1–11/12 or 92% ∑ 39Ar
t = dwell time in minutes.
40(mol) = moles corrected for blank and reactor-produced 40.
Ratios are corrected for blanks, decay, and interference.
∑39Ar is cumulative, 40Ar* = rad fraction.

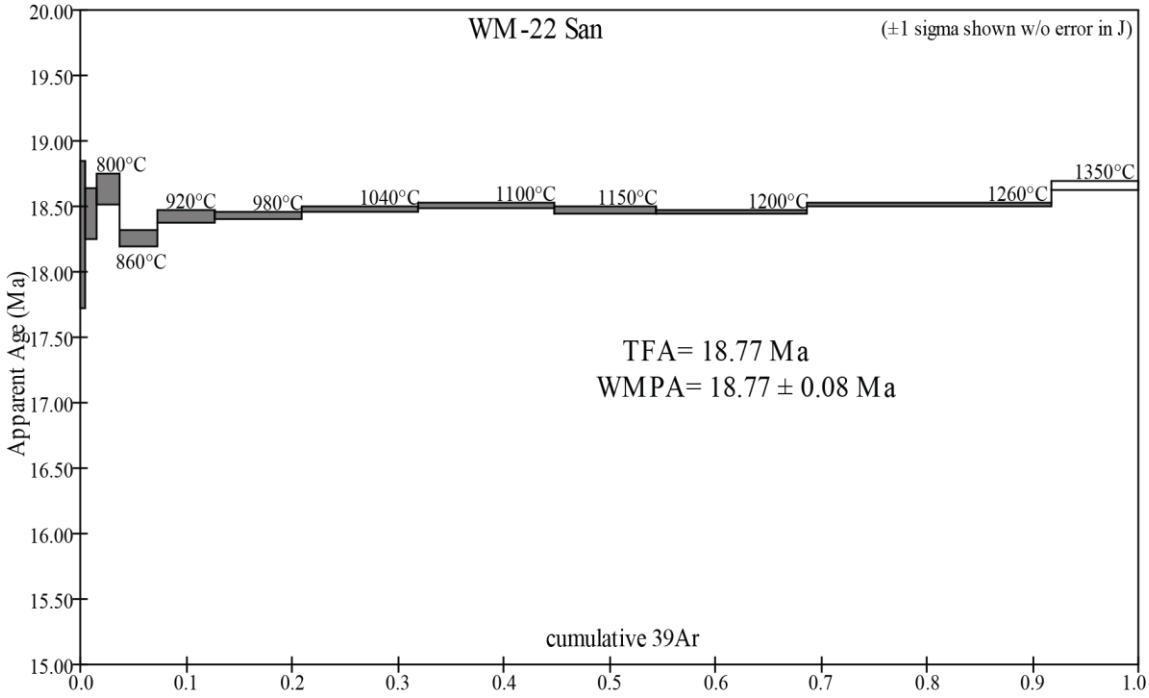

Sample: SB63-72; WM-23 GM; J=0.0034937

T	t	40(mol)	40/39	38/39	37/39	36/39	K/Ca	∑ 39Ar	40Ar*	Age (Ma)
500	30	4.0e-14	13.1165	1.1e-3	0.8177	0.0360	0.60	0.02946	0.188	15.5 ± 0.2
540	20	1.8e-14	9.2298	5.5e-4	0.6628	0.0220	0.74	0.04866	0.295	17.1 ± 0.2
580	20	2.1e-14	6.4977	0.0e+0	0.8259	0.0121	0.59	0.07936	0.449	18.3 ± 0.1
630	20	2.7e-14	4.8890	0.0e+0	1.0014	0.0061	0.49	0.13310	0.628	19.3 ± 0.1
680	20	3.3e-14	4.1776	0.0e+0	1.0424	0.0036	0.47	0.21055	0.742	19.4 ± 0.1
730	20	4.0e-14	4.0519	0.0e+0	0.8925	0.0034	0.55	0.30638	0.750	19.1 ± 0.1
780	20	4.5e-14	3.9590	0.0e+0	0.8032	0.0032	0.61	0.41603	0.761	18.9 ± 0.1
840	20	4.8e-14	4.2092	0.0e+0	0.6235	0.0041	0.79	0.52752	0.712	18.8 ± 0.1
900	20	4.5e-14	4.9297	0.0e+0	0.6965	0.0066	0.70	0.61643	0.606	18.7 ± 0.1
960	20	7.5e-14	7.0157	0.0e+0	0.7141	0.0138	0.69	0.72094	0.419	18.5 ± 0.1
1040	20	1.8e-13	11.2209	0.0e+0	0.6333	0.0280	0.77	0.87716	0.263	18.5 ± 0.1
1110	20	8.1e-14	13.6174	0.0e+0	1.0678	0.0357	0.46	0.93517	0.226	19.3 ± 0.1
1180	20	6.4e-14	14.7863	0.0e+0	4.4061	0.0390	0.11	0.97733	0.220	20.4 ± 0.2
1250	20	3.1e-14	13.6482	0.0e+0	13.1143	0.0354	0.04	1.00000	0.233	19.9 ± 0.2

Total fusion age, TFA= 18.79 ± 0.04 Ma (including J)
Weighted mean plateau age, WMPA= 18.48 ± 0.06 Ma (including J)
Inverse isochron age =18.93 ± 0.17 Ma. (MSWD =37.82; 40Ar/36Ar=295.2 ± 2.1)
Steps used: 960, 1040, (10–11/14 or 26% ∑ 39Ar
t = dwell time in minutes.
40(mol) = moles corrected for blank and reactor-produced 40.
Ratios are corrected for blanks, decay, and interference.
∑39Ar is cumulative, 40Ar* = rad fraction.

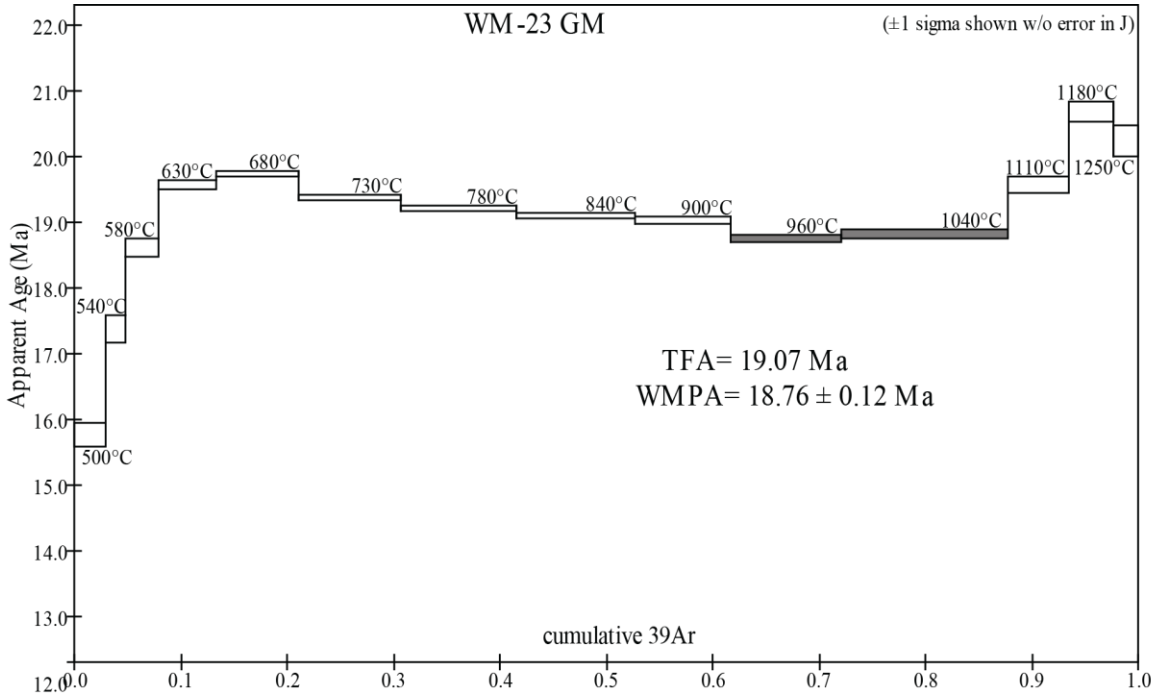

Sample: SB63-54; WM-29 Plag; J=0.0035920

T	t	40(mol)	40/39	38/39	37/39	36/39	K/Ca	∑ 39Ar	40Ar*	Age (Ma)
650	18	2.3e-14	14.4068	1.9e-3	4.4256	0.0390	0.11	0.02469	0.200	18.6 ± 0.3
730	18	2.3e-14	5.4361	0.0e+0	5.1541	0.0083	0.095	0.09197	0.547	19.2 ± 0.1
800	18	3.0e-14	3.9747	0.0e+0	5.3998	0.0034	0.091	0.20946	0.744	19.1 ± 0.1
860	18	3.5e-14	3.5847	0.0e+0	5.3977	0.0020	0.091	0.36113	0.833	19.3 ± 0.1
920	18	4.1e-14	3.4336	0.0e+0	5.3128	0.0015	0.092	0.54636	0.867	19.2 ± 0.1
990	18	4.6e-14	3.4165	0.0e+0	5.1367	0.0015	0.095	0.75569	0.872	19.2 ± 0.0
1050	18	3.2e-14	3.8402	0.0e+0	4.8864	0.0029	0.10	0.88414	0.777	19.2 ± 0.1
1100	18	2.2e-14	7.0507	0.0e+0	4.7486	0.0138	0.10	0.93225	0.422	19.2 ± 0.1
1150	18	1.5e-14	17.2904	0.0e+0	4.8934	0.0483	0.10	0.94597	0.175	19.5 ± 0.5
1200	18	1.9e-14	25.4624	0.0e+0	5.3178	0.0766	0.092	0.95778	0.112	18.3 ± 0.6
1300	18	3.3e-14	20.3641	0.0e+0	6.0940	0.0581	0.080	0.98286	0.156	20.5 ± 0.3
1400	18	1.3e-14	11.6476	0.0e+0	6.8534	0.0244	0.071	1.00000	0.381	28.6 ± 0.3

Total fusion age, TFA= 19.36 ± 0.05 Ma (including J)
Weighted mean plateau age, WMPA= 19.20 ± 0.04 Ma (including J)
Inverse isochron age =19.19 ± 0.05 Ma. (MSWD =1.02; 40Ar/36Ar=295.6 ± 1.2)
Steps used: 730, 800, 860, 920, 990, 1050, 1100, 1150, (2–9/12 or 92% ∑ 39Ar
t = dwell time in minutes.
40(mol) = moles corrected for blank and reactor-produced 40.
Ratios are corrected for blanks, decay, and interference.
∑39Ar is cumulative, 40Ar* = rad fraction.

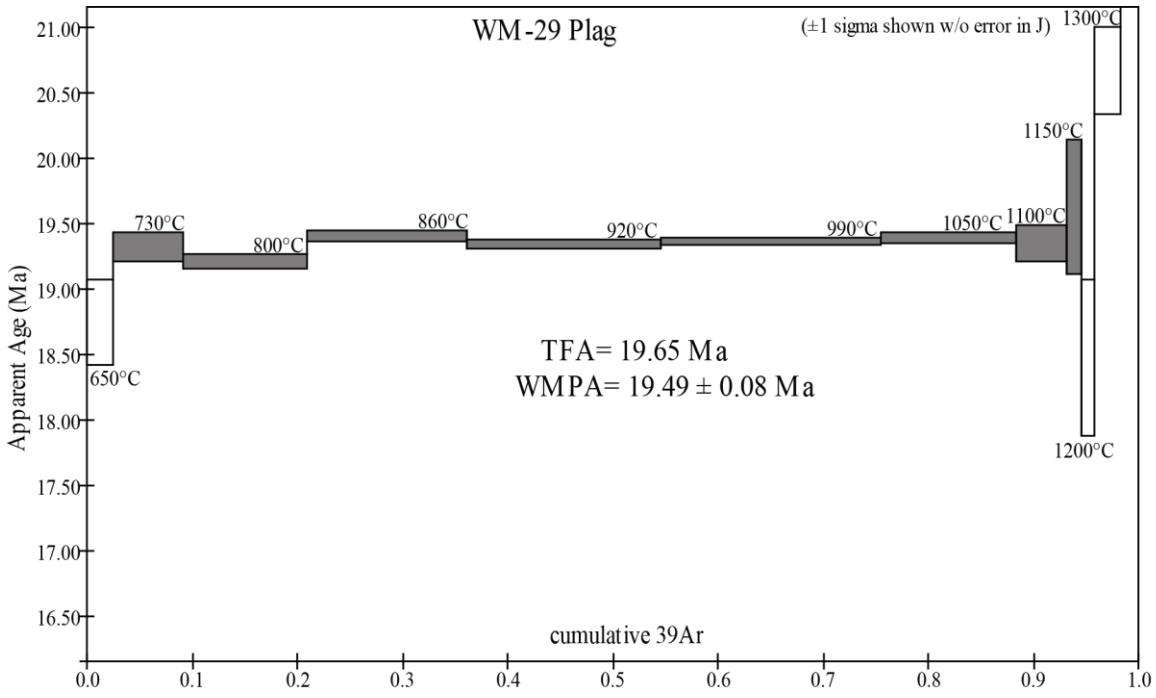

Sample: SB67-110; WM-32 gm; J=0.0029640

T	t	40(mol)	40/39	38/39	37/39	36/39	K/Ca	∑ 39Ar	40Ar*	Age (Ma)
670	14	1.1e-14	9.1238	0.0e+0	6.5045	0.0196	0.075	0.14238	0.366	17.7 ± 0.4
740	14	9.4e-15	6.5784	0.0e+0	5.3119	0.0105	0.092	0.31036	0.528	18.5 ± 0.4
810	14	7.8e-15	6.0879	0.0e+0	4.1732	0.0087	0.12	0.45997	0.580	18.8 ± 0.4
880	14	7.1e-15	5.9667	0.0e+0	5.0847	0.0083	0.096	0.59914	0.591	18.7 ± 0.4
960	14	8.1e-15	6.6253	0.0e+0	6.2092	0.0108	0.079	0.74368	0.519	18.3 ± 0.4
1040	14	1.0e-14	10.8076	0.0e+0	5.2060	0.0248	0.094	0.85657	0.321	18.4 ± 0.4
1120	14	8.3e-15	13.3990	0.0e+0	7.4674	0.0332	0.066	0.92931	0.268	19.1 ± 0.7
1200	14	6.5e-15	11.2255	0.0e+0	53.2712	0.0260	0.009	1.00000	0.317	18.9 ± 1.6

Total fusion age, TFA= 18.50 ± 0.19 Ma (including J)
Weighted mean plateau age, WMPA= 18.46 ± 0.16 Ma (including J)
Inverse isochron age =18.55 ± 0.33 Ma. (MSWD =1.04; 40Ar/36Ar=294.2 ± 3.9)
Steps used: 670, 740, 810, 880, 960, 1040, 1120, 1200, (1–8/8 or 100% ∑ 39Ar
t = dwell time in minutes.
40(mol) = moles corrected for blank and reactor-produced 40.
Ratios are corrected for blanks, decay, and interference.
∑39Ar is cumulative, 40Ar* = rad fraction.

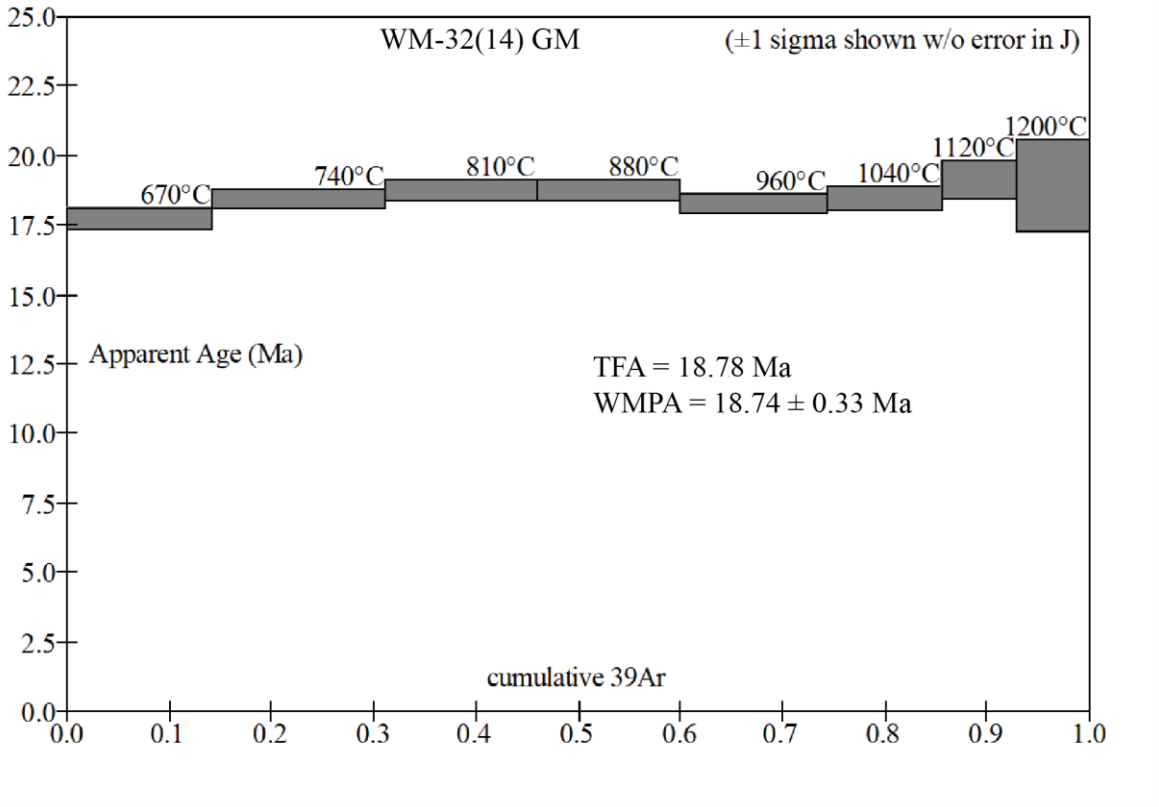

SB67-112 **Sample: WM-34 plag** **J=0.0029470**

T	t	40(mol)	40/39	38/39	37/39	36/39	K/Ca	∑ 39Ar	40Ar*	Age (Ma)
750	14	8.2e-15	4.4250	0.0e+0	8.0649	0.0026	0.061	0.08266	0.824	19.3 ± 0.3
840	14	1.5e-14	4.0240	0.0e+0	8.2546	0.0010	0.059	0.24665	0.924	19.7 ± 0.2
930	14	2.1e-14	3.9127	0.0e+0	8.3329	0.0008	0.059	0.48877	0.943	19.5 ± 0.2
1020	14	2.4e-14	4.0897	0.0e+0	8.1182	0.0013	0.060	0.74575	0.906	19.6 ± 0.2
1110	14	1.1e-14	4.6047	0.0e+0	7.7727	0.0030	0.063	0.85537	0.810	19.7 ± 0.2
1200	14	7.0e-15	5.2579	0.0e+0	7.9434	0.0050	0.062	0.91480	0.718	20.0 ± 0.3
1290	14	6.9e-15	5.6801	0.0e+0	6.8825	0.0056	0.071	0.96905	0.707	21.2 ± 0.4
1380	14	5.4e-15	7.7617	0.0e+0	6.9145	0.0096	0.071	1.00000	0.635	26.0 ± 0.5

Total fusion age, TFA= 19.88 ± 0.11 Ma (including J)
Weighted mean plateau age, WMPA= 19.61 ± 0.11 Ma (including J)
Inverse isochron age =19.45 ± 0.17 Ma. (MSWD =0.53; 40Ar/36Ar=311.2 ± 9.7)
Steps used: 750, 840, 930, 1020, 1110, 1200, (1–6/8 or 91% ∑ 39Ar
t = dwell time in minutes.
40(mol) = moles corrected for blank and reactor-produced 40.
Ratios are corrected for blanks, decay, and interference.
∑39Ar is cumulative, 40Ar* = rad fraction.

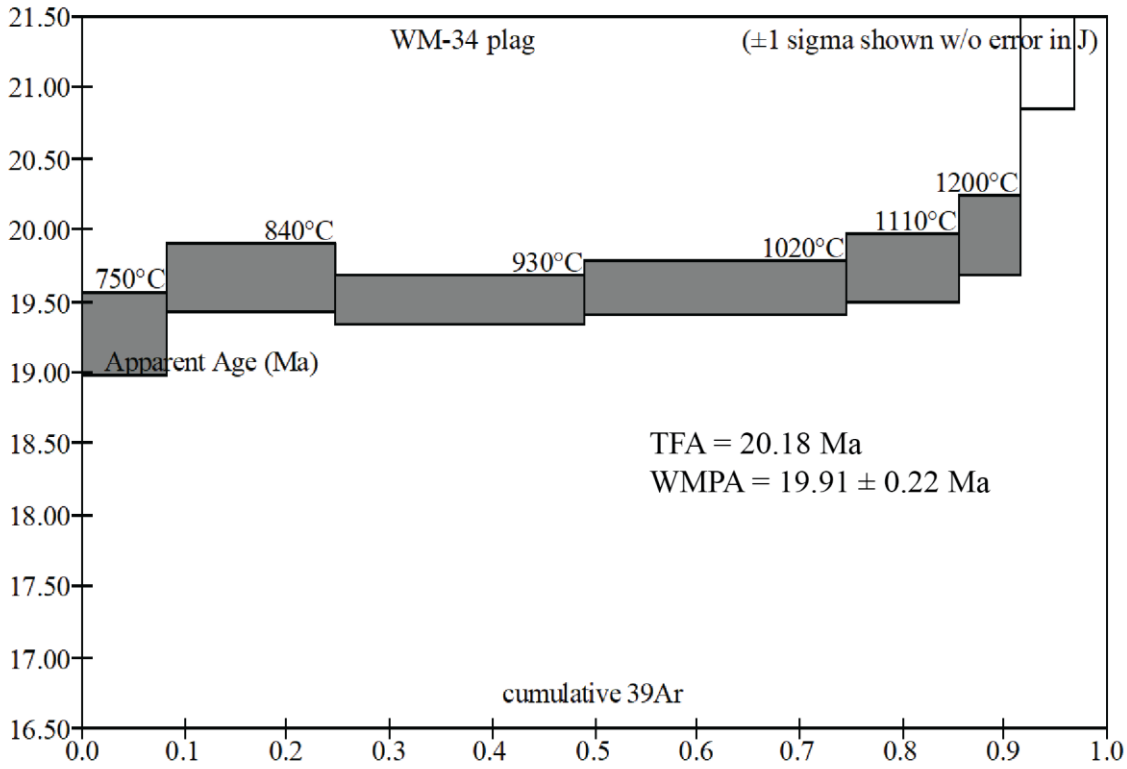

SB67-114 **Sample: WM-35 plag** **J=0.0029260**

T	t	40(mol)	40/39	38/39	37/39	36/39	K/Ca	∑ 39Ar	40Ar*	Age (Ma)
750	14	7.4e-13	387.6681	4.6e-3	7.2401	1.3183	0.068	0.11442	-0.005	-10.0 ± 0.9
750	14	3.8e-13	399.0011	1.5e-3	7.8895	1.3539	0.062	0.17217	-0.003	-5.7 ± 1.3
800	14	1.6e-13	155.2244	0.0e+0	7.8075	0.5182	0.063	0.23329	0.014	11.0 ± 1.5
920	14	3.7e-13	80.6620	0.0e+0	7.6409	0.2624	0.064	0.50684	0.039	16.3 ± 0.2
920	12	2.3e-13	107.9488	0.0e+0	7.5707	0.3535	0.065	0.63435	0.032	18.3 ± 0.8
960	14	2.7e-13	112.8432	0.0e+0	7.3817	0.3691	0.066	0.77973	0.033	19.8 ± 0.3
960	14	2.1e-13	154.3711	6.6e-4	7.2923	0.5098	0.067	0.85985	0.024	19.6 ± 1.3
1000	14	2.6e-13	209.5210	1.4e-3	7.1520	0.6928	0.069	0.93398	0.023	25.1 ± 1.6
1020	14	2.7e-13	379.5595	3.2e-3	7.1264	1.2612	0.069	0.97650	0.018	36.0 ± 3.4
1040	14	2.7e-13	684.2760	3.3e-3	7.3094	2.2898	0.067	1.00000	0.011	39.8 ± 8.3

Total fusion age, TFA= 14.82 ± 0.36 Ma (including J)
Weighted mean plateau age, WMPA= 17.35 ± 0.15 Ma (including J)
Inverse isochron age =10.20 ± 1.54 Ma. (MSWD =8.79; 40Ar/36Ar=300.1 ± 1.0)
Steps used: 920, 920, 960, 960, (4–7/10 or 63% ∑ 39Ar
t = dwell time in minutes.
40(mol) = moles corrected for blank and reactor-produced 40.
Ratios are corrected for blanks, decay, and interference.
∑39Ar is cumulative, 40Ar* = rad fraction.

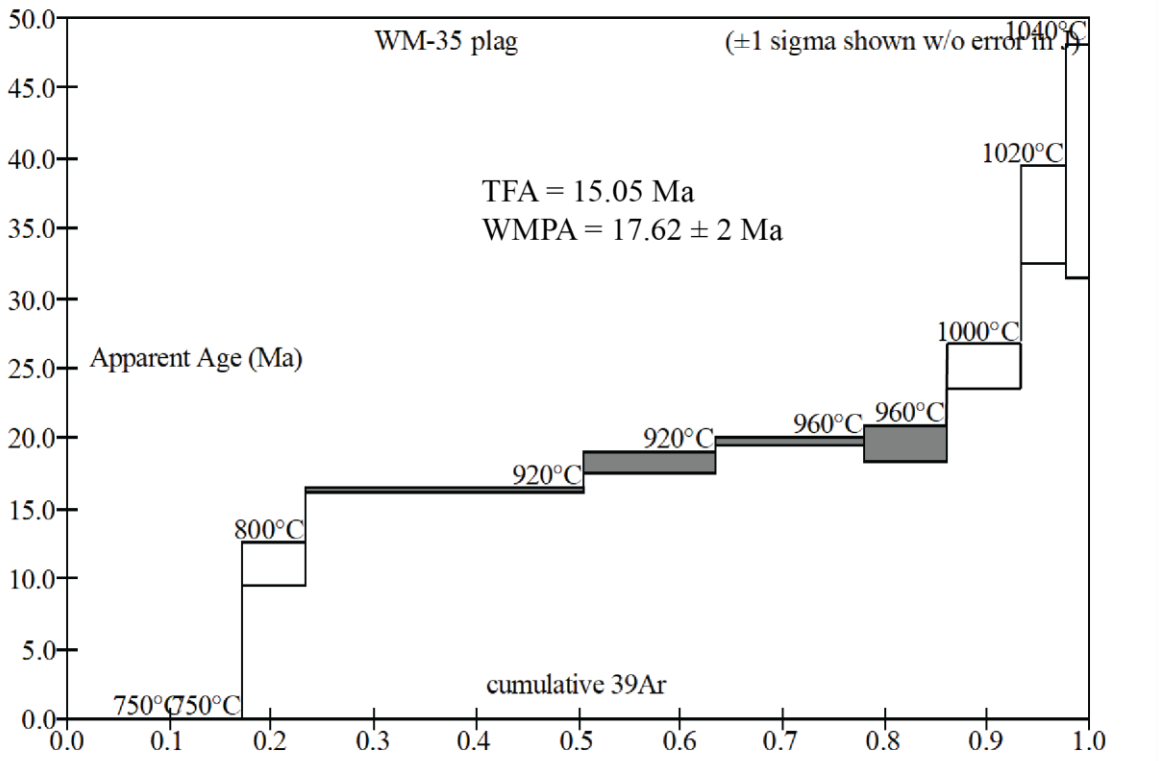

SB67-116 **Sample: WM-36 plag** **J=0.0029060**

T	t	40(mol)	40/39	38/39	37/39	36/39	K/Ca	∑ 39Ar	40Ar*	Age (Ma)
750	14	8.8e-13	580.5408	7.7e-3	8.8069	1.9743	0.056	0.14674	-0.005	-15.1 ± 1.4
750	14	4.6e-13	534.6042	0.0e+0	8.6930	1.8129	0.056	0.22868	-0.002	-5.8 ± 2.2
900	14	3.5e-13	148.7720	0.0e+0	8.3110	0.4945	0.059	0.45793	0.018	13.9 ± 0.4
900	10	1.3e-13	166.9903	0.0e+0	8.2985	0.5548	0.059	0.53487	0.018	15.9 ± 1.8
920	10	1.3e-13	165.3847	2.2e-3	8.2464	0.5485	0.059	0.61192	0.020	17.2 ± 1.6
940	10	1.4e-13	167.1821	5.9e-4	8.1744	0.5546	0.060	0.69042	0.020	17.3 ± 1.8
960	10	1.4e-13	177.9626	3.3e-4	8.2070	0.5907	0.060	0.76598	0.019	17.8 ± 2.0
970	10	1.3e-13	212.3970	1.3e-3	8.1545	0.7059	0.060	0.82301	0.018	19.8 ± 2.5
1000	10	1.6e-13	265.8042	1.3e-3	8.1175	0.8852	0.060	0.87985	0.016	22.1 ± 3.1
1030	10	2.4e-13	429.8838	2.8e-3	8.2363	1.4308	0.059	0.93285	0.016	36.7 ± 4.5
1060	10	3.1e-13	670.1771	8.4e-3	8.4652	2.2360	0.058	0.97713	0.014	48.7 ± 3.9
1060	10	1.9e-13	800.6318	1.6e-2	8.4521	2.6772	0.058	1.00000	0.012	49.1 ± 11.9

Total fusion age, TFA= 13.41 ± 0.61 Ma (including J)
Weighted mean plateau age, WMPA= 18.09 ± 0.90 Ma (including J)
Inverse isochron age =8.99 ± 3.76 Ma. (MSWD =0.01; 40Ar/36Ar=298.4 ± 0.1)
Steps used: 920, 940, 960, 970, 1000, (5–9/12 or 34% ∑ 39Ar
t = dwell time in minutes.
40(mol) = moles corrected for blank and reactor-produced 40.
Ratios are corrected for blanks, decay, and interference.
∑39Ar is cumulative, 40Ar* = rad fraction.

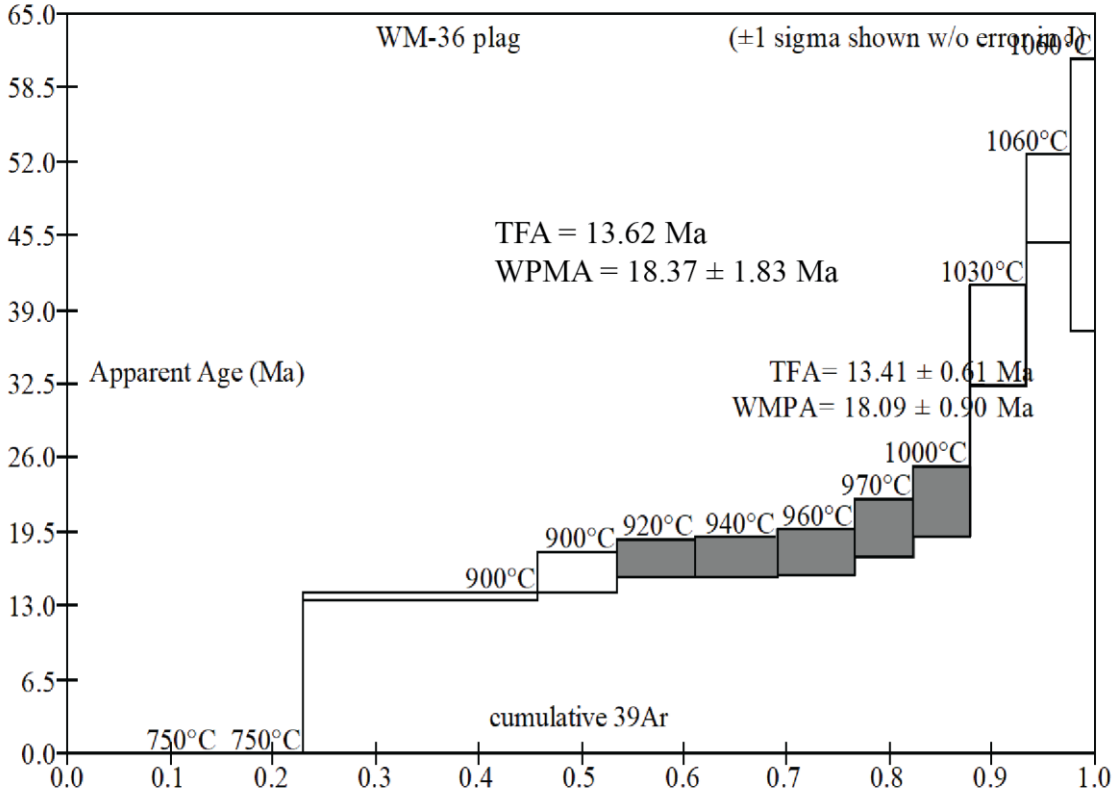

SB67-122 **Sample: WM-38 plag** **J=0.0032230**

T	t	40(mol)	40/39	38/39	37/39	36/39	K/Ca	∑ 39Ar	40Ar*	Age (Ma)
800	14	8.6e-15	4.1085	0.0e+0	7.7882	0.0026	0.063	0.16327	0.811	19.3 ± 0.4
890	14	1.1e-14	3.7810	0.0e+0	8.3068	0.0013	0.059	0.39264	0.900	19.7 ± 0.3
980	14	1.4e-14	3.7884	0.0e+0	8.3449	0.0013	0.059	0.67868	0.898	19.7 ± 0.3
1070	14	9.0e-15	4.2250	0.0e+0	8.1133	0.0026	0.060	0.84479	0.817	19.9 ± 0.4
1190	14	5.8e-15	5.7751	0.0e+0	7.6605	0.0077	0.064	0.92281	0.607	20.3 ± 0.6
1350	14	9.9e-15	10.0624	0.0e+0	7.0704	0.0208	0.069	1.00000	0.390	22.7 ± 0.6

Total fusion age, TFA= 19.93 ± 0.16 Ma (including J)
Weighted mean plateau age, WMPA= 19.68 ± 0.16 Ma (including J)
Inverse isochron age =19.49 ± 0.27 Ma. (MSWD =0.69; 40Ar/36Ar=310.6 ± 14.7)
Steps used: 800, 890, 980, 1070, 1190, (1–5/6 or 92% ∑ 39Ar
t = dwell time in minutes.
40(mol) = moles corrected for blank and reactor-produced 40.
Ratios are corrected for blanks, decay, and interference.
∑39Ar is cumulative, 40Ar* = rad fraction.

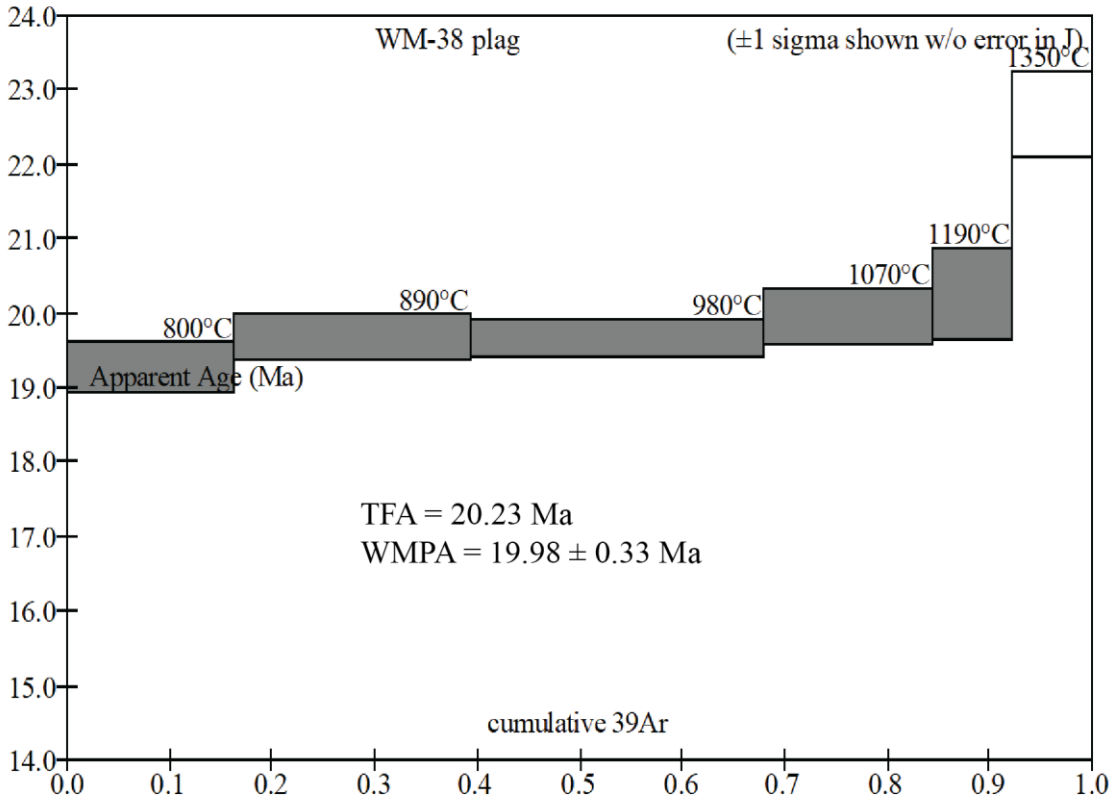

SB67-124 **Sample: WM-39 plag** **J=0.0032230**

T	t	40(mol)	40/39	38/39	37/39	36/39	K/Ca	∑ 39Ar	40Ar*	Age (Ma)
800	14	1.7e-14	5.1870	0.0e+0	9.6208	0.0059	0.051	0.14886	0.666	20.0 ± 0.3
880	14	2.0e-14	4.2621	0.0e+0	9.6737	0.0028	0.051	0.35484	0.806	19.9 ± 0.3
960	14	2.4e-14	4.0019	0.0e+0	9.4939	0.0020	0.052	0.61947	0.853	19.7 ± 0.2
1040	14	2.0e-14	4.1006	0.0e+0	9.0571	0.0022	0.054	0.83340	0.841	19.9 ± 0.2
1160	14	9.6e-15	5.0972	0.0e+0	8.4111	0.0046	0.058	0.91715	0.735	21.7 ± 0.3
1350	14	1.5e-14	8.1560	0.0e+0	8.3766	0.0146	0.058	1.00000	0.470	22.2 ± 0.4

Total fusion age, TFA= 20.21 ± 0.12 Ma (including J)
Weighted mean plateau age, WMPA= 19.86 ± 0.13 Ma (including J)
Inverse isochron age =19.74 ± 0.30 Ma. (MSWD =0.16; 40Ar/36Ar=302.9 ± 6.7)
Steps used: 800, 880, 960, 1040, (1–4/6 or 83% ∑ 39Ar
t = dwell time in minutes.
40(mol) = moles corrected for blank and reactor-produced 40.
Ratios are corrected for blanks, decay, and interference.
∑39Ar is cumulative, 40Ar* = rad fraction.

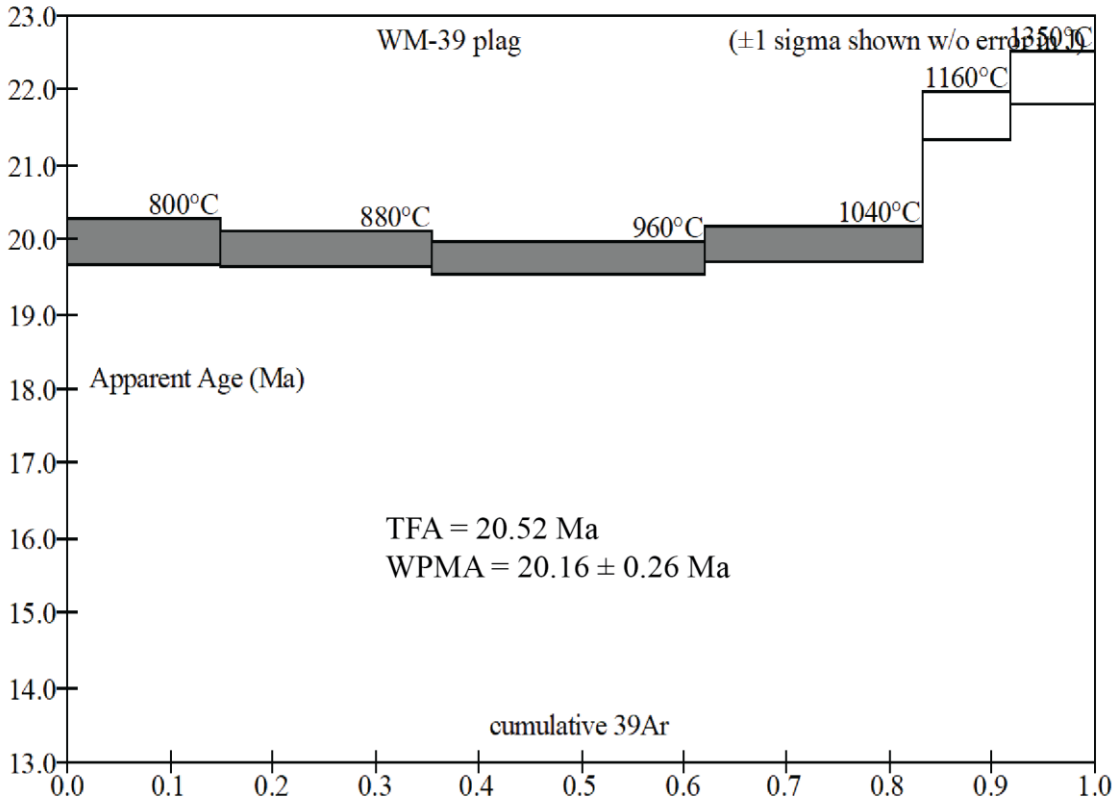

SB67-125 **Sample: WM-41 gm** **J=0.0032230**

T	t	40(mol)	40/39	38/39	37/39	36/39	K/Ca	∑ 39Ar	40Ar*	Age (Ma)
680	12	2.7e-14	6.3848	0.0e+0	1.1851	0.0106	0.41	0.07476	0.509	18.8 ± 0.1
750	12	3.6e-14	4.9074	0.0e+0	1.0167	0.0056	0.48	0.20112	0.663	18.8 ± 0.1
820	12	4.5e-14	5.0602	0.0e+0	0.7719	0.0062	0.63	0.35557	0.637	18.7 ± 0.1
900	12	5.8e-14	5.9272	0.0e+0	0.6133	0.0092	0.80	0.52480	0.539	18.5 ± 0.1
980	12	9.7e-14	9.7676	0.0e+0	0.4264	0.0226	1.1	0.69712	0.318	18.0 ± 0.1
1070	12	1.8e-13	12.6039	0.0e+0	0.4644	0.0319	1.1	0.93898	0.252	18.3 ± 0.1
1150	12	5.0e-14	14.2219	0.0e+0	3.1753	0.0374	0.15	1.00000	0.224	18.4 ± 0.2

Total fusion age, TFA= 18.45 ± 0.06 Ma (including J)
Weighted mean plateau age, WMPA= 18.30 ± 0.07 Ma (including J)
Inverse isochron age =18.99 ± 0.11 Ma. (MSWD =1.61; 40Ar/36Ar=287.4 ± 1.3)
Steps used: 900, 980, 1070, 1150, (4–7/7 or 64% ∑ 39Ar
t = dwell time in minutes.
40(mol) = moles corrected for blank and reactor-produced 40.
Ratios are corrected for blanks, decay, and interference.
∑39Ar is cumulative, 40Ar* = rad fraction.

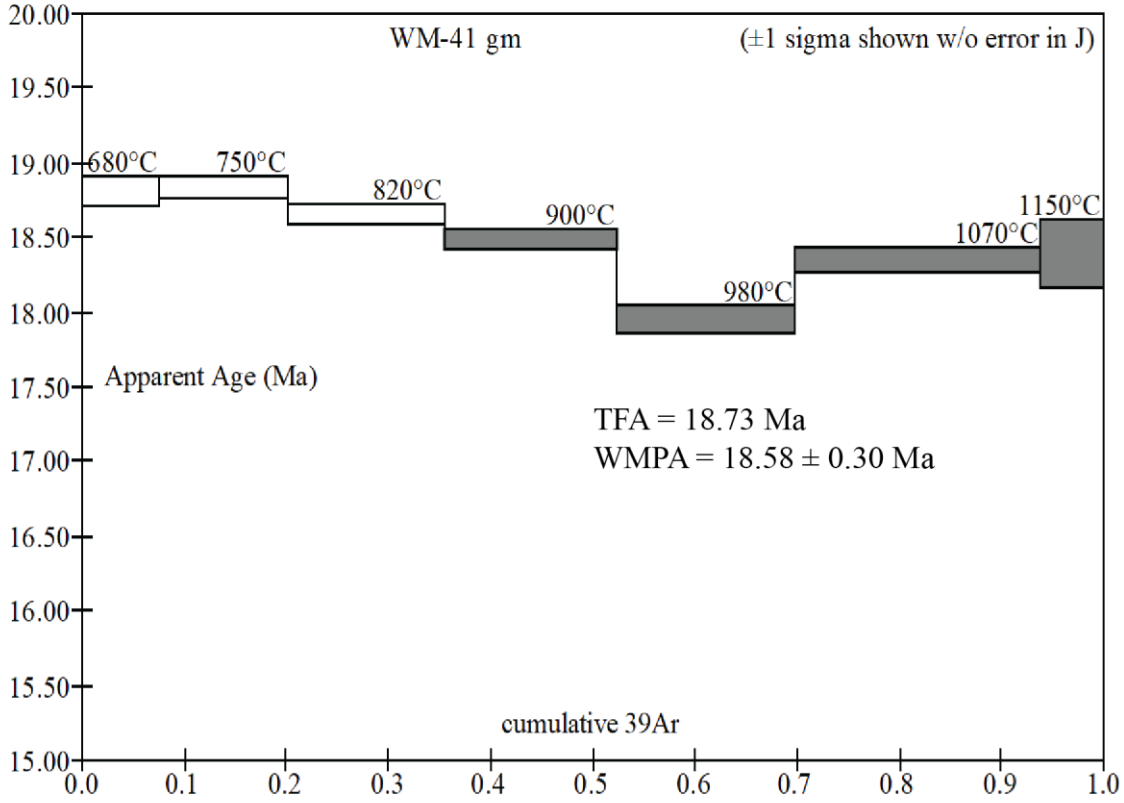

SB67-127 Sample: WM-43 plag J=0.0032230

T	t	40(mol)	40/39	38/39	37/39	36/39	K/Ca	∑ 39Ar	40Ar*	Age (Ma)
800	14	3.7e-14	11.4521	0.0e+0	10.5314	0.0279	0.047	0.17140	0.280	18.5 ± 0.3
880	14	3.9e-14	9.8906	0.0e+0	10.6657	0.0225	0.046	0.38340	0.326	18.7 ± 0.3
960	14	4.5e-14	9.8834	0.0e+0	10.3602	0.0225	0.047	0.62757	0.326	18.7 ± 0.3
1040	14	4.8e-14	13.2996	0.0e+0	9.8425	0.0342	0.050	0.81833	0.240	18.5 ± 0.3
1160	14	4.2e-14	26.1548	0.0e+0	9.7042	0.0784	0.050	0.90394	0.115	17.4 ± 0.5
1350	14	4.6e-14	25.3953	0.0e+0	9.7494	0.0723	0.050	1.00000	0.159	23.3 ± 0.5

Total fusion age, TFA= 18.94 ± 0.14 Ma (including J)
Weighted mean plateau age, WMPA= 18.60 ± 0.14 Ma (including J)
Inverse isochron age =19.02 ± 0.74 Ma. (MSWD =0.02; 40Ar/36Ar=292.7 ± 0.6)
Steps used: 800, 880, 960, 1040, (1–4/6 or 82% ∑ 39Ar
t = dwell time in minutes.
40(mol) = moles corrected for blank and reactor-produced 40.
Ratios are corrected for blanks, decay, and interference.
∑39Ar is cumulative, 40Ar* = rad fraction.

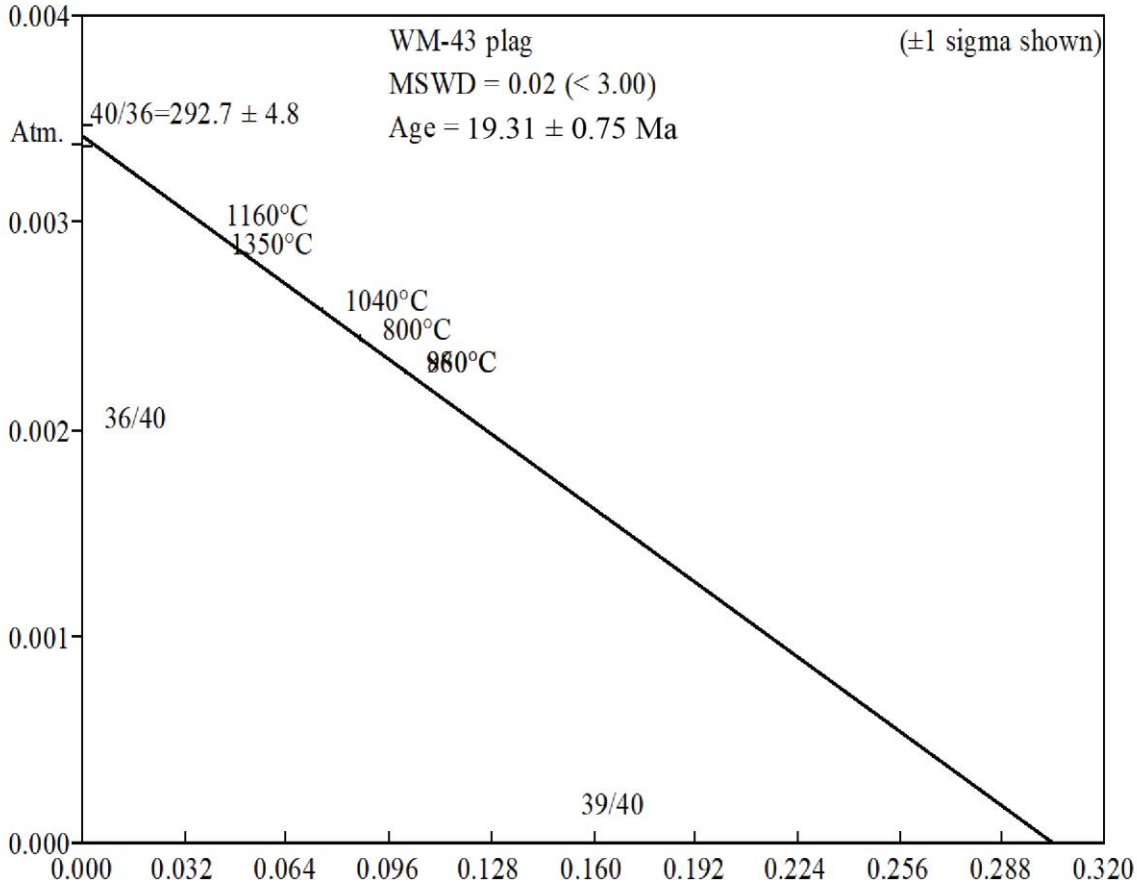

SB67-130 **Sample: WM-44 plag** **J=0.0032090**

T	t	40(mol)	40/39	38/39	37/39	36/39	K/Ca	∑ 39Ar	40Ar*	Age (Ma)
800	14	2.2e-14	4.3812	0.0e+0	6.5045	0.0037	0.075	0.20293	0.752	19.0 ± 0.2
880	15	2.3e-14	3.9735	0.0e+0	6.7768	0.0021	0.072	0.43063	0.846	19.3 ± 0.2
950	15	2.0e-14	4.0401	0.0e+0	6.5831	0.0023	0.074	0.62415	0.832	19.4 ± 0.2
1030	15	1.9e-14	5.0797	0.0e+0	6.2413	0.0060	0.079	0.77361	0.653	19.1 ± 0.2
1160	14	1.9e-14	7.6334	0.0e+0	5.9784	0.0146	0.082	0.87259	0.435	19.1 ± 0.3
1350	14	2.3e-14	7.3278	0.0e+0	6.0537	0.0120	0.081	1.00000	0.515	21.7 ± 0.2

Total fusion age, TFA= 19.51 ± 0.10 Ma (including J)
Weighted mean plateau age, WMPA= 19.18 ± 0.10 Ma (including J)
Inverse isochron age =19.25 ± 0.15 Ma. (MSWD =1.00; 40Ar/36Ar=292.9 ± 3.9)
Steps used: 800, 880, 950, 1030, 1160, (1–5/6 or 87% ∑ 39Ar
t = dwell time in minutes.
40(mol) = moles corrected for blank and reactor-produced 40.
Ratios are corrected for blanks, decay, and interference.
∑39Ar is cumulative, 40Ar* = rad fraction.

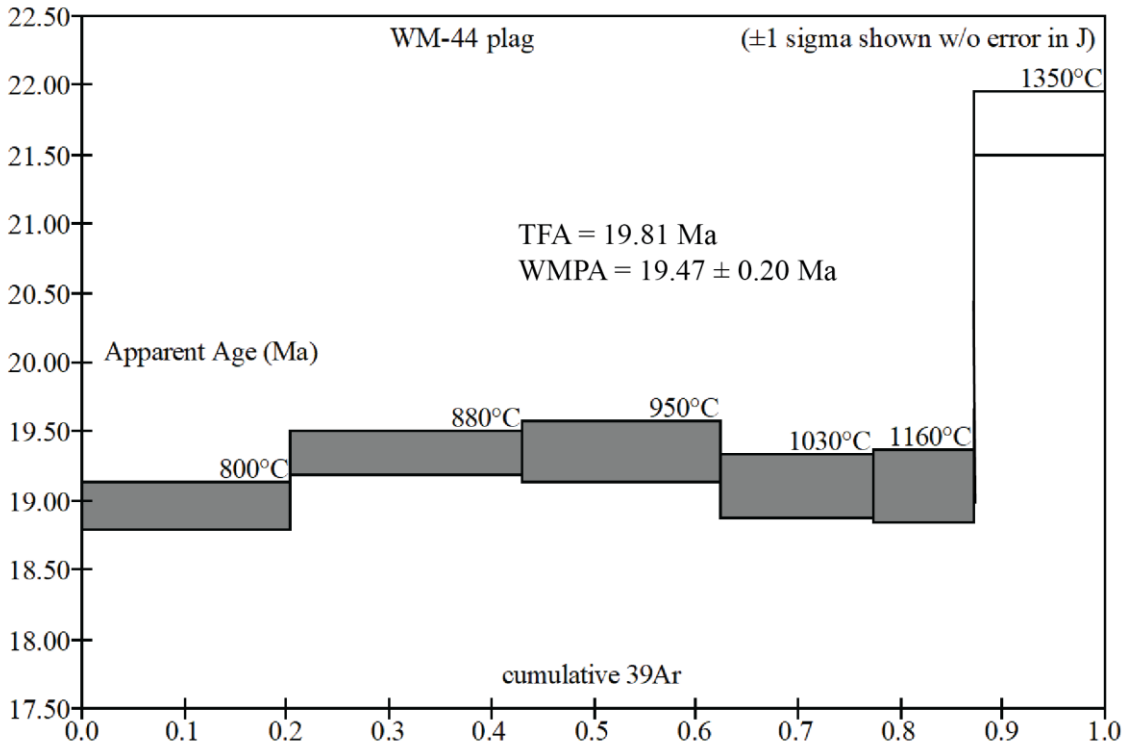

SB67-153 Sample: WM-48 gm J=0.0030420

T	t	40(mol)	40/39	38/39	37/39	36/39	K/Ca	∑ 39Ar	40Ar*	Age (Ma)
660	12	3.0e-14	6.5511	0.0e+0	0.7990	0.0127	0.61	0.12408	0.426	15.3 ± 0.1
720	12	3.4e-14	6.3749	0.0e+0	0.7744	0.0117	0.63	0.27116	0.459	16.0 ± 0.1
790	12	4.1e-14	6.1574	0.0e+0	0.6319	0.0108	0.78	0.45630	0.484	16.3 ± 0.1
860	12	4.0e-14	6.4708	0.0e+0	0.5902	0.0118	0.83	0.62527	0.463	16.3 ± 0.1
930	12	3.3e-14	7.1325	0.0e+0	0.7910	0.0140	0.62	0.75410	0.419	16.3 ± 0.1
1000	12	3.3e-14	8.0160	0.0e+0	1.0602	0.0172	0.46	0.86682	0.364	16.0 ± 0.1
1080	12	4.1e-14	11.0052	0.0e+0	1.6218	0.0272	0.30	0.96836	0.271	16.3 ± 0.2
1160	12	1.7e-14	14.5425	0.0e+0	8.4612	0.0392	0.058	1.00000	0.204	16.2 ± 0.5

Total fusion age, TFA= 16.09 ± 0.06 Ma (including J)
Weighted mean plateau age, WMPA= 16.27 ± 0.07 Ma (including J)
Inverse isochron age =16.38 ± 0.18 Ma. (MSWD =1.53; 40Ar/36Ar=294.1 ± 2.1)
Steps used: 790, 860, 930, 1000, 1080, 1160, (3–8/8 or 73% ∑ 39Ar
t = dwell time in minutes.
40(mol) = moles corrected for blank and reactor-produced 40.
Ratios are corrected for blanks, decay, and interference.
∑39Ar is cumulative, 40Ar* = rad fraction.

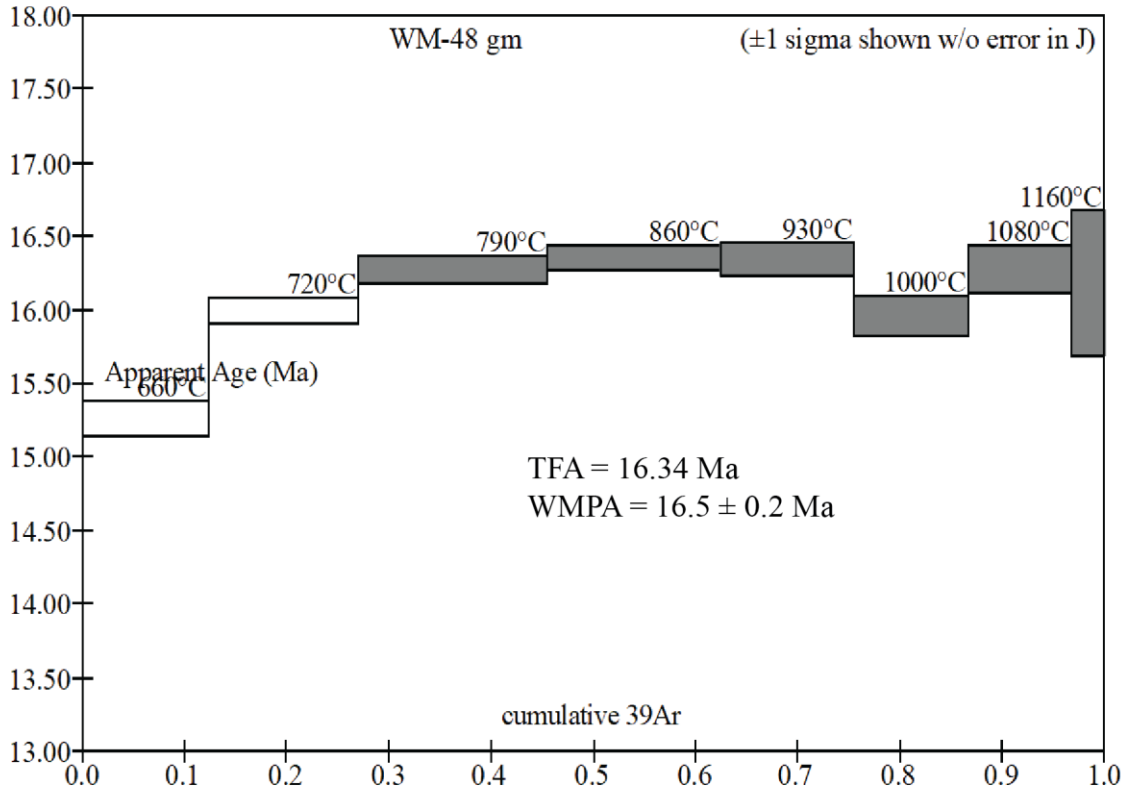

SB67-154 Sample: WM-49 gm J=0.0030310

T	t	40(mol)	40/39	38/39	37/39	36/39	K/Ca	∑ 39Ar	40Ar*	Age (Ma)
660	12	4.3e-14	6.1958	0.0e+0	0.8740	0.0103	0.56	0.17072	0.511	17.2 ± 0.1
720	12	3.6e-14	4.4646	0.0e+0	0.8867	0.0043	0.55	0.36997	0.717	17.4 ± 0.1
790	12	2.6e-14	4.3246	0.0e+0	0.8377	0.0039	0.58	0.51508	0.731	17.2 ± 0.1
860	12	2.1e-14	5.1460	0.0e+0	0.8305	0.0068	0.59	0.61445	0.611	17.1 ± 0.1
930	12	2.8e-14	6.8521	0.0e+0	0.6262	0.0128	0.78	0.71626	0.449	16.7 ± 0.1
1000	12	4.9e-14	10.5349	0.0e+0	0.6432	0.0255	0.76	0.82985	0.284	16.3 ± 0.1
1080	12	9.2e-14	15.6277	0.0e+0	0.9789	0.0427	0.50	0.97522	0.192	16.3 ± 0.1
1160	12	1.8e-14	17.6310	1.5e-3	4.6633	0.0502	0.11	1.00000	0.159	15.3 ± 0.5

Total fusion age, TFA= 16.91 ± 0.06 Ma (including J)
Weighted mean plateau age, WMPA= 16.29 ± 0.10 Ma (including J)
Inverse isochron age =17.42 ± 0.12 Ma. (MSWD =4.21; 40Ar/36Ar=289.6 ± 1.2)
Steps used: 1000, 1080, (6–7/8 or 26% ∑ 39Ar
t = dwell time in minutes.
40(mol) = moles corrected for blank and reactor-produced 40.
Ratios are corrected for blanks, decay, and interference.
∑39Ar is cumulative, 40Ar* = rad fraction.

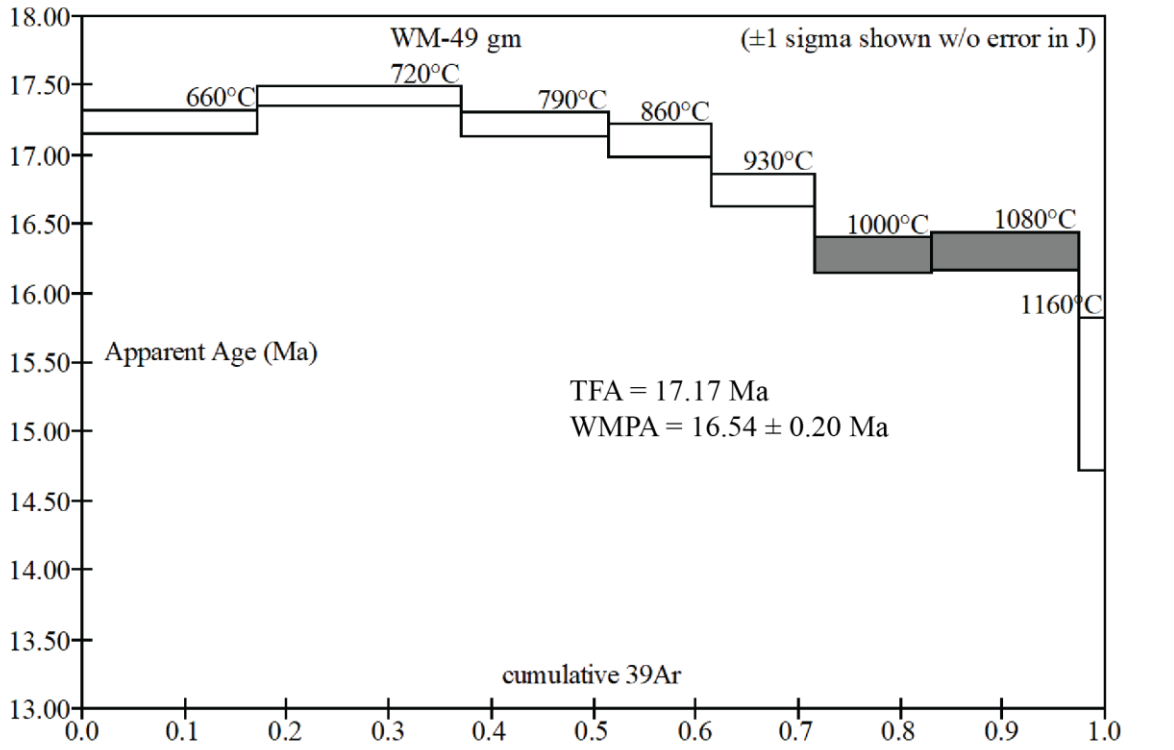

SB67-155 Sample: WM-51 gm J=0.0030210

T	t	40(mol)	40/39	38/39	37/39	36/39	K/Ca	∑ 39Ar	40Ar*	Age (Ma)
660	12	3.5e-14	6.3787	0.0e+0	0.7334	0.0106	0.67	0.09818	0.509	17.6 ± 0.1
720	12	3.8e-14	4.9218	0.0e+0	0.7427	0.0057	0.66	0.23821	0.661	17.6 ± 0.1
790	12	4.7e-14	5.0811	0.0e+0	0.6150	0.0065	0.80	0.40433	0.624	17.2 ± 0.1
860	12	5.8e-14	7.0404	0.0e+0	0.5291	0.0134	0.93	0.55304	0.436	16.6 ± 0.1
930	12	8.4e-14	11.3193	0.0e+0	0.4786	0.0283	1.0	0.68689	0.262	16.1 ± 0.1
1000	12	1.3e-13	15.7267	0.0e+0	0.4441	0.0432	1.1	0.83187	0.188	16.0 ± 0.1
1080	12	1.4e-13	17.4008	0.0e+0	0.7738	0.0481	0.63	0.97920	0.183	17.2 ± 0.1
1160	12	2.0e-14	17.5645	1.1e-4	4.3746	0.0485	0.11	1.00000	0.184	17.5 ± 0.5

Total fusion age, TFA= 16.91 ± 0.06 Ma (including J)
Weighted mean plateau age, WMPA= 16.05 ± 0.09 Ma (including J)
Inverse isochron age =17.39 ± 0.30 Ma. (MSWD =32.01; 40Ar/36Ar=291.3 ± 2.4)
Steps used: 930, 1000, (5–6/8 or 28% ∑ 39Ar
t = dwell time in minutes.
40(mol) = moles corrected for blank and reactor-produced 40.
Ratios are corrected for blanks, decay, and interference.
∑39Ar is cumulative, 40Ar* = rad fraction.

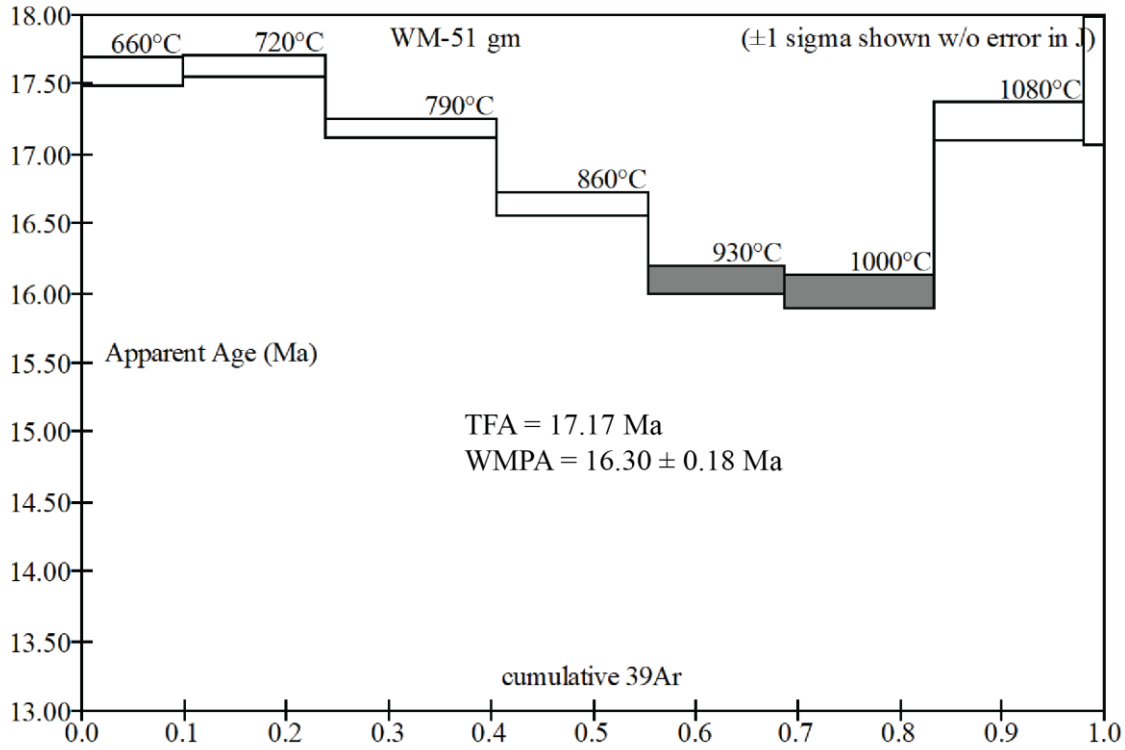

Appendix III

Volcanic volume calculation corrections and uncertainties:

The greatest source of uncertainty for the realistic volume estimates of older steeply dipping units is cover by younger units and alluvium. For these calculations, we assume that all exposed dipping units continue along strike beneath younger units to the map edges. Though individual units may pinch out along strike, we believe that this is a relatively safe assumption when considering the rocks of an entire volcanic stage based on what we see in exposed areas.

We do not attempt to correct for volume lost to erosion for steeply dipping Stage 1 and 2 lavas because our down-dip length estimates are independent of modern surface erosion (Fig. 14; down-dip surface lengths projected into both the air and subsurface to the map edges) there is little stratigraphic evidence of erosion between eruptions. For Stage 3 and 4 lavas which either dip moderately or are flat lying, the volume lost due to erosion is a large uncertainty. Along strike and down-dip surface lengths for these units (length and width of surface exposure for flat lying units) are greater than the actual exposure lengths to account for some erosion and partial burial by alluvium (Fig. 14). The amount of lateral erosion and partial burial is unconstrained, and are likely underrepresented in our estimates, and vertical erosion (effecting unit thickness) is not corrected for at all. Thus, the realistic volume estimates for Stage 3 and 4 units should be considered minimum values.

Making corrections for volume lost to erosion and cover by younger units both serve to increase volume estimates. The interpreted dip of faults in the field area also effects volume estimates. Because almost all of the major faults in the study area are either poorly

exposed or buried by quaternary units, fault dips are largely interpretive and are estimated based on relative ages and unit dips. Because down-dip surface lengths are measured directly using Cross-Sections A and B, our interpreted fault dips effect these measurements. Steeper faults will increase volume estimates while shallower faults will decrease volume estimates within the field area (Fig. 14).

Lastly, we did not calculate volumes for any exposures of Tts or calculate a dense rock equivalent for this texturally variable unit. Because Tts makes up a small percentage of the total erupted volume and occurs primarily in discontinuous lenses of variable thickness (many of which are not map scale), we excluded the unit for the sake of simplicity and believe it is a negligible contribution to the total locally erupted volume. We also did not include the Peach Springs Tuff in our total volume estimate as it is sourced from outside the map area.

Appendix IV

Sample locations, rock type, and context for samples unique to Chapters 2 and 3

Sample	Context	Latitude	Longitude
AB-01	Pre-extensional	34°24'42.28"N	114°13'6.21"W
AB-02	Pre-extensional	34°26'29.89"N	114°16'3.06"W
MHV-01	Syn-extensional	34°28'57.43"N	114°15'12.92"W
MHV-04	Syn-extensional	34°29'6.47"N	114°15'8.18"W
MHV-10	Pre-extensional	34°29'32.32"N	114°14'30.24"W
MHV-12	Syn-extensional	34°40'54.39"N	114°18'42.09"W
MHV-14	Pre-extensional	34°41'14.85"N	114°18'58.63"W
MK13-2.1	Pre-extensional	34°25'24.11"N	114°13'55.29"W
MK13-2.3	Pre-extensional	34°24'40.69"N	114°14'7.58"W
MK13-2.4	Pre-extensional	34°24'41.35"N	114°13'2.07"W
MK13-4.1	Post-extensional	34°27'48.83"N	114°10'46.56"W
MK13-4.2	Pre-extensional	34°28'11.62"N	114°10'51.36"W
MK13-4.3	Pre-extensional	34°28'11.15"N	114°10'53.30"W
MK13-4.4	Pre-extensional	34°28'32.62"N	114°11'1.35"W
MK13-4.6	Pre-extensional	34°28'21.54"N	114°10'4.23"W
MK13-7.1	Pre-extensional	34°22'52.84"N	114°46'27.47"W
MK13-7.4	Pre-extensional	34°20'45.19"N	114°46'21.00"W
SWM-03	Post-extensional	34°12'57.71"N	114°18'2.20"W
TTM-01	Pre-extensional	34° 7'25.32"N	114°48'40.19"W
TTM-02	Pre-extensional	34° 7'27.12"N	114°48'40.99"W
WM-4	Pre-extensional	34°16'49.37"N	114°34'6.24"W
WM-6	Pre-extensional	34°16'20.06"N	114°34'12.76"W
WM-7	Pre-extensional	34°15'25.92"N	114°33'43.13"W
WM-8	Pre-extensional	34°15'29.41"N	114°33'45.11"W
WM-9	Pre-extensional	34°15'25.96"N	114°33'54.68"W
WM-13	Pre-extensional	34°15'11.09"N	114°34'2.24"W
WM-14	Syn-extensional	34°14'59.21"N	114°34'19.78"W
WM-15	Syn-extensional	34°15'1.26"N	114°34'20.42"W

Appendix V

Tabulated $^{40}Ar/^{39}Ar$ data and age spectra discussed in Chapter 2. All mineral separations and analyses were performed at UCSB's $^{40}Ar/^{39}Ar$ geochronology laboratory.

Sample: SB65-121; MK13-7.1 Plag; J=0.0028909

T	t	40(mol)	40/39	38/39	37/39	36/39	K/Ca	∑ 39Ar	40Ar*	Age (Ma)
700	14	1.4e-14	6.0661	0.0e+0	10.1837	0.0076	0.048	0.03751	0.631	19.9 ± 0.2
750	14	1.7e-14	4.7947	0.0e+0	10.3588	0.0031	0.047	0.09277	0.809	20.1 ± 0.1
790	14	1.9e-14	4.4092	0.0e+0	10.2959	0.0019	0.048	0.16104	0.875	20.0 ± 0.1
830	14	2.2e-14	4.2254	0.0e+0	10.1823	0.0012	0.048	0.24460	0.917	20.1 ± 0.1
870	14	2.6e-14	4.1193	0.0e+0	10.1021	0.0009	0.049	0.34559	0.936	20.0 ± 0.1
910	14	2.8e-14	4.0617	0.0e+0	10.0719	0.0008	0.049	0.45725	0.945	19.9 ± 0.1
950	14	3.0e-14	4.0378	0.0e+0	9.9347	0.0006	0.049	0.57445	0.959	20.1 ± 0.1
990	14	2.8e-14	4.0235	0.0e+0	9.7755	0.0006	0.050	0.68709	0.956	20.0 ± 0.1
1030	14	2.4e-14	4.0570	0.0e+0	9.6366	0.0006	0.051	0.78231	0.960	20.2 ± 0.1
1090	14	2.1e-14	4.1525	0.0e+0	9.4356	0.0009	0.052	0.86176	0.937	20.2 ± 0.1
1150	14	1.1e-14	4.4984	0.0e+0	9.2008	0.0019	0.053	0.90251	0.876	20.4 ± 0.1
1230	14	9.5e-15	5.0391	0.0e+0	9.0285	0.0031	0.054	0.93253	0.815	21.3 ± 0.2
1350	14	3.2e-14	7.4768	0.0e+0	7.9732	0.0105	0.061	1.00000	0.585	22.7 ± 0.1

Total fusion age, TFA= 20.27 ± 0.04 Ma (including J)
Weighted mean plateau age, WMPA= 20.01 ± 0.04 Ma (including J)
Inverse isochron age =20.02 ± 0.05 Ma. (MSWD =0.82; 40Ar/36Ar=293.7 ± 3.9)
Steps used: 700, 750, 790, 830, 870, 910, 950, 990, (1–8/13 or 69% ∑ 39Ar
t = dwell time in minutes.
40(mol) = moles corrected for blank and reactor-produced 40.
Ratios are corrected for blanks, decay, and interference.
∑39Ar is cumulative, 40Ar* = rad fraction.

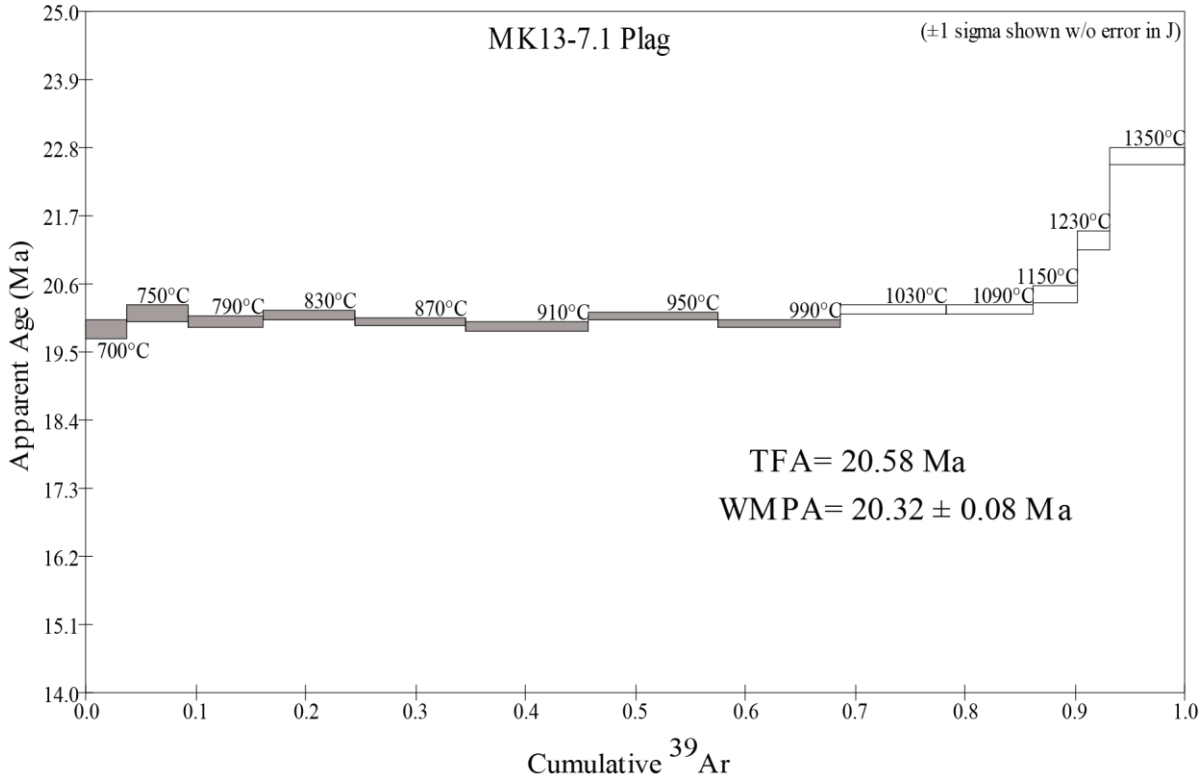

Sample: SB65-114; MK13-7.4 Plag; J=0.0029690

T	t	40(mol)	40/39	38/39	37/39	36/39	K/Ca	∑ 39Ar	40Ar*	Age (Ma)
700	14	1.4e-14	4.1215	2.4e-3	7.7615	0.0014	0.063	0.04682	0.903	19.8 ± 0.1
750	14	2.0e-14	3.9563	0.0e+0	7.7499	0.0008	0.063	0.11463	0.944	19.9 ± 0.1
790	14	2.3e-14	3.9012	0.0e+0	7.7651	0.0006	0.063	0.19726	0.958	19.9 ± 0.1
830	14	2.8e-14	3.8750	0.0e+0	7.7646	0.0004	0.063	0.29531	0.968	20.0 ± 0.1
870	14	3.2e-14	3.8591	0.0e+0	7.7677	0.0004	0.063	0.40957	0.968	19.9 ± 0.1
910	14	3.4e-14	3.8545	0.0e+0	7.7633	0.0003	0.063	0.53199	0.974	20.0 ± 0.1
950	14	3.5e-14	3.8614	0.0e+0	7.7032	0.0004	0.064	0.65554	0.972	20.0 ± 0.1
990	14	3.1e-14	3.8912	0.0e+0	7.6077	0.0004	0.064	0.76466	0.973	20.2 ± 0.1
1030	14	2.3e-14	3.9654	0.0e+0	7.4931	0.0006	0.065	0.84541	0.956	20.2 ± 0.1
1080	14	1.7e-14	4.5030	0.0e+0	7.2842	0.0012	0.067	0.89756	0.919	22.0 ± 0.1
1130	14	9.9e-15	5.6748	0.0e+0	7.0494	0.0041	0.070	0.92156	0.787	23.8 ± 0.2
1190	14	1.9e-14	12.9100	0.0e+0	5.9853	0.0060	0.082	0.94141	0.862	58.6 ± 0.2
1250	14	1.6e-14	11.4207	0.0e+0	6.0177	0.0085	0.081	0.96071	0.780	47.1 ± 0.2
1350	14	2.4e-14	8.3678	0.0e+0	6.3225	0.0096	0.078	1.00000	0.661	29.4 ± 0.2

Total fusion age, TFA= 21.86 ± 0.04 Ma (including J)
Weighted mean plateau age, WMPA= 19.95 ± 0.04 Ma (including J)
Inverse isochron age =20.03 ± 0.06 Ma. (MSWD =0.33; 40Ar/36Ar=263.4 ± 10.0)
Steps used: 700, 750, 790, 830, 870, 910, 950, (1–7/14 or 66% ∑ 39Ar
t = dwell time in minutes.
40(mol) = moles corrected for blank and reactor-produced 40.
Ratios are corrected for blanks, decay, and interference.
∑39Ar is cumulative, 40Ar* = rad fraction.

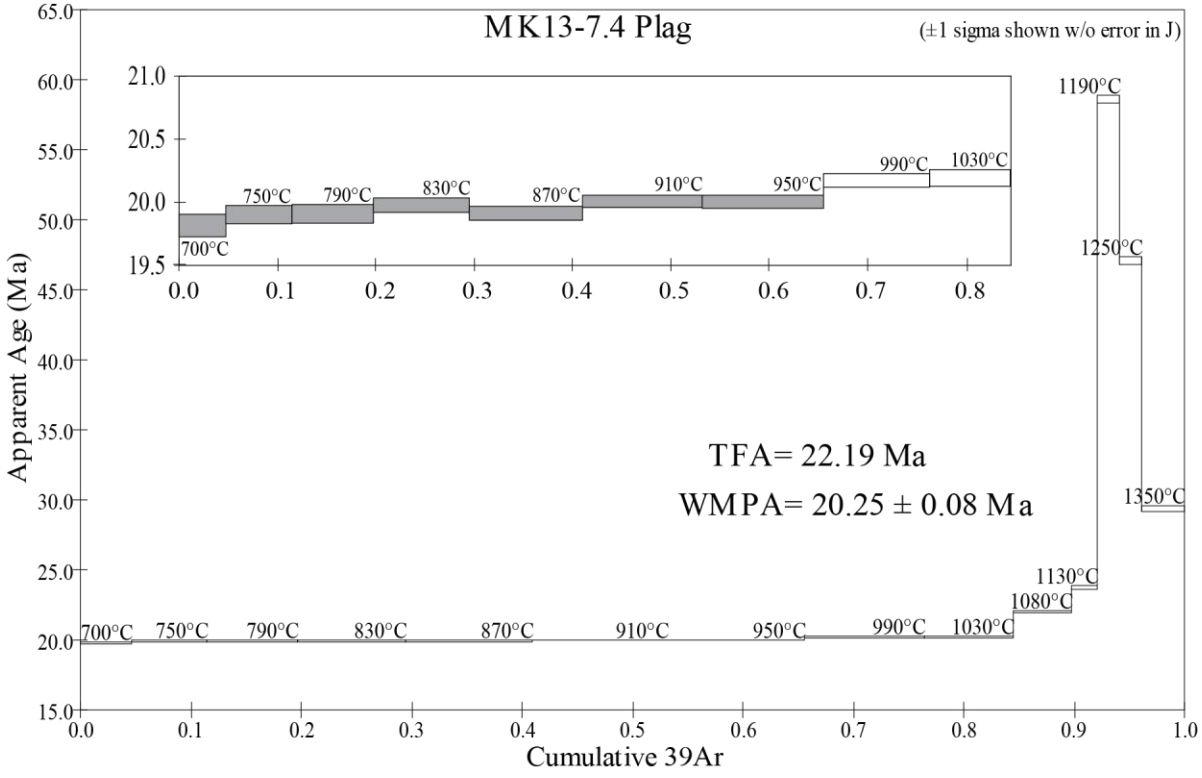

Sample: SB66-116; AB-01 GM; J=0.0041919

T	t	40(mol)	40/39	38/39	37/39	36/39	K/Ca	∑ 39Ar	40Ar*	Age (Ma)
500	14	6.2e-15	8.9490	0.0e+0	0.9545	0.0210	0.51	0.00554	0.306	20.6 ± 0.8
550	14	7.1e-15	4.8058	0.0e+0	0.7240	0.0065	0.68	0.01746	0.601	21.7 ± 0.3
600	14	1.1e-14	3.5476	0.0e+0	0.6913	0.0025	0.71	0.04137	0.792	21.1 ± 0.2
650	14	1.7e-14	3.1331	0.0e+0	0.6986	0.0012	0.70	0.08450	0.885	20.9 ± 0.1
700	14	2.2e-14	2.9481	0.0e+0	0.6806	0.0006	0.72	0.14398	0.942	20.9 ± 0.1
750	14	2.3e-14	2.9088	0.0e+0	0.5361	0.0004	0.91	0.20817	0.956	20.9 ± 0.1
800	14	2.4e-14	2.9447	0.0e+0	0.3984	0.0006	1.2	0.27285	0.944	20.9 ± 0.1
860	14	2.9e-14	2.9454	0.0e+0	0.3576	0.0006	1.4	0.35123	0.940	20.8 ± 0.1
920	14	3.0e-14	2.9043	0.0e+0	0.3769	0.0006	1.3	0.43310	0.940	20.5 ± 0.1
980	14	5.1e-14	2.8697	0.0e+0	0.4099	0.0006	1.2	0.57540	0.941	20.3 ± 0.1
1040	14	8.4e-14	2.8870	0.0e+0	0.4592	0.0006	1.1	0.80803	0.934	20.3 ± 0.0
1100	14	3.3e-14	3.0908	0.0e+0	1.2530	0.0013	0.39	0.89446	0.877	20.4 ± 0.1
1160	14	3.5e-14	3.3331	0.0e+0	5.1137	0.0020	0.096	0.98002	0.826	20.7 ± 0.1
1250	14	1.1e-14	4.2817	0.0e+0	4.7921	0.0038	0.10	1.00000	0.739	23.8 ± 0.2

Total fusion age, TFA= 20.64 ± 0.04 Ma (including J)
Weighted mean plateau age, WMPA= 20.30 ± 0.04 Ma (including J)
Inverse isochron age =20.21 ± 0.10 Ma. (MSWD =0.43; 40Ar/36Ar=312.7 ± 10.5)
Steps used: 980, 1040, 1100, (10–12/14 or 46% ∑ 39Ar
t = dwell time in minutes.
40(mol) = moles corrected for blank and reactor-produced 40.
Ratios are corrected for blanks, decay, and interference.
∑39Ar is cumulative, 40Ar* = rad fraction.

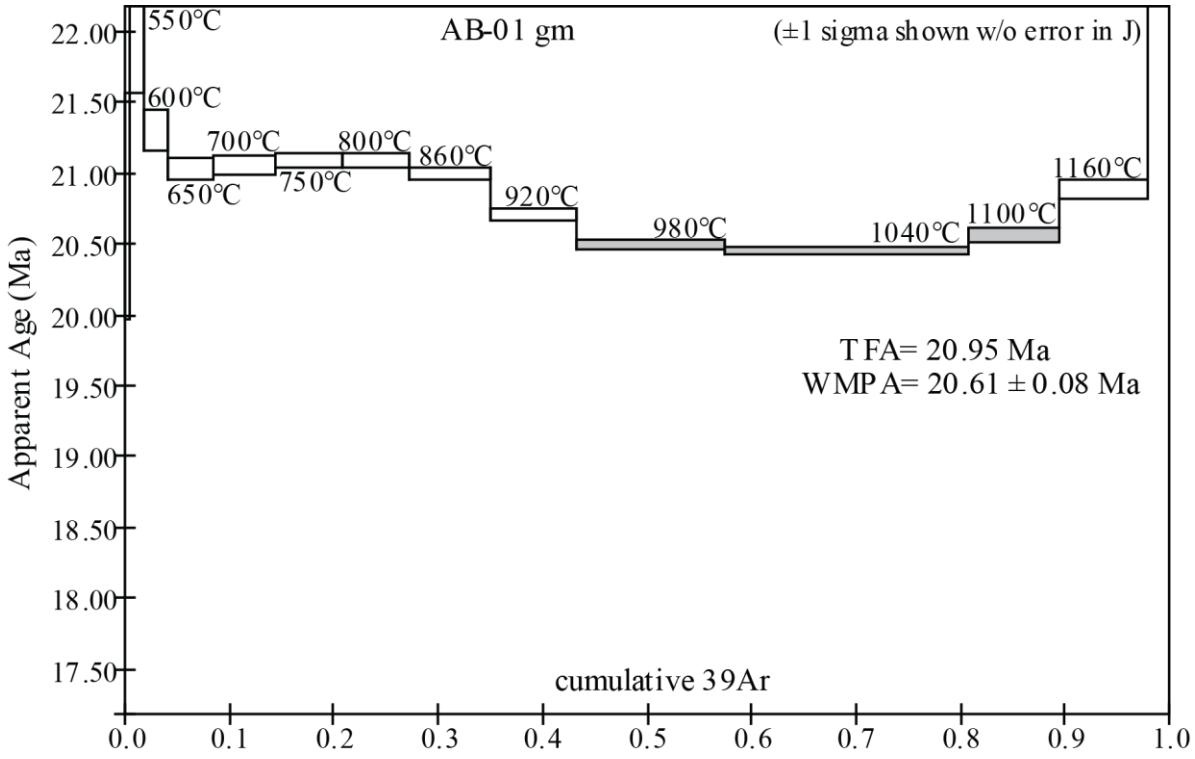

Sample: SB66-124; MK-2.4 GM; J=0.0041503

T	t	40(mol)	40/39	38/39	37/39	36/39	K/Ca	∑ 39Ar	40Ar*	Age (Ma)
550	14	1.6e-14	6.1920	0.0e+0	0.4557	0.0124	1.1	0.01920	0.406	18.7 ± 0.3
600	14	1.4e-14	3.7555	0.0e+0	0.4700	0.0038	1.0	0.04663	0.699	19.5 ± 0.2
650	14	1.6e-14	3.2624	0.0e+0	0.5148	0.0022	0.95	0.08327	0.803	19.5 ± 0.1
700	14	1.9e-14	3.0670	0.0e+0	0.6411	0.0013	0.76	0.12980	0.877	20.0 ± 0.1
750	14	2.1e-14	3.0031	0.0e+0	0.5470	0.0009	0.90	0.18239	0.911	20.4 ± 0.1
800	14	2.3e-14	2.9975	0.0e+0	0.3677	0.0010	1.3	0.23992	0.903	20.2 ± 0.1
850	14	3.1e-14	3.0115	0.0e+0	0.2991	0.0009	1.6	0.31791	0.909	20.4 ± 0.1
900	14	3.1e-14	2.9567	0.0e+0	0.2707	0.0008	1.8	0.39612	0.919	20.2 ± 0.1
950	14	3.5e-14	2.9921	0.0e+0	0.2669	0.0012	1.8	0.48515	0.883	19.7 ± 0.1
1000	14	5.5e-14	3.0052	0.0e+0	0.3273	0.0014	1.5	0.62302	0.863	19.3 ± 0.1
1050	14	9.0e-14	3.0812	0.0e+0	0.3432	0.0016	1.4	0.84386	0.850	19.5 ± 0.0
1110	14	4.5e-14	3.2943	0.0e+0	0.9687	0.0025	0.51	0.94705	0.778	19.1 ± 0.1
1200	14	3.2e-14	4.5983	0.0e+0	5.3201	0.0069	0.092	1.00000	0.556	19.0 ± 0.1

Total fusion age, TFA= 19.64 ± 0.04 Ma (including J)
Weighted mean plateau age, WMPA= 19.48 ± 0.04 Ma (including J)
Inverse isochron age =19.90 ± 1.12 Ma. (MSWD =17.98; 40Ar/36Ar=255.8 ± 104.6)
Steps used: 950, 1000, 1050, (9–11/13 or 45% ∑ 39Ar
t = dwell time in minutes.
40(mol) = moles corrected for blank and reactor-produced 40.
Ratios are corrected for blanks, decay, and interference.
∑39Ar is cumulative, 40Ar* = rad fraction.

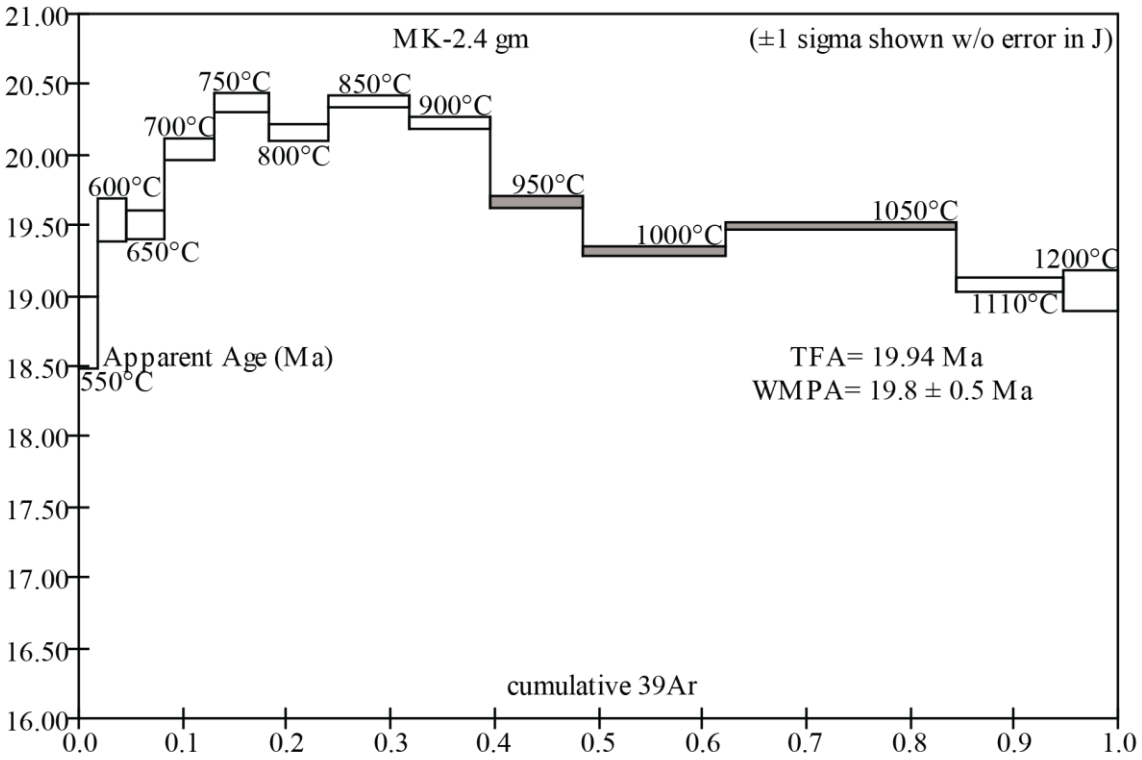

Sample: SB66-127; MK-4.4 GM; J=0.0041390

T	t	40(mol)	40/39	38/39	37/39	36/39	K/Ca	∑ 39Ar	40Ar*	Age (Ma)
550	14	4.0e-14	7.8304	0.0e+0	0.4272	0.0179	1.1	0.06411	0.325	18.9 ± 0.2
600	14	3.7e-14	4.8339	0.0e+0	0.6091	0.0077	0.80	0.16041	0.530	19.0 ± 0.1
650	14	3.0e-14	3.9390	0.0e+0	0.5512	0.0046	0.89	0.25754	0.653	19.1 ± 0.1
700	14	2.0e-14	3.9025	0.0e+0	0.2460	0.0047	2.0	0.32323	0.641	18.6 ± 0.1
750	14	1.4e-14	4.3081	0.0e+0	0.2156	0.0061	2.3	0.36474	0.584	18.7 ± 0.2
800	14	1.4e-14	5.3696	0.0e+0	0.2886	0.0097	1.7	0.39710	0.466	18.6 ± 0.3
850	14	1.4e-14	6.1288	0.0e+0	0.2840	0.0123	1.7	0.42610	0.408	18.6 ± 0.3
900	14	2.2e-14	6.6521	0.0e+0	0.2915	0.0139	1.7	0.46808	0.381	18.8 ± 0.2
950	14	4.1e-14	6.8141	0.0e+0	0.3800	0.0146	1.3	0.54430	0.367	18.6 ± 0.2
1000	14	8.5e-14	7.3294	0.0e+0	0.4600	0.0167	1.1	0.69152	0.326	17.7 ± 0.1
1050	14	1.3e-13	10.2752	0.0e+0	0.7719	0.0270	0.63	0.84560	0.224	17.1 ± 0.2
1110	14	1.5e-13	21.7573	5.3e-4	1.9749	0.0649	0.25	0.93585	0.119	19.2 ± 0.4
1200	14	1.6e-13	32.2074	3.4e-4	6.5728	0.0999	0.075	1.00000	0.084	20.0 ± 0.5

Total fusion age, TFA= 18.51 ± 0.07 Ma (including J)
Weighted mean plateau age, WMPA= 18.64 ± 0.08 Ma (including J)
Inverse isochron age =18.57 ± 0.18 Ma. (MSWD =0.22; 40Ar/36Ar=296.5 ± 1.1)
Steps used: 700, 750, 800, 850, 900, 950, (4–9/13 or 29% ∑ 39Ar
t = dwell time in minutes.
40(mol) = moles corrected for blank and reactor-produced 40.
Ratios are corrected for blanks, decay, and interference.
∑39Ar is cumulative, 40Ar* = rad fraction.

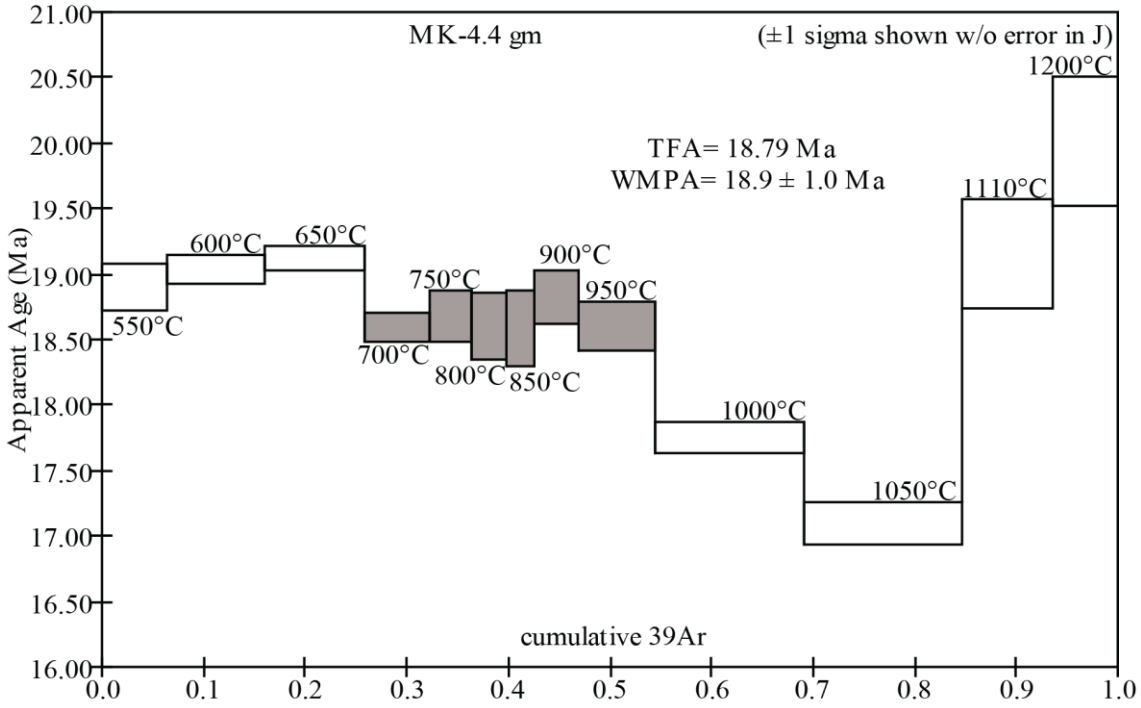

Sample: SB66-129; MK-4.6 GM; J=0.0041286

T	t	40(mol)	40/39	38/39	37/39	36/39	K/Ca	∑ 39Ar	40Ar*	Age (Ma)
550	14	1.4e-14	7.1482	0.0e+0	1.3106	0.0139	0.37	0.01923	0.426	22.5 ± 0.3
600	14	1.4e-14	4.7632	0.0e+0	1.4259	0.0060	0.34	0.04810	0.628	22.1 ± 0.2
650	14	2.0e-14	3.7383	0.0e+0	1.2261	0.0027	0.40	0.09851	0.789	21.8 ± 0.1
700	14	2.6e-14	3.1902	0.0e+0	1.2491	0.0010	0.39	0.17614	0.905	21.4 ± 0.1
750	14	2.9e-14	3.0509	0.0e+0	0.9444	0.0007	0.52	0.26608	0.935	21.1 ± 0.1
800	14	3.6e-14	3.1429	0.0e+0	0.6691	0.0010	0.73	0.37609	0.906	21.1 ± 0.1
850	14	3.5e-14	3.0233	0.0e+0	0.5463	0.0006	0.90	0.48693	0.938	21.0 ± 0.1
900	14	3.0e-14	2.9912	0.0e+0	0.4271	0.0006	1.1	0.58379	0.945	20.9 ± 0.1
950	14	2.9e-14	3.0493	0.0e+0	0.4818	0.0008	1.0	0.67654	0.918	20.7 ± 0.1
1000	14	3.3e-14	3.0430	0.0e+0	0.6620	0.0009	0.74	0.78217	0.915	20.6 ± 0.1
1050	14	4.1e-14	3.0308	0.0e+0	0.6241	0.0008	0.79	0.91161	0.921	20.7 ± 0.1
1110	14	2.4e-14	3.1155	8.6e-5	1.8314	0.0011	0.27	0.98661	0.896	20.7 ± 0.1
1200	14	6.4e-15	4.6859	0.0e+0	16.5279	0.0060	0.030	1.00000	0.619	21.5 ± 0.4

Total fusion age, TFA= 21.02 ± 0.05 Ma (including J)
Weighted mean plateau age, WMPA= 20.68 ± 0.05 Ma (including J)
Inverse isochron age =20.68 ± 0.29 Ma. (MSWD =0.80; 40Ar/36Ar=295.5 ± 40.3)
Steps used: 950, 1000, 1050, 1110, (9–12/13 or 40% ∑ 39Ar
t = dwell time in minutes.
40(mol) = moles corrected for blank and reactor-produced 40.
Ratios are corrected for blanks, decay, and interference.
∑39Ar is cumulative, 40Ar* = rad fraction.

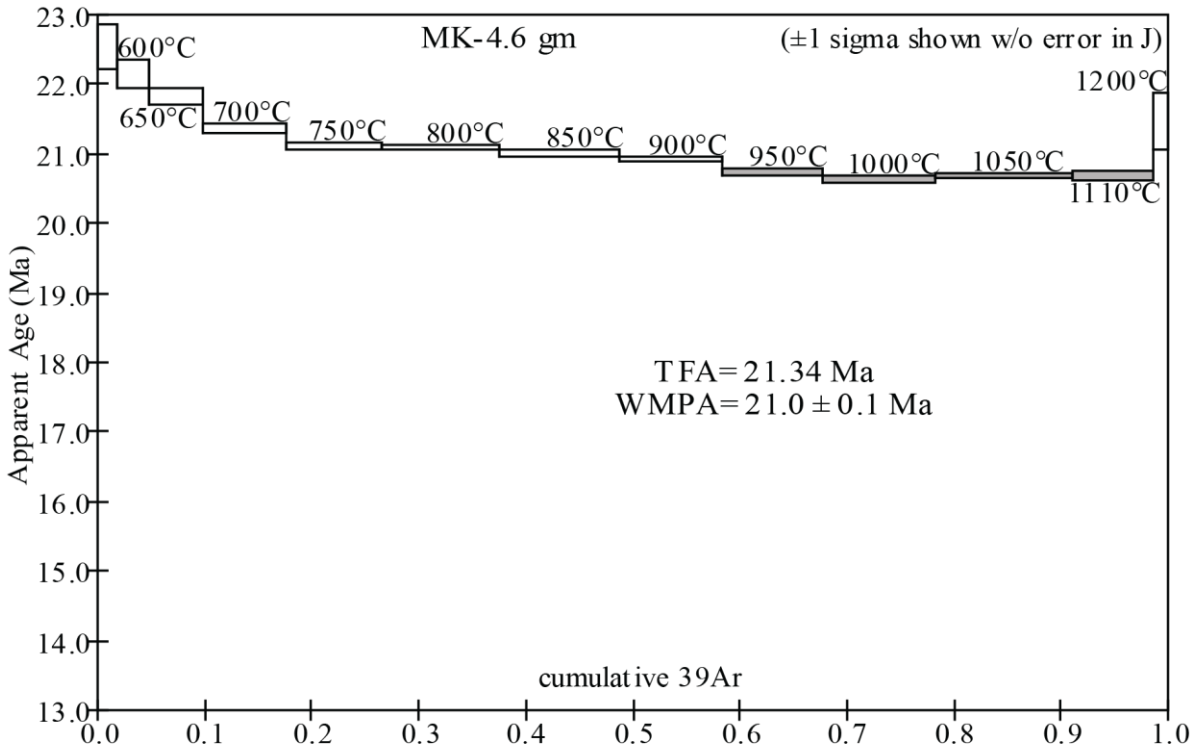

Sample: SB69-95 TTM-01 gm J=0.0041909 FINAL J (28.1 FCT)

T	t	40(mol)	40/39	38/39	37/39	36/39	K/Ca	∑ 39Ar	40Ar*	Age (Ma)
550	14	4.0e-15	6.2925	0.0e+0	1.7779	0.0112	0.28	0.01130	0.476	22.5 ± 0.6
600	14	7.5e-15	4.3086	0.0e+0	1.7660	0.0046	0.28	0.04218	0.683	22.1 ± 0.2
650	14	1.3e-14	3.4385	0.0e+0	1.4922	0.0018	0.33	0.11149	0.844	21.8 ± 0.1
700	14	1.8e-14	3.2094	0.0e+0	1.2762	0.0012	0.38	0.21072	0.890	21.5 ± 0.1
750	14	1.5e-14	3.1873	0.0e+0	1.0464	0.0012	0.47	0.29548	0.886	21.2 ± 0.1
800	14	1.5e-14	3.2159	0.0e+0	1.0154	0.0013	0.48	0.38036	0.879	21.2 ± 0.1
860	14	1.7e-14	3.1744	0.0e+0	1.1128	0.0011	0.44	0.47749	0.893	21.3 ± 0.1
920	14	1.3e-14	3.1994	0.0e+0	1.0264	0.0013	0.48	0.55037	0.881	21.2 ± 0.1
980	14	2.0e-14	3.1518	0.0e+0	0.9730	0.0012	0.50	0.66189	0.890	21.1 ± 0.1
1040	14	2.4e-14	3.3119	0.0e+0	1.1897	0.0017	0.41	0.79151	0.848	21.1 ± 0.1
1100	14	1.5e-14	3.6814	0.0e+0	2.6260	0.0030	0.19	0.86216	0.761	21.0 ± 0.1
1170	14	2.4e-14	4.7171	0.0e+0	15.2531	0.0064	0.032	0.95366	0.598	21.2 ± 0.2
1240	14	1.2e-14	4.5595	0.0e+0	12.3132	0.0058	0.040	1.00000	0.625	21.4 ± 0.2

Total fusion age, TFA= 21.30 ± 0.05 Ma (including J)
Weighted mean plateau age, WMPA= 21.17 ± 0.05 Ma (including J)
Inverse isochron age =21.20 ± 0.08 Ma. (MSWD =0.81; 40Ar/36Ar=293.2 ± 4.0)
Steps used: 750, 800, 860, 920, 980, 1040, 1100, 1170, (5–12/13 or 74% ∑ 39Ar
t = dwell time in minutes.
40(mol) = moles corrected for blank and reactor-produced 40.
Ratios are corrected for blanks, decay, and interference.
∑39Ar is cumulative, 40Ar* = rad fraction.

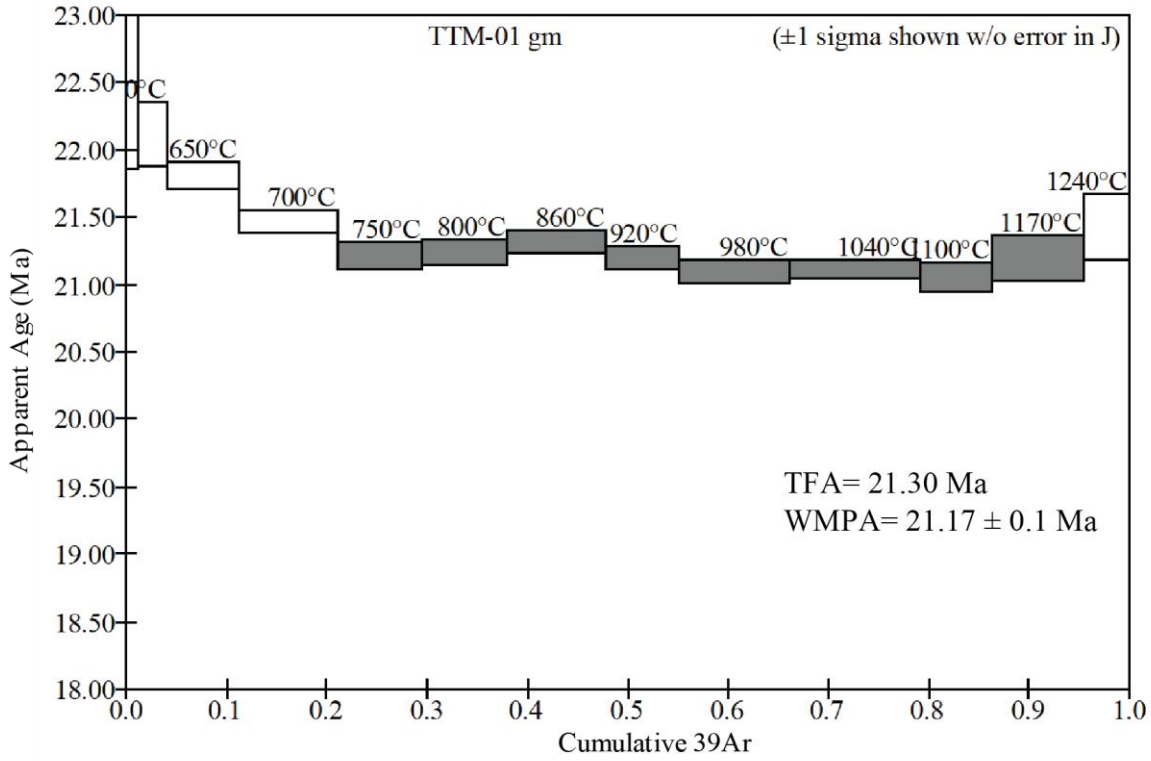

Sample: SB69-98 TTM-02 gm J=0.0041818 FINAL J (28.1 FCT)

T	t	40(mol)	40/39	38/39	37/39	36/39	K/Ca	∑ 39Ar	40Ar*	Age (Ma)
600	14	1.7e-14	4.6050	0.0e+0	1.0845	0.0058	0.45	0.02688	0.626	21.6 ± 0.1
650	14	2.4e-14	3.4539	0.0e+0	0.9401	0.0018	0.52	0.07808	0.842	21.8 ± 0.1
700	14	4.0e-14	3.1307	0.0e+0	0.7495	0.0008	0.65	0.16950	0.921	21.6 ± 0.1
750	14	4.5e-14	3.0221	0.0e+0	0.6180	0.0006	0.79	0.27834	0.945	21.4 ± 0.1
800	14	4.5e-14	2.9640	0.0e+0	0.5400	0.0005	0.91	0.38747	0.955	21.2 ± 0.1
860	14	6.2e-14	2.9033	0.0e+0	0.4976	0.0003	0.98	0.54091	0.973	21.2 ± 0.1
920	14	5.5e-14	2.8966	0.0e+0	0.4612	0.0003	1.1	0.67814	0.972	21.1 ± 0.0
980	14	5.1e-14	2.9444	0.0e+0	0.4895	0.0005	1.0	0.80310	0.947	20.9 ± 0.1
1040	14	4.1e-14	3.1773	0.0e+0	0.6626	0.0013	0.74	0.89588	0.876	20.9 ± 0.1
1100	14	2.3e-14	3.6595	9.9e-4	1.7117	0.0032	0.29	0.94098	0.744	20.4 ± 0.1
1170	14	1.8e-14	4.6075	1.7e-3	7.5293	0.0064	0.065	0.96859	0.592	20.4 ± 0.2
1240	14	2.1e-14	4.7916	1.1e-3	8.9313	0.0070	0.055	1.00000	0.571	20.5 ± 0.2

Total fusion age, TFA= 21.15 ± 0.04 Ma (including J)
Weighted mean plateau age, WMPA= 21.07 ± 0.04 Ma (including J)
Inverse isochron age =21.20 ± 0.11 Ma. (MSWD =5.73; 40Ar/36Ar=261.1 ± 19.7)
Steps used: 800, 860, 920, 980, 1040, (5–9/12 or 62% ∑ 39Ar
t = dwell time in minutes.
40(mol) = moles corrected for blank and reactor-produced 40.
Ratios are corrected for blanks, decay, and interference.
∑39Ar is cumulative, 40Ar* = rad fraction.

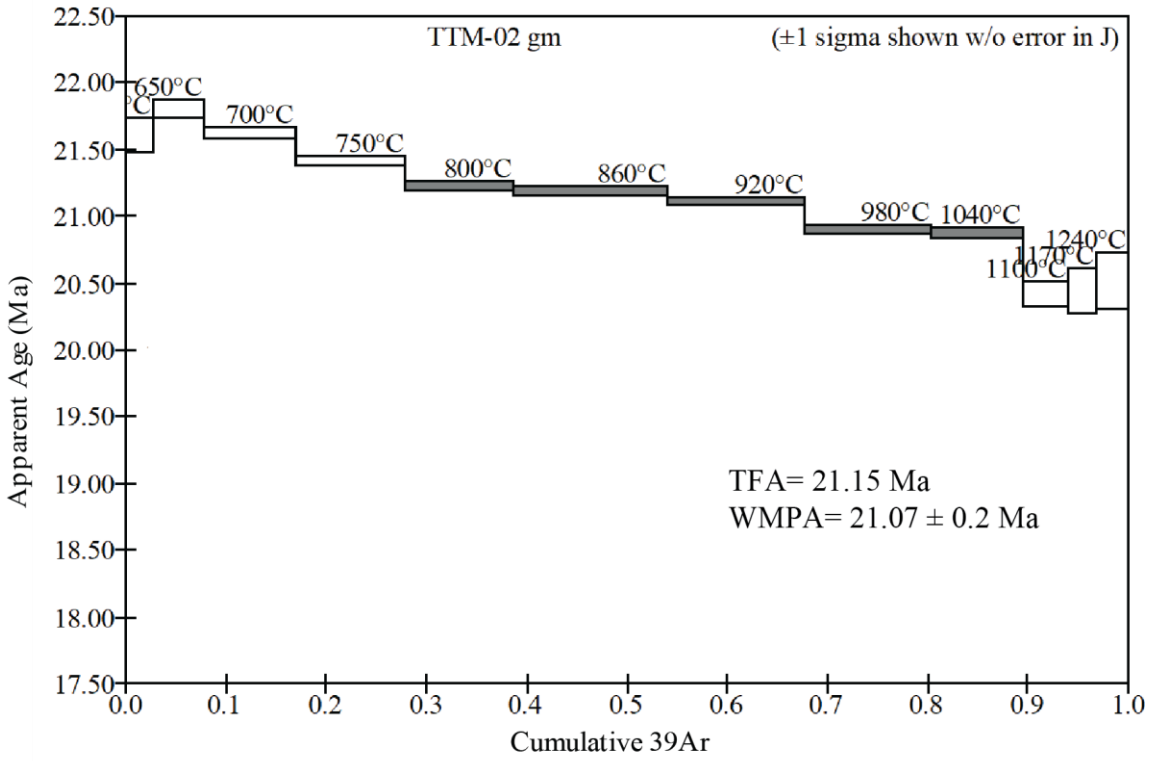

Sample: SB69-103 MHV-01 gm J=0.0041574 FINAL J (28.1 FCT)

T	t	40(mol)	40/39	38/39	37/39	36/39	K/Ca	∑ 39Ar	40Ar*	Age (Ma)
600	14	1.9e-14	5.5284	0.0e+0	1.5396	0.0096	0.32	0.03172	0.487	20.1 ± 0.2
650	14	1.8e-14	3.4987	0.0e+0	1.2666	0.0026	0.39	0.07883	0.782	20.4 ± 0.1
700	14	2.5e-14	3.0906	0.0e+0	0.9727	0.0014	0.50	0.15258	0.869	20.0 ± 0.1
750	14	2.5e-14	2.9650	0.0e+0	0.7391	0.0010	0.66	0.22943	0.904	20.0 ± 0.1
800	14	2.5e-14	2.9688	0.0e+0	0.6473	0.0011	0.76	0.30738	0.892	19.7 ± 0.1
860	14	4.0e-14	2.9179	0.0e+0	0.8553	0.0009	0.57	0.43080	0.912	19.9 ± 0.1
920	14	2.8e-14	2.8082	0.0e+0	0.7046	0.0006	0.70	0.52242	0.939	19.7 ± 0.1
980	14	3.5e-14	2.9150	0.0e+0	0.7238	0.0010	0.68	0.63136	0.901	19.6 ± 0.1
1040	14	4.2e-14	3.0467	0.0e+0	0.8973	0.0015	0.55	0.75781	0.855	19.4 ± 0.1
1100	14	3.8e-14	3.0418	0.0e+0	1.5082	0.0015	0.32	0.87086	0.852	19.3 ± 0.1
1170	14	1.7e-14	3.4927	2.5e-4	6.5579	0.0029	0.075	0.91607	0.753	19.6 ± 0.1
1240	14	3.4e-14	3.6723	0.0e+0	5.7871	0.0035	0.085	1.00000	0.717	19.6 ± 0.1

Total fusion age, TFA= 19.71 ± 0.04 Ma (including J)
Weighted mean plateau age, WMPA= 19.52 ± 0.04 Ma (including J)
Inverse isochron age =19.55 ± 0.13 Ma. (MSWD =5.16; 40Ar/36Ar=293.0 ± 10.5)
Steps used: 920, 980, 1040, 1100, 1170, 1240, (7–12/12 or 57% ∑ 39Ar
t = dwell time in minutes.
40(mol) = moles corrected for blank and reactor-produced 40.
Ratios are corrected for blanks, decay, and interference.
∑39Ar is cumulative, 40Ar* = rad fraction.

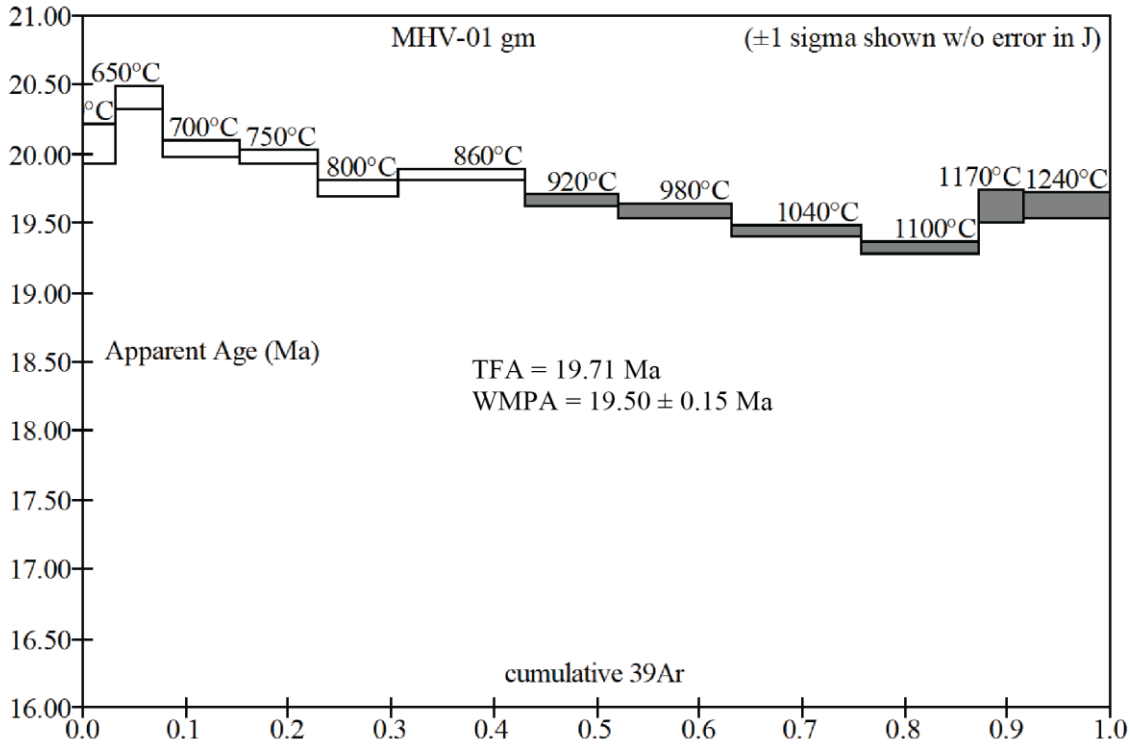

Sample: SB69-110 MHV-04 gm J=0.0041065 FINAL J (28.1 FCT)

T	t	40(mol)	40/39	38/39	37/39	36/39	K/Ca	∑ 39Ar	40Ar*	Age (Ma)
600	14	2.2e-14	6.4398	0.0e+0	1.3416	0.0123	0.37	0.03755	0.436	20.7 ± 0.2
650	14	2.4e-14	4.2142	0.0e+0	1.3213	0.0048	0.37	0.09991	0.667	20.7 ± 0.1
700	14	3.2e-14	3.5221	0.0e+0	1.2388	0.0025	0.40	0.20219	0.792	20.5 ± 0.1
750	14	3.6e-14	3.2583	0.0e+0	1.0765	0.0018	0.46	0.32360	0.841	20.2 ± 0.1
800	14	3.1e-14	3.1262	0.0e+0	0.9887	0.0014	0.50	0.43523	0.866	19.9 ± 0.1
860	14	4.1e-14	2.9055	0.0e+0	0.8842	0.0008	0.55	0.59325	0.923	19.8 ± 0.1
920	14	3.4e-14	2.8710	0.0e+0	0.8662	0.0005	0.57	0.72314	0.944	20.0 ± 0.1
980	14	2.9e-14	2.9226	0.0e+0	0.7929	0.0008	0.62	0.83309	0.914	19.7 ± 0.1
1040	14	2.3e-14	3.1479	0.0e+0	0.8867	0.0018	0.55	0.91281	0.827	19.2 ± 0.1
1100	14	1.4e-14	3.3931	0.0e+0	2.2386	0.0027	0.22	0.95870	0.763	19.1 ± 0.1
1170	14	9.0e-15	3.7504	1.5e-3	14.6715	0.0040	0.033	0.98560	0.686	19.0 ± 0.3
1240	14	5.5e-15	4.2746	1.8e-3	20.3947	0.0056	0.024	1.00000	0.615	19.4 ± 0.4

Total fusion age, TFA= 19.92 ± 0.04 Ma (including J)
Weighted mean plateau age, WMPA= 19.42 ± 0.05 Ma (including J)
Inverse isochron age =19.95 ± 0.22 Ma. (MSWD =4.78; 40Ar/36Ar=245.5 ± 17.7)
Steps used: 980, 1040, 1100, (8–10/12 or 24% ∑ 39Ar
t = dwell time in minutes.
40(mol) = moles corrected for blank and reactor-produced 40.
Ratios are corrected for blanks, decay, and interference.
∑39Ar is cumulative, 40Ar* = rad fraction.

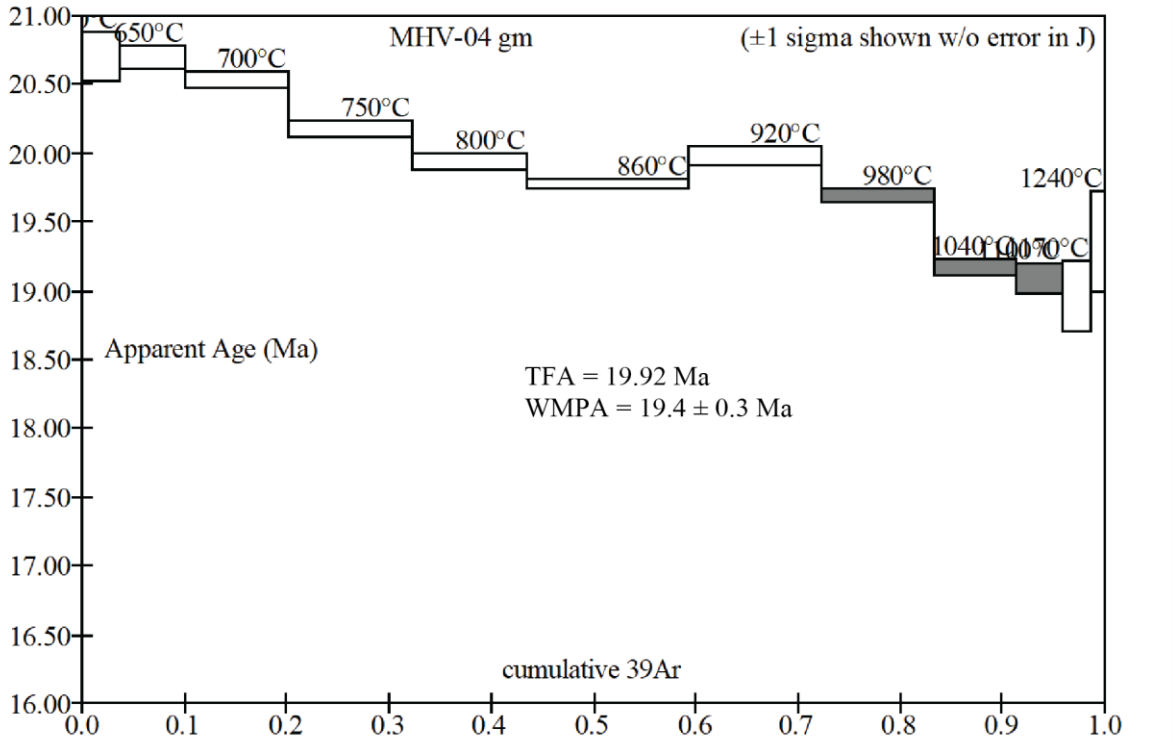

Sample: SB69-100 MHV-10 gm J=0.0041711 FINAL J (28.1 FCT)

T	t	40(mol)	40/39	38/39	37/39	36/39	K/Ca	∑ 39Ar	40Ar*	Age (Ma)
600	14	2.1e-14	4.5488	0.0e+0	0.8605	0.0044	0.57	0.03112	0.713	24.2 ± 0.1
650	14	2.6e-14	3.4182	0.0e+0	0.5982	0.0013	0.82	0.08311	0.884	22.6 ± 0.1
700	14	3.8e-14	3.0696	0.0e+0	0.4975	0.0007	0.98	0.16741	0.935	21.5 ± 0.1
750	14	4.8e-14	2.9579	0.0e+0	0.4842	0.0004	1.0	0.27820	0.958	21.2 ± 0.1
800	14	4.8e-14	3.0182	0.0e+0	0.4391	0.0006	1.1	0.38751	0.937	21.1 ± 0.1
860	14	5.7e-14	2.9650	0.0e+0	0.3683	0.0005	1.3	0.51830	0.953	21.1 ± 0.0
920	14	4.4e-14	2.9738	0.0e+0	0.3910	0.0005	1.3	0.61917	0.947	21.1 ± 0.1
980	14	4.5e-14	3.0744	0.0e+0	0.5357	0.0010	0.91	0.71786	0.908	20.9 ± 0.1
1040	14	6.2e-14	2.9455	0.0e+0	0.4602	0.0005	1.1	0.86125	0.946	20.9 ± 0.0
1100	14	3.4e-14	3.0121	0.0e+0	0.9304	0.0008	0.53	0.93817	0.925	20.8 ± 0.1
1170	14	1.6e-14	3.4598	0.0e+0	8.2228	0.0023	0.060	0.96967	0.805	20.8 ± 0.1
1240	14	1.6e-14	3.7129	0.0e+0	12.1705	0.0031	0.040	1.00000	0.754	21.0 ± 0.2

Total fusion age, TFA= 21.23 ± 0.04 Ma (including J)
Weighted mean plateau age, WMPA= 20.86 ± 0.04 Ma (including J)
Inverse isochron age =20.84 ± 0.07 Ma. (MSWD =0.18; 40Ar/36Ar=298.4 ± 3.0)
Steps used: 980, 1040, 1100, 1170, 1240, (8–12/12 or 38% ∑ 39Ar
t = dwell time in minutes.
40(mol) = moles corrected for blank and reactor-produced 40.
Ratios are corrected for blanks, decay, and interference.
∑39Ar is cumulative, 40Ar* = rad fraction.

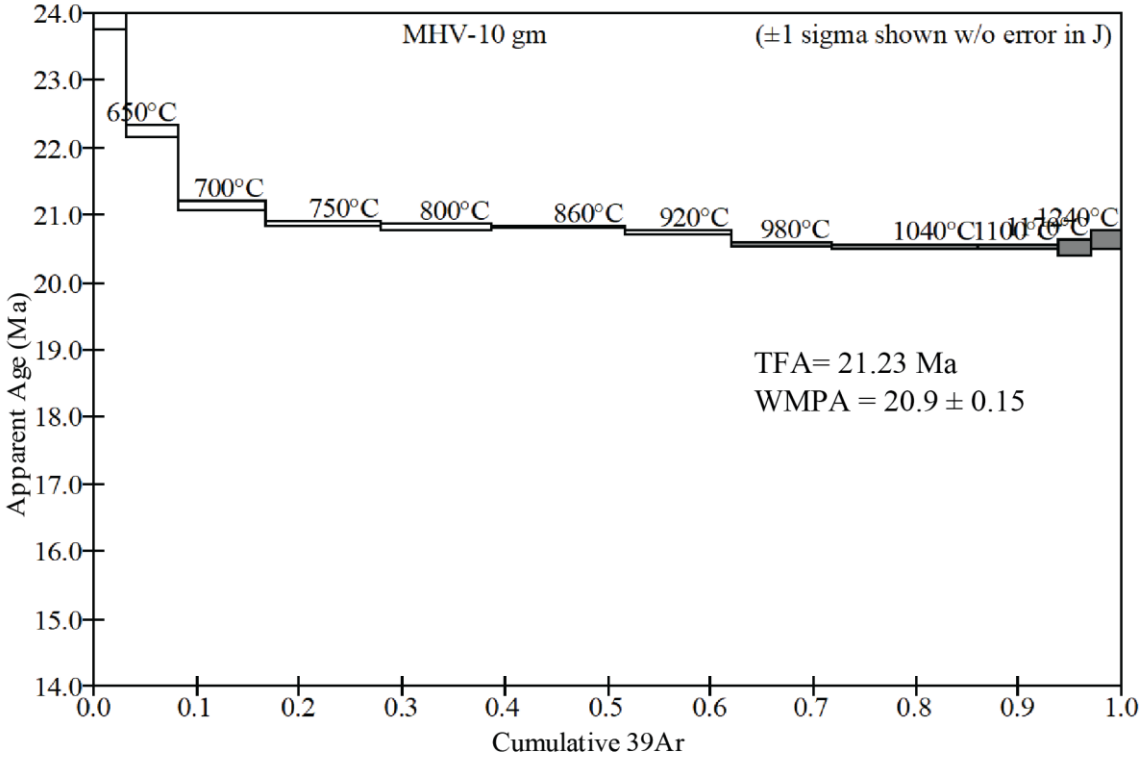

Sample: SB69-105 MHV-12 gm J=0.0041441 FINAL J (28.1 FCT)

T	t	40(mol)	40/39	38/39	37/39	36/39	K/Ca	∑ 39Ar	40Ar*	Age (Ma)
600	14	2.5e-14	5.7997	0.0e+0	1.2278	0.0112	0.40	0.05048	0.429	18.5 ± 0.2
650	14	2.2e-14	3.7565	0.0e+0	1.5335	0.0040	0.32	0.12166	0.686	19.2 ± 0.1
700	14	2.5e-14	3.1991	0.0e+0	1.4420	0.0021	0.34	0.21543	0.808	19.2 ± 0.1
750	14	2.4e-14	3.0759	0.0e+0	1.0813	0.0018	0.45	0.30942	0.828	18.9 ± 0.1
800	14	2.3e-14	3.1989	0.0e+0	0.8270	0.0022	0.59	0.39628	0.797	19.0 ± 0.1
860	14	3.1e-14	3.3396	0.0e+0	0.7646	0.0027	0.64	0.50495	0.760	18.9 ± 0.1
920	14	3.6e-14	3.8896	0.0e+0	0.9425	0.0046	0.52	0.61419	0.651	18.8 ± 0.1
980	14	7.1e-14	6.0911	0.0e+0	0.9167	0.0121	0.53	0.75271	0.415	18.8 ± 0.1
1040	14	7.9e-14	6.7858	0.0e+0	1.0676	0.0144	0.46	0.89205	0.373	18.8 ± 0.1
1100	14	3.1e-14	6.7047	0.0e+0	2.3331	0.0141	0.21	0.94646	0.380	18.9 ± 0.2
1170	14	1.7e-14	7.7443	5.2e-4	12.3018	0.0173	0.040	0.97311	0.341	19.6 ± 0.3
1240	14	1.7e-14	7.6027	0.0e+0	16.9769	0.0166	0.029	1.00000	0.354	20.0 ± 0.3

Total fusion age, TFA= 18.96 ± 0.05 Ma (including J)
Weighted mean plateau age, WMPA= 18.89 ± 0.04 Ma (including J)
Inverse isochron age =18.93 ± 0.06 Ma. (MSWD =0.50; 40Ar/36Ar=294.4 ± 0.6)
Steps used: 750, 800, 860, 920, 980, 1040, 1100, (4–10/12 or 73% ∑ 39Ar
t = dwell time in minutes.
40(mol) = moles corrected for blank and reactor-produced 40.
Ratios are corrected for blanks, decay, and interference.
∑39Ar is cumulative, 40Ar* = rad fraction.

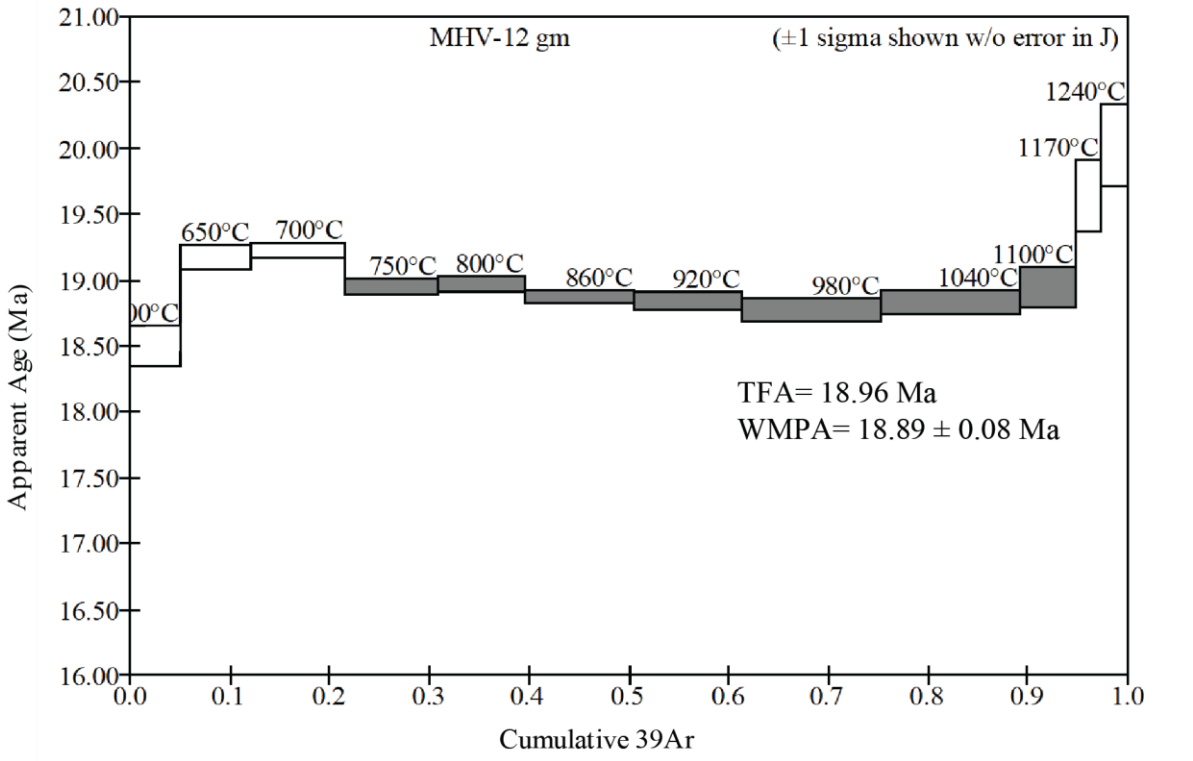

Sample: SB69-107		MHV-14 gm		J=0.0041305			FINAL J (28.1 FCT)			
T	t	40(mol)	40/39	38/39	37/39	36/39	K/Ca	∑ 39Ar	40Ar*	Age (Ma)
600	14	4.2e-14	3.7775	0.0e+0	0.2010	0.0052	2.4	0.04903	0.593	16.6 ± 0.1
650	14	3.9e-14	2.9490	0.0e+0	0.2247	0.0021	2.2	0.10725	0.785	17.2 ± 0.1
700	14	4.5e-14	2.8619	0.0e+0	0.2581	0.0014	1.9	0.17561	0.850	18.0 ± 0.0
750	14	4.9e-14	2.8884	0.0e+0	0.2345	0.0012	2.1	0.24998	0.877	18.8 ± 0.1
800	14	5.2e-14	2.9927	0.0e+0	0.2088	0.0014	2.3	0.32611	0.860	19.1 ± 0.0
860	14	6.4e-14	3.1287	0.0e+0	0.1724	0.0019	2.8	0.41486	0.825	19.1 ± 0.1
920	14	7.6e-14	3.2405	0.0e+0	0.1821	0.0023	2.7	0.51781	0.790	19.0 ± 0.0
980	14	9.8e-14	3.3899	0.0e+0	0.2342	0.0030	2.1	0.64400	0.741	18.6 ± 0.1
1040	14	1.0e-13	3.6166	0.0e+0	0.2923	0.0038	1.7	0.76922	0.691	18.5 ± 0.1
1100	14	9.7e-14	3.9074	0.0e+0	0.4641	0.0049	1.1	0.87795	0.630	18.2 ± 0.1
1170	14	7.4e-14	4.6350	5.4e-5	1.5697	0.0075	0.31	0.94799	0.524	18.0 ± 0.1
1240	14	6.0e-14	5.0568	0.0e+0	3.3251	0.0092	0.15	1.00000	0.463	17.4 ± 0.1

Total fusion age, TFA= 18.37 ± 0.04 Ma (including J)
Weighted mean plateau age, WMPA= 18.46 ± 0.04 Ma (including J)
Inverse isochron age =19.26 ± 0.16 Ma. (MSWD =0.92; 40Ar/36Ar=268.0 ± 5.1)
Steps used: 980, 1040, 1100, (8–10/12 or 36% ∑ 39Ar
t = dwell time in minutes.
40(mol) = moles corrected for blank and reactor-produced 40.
Ratios are corrected for blanks, decay, and interference.
∑39Ar is cumulative, 40Ar* = rad fraction.